University of Naples Federico II

Polytechnic and Basic Sciences School

Department of Chemical Sciences

Ph.D. in Chemical Sciences

Use of levulinic acid to produce chemicals

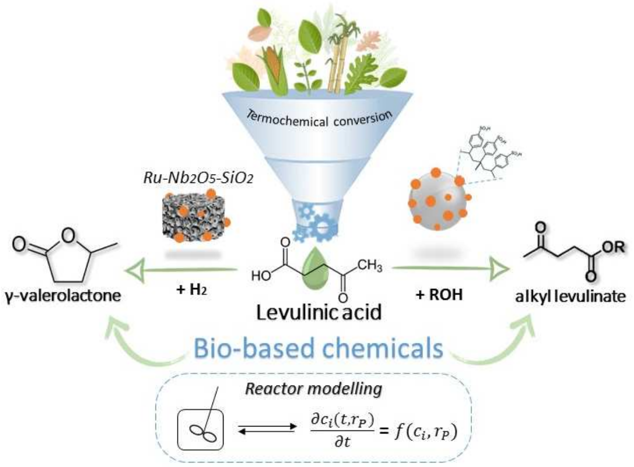

Carmelina Rossano

Supervisor	Tutor
Prof. Angela Lombardi	Prof. Martino Di Serio

XXIII Cycle 2018 – 2021

Coordinator: Prof. Angela Lombardi

Abstract

Introduction

The non-edible Biomass is an abundant and relatively cheap carbon source that can be quickly reintegrated and that is ethically accepted because they cannot be used as a food source. They represent the best candidate to supply both energy and non-fossil carbon for our industrial society and have an enormous potential since they can be transformed into useful platform chemicals through biotechnological or thermochemical conversion steps. ***Levulinic acid*** (LA) was highlighted as one of the most promising platform chemicals mainly obtained from acid hydrolysis of lignocellulosic biomass because its synthesis is easier respect to other possible building block derived from cellulose. However, the actual chemical processes limit an economically convenient production in commercial quantities. Levulinic acid esters (LAEs) or alkyl levulinates fall certainly within the most important derivatives of levulinic acid and represent strategic value-added chemicals from a biofuel-market perspective, as biofuel additives, replacing current chemicals synthetized from petrochemicals. At the present, ethyl levulinate (EL) is the most widely studied alkyl levulinate since it provides a better blending option with fuel likewise other higher alcohols (butyl levulinate). The big advantage of EL is that it is synthetized with ethanol, which is traditionally produced from renewable resources.

In this thesis work, the use of heterogenous catalysts for esterification reaction, with a deep investigation on kinetic aspects to design and optimize industrial reactors, will be investigated. By hydrogenation of levulinic acid it is possible to obtain γ-valerolactone, that is a very interesting solvent that can substitute the traditional solvents. This reaction is the second object of these project.

Thesis organization

The thesis after a general introduction to the production and uses of Levulinic Acid (Chapter I) is organized in 2 parts: levulinic acid esterification (part A) and levulinic acid hydrogenation (part B)

Part A

The first chapter of Part A is devoted to the state of art on levulinic acid Esterification (Chapter II). The successive chapters describe the experimental work. In Chapter III the results on the influence of reaction parameters on the esterification reaction of Levulinic acid with different catalysts (Amberlyst-15, Amberlite IR120 and Dowex 50Wx8) is reported. Chapter IV is devoted to the study of process intensification from batch to continuous reactor for the ethyl levulinate synthesis with Amberlite IR120 as catalyst. The possibility to use a chromatographic reactor, to integrate reaction and separation stages, is described at the end of Part A in Chapter V

Part B

In Chapter VI the state of art on levulinic acid hydrogenation is reported.

The experimental work, reported in Chapter VII, was devoted to elucidate the influence of catalyst acidity in γ-valerolactone yield, and a deeper analysis on the performances of $SiO_2/Nb_2O_5/RuO$ catalysts, prepared via sol-gel technique was conducted.

List of Publications

The thesis consists of the following publications, which are referred to, in the text, by their Roman numerals.

I. V. Russo, C. Rossano, E. Salucci, R. Tesser, T. Salmi, M. Di Serio, "Intraparticle Diffusion Model to Determine the Intrinsic Kinetics of Ethyl Levulinate Synthesis Promoted by Amberlyst-15". *Chem. Eng. Sci.* (**2020)** *228*, 115974

II. V. Russo, R. Tesser, C. Rossano, T. Cogliano, R. Vitiello, S. Leveneur, M. Di Serio, "Kinetic Study of Amberlite IR120 Catalyzed Acid Esterification of Levulinic Acid with Ethanol: From Batch to Continuous Operation". *Chem. Eng. J.* (**2020)** *401*, 126126

III. V. Russo, R. Tesser, C. Rossano, R. Vitiello, R. Turco, T. Salmi, M. Di Serio, " Chromatographic Reactor Modelling"*Chem. Eng. J.* (**2019)**, *377*, 119692.

IV. C. Rossano, C.L. Pizzo, R. Tesser, M. Di Serio, V. Russo, "Reactive Chromatography Applied to Ethyl Levulinate Synthesis: A Proof of Concept" *Processes* (**2021)** *9* (9)

V. S. Esposito, B. Silvestri, C. Rossano, V. Vermile, C. Imparato, M. Manzoli, B. Bonelli, V. Russo, E. M. Gaigneaux, A. Aronne, M. Di Serio, "The Role of Metallic and Acid Sites of Ru-Nb-Si Catalysts in the Transformation of Levulinic Acid to γ-Valerolactone" (Submitted to Applied Catalysis B: Environmental)

Other publication not concerning the thesis topics:

- R. Vitiello, C. Rossano, I. Russo Krauss, G. D'Errico, M. Di Serio, "Hydrophobically Modified Alkali Soluble Emulsion Polymers: Literature Review". *J. Surfactants Deterg.* **2020**, *23* (1), 5–19.

Index

CHAPTER I

Levulinic acid as a building block for chemistry

State of the art

Preamble

In this chapter the background (paragraph 1.1) of the research project, highlighting the necessity of bio-chemicals to decrease the world's dependence on fossil resources is presented. From hydrolysis of lignocellulosic biomass, it is possible to produce ***levulinic acid*** that was considered as one of the most promising platform chemicals (paragraph 1.2) and the literature about the continuous processes for the commercial production of levulinic acid is described (paragraph 1.3). In paragraph 1.4, derivatives of levulinic acid and their application is listed and briefly explained; while paragraph 1.5 provides an outline of the research aim that will be focused on their dedicated chapters.

1.1.Introduction

To satisfy the ever-growing global energy demand fossil resources such as coal, oil and natural gas are still extensively used. Nevertheless, at the current consumption rhythm, the global resources will eventually run out. Based on BP's Statistical Review of World Energy 2016, we would have about 115 years of coal production, and roughly 50 years of both oil and natural gas remaining (Figure 1). [1, 2]

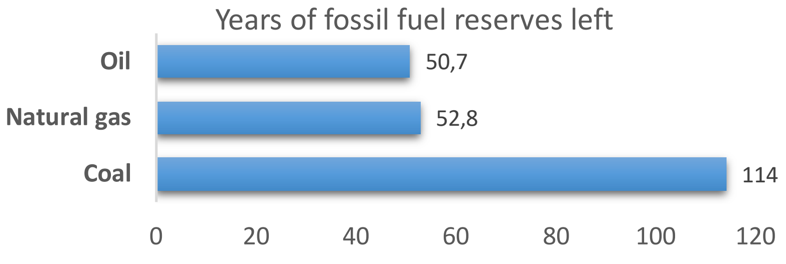

Figure 1.1. Years of global oil, natural gas and coal left, reported as the reserves-to-product ratio which measures the remaining amount of a non-renewable resource, expressed in time.

In this scenario to safeguard our future and to bring it towards "green chemistry" perspective, sustainable alternatives have been taken in account. Biomass is the best candidate to supply both energy and non-fossil carbon for our industrial society. Biomasses are relatively cheap, quickly reintegrated and ethically accepted by the society because they cannot be used as a food source and for that they are considered as a second-generation raw material. [3,4]

Moreover, the substitution of fossil source with biomasses is fundamental for the solution of the greenhouse gas emissions problem (changing global climate), indeed the CO_2 generated by its transformation into chemical products and biofuels or by the combustion of the latter, it is reused by existing plants for the photosynthesis process and for biomass regrowth.

In the last decade, many studies have highlighted the enormous potential of ***lignocellulosic biomass***, in the large framework of opportunities deriving from renewable energy sources, as a key resource for the development of a more sustainable chemical and energy industry. [3,5,6]

Also, lignocellulosic biomass is considered as "second generation biomass" and includes non-food crops such as wood, agriculture waste, paper mill discards, grass and organic waste. The composition of lignocellulosic biomass could be roughly represented by a ratio of *ca.* 38–50% of cellulose, *ca.* 23–32% hemicellulose and *ca.* 15–25% lignin, but it differs for different types of biomass and geographical origin. *Cellulose* is a linear polymer of glucose linked by bond β-1,4 and have a crystalline structure obtained through intra- and intermolecular hydrogen bonding networks, that give structural strength to the plants. *Hemicellulose* is also a polymeric material consisting of C_6-sugars (glucose, mannose and galactose) and C_5-sugars (mainly arabinose and xylose). Hemicelluloses have random, amorphous structure that provide structural strength by linking cellulose fibers into microfibrils and cross-linking with lignin through hydrogen bonds and van der Waals forces. *Lignin* is an amorphous, mononuclear aromatic compounds that fills the spaces in the cell wall between cellulose and hemicellulose through combinations of hydrogen bonds, ionic - interactions, ester and ether linkages and van der Waals interactions. [7–10]

The pre-treatment of lignocellulosic biomass is not an easy step since the lignin creates a barrier effect limiting the accessibility to cellulose and hemicellulose. Therefore, the purpose is to break the lignin structure and separate the cellulose in order to increase exposure to enzymes in the hydrolysis phase.

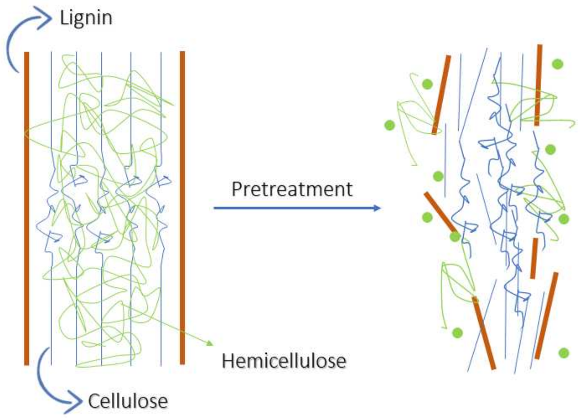

Figure 1.2. Pretreatment effect on the lignocellulosic biomass.

Principally, the treatment methods include physical, chemical, thermophysical, thermochemical, and biological. Through thermochemical processes (i.e. gasification, hydrolysis and pyrolysis) the entire biomass is considered as feedstock and is pre-treated in order to extract polysaccharides, and it is a very significant step. Formation of monosaccharides, such as hexoses and pentoses, occurs after polysaccharides hydrolysis.[11–14] Then, there are several processes for transforming each sugar to the key intermediate, such as furfural, 5-hydroxymethylfurfural (5-HMF) and levulinic acid (LA). [9]

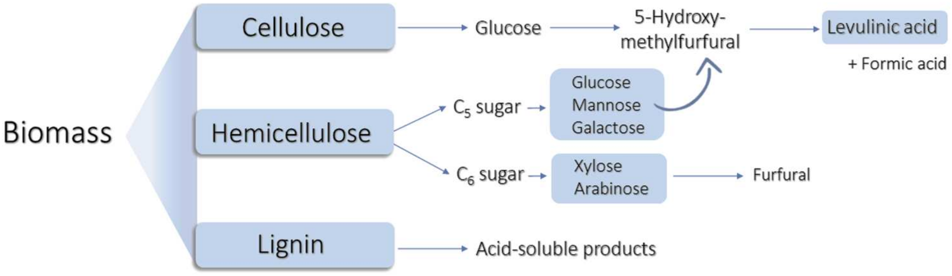

Figure 1.3. Reaction scheme for the conversion of lignocellulosic biomass. (Adapted from [15])

These products are highly desired: the glucose, for example, is important in the conversion process to bioethanol; the 5-HMF is the ideal candidate in the production of the biofuel precursors and polymers and the levulinic acid can be utilized to produce various bio-chemicals (succinic acid, resins, polymers, pharmaceuticals) and oxygenated fuel additives. Furthermore, in the conversion of hexose sugars to levulinic acid there is also a parallel formation of formic acid that is a low value chemical product used specially in the production of plasticizers, formaldehyde, textiles and pharmaceuticals. As well, formic acid find application as a source for hydrogen production and it can be used in the reaction of levulinic acid to higher value products via transfer hydrogenation. [16–18]

The facility in which are collected all the biomass conversion processes, at the purpose to transform it in products that find an application in the production of fuels, power, heat and platform chemicals, is defined Bio-refinery as described by the American National Renewable Energy Laboratory (NREL). [19–21] The bio-refinery of the future will be similar to the hodiern petrochemical refinery. It will be a highly integrated system of optimized processes from the point of view of energy efficiency and use of resources.

1.2. Top-value added chemicals: levulinic acid

Researchers from Department of Energy of the National Renewable Energy Laboratory Documents (DOE/NREL) have identified twelve sugar-based building blocks, after screened approximately 300 substances, by evaluating the potential markets of their derivatives and the complexity of the synthetic pathways.[11,22] Among these, ***levulinic acid*** was highlighted as one of the most promising platform chemicals from hydrolysis of lignocellulosic biomass (Fig.2) for fuels and chemicals and because it can be obtained from a wide range of feedstocks, becoming a chemical bridge between petroleum processing and biomasses.

Levulinic acid (LA), is a crystalline γ-ketoacid also known as 4-oxopentanoic acid (or 4-oxovaleric acid).

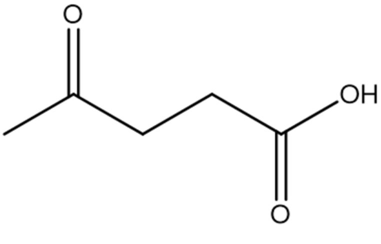

Figure 1.4. Levulinic acid molecular structure.

In 1840 the Dutch professor G. J. Mulder mentioned levulinic acid for the first time, he prepared LA by heating fructose with mineral acids at high temperature (reaction 1), but there aren’t details about reaction conditions and LA yield.[23]

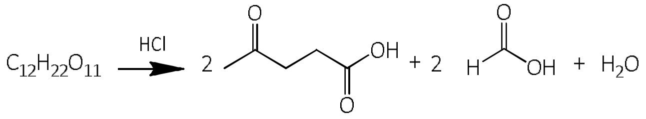
(1)

LA is readily soluble in water (675 g/L at 293.15 K), ethanol, diethyl ether, acetone and many other organic solvents, and it crystallizes at room temperature. The main physical properties of LA are given in Table 1.1. [3,24]

Table 1.1. Physical properties of levulinic acid.

Physical properties	Value
Color	Clear yellow
pKa	4.65 (at T=273 K)
Melting point	306 to 308 K
Boiling point	518 to 519 K
Density	1.1447 g/mL (at T=298,15 K)
Heat of vaporization (423.15 K)	0.58 kJ/mol
Heat of fusion	79.8 kJ/mol

The feedstock and processing conditions determine the levulinic acid production as showed by technoeconomic evaluations and there are a lot of reasons why its production does not reach commercial quantities. [25] The main reason is the raw material costs, used for production of high purity levulinic acid, that involves petrochemical feedstocks as maleic anhydride and furfuryl alcohol. The recovery problems of the levulinic acid due to its inherent physical properties, then the equipment costs which should include also a catalyst recovery plant and, in the end, the high temperatures required for the conversion reaction. [18] Today the best approach is the investigation of the conversion of lignocellulosic materials and its reaction to produce LA with catalysts, both homogeneous and heterogeneous, thanks to which the reaction speeded-up and numerous studies have been published in the last decades in this regard, in particular there are some new in- depth reviews on this topic. [26–28]

- ***Homogeneous catalysts***

In table 1.2 are show an overview of different biomasses as starting materials in the LA synthesis using homogeneous catalysts. The most used are HCl and H_2SO_4

through which 73% and 81% as maximum LA yields are respectively obtained from fructose while using glucose as feedstock, lower yields of LA are obtained. Several factors have an impact on the activity and reactivity of mineral acids: catalyst concentration and strength, typology and concentration of used feedstock and finally the reaction conditions (time and temperature). [26] However, the major challenge is still the separation of LA from mineral acid, assuming that these acid catalysts are difficult to recycle and are harmful to the equipment. Generally, the homogeneous catalyst separation requires flash separation and organic solvent extraction respectively for HCl and H_2SO_4 from LA. Nowadays, ionic liquids (ILs) have gained wide interest in green catalysis field due to their properties such as low volatility, high boiling point and high polarity. SO_3H-functionalized ionic liquids (SFILs) are an optimum alternative in term of separation and reuse.

Ren et al.[29] using 1-methyl-3-(3-sulfopropyl) imidazolium hydrogen sulfate ([C_3SO_3Hmim]HSO_4) has reached 86.1% LA yield starting from depolymerized cellulose. Shen et al. [30] has studied the 1-(4-sulfonic acid) butyl-3-methylimidazolium hydrogen sulphate ([BSmim]HSO_4)$_4$ achieving a LA yield to 39.4%. In this work, the ([BSmim]HSO_4)$_4$ was also used to study the reusability of the IL catalysts and it show a good catalytic activity after four repeated runs. A drawbacks in the use of ILs is their high cost and their difficult to purification.[31]

Table 1.2. Overview of LA yield from different feedstocks with homogeneous catalysts in water.

Feedstock	**Catalyst**	**T (°C)**	**Reaction time**	**Y_{LA} (wt%)***	**Y_{LA} (mol %)**	**Ref.**
Glucose	H_2SO_4 1 M	140	1 h	-	59	[32]
	H_2SO_4 2 M	170	2 h	41	80.7	[33]
	HCl 2M	170	30 min	49	-	[33]
Fructose	H_2SO_4 1 M	140	30 min	-	74	[34]
	H_2SO_4 2 M	170	30 min	43	-	[33]
	HCl 2M	100	24 h	81	-	[35]
Extruded starch	4% H_2SO_4	200	40 min	-	67	[35]
Paper sludge	98% H_2SO_4	200	1 h	15.4	27.1	[26]
	37% HCl	200	1 h	31.4	55.1	[26]
Bagasse	HCl 4.5 wt%	220	45 min	22.8	82.7	[36]
Poplar sawdust	37% HCl	200	1 h	29.3	51.0	[36]
Cellulose	H_2SO_4 2 M	170	50 min	34	-	[33]
	HCl 0.927 M	180	20 min	60	-	[35]
	$[C_3SO_3Hmim]HSO_4$ 16.7 wt%	170	5 h	-	86.1	[29]
	$[BSMim]HSO_4$	120	2 h	39.4	-	[30]

*LA yields measured using HPLC or GC analysis and based on the amount of C6 sugars in the feedstock

Despite this is a promising result, the application in large-scale is difficult due to the complex synthesis process and the high cost.

- ***Heterogeneous catalysts***

Even though homogeneous catalysts are successful, heterogeneous ones offer a promising alternative due to their ease recovery and separation and their handling nature thus overcoming also technological disadvantages (i.e., environment pollution and equipment corrosion). Despite this the deposition of humins on the catalyst surface lead to the deactivation of the active sites, therefore low LA yields are obtained. The humins are insoluble by-products from acid catalyzed hydrolysis/dehydration reactions of biomasses. However, most studies have already reviewed reported zeolite, ionic exchange resins (i.e. Amberlyst) and among new polymer catalyst designs, a 5-chloro-sulfonated hyper branched poly-(arylene oxindole)s) as heterogeneous catalysts that provided the highest LA yield. The most representative results are shown in Table 1.3. Already, in 1987 Jow et al.[37] used LZY zeolite (Faujasite) powder starting from d-fructose to prepare LA achieved the highest yields of up to 66 %. As show in Table 1.3, LA yields obtained from low molecular weight sugars (i.e. fructose and glucose) and lignocellulosic biomasses are comparable with yield achieved with homogeneous catalysts and to get similar quantities of LA prolonged reaction time are required. [18]

Table 1.3. Overview of LA yield from different feedstocks with heterogeneous catalysts.

Feedstock	Catalyst	T (°C)	Reaction time	Y_{LA} (%)*	Y_{LA} (mol%)	Ref.
Glucose	Amberlyst-70	180	25 h	-	50	[38]
	Fe/HY zeolite	180	4 h	66	-	[39]
	5-Cl-SHPAOs	165	5 h	51	-	[40]
Fructose	Amberlyst-15	120	24 h	52		[41]
	LZY- zeolite	140	15 h	66	43.2	[37]
	5-Cl-SHPAOs	165	1 h	66	-	[40]
Starch	5-Cl-SHPAOs	165	7 h	50	-	[40]
Nordic pulp	Amberlyst-70	180	60 h	-	57	[38]
Cellulose	Amberlyst-70	160	16 h	-	69	[42]
	5-Cl-SHPAOs	165	5 h	48	-	[40]

*LA yields measured using HPLC or GC analysis. The yield calculated in the respective paper is not clear.

Even though heterogeneous catalysts have received extensive attention, in order to promote the biomass large-scale application a depth exploration of the catalytic mechanism on the reaction of biomass conversion is required. To improve the LA yields, other important research topics for the future are also to prevent the catalyst deactivation due to the humins deposition, designing new catalysts structure involving likewise different organization of the acid sites.

1.3. Continuous process for the commercial production of levulinic acid

A typical laboratory batch reactor has been used to obtain the results shown in Table 1.2 and 1.3 in the previous paragraph. As already mentioned, is not very simple to achieve high LA yields and the first application in large scale dates from 1957 and was proposed by Dunlop and Wells [43] starting from furfural corn cob residues. In this process, sulphuric acid was used as catalysts and the corn cob furfural residue is mixed with it and with water. The mixture is continuously passed through a reactor at a flow rate such that the residence time of the material within the reactor is of 2 h, at 169°C. At this point, the humins that are formed during the reaction are separated in a filter unit.

Thereafter the aqueous mixture, that contain LA, acid catalyst, and formic acid, is passed through an upper portion of a solvent extraction column and at the same time a water-immiscible solvent (methyl isobutyl ketone) is passed into the bottom of column. The acid so separated is recycled and sent back to the mixer prior the reactor. Finally, the extraction solvent is separated from the LA and is recycled to the extraction column. Through a vacuum distillation, a further concentration and purification of LA is carried out in a fractionation unit achieving a LA yield of 19.9 wt % (based on the weight of the dry feedstock).

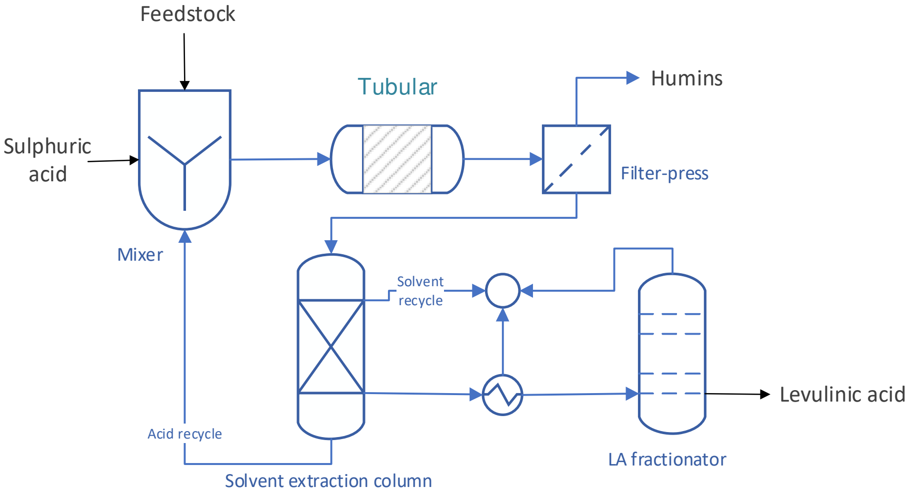

Figure 1.5. Continuous process to produce levulinic acid from corncob feedstock. Adapted from [15].

The first consolidated technology to commercialize the LA production was based on Biofine process patented by Fitzpatrick in 1990 [44] and in 1997 [45]. A block diagram of the system is shown in Figure 1.6.

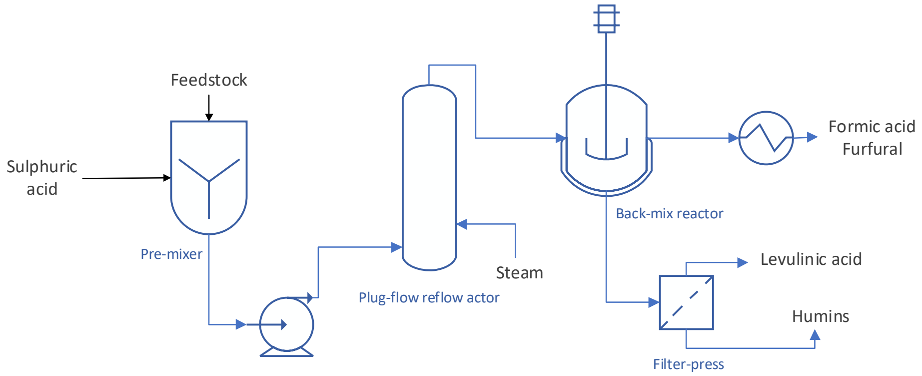

Figure 1.6. Continuous process to produce levulinic acid based on Biofine technology. Adapted from [15].

The Biofine Process, using a polymerization inhibitor, reduces excessive char formation, achieves from cellulose LA yields of 70–80% of the theoretical maximum. To reach this goal, feedstock materials for a Biofine plant must be of appropriate particle size (ca 0.5 to 1 cm) this guarantees, above all, efficient hydrolysis. The feedstock, initially shredded is passed through to a mixing tank in which there is sulphuric acid recycled. The process consists of two stages, with two reactors. In the first stage, the reaction occurs in a plug-flow reactor at a temperature of 210–220°C and a pressure of 25 bar at a mean residence time of 12 s to effectively hydrolyze the polysaccharides into soluble sugar monomers and oligomers. Obviously, considering that the products are removed in continuous, and take into account the short residence time, the diameter of the reactor is small.

The second stage is slower than the first one and requires mean residence time of 20 min. In this step the reaction occurs in a back-mix reactor, and the operating conditions are less severe (190–200 °C, 14 bar). LA is removed from the remaining product (formic acid and furfural), while solid by-products are removed in a filter-press unit. Based on this technology, the first pilot plant was built in New York at South Glen Falls (1996-2000) with a capacity of 1 ton per day.[21]

A 50 TPD demonstration plant was also built in Caserta, Italy during between 2000 and 2005 by GF Biochemicals, starting from local tobacco bagasse and paper mill sludge. In 2015, GF Biochemicals announced that has started the commercial production of levulinic acid. [46]

1.4. Potential Applications of LA and Its Derivatives

Levulinic acid is a precursor for the production of a wide variety of utilizable chemicals such as levulinate esters, γ-valerolactone (GVL), succinic acid, α-angelica lactone, 2-methyltetrahydrofuran (MTHF), δ-aminolevulinic acid (DALA), and so on (Fig. 1.7) and it finds applications for several commercial purposes: additives, fragrances, solvents, resins, printer ink, drug delivery systems, antifreezing agents, polymers, pharmaceuticals, and plasticizers (Table 1.4).

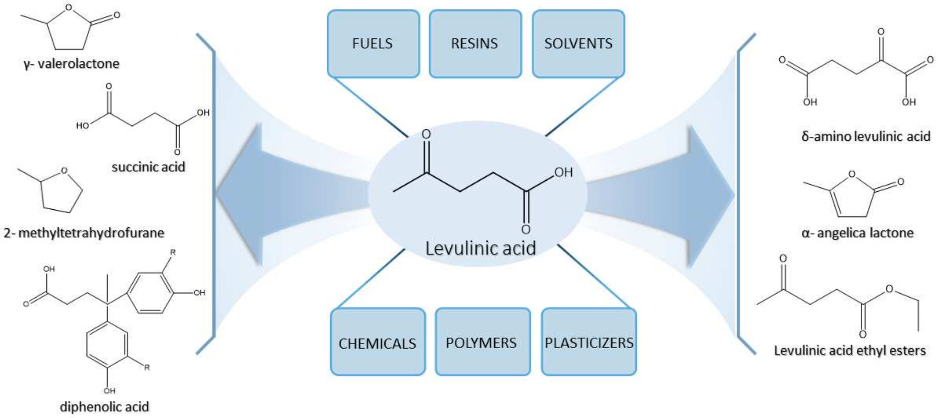

Figure 1.7. Derivatives of levulinic acid and their application.

Table 1.4. Levulinic acid derivatives and their potential application (Adapted from [47]).

Levulinic acid derivatives	*Applications*
Levulinate esters	Solvents, plasticizers
Ethyl levulinate	Food flavoring, fuel additives, fragrance
γ-valerolactone (GVL)	Solvents, biofuels, polymers, fuel additive
Succinic acid	Pesticides, solvents, polymers, lubricants
α-angelica lactone	Solvents, fuel additive
2-methyltetrahydrofuran (MTHF)	Solvents, fuel additive
δ-aminolevulinic acid (DALA)	Cancer treatment, insecticides, herbicides
Diphenolic acid	Epoxy resins, adhesives, lubricants, paints, polymers
Levulinic Ketals	Plasticizers for PVC, polyols for polyurethane materials, polymer synthesis

The potential applications of LA derivatives have been already reviewed largely [21,27,35,48], following are list some of the more promising chemicals which potentially have the largest markets.

- ***Diphenolic acid***

Diphenolic acid (DPA) is a chemical that can find some application specially for the synthesis of epoxy resins and polycarbonates. DPA can be synthesized from the condensation reaction of LA with two moles of phenol in the presence of Brönsted acid [49].

Initially, DPA was replaced by bisphenol A (BPA), a petrolchemical derived with a low cost. Now, the reduced cost of LA production due to the Biofine process made possible to reclaim its marketplace. DPA is a structurally analog to BPA but also contains a carboxyl group that offers more functionality in the polymer synthesis and this will ensure new sustainable opportunities for the chemical industry.

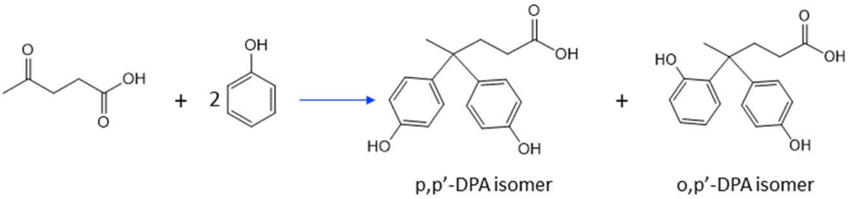

Figure 1.8. Synthesis of diphenolic acid from levulinic acid and phenol.

The molar ratio of both isomers has an important effect on the final polycarbonate properties, as for example the crystallinity and color stability and the formation of o,p'-DPA isomer is undesirable. [35]

Homogeneous and heterogeneous catalysts have been used for the synthesis of DPA, and Table 1.5 gives DPA yields for some selected catalysts.

Table 1.5. Diphenolic acid yields for selected catalysts. (Adapted from [27])

Catalyst	**T (°C)**	**Reaction time (h)**	**Y_{LA} (%)***	**Ref.**
HCl (40%-mol of LA)	100	6	28	[50]
H_2SO_4 (300%-wt of LA)	25	20	60	[51]
$H_3PW_{12}O_{40}$/SBA-15	100	8	80	[52]
Sulfonated hyperbranched poly(arylene oxindoles)	100	16	52	[53]
[BSMim]HSO_4	60	24	93	[54]

* The yield calculated in the respective paper is not clear.

As showed in Table 1.5, the ionic liquids [BSMim]HSO_4 exhibited higher catalytic activity with 100% selectivity to p,p′-DPA isomer. For that reason and because [BSMim]HSO_4 can be re-used multiple times, at now this catalyst has been claimed as best catalyst for the green production of DPA. [54]

- ***Succininc acid***

Succinic acid (SA) is a versatile compound and different important compounds can be derivated from it as γ-butyrolactone, 1,4-butanediol and tetrahydrofuran. In addition to the application reported in Table 1.4, SA is largely used in the food and beverage industry as an acidity regulator.

The reaction from which it is possible to obtain SA from levulinic acid is through catalytic oxidation with oxidants such as oxygen and peroxides (Fig. 1.9).

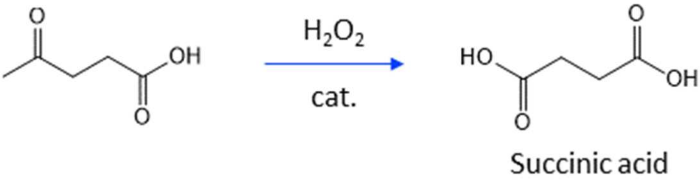

Figure 1.9. Synthesis of succinic acid from levulinic acid.

Some catalysts with relative reaction conditions used for the conversion of LA to SA are summarized in Table 1.6.

Table 1.6. Succinic acid yields for selected catalysts. (Adapted from [27])

Catalyst	**T (°C)**	**Reaction time (h)**	**Solvent**	**Y_{LA} (%)***	**Ref.**
Ru(III)- MNP	150	6	-	98	[55]
Amberlyst-15	80	6	Methanol	36	[56]
I_2/t-BuOK	RT	1	Water	87	[57]
H_2WO_4	100	6	-	47	[58]

* The yield calculated in the respective paper is not clear.

Ruthenium based magnetic nanoparticles, Ru(III)-MNP, was found to be highly active for oxidation reaction, it is easily recoverable and no oxygen was used as an oxidant, thus this method could be a green catalytic oxidation process. [55]

- ***Levulinic ketals***

Levulinic ketals are a class of compounds that are involved as plasticizers for PVC, or in polyols for polyurethane materials and in polymer synthesis. LA ketals and esters have attracted attention as biodegradable surfactants. They can be synthetized from LA or levulinate esters in reaction with an alcohol or a diol/triol in the presence of an acid catalysts. [35]

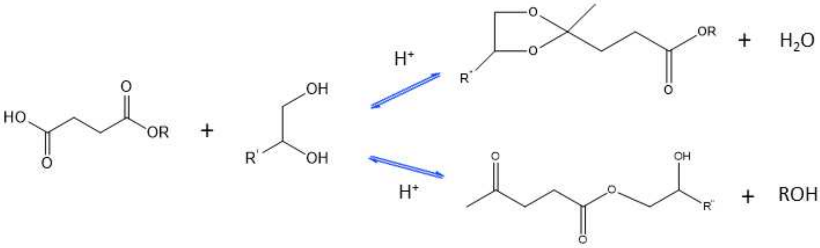

Figure 1.10. Synthesis of levulinic ketals from levulinic acid or levulinate esters.

Generally, most studies reported ketalization of levulinic acid esters rather than the direct use of levulinic acid that is a relatively unexplored area. The bifunctionality of LA provide the possibility to react with polyols (as glycerol, for example) in two different reaction way: the keto group can form ketals with 1,2 or 1,3 hydroxyls, and the carboxylic acid may sustain esterification.

- ***δ-aminolaevulinic acid***

δ-Aminolaevulinic acid (DALA) is a very expensive product and it is used sparingly only for highly selective herbicidal treatment and some brain cancer therapies. The conventional mechanism expected the bromination of LA in an alcohol medium to give mixtures of 5-bromo- and 3-bromoesters that are separated by distillation. Successively, using a nucleophilic nitrogen species (such as sodium azide or potassium phthalimide), the 5-bromolevulinate is aminated. This synthesis gives low yields at very high cost. The National Renewable Energy Laboratory (NREL) showed that DALA can be prepared from LA using sodium diformyalmide as the N-nucleophile achieving high yields (> 80 mol %) and purity (> 90%). [21,35]

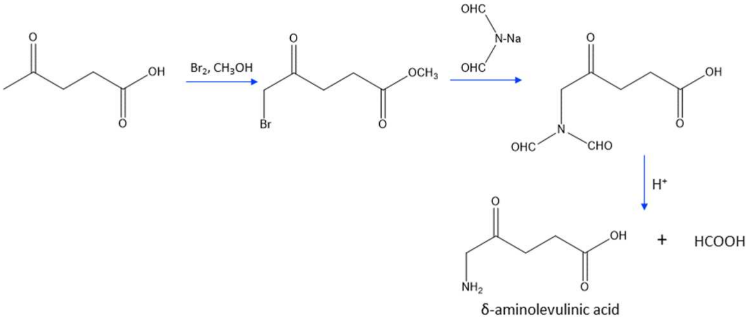

Figure 1.11. Synthesis of δ-aminolaevulinic acid from levulinic acid.

- ***Levulinate esters***

The carboxylic group of LA is implicated in an important reaction, i.e. the esterification through which are produced levulinate esters using acid catalyst, both homogeneous and heterogeneous.

The esterification reaction of LA is also possible without catalyst, but longer reaction time and higher temperature and pressure are required.

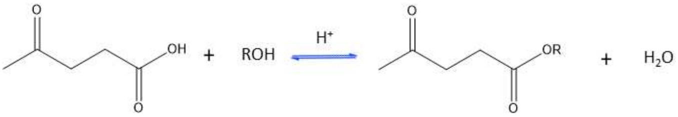

Figure 12. Synthesis of levulinate esters from levulinic acid.

Another way to obtain levulinate esters is the direct synthesis with an alcohol and in the presence of a catalyst from monosaccharides, polysaccharides, and lignocellulosic biomass. However, the formation of by-products (as formate ester, humins, HMF and HMF ethers) lower the yields, for that reason the best method to synthetize levulinate esters is to start from LA.

An in-depth review about the esterification of LA and application of levulinate esters will be dealt in a dedicated chapter (Chapter II).

- ***γ-valerolactone (GVL)***

GVL can be synthetized through a hydrogenation reaction of LA using hydrogen gas as the source for hydrogen and suitable catalysts, among the most used there are platinum oxide, Raney nickel, rhenium catalysts and rhodium complexes. Different pathways involved in the γ-valerolactone synthesis (see Fig. 13) and they depend on the conditions adopted.

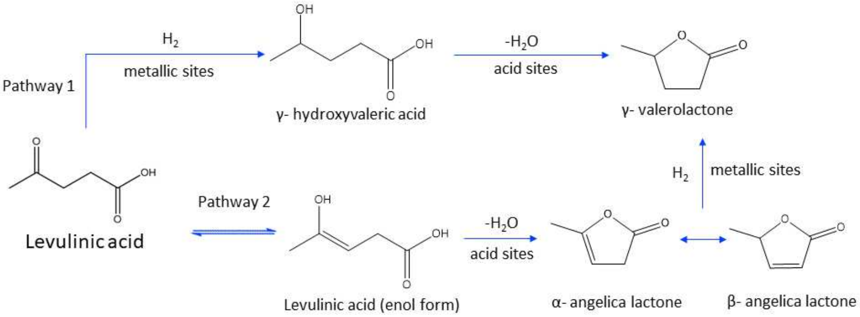

Figure 1.13. Synthesis of γ-valerolactone from levulinic acid.

In a greener and low-cost perspective noble metal-free LA to GVL conversion is also possible via catalytic transfer hydrogenation (CTH) using alcohols as hydrogen donor. An in-depth review about the hydrogenation of LA and application of GVL will be dealt in a dedicated chapter (Chapter VI).

References

(1) Dudley, B. BP Statistical Review of World Energy About This Review. *BP Stat. Rev. World Energy Juny 2016* **2016**, No. June, 10.

(2) Ritchie, H. Fossil Fuels. *Our World Data* **2017**.

(3) Yan, K.; Jarvis, C.; Gu, J.; Yan, Y. Production and Catalytic Transformation of Levulinic Acid: A Platform for Speciality Chemicals and Fuels. *Renew. Sustain. Energy Rev.* **2015**, *51*, 986–997. https://doi.org/https://doi.org/10.1016/j.rser.2015.07.021.

(4) Kudakasseril Kurian, J.; Raveendran Nair, G.; Hussain, A.; Vijaya Raghavan, G. S. Feedstocks, Logistics and Pre-Treatment Processes for Sustainable Lignocellulosic Biorefineries: A Comprehensive Review. *Renew. Sustain. Energy Rev.* **2013**, *25*, 205–219. https://doi.org/https://doi.org/10.1016/j.rser.2013.04.019.

(5) Takkellapati, S.; Li, T.; Gonzalez, M. A. An Overview of Biorefinery-Derived Platform Chemicals from a Cellulose and Hemicellulose Biorefinery. *Clean Technol. Environ. Policy* **2018**, *20* (7), 1615–1630. https://doi.org/10.1007/s10098-018-1568-5.

(6) Esposito, D.; Antonietti, M. Redefining Biorefinery: The Search for Unconventional Building Blocks for Materials. *Chem. Soc. Rev.* **2015**, *44* (16), 5821–5835. https://doi.org/10.1039/C4CS00368C.

(7) Rinaldi, R.; Schüth, F. Acid Hydrolysis of Cellulose as the Entry Point into Biorefinery Schemes. *ChemSusChem* **2009**, *2* (12), 1096–1107. https://doi.org/10.1002/cssc.200900188.

(8) Serrano-Ruiz, J. C.; Luque, R.; Sepúlveda-Escribano, A. Transformations of Biomass-Derived Platform Molecules: From High Added-Value Chemicals to Fuelsvia Aqueous-Phase Processing. *Chem. Soc. Rev.* **2011**, *40* (11), 5266–5281. https://doi.org/10.1039/C1CS15131B.

(9) Isikgor, F. H.; Becer, C. R. Lignocellulosic Biomass: A Sustainable Platform for the Production of Bio-Based Chemicals and Polymers. *Polym. Chem.* **2015**, *6* (25), 4497–4559. https://doi.org/10.1039/C5PY00263J.

(10) Lange, J.-P.; van der Heide, E.; van Buijtenen, J.; Price, R. Furfural--a Promising Platform for Lignocellulosic Biofuels. *ChemSusChem* **2012**, *5* (1), 150–166. https://doi.org/10.1002/cssc.201100648.

(11) Alonso, D. M.; Bond, J. Q.; Dumesic, J. A. Catalytic Conversion of Biomass to Biofuels. *Green Chem.* **2010**, *12* (9), 1493–1513. https://doi.org/10.1039/C004654J.

(12) Geboers, J. A.; Van de Vyver, S.; Ooms, R.; Op de Beeck, B.; Jacobs, P. A.; Sels, B. F. Chemocatalytic Conversion of Cellulose: Opportunities, Advances and Pitfalls. *Catal. Sci. Technol.* **2011**, *1* (5), 714. https://doi.org/10.1039/c1cy00093d.

(13) Onda, A.; Ochi, T.; Yanagisawa, K. Hydrolysis of Cellulose Selectively into Glucose Over Sulfonated Activated-Carbon Catalyst Under Hydrothermal Conditions. *Top. Catal.* **2009**, *52* (6), 801–807. https://doi.org/10.1007/s11244-009-9237-x.

(14) Tompsett, G. A.; Li, N.; Huber, G. W. Catalytic Conversion of Sugars to Fuels. In *Thermochemical Processing of Biomass*; John Wiley & Sons, Ltd: Chichester, UK, 2011; pp 232–279. https://doi.org/10.1002/9781119990840.ch8.

(15) Girisuta, B. *Levulinic Acid from Lignocellulosic Biomass*; 2007.

(16) Loges, B.; Boddien, A.; Junge, H.; Beller, M. Controlled Generation of Hydrogen from Formic Acid Amine Adducts at Room Temperature and Application in H2/O2 Fuel Cells. *Angew. Chem. Int. Ed. Engl.* **2008**, *47* (21), 3962–3965. https://doi.org/10.1002/anie.200705972.

(17) Heeres, H.; Handana, R.; Chunai, D.; Borromeus Rasrendra, C.; Girisuta, B.; Jan Heeres, H. Combined Dehydration/(Transfer)-Hydrogenation of C6-Sugars (D-Glucose and D-Fructose) to γ-Valerolactone Using Ruthenium Catalysts. *Green Chem.* **2009**, *11* (8), 1247–1255. https://doi.org/10.1039/B904693C.

(18) Rackemann, D. W.; Doherty, W. O. The Conversion of Lignocellulosics to Levulinic Acid. *Biofuels, Bioprod. Biorefining* **2011**, *5* (2), 198–214. https://doi.org/10.1002/bbb.267.

(19) Bozell, J. J.; Petersen, G. R. Technology Development for the Production of Biobased Products from Biorefinery Carbohydrates—the US Department of Energy's "Top 10" Revisited. *Green Chem.* **2010**, *12* (4), 539. https://doi.org/10.1039/b922014c.

(20) Putra, Z. A. Lignocellulosic Biomass Pretreatment for Biorefinery: A Review. *Indones. J. Sci. Technol.* **2018**, *3* (1), 75. https://doi.org/10.17509/ijost.v3i1.10796.

(21) Hayes, D. J.; Fitzpatrick, S.; Hayes, M. H. B.; Ross, J. R. H. The Biofine Process– Production of Levulinic

Acid, Furfural, and Formic Acid from Lignocellulosic Feedstocks. In *Biorefineries-Industrial Processes and Products*; Wiley-VCH Verlag GmbH: Weinheim, Germany; pp 139–164. https://doi.org/10.1002/9783527619849.ch7.

(22) Werpy, T.; Petersen, G. Top Value Added Chemicals from Biomass Volume I. *Us Nrel* **2004**, Medium: ED; Size: 76 pp. pages. https://doi.org/10.2172/15008859.

(23) Mulder, G. J. Untersuchungen Über Die Humussubstanzen. *J. für Prakt. Chemie* **1840**, *21* (1), 203–240. https://doi.org/10.1002/prac.18400210121.

(24) Timokhin, B. V; Baransky, V. A.; Eliseeva, G. D. Levulinic Acid in Organic Synthesis. *Russ. Chem. Rev.* **1999**, *68* (1), 73–84. https://doi.org/10.1070/rc1999v068n01abeh000381.

(25) Wyman, C. E. What Is (and Is Not) Vital to Advancing Cellulosic Ethanol. *Trends Biotechnol.* **2007**, *25* (4), 153–157. https://doi.org/10.1016/j.tibtech.2007.02.009.

(26) Liu, C.; Lu, X.; Yu, Z.; Xiong, J.; Bai, H.; Zhang, R. Production of Levulinic Acid from Cellulose and Cellulosic Biomass in Different Catalytic Systems. *Catalysts* **2020**, *10* (9), 1–22. https://doi.org/10.3390/catal10091006.

(27) Malu, T. J.; Manikandan, K.; Cheralathan, K. K. *Levulinic Acid-a Potential Keto Acid for Producing Biofuels and Chemicals*; Elsevier B.V., 2019. https://doi.org/10.1016/B978-0-444-64307-0.00006-8.

(28) Signoretto, M.; Taghavi, S.; Ghedini, E.; Menegazzo, F. Catalytic Production of Levulinic Acid (LA) from Actual Biomass. *Molecules* **2019**, *24*, 2760. https://doi.org/10.3390/molecules24152760.

(29) Ren, H.; Girisuta, B.; Zhou, Y.; Liu, L. Selective and Recyclable Depolymerization of Cellulose to Levulinic Acid Catalyzed by Acidic Ionic Liquid. *Carbohydr. Polym.* **2015**, *117*, 569–576. https://doi.org/10.1016/j.carbpol.2014.09.091.

(30) Shen, Y.; Sun, J.-K.; Yi, Y.-X.; Wang, B.; Xu, F.; Sun, R.-C. One-Pot Synthesis of Levulinic Acid from Cellulose in Ionic Liquids. *Bioresour. Technol.* **2015**, *192*, 812–816. https://doi.org/10.1016/j.biortech.2015.05.080.

(31) Rackemann, D. W.; Doherty, W. O. S.; Crops, T. The Conversion of Lignocellulosics to Levulinic Acid. **2011**, *5*, 115–126. https://doi.org/10.1002/bbb.267.

(32) Girisuta, B.; Janssen, L. P. B. M.; Heeres, H. J. Green Chemicals. *Chem. Eng. Res. Des.* **2006**, *84* (5), 339–349. https://doi.org/10.1205/cherd05038.

(33) Szabolcs, Á.; Molnár, M.; Dibó, G.; Mika, L. T. Microwave-Assisted Conversion of Carbohydrates to Levulinic Acid: An Essential Step in Biomass Conversion. *Green Chem.* **2013**, *15* (2), 439–445. https://doi.org/10.1039/C2GC36682G.

(34) Fachri, B. A.; Abdilla, R. M.; Bovenkamp, H. H. van de; Rasrendra, C. B.; Heeres, H. J. Experimental and Kinetic Modeling Studies on the Sulfuric Acid Catalyzed Conversion of d -Fructose to 5-Hydroxymethylfurfural and Levulinic Acid in Water. *ACS Sustain. Chem. Eng.* **2015**, *3* (12), 3024–3034. https://doi.org/10.1021/acssuschemeng.5b00023.

(35) Girisuta, B.; Heeres, H. J. Levulinic Acid from Biomass: Synthesis and Applications; Fang, Z., Smith, R. L., Qi, X., Eds.; Biofuels and Biorefineries; Springer Singapore: Singapore, 2017; pp 143–169. https://doi.org/10.1007/978-981-10-4172-3_5.

(36) Yan, L.; Yang, N.; Pang, H.; Liao, B. Production of Levulinic Acid from Bagasse and Paddy Straw by Liquefaction in the Presence of Hydrochloride Acid. *CLEAN – Soil, Air, Water* **2008**, *36* (2), 158–163. https://doi.org/10.1002/clen.200700100.

(37) Jow, J.; Rorrer, G. L.; Hawley, M. C.; Lamport, D. T. A. Dehydration of D-Fructose to Levulinic Acid over LZY Zeolite Catalyst. *Biomass* **1987**, *14* (3), 185–194. https://doi.org/10.1016/0144-4565(87)90046-1.

(38) Ahlkvist, J.; Ajaikumar, S.; Larsson, W.; Mikkola, J.-P. One-Pot Catalytic Conversion of Nordic Pulp Media into Green Platform Chemicals. *Appl. Catal. A Gen.* **2013**, *454*, 21–29. https://doi.org/10.1016/j.apcata.2013.01.004.

(39) Ramli, N. A. S.; Amin, N. A. S. Kinetic Study of Glucose Conversion to Levulinic Acid over Fe/HY Zeolite Catalyst. *Chem. Eng. J.* **2016**, *283*, 150–159. https://doi.org/10.1016/j.cej.2015.07.044.

(40) Yu, F.; Thomas, J.; Smet, M.; Dehaen, W.; Sels, B. F. Molecular Design of Sulfonated Hyperbranched Poly(Arylene Oxindole)s for Efficient Cellulose Conversion to Levulinic Acid. *Green Chem.* **2016**, *18* (6), 1694–1705. https://doi.org/10.1039/C5GC01971K.

(41) Son, P. A.; Nishimura, S.; Ebitani, K. Synthesis of Levulinic Acid from Fructose Using Amberlyst-15 as a Solid Acid Catalyst. *React. Kinet. Mech. Catal.* **2012**, *106* (1), 185–192. https://doi.org/10.1007/s11144-012-0429-1.

(42) Alonso, D. M.; Gallo, J. M. R.; Mellmer, M. A.; Wettstein, S. G.; Dumesic, J. A. Direct Conversion of Cellulose to Levulinic Acid and Gamma-Valerolactone Using Solid Acid Catalysts. *Catal. Sci. Technol.* **2013**, *3* (4), 927–931. https://doi.org/10.1039/c2cy20689g.

(43) Duniop, A. P.; Weiis, Process for producing levulinic acid P. A. United States Patent Office No 2,813,900, 19 November **1957**

(44) Fitzpatrick, W. S., Lignocellulose Degradation To Furfural And Levulinic Acid. U.S. Patent 4,897,497, 30 January **1990**.

(45) W, F. S. Production Of Levulinic Acid From Carbohydrate-Containing Materials. U.S. Patent 5,608,105, 4 March **1997**

(46) GFBiochemicals. No Title GF Biochemicals press release. [Accessed 22 June 2017]; available at (accessed Jan 13, 2021).

(47) Khan, A. S.; Man, Z.; Nasrullah, A.; Ullah, Z.; Muhammad, N.; Rahim, A.; Bustam, A.; Idris, A. Conversion of Biomass to Chemicals Using Ionic Liquids. *Green Sustain. Process Chem. Environ. Eng. Sci. Ion. Liq. as Green Solvents* **2019**, 1–30. https://doi.org/10.1016/B978-0-12-817386-2.00001-9.

(48) Bozell, J. J.; Moens, L.; Elliott, D. C.; Wang, Y.; Neuenscwander, G. G.; Fitzpatrick, S. W.; Bilski, R. J.; Jarnefeld, J. L. Production of Levulinic Acid and Use as a Platform Chemical for Derived Products. *Resour. Conserv. Recycl.* **2000**, *28* (3), 227–239. https://doi.org/https://doi.org/10.1016/S0921-3449(99)00047-6.

(49) Isoda Y, A. M. Preparation of Bis(Hydroxyaryl)Pentanoic Acids. JP08053390. Japanese patent 08053390, 1996.

(50) Yu, X.; Guo, Y.; Li, K.; Yang, X.; Xu, L.; Guo, Y.; Hu, J. Catalytic Synthesis of Diphenolic Acid from Levulinic Acid over Cesium Partly Substituted Wells–Dawson Type Heteropolyacid. *J. Mol. Catal. A Chem.* **2008**, *290* (1–2), 44–53. https://doi.org/10.1016/j.molcata.2008.04.023.

(51) Bader, A. R.; Kontowicz, A. D. γ,γ-Bis-(p-Hydroxyphenyl)-Valeric Acid. *J. Am. Chem. Soc.* **1954**, *76* (17), 4465–4466. https://doi.org/10.1021/ja01646a053.

(52) Guo, Y.; Li, K.; Clark, J. H. The Synthesis of Diphenolic Acid Using the Periodic Mesoporous H3PW12O40-Silica Composite Catalysed Reaction of Levulinic Acid. *Green Chem.* **2007**, *9* (8), 839–841. https://doi.org/10.1039/B702739G.

(53) Van de Vyver, S.; Geboers, J.; Helsen, S.; Yu, F.; Thomas, J.; Smet, M.; Dehaen, W.; Sels, B. F. Thiol-Promoted Catalytic Synthesis of Diphenolic Acid with Sulfonated Hyperbranched Poly(Arylene Oxindole)S. *Chem. Commun.* **2012**, *48* (29), 3497. https://doi.org/10.1039/c2cc30239j.

(54) Shen, Y.; Sun, J.; Wang, B.; Xu, F.; Sun, R. Catalytic Synthesis of Diphenolic Acid from Levulinic Acid over Bronsted Acidic Ionic Liquids. *BioResources* **2014**, *9* (2), 3264–3275. https://doi.org/10.15376/biores.9.2.3264-3275.

(55) Podolean, I.; Kuncser, V.; Gheorghe, N.; MacOvei, D.; Parvulescu, V. I.; Coman, S. M. Ru-Based Magnetic Nanoparticles (MNP) for Succinic Acid Synthesis from Levulinic Acid. *Green Chem.* **2013**, *15* (11), 3077–3082. https://doi.org/10.1039/c3gc41120f.

(56) Wang, Y.; Vogelgsang, F.; Román-Leshkov, Y. Acid-Catalyzed Oxidation of Levulinate Derivatives to Succinates under Mild Conditions. *ChemCatChem* **2015**, *7* (6), 916–920. https://doi.org/10.1002/cctc.201403014.

(57) Kawasumi, R.; Narita, S.; Miyamoto, K.; Tominaga, K.; Takita, R.; Uchiyama, M. One-Step Conversion of Levulinic Acid to Succinic Acid Using I2/t-BuOK System: The Iodoform Reaction Revisited. *Sci. Rep.* **2017**, *7* (1), 17967. https://doi.org/10.1038/s41598-017-17116-4.

(58) Carnevali, D.; Rigamonti, M. G.; Tabanelli, T.; Patience, G. S.; Cavani, F. Levulinic Acid Upgrade to Succinic Acid with Hydrogen Peroxide. *Appl. Catal. A Gen.* **2018**, *563*, 98–104. https://doi.org/10.1016/j.apcata.2018.06.034.

CHAPTER II

Levulinic acid esters from levulinic acid

State of the art

Preamble

A brief state of the art on levulinic acid esters and the importance of their application as biofuel additives are outlined (paragraph 2.1). The synthesis mechanism of levulinic acid esters production and the catalysts used are outlined in this chapter and current and potential applications of LA and its derivatives are explained (paragraph 2.2). Paragraph 2.3 is dedicated to highlighting the importance of the chemical reaction kinetics study to optimize the esterification reaction.

2.1. Introduction

Levulinic acid esters (LAEs) or alkyl levulinates fall certainly within the most important derivatives of levulinic acid and represent strategic value-added chemicals from a biofuel-market perspective, as biofuel additives [1], replacing current chemicals synthetized from petrochemicals.

These compounds, among other, can be used as substrates for various types of reactions (as addition and condensation) at the ester and keto groups and they found applications as bio lubricants[2], flavoring and fragrances agents[3], plasticizers[4,5], green solvents[6,7], personal care products[8] , latex coating compositions[9] and polymer and resin precursors [10,11].

Above all, is the use of LAEs as biofuel additives to attract a lot of interest due to the ability of this oxygenated compounds to modify some physical properties of diesel and gasoline fuels [12–16] replacing in sustainable way aggressive additives as tetraethyl lead and according to a report by Grand View Research Inc., in 2022 the demand of these compounds to reach almost 49.1 tons and an annual growth rate of 3.6%, just consider that the request in the 2014 was of 32.4 tons. [17,18]

Biofuel additives based on LAEs, other than having the common uses like to prevent the engine parts corrosion, to enhance the complete combustion of the fuel and help to reach the suitable lubricity; after mixed in appropriate compositions (generally LAEs/fuel ratio is between 0.5-20 vol%) they exhibit excellent properties that make them suitable for such application as good oxidative stability, flow-property, flash point-, cloud-point- stability. [19]

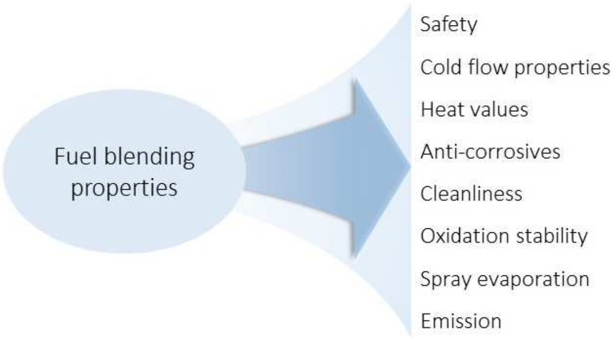

Figure 2.1. Summary of properties to have for blended fuels. Adapted from Badgujar et al. [18]

Furthermore, very important for a green and sustainable future, is that levulinates blended with fuels enhance the cleaner combustion process avoiding the formation of exhausting pollutants like CO, CO_2, hydrocarbon, sulfur and lower NOx emissions. [1] Consequently, LAEs are ever more reason of R&D initiatives in this field, also due to the easiness of synthesis from levulinic acid. There are four different synthetic routes to obtain levulinate ester compounds as shown in Figure 2.2. [18]

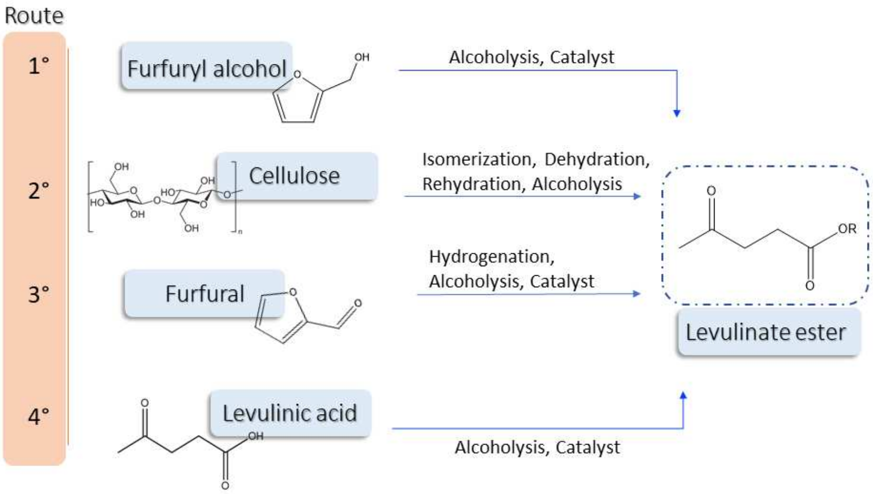

Figure 2.2. Different synthesis routes to produce levulinate esters. Adapted from Badgujar et al. [18]

First route starts from furfuryl alcohol and LAEs are obtained in high yield through an easy reaction under relatively mild conditions. This pathway has a disadvantage which is production and availability of the furfuryl alcohol. [1,18,20]

The second route is the one-pot synthesis of LAEs from cellulose follows a series of acid-catalyzed steps, as shown in Fig. 2.2. This process has the advantage to by-pass several intermediate reactions but suffer of different drawbacks as humin formation, lower yield and selectivity, and is really limited by harsh reaction conditions with high catalyst amounts. [21] The third route expect to start from furfural which is firstly reduced to furfuryl alcohol and then through an acid-catalyzed alcoholysis transformed in LAEs. In this case, disadvantage is the use of hazardous H_2 gas for reduction at high reaction temperature and pressure. [18,22]

Therefore, all the routes provide for the acid catalyzed alcoholysis and the simplest pathway is the fourth, consisting in a direct esterification of levulinic acid with alcohols (i.e., methanol, ethanol, propanol and butanol) and in high LAE yields using different catalytic systems.[23–26]

At the present, ethyl levulinate is the most widely studied alkyl levulinate since provide a better blending option with fuel likewise other higher alcohols (butyl levulinate). The big advantage of EL is that it is synthetize with ethanol, which is traditionally produced from renewable resources and with lower total costs respect methanol and butanol. In mixtures with fuels, ethyl levulinate enhance the engine efficiency prolonging the operating life; moreover, thanks to the high oxygen content about 33% reduces NOx and CO emissions.[27]

2.2. Esterification reaction

The mechanism proposed for acid catalyzed synthesis of LA (Fig. 2.3) involves the coordination of the carbonyl oxygen with the active site of catalyst, and the formation of a carbocation to which occurs a nucleophilic attack of the alcohol.

A tetrahedral intermediate is obtained in which there are two equivalent hydroxyl groups. One of these hydroxyl groups is eliminated after a proton shift (tautomerism) to give water and the ester. [25,26]

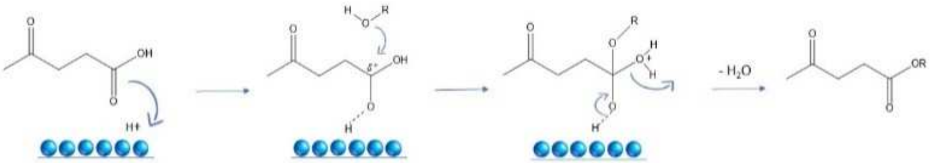

Figure 2.3. Mechanism of acid catalyzed esterification reaction of LA with alcohols to produce levulinate esters.

The direct esterification of LA with alcohols to produce levulinate esters has been studied since about 150 years ago. [28,29] Some years later, study about LAEs synthesis was progressively intensified and Sah[30] and then Schuette[31] et al. were the first that published the formation of alkyl levulinates starting with an excess of the corresponding alcohols and in the presence of HCl. Earlier studies employed mostly homogeneous catalysts (i.e. sulfuric acid, phosphoric acid, p-toluene sulphonic acid, etc.) which are low cost and easy to handle specially in modulating the acidic strength required for the reaction.[1,32] Literature concerning ethyl levulinate production with the use of homogeneous catalyst is very poor and mostly belonging from the past. [33–35]
Nowadays, the esterification of LA has been carried out using heterogeneous catalyst (i.e., solids with Brønsted acidity) that are now the preferred catalysts giving moderate to high yields of alkyl levulinates. Very recently, one in-dept review article was published by Badgujar et al. [18] in which are summarized the scientific progress about the use of various kinds of solid acid catalysts (silica based, resins, zeolites, heteropoly- acids, mixed metal oxide, nano-catalyst etc.); also the process, advantage and disadvantage, and challenge of the various catalytic systems to obtain LAEs from levulinic acid was highlighting.

- Heterogeneous catalysts

Some of heterogeneous acid catalysts are summarized in Table 2.1 and reported in the Badgujar [18] review. As we well know, the choice in the use of solid catalysts is due both to their easy separation steps from the products and recovery and reuse in various reaction cycles. In the development of new catalysts, from an economic and environmental perspective, they must be easy to prepare, low cost and have high selectivity to the product. Using solid catalyst, the adsorption of reagents on the catalyst surface must be take into account since its significantly influence the rate of the reaction. Therefore, the catalyst needs to be designed also considering the porosity and channel size, adaptable surface functionalities, the surface area, and the chemical and thermal stability.

Table 2.1. Heterogeneous acid catalysts reported in literature [18].

	Catalyst	LAEs	Time (h)	Temperature (°C)	Yield (%)	Ref.
Silica catalyst	$HClO_4/SiO_2$ nanoporous solid-acid (10% w/w)	EL	5	100	99	[36]
	$HClO_4/SiO_2$ nanoporous solid-acid (10% w/w)	BL	5	100	90	[36]
	Tungsten oxide incorporated SBA-16 catalyst (0.5 g)	ML	-	250	96	[37]
	Tungsten oxide incorporated SBA-16 catalyst (0.5 g)	EL	-	250	95	[37]
Resin catalyst	Amberlyst-15 (30%)	ML	5	64.7	82	[23]
	Amberlyst-15 (30%)	EL	5	78.4	71	[23]
	Amberlyst-15 (30%)	BL	5	117.7	55	[23]
	Dowex 50Wx2 (0.8%)	BL	8	80	94	[32]
	Aquivion mP90 (10 mol%)	PL	24	90	92	[38]
Zeolite catalyst	H-Y catalyst (10 wt%)	BL	4	120	32.2	[39]
	H-ZSM-5	BL	4	120	30.6	[39]
	Micro/Meso-HZ-5 catalyst (20 wt%)	ML	5	120	91	[40]
	Micro/Meso-HZ-5 catalyst (20 wt%)	EL	5	120	95	[40]
MOF catalyst	Zirconia containing MOF UIO-66 (1.8 mol%)	BL	5	120	99	[41]
	Zirconia containing MOF UIO-66-NH_2 (1.8 mol%)	BL	5	120	99	[41]

LAEs: alkyl levulinates, ML: methyl levulinate, EL: ethyl levulinate, BL: butyl levulinate, PL: pentyl levulinate MOF: metal organic framework.

Silica based catalyst aroused great interest from researchers given that can be acid functionalized (for example with $HClO_4$, H_2SO_4, PTSA). Yang and Tang [36] synthetize alkyl levulinate using $HClO_4$ as acid sites and nano-porous silica gel as support, showing that it is possible to reach high yield. Enumula et al. [37] demonstrated that the uniform insertion of tungsten oxide into a ordered mesoporous silica SBA-16 lead to high yield and showed enhanced acidity and activity. Unfortunately, these silica-based catalysts suffer from leaching phenomena losing the activity because the formation of H-bonding in polar solvent. In the field of catalyst morphology design, polystyrene sulphonic **acid resins** represent the challenge, thanks to the high ion-exchange capacity, the swelling properties and the living polymerization methods that allows for different range of structures, modulating acid sites along polymers. Alkyl levulinates synthesis from LA on various resin-supported acid catalysts was studied, among others, by Tejero et al. [32] who demonstrated the potential of a gel-type resin as Dowex 50Wx2 to produce butyl levulinate with a yield of 94%. Ramli et al. [24] used Amberlyst-15 as catalyst for the synthesis of short-chain levulinates, while Trombettoni et al. [38] using long chain alcohols to produce LAEs with a cation exchange resins, named Aquivion mP90.

Zeolites represent another group of solid with great catalytic potential. Zeolites can be natural or synthetic materials. They are microporous aluminosilicate minerals with well-defined channel, pores and cavities that contribute to the catalytic activity. They are noted for their ability toward ion-exchange, water molecules trap (esterification side product) and adsorption capacity. Even the zeolites can be functionalized enhancing the acidic properties. Maheria et al.[39] synthetize butyl levulinate (BL) founding that the preferential order to high yield was HY> H-ZSM-5. Nandiwale et al.[40] demonstrated the great potential of zeolites, in particular of micro/meso-HZ-5 at 20 wt% to produce renewable alkyl levulinate reaching high yield 91-95%.

Among the class of **metal organic frameworks** (MOF), Zirconium-MOFs formed by terephthalate (UiO-66)[41] are active and stable catalysts used for the acid catalyzed esterification of LA. MOFs are a crystalline micro/mesoporous material formed by metal ions or metal clusters interconnected by hydrophobic linkers. Even in this case it is possible to modulate the acidity, the cavity size, and the stability of the catalyst itself ensuring wide range of features.

A very interesting paper concerning the production of ethyl levulinate, was published by Fernandes et al.[26] that have compared different heterogeneous catalysts such as zeolite (HUSY, HBEA, HMOR, HZSM-5, HMCM-22) sulfated oxides (SnO_2, ZrO_2, Nb_2O_5, TiO_2) and a commercial sulfonic resin (Amberlyst-15).

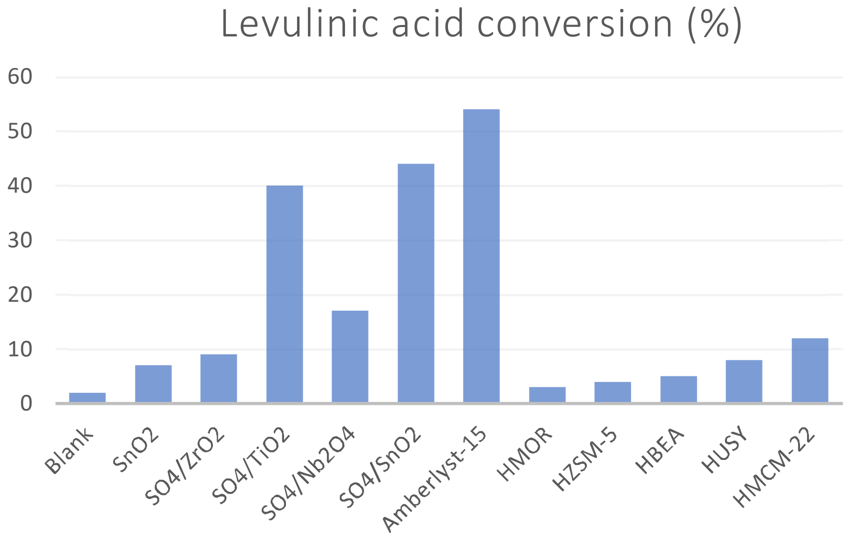

Figure 2.4. Catalysts screening for the esterification of levulinic acid with ethanol. (Adapted from [26])

As a conclusion of their own study Fernandes et al.[26] demonstrated that the activity of the zeolites is correlate to the pore channels rather than the total acidity, that is more important in the sulfated oxide catalysts (Fig. 2.4). This latter correlation has suggested that strong acidic sites are needed to synthetize ethyl levulinate from levulinic acid. Despite zeolites are cheapest materials (prize for laboratory application 0.1€/g) they showed low activity (levulinic acid conversion lower than 15%). However, Amberlyst-15 is a good candidate as catalyst for the levulinic acid esterification reaction, achieving a yield of 54%.

This promising result is due to the presence of SO_3H functional groups supported on a polymer matrix made of polystyrene cross-linked with divinylbenzene (DVB) that provide the acidic character to the resin and through the which start the reaction. The main catalytic resins are Amberlyst 15, Amberlyst 36, Amberlite IR120, Purolite, Smopex101 and Dowex. These ion-exchange resins have a lot of good characteristics as high surface area, accessibility to the active sites, appropriate pore structures, high thermal stability, and the peculiarity of swelling property in polar media. They are commercially provided as beads that can have either a dense internal structure with or without pores, dividing in gel-type and macroreticular resins respectively. Among others, safe to use, readily to remove at the end of the reaction, possibility to regenerate and then use several times are the major advantages. The most important parameter that characterizes different resins is the cross-linking content (due to the divinylbenzene amount), which determines the surface area, the pore size distribution and hence the accessibility to the active sites. When the resin is put in contact with the polar media, based on the different affinity, the polymeric matrix changes its morphology, and this phenomenon is called swelling. Lower the cross-linking content, higher is the swelling due to the flexibility of the polymeric matrix. During swelling phenomena, enlargement of pore size occurs enhancing the mass transfer and the reaction rate. [23]

2.3 Kinetic aspects of esterification reaction

The study of the chemical reaction kinetics plays an important rule to do an accurate and safe chemical reactor design. The R&D about this theme already begin in the academic laboratories and in research institute at the purpose to understand the chemical processes and their reaction kinetics and convert this information into a mathematical rate expression. That kinetic expression will allow us to understand the influence of the main parameters as temperature, composition, speed of agitation and concentration of catalytic active sites. Hence, only in this way it is possible to determine the size of the catalytic reactor, evaluate the potential industrial applicability of the catalysts, estimate the overall costs to realize a production plant and without reliable kinetics is not possible predict how eventual secondary reactions may effect on the operational safety and the environmental impact of chemicals production unit.[42]

Kinetic study on the esterification reaction of LA is relatively well-know, but related to specific processes, many gaps exist and only few kinetic investigations have been published in the literature on the ethyl levulinate synthesis. Bart et al.[34] was the first, in the early 1990s, to publish the kinetics of the reaction between LA and n-butanol in the presence of sulfuric acid. About LA esterification with ethanol Nandiwale et al.[43] presented a kinetic study based on pseudo-homogeneous (P-H) model and a second order kinetics using DTPA (dodecatungstophosphoric acid [$H_3PO_4 \cdot 12WO_3 \cdot xH_2O$]) supported on desilicated H-ZSM-5 as catalyst.

In this thesis results obtained a in dept kinetic research program on esterification of LA with ethanol promoted by different heterogeneous catalysts (Amberlyst-15, Amberlite IR120 and Dowex 50Wx8) are reported in the next Chapters.

References

(1) Démolis, A.; Essayem, N.; Rataboul, F. Synthesis and Applications of Alkyl Levulinates. *ACS Sustain. Chem. Eng.* **2014**, *2* (6), 1338–1352. https://doi.org/10.1021/sc500082n.

(2) Mukherjee, A.; Dumont, M.-J.; Raghavan, V. Review: Sustainable Production of Hydroxymethylfurfural and Levulinic Acid: Challenges and Opportunities. *Biomass and Bioenergy* **2015**, 143–183. https://doi.org/DOI:101016/jbiombioe201411007.

(3) Yontz D.J. Fragrant formulations, methods of manufacture thereof and articles comprising the same. US 2011/0274.643 A1, 2011.

(4) Paul, B. Levulinic Acid Ester Derivatives as Reactive Plasticizers and Coalescent Solvents. WO 2007094922A2, 2007.

(5) Xuan, W.; Hakkarainen, M.; Odelius, K. Levulinic Acid as a Versatile Building Block for Plasticizer Design. *ACS Sustain. Chem. Eng.* **2019**, *7* (14), 12552–12562. https://doi.org/10.1021/acssuschemeng.9b02439.

(6) Lomba, L.; Giner, B.; Bandrés, I.; Lafuente, C.; Pino, M. a R. Physicochemical Properties of Green Solvents Derived from Biomass. *Green Chem.* **2011**, *13* (8), 2062–2070. https://doi.org/10.1039/C0GC00853B.

(7) Lomba, L.; Lafuente, C.; García-Mardones, M.; Gascón, I.; Giner, B. Thermophysical Study of Methyl Levulinate. *J. Chem. Thermodyn.* **2013**, *65*, 34–41. https://doi.org/https://doi.org/10.1016/j.jct.2013.05.025.

(8) Tsucha J., Y. K. Skin Cosmetics Containing Levulinates, Glycyrrizates, and Resorcinol or Isopropylmethylphenol, 1994.

(9) Rieth, L.R., Leibig, C.M., Pratt, J., Jackson, M. Latex Coating Compositions Including Carboxy Ester Ketal Coalescents, Coalescent Evaluation and Use of Coalescents in Coatings. Patent WO2012021826A2, 2012.

(10) Allaoua, I.; Goi, B. E.; Obadia, M. M.; Debuigne, A.; Detrembleur, C.; Drockenmuller, E. (Co)Polymerization of Vinyl Levulinate by Cobalt-Mediated Radical Polymerization and Functionalization by Ketoxime Click Chemistry. *Polym. Chem.* **2014**, *5* (8), 2973–2979. https://doi.org/10.1039/C3PY01505J.

(11) Harmer, M. A.; Kapur, V.; Williams, S. R. Closed-Cell Tannin- Based Foams Comprising Polymer and Blowing Agent, 2012.

(12) Manzer, L. E. Preparation of Levulinic Acid Esters from α- Angelica Lactone and Alcohols.

(13) Rae, A.; Hodgson, W. Gasoline and Diesel Fuels Containing Alcohols, Alcohol Derivatives, and Levulinic Acid Derivatives.

(14) Groves, A. P.; Morley, C.; Smith, J. Gasoline Compositions.

(15) Clark, R. H.; Groves, A. P.; Morley, C. . S. Fuel Compositions, 2004.

(16) Lake, M. A.; Burton, S. W. Diesel Fuel Compositions Containing Levulinate Ester. *U.S. Pat. US20100313467, 2010.*

(17) https://www.grandviewresearch.com/industry-analysis/ethyl-levulinate-market (17/04/2021, data accessed)

(18) Badgujar, K. C.; Badgujar, V. C.; Bhanage, B. M. A Review on Catalytic Synthesis of Energy Rich Fuel Additive Levulinate Compounds from Biomass Derived Levulinic Acid. *Fuel Process. Technol.* **2020**, *197* (September 2019), 106213. https://doi.org/10.1016/j.fuproc.2019.106213.

(19) Fagan, P.J. , Korovessi, E. , Manzer, L.E., Mehta, R., Thomas, S. M. Levulinic and Formic Acid Esters, as Gasoline and Diesel Fuel Oxygenate Additives, Prepared from Biomass by Hydrolysis and Esterification with Olefins. *Pat. WO2003085071, 2003.*

(20) Peng, L.; Li, H.; Xi, L.; Chen, K.; Chen, H. Facile and Efficient Conversion of Furfuryl Alcohol into N-Butyl Levulinate Catalyzed by Extremely Low Acid Concentration. *Bioresources* **2014**, *9*, 3825–3834. https://doi.org/10.15376/biores.9.3.3825-3834.

(21) Amarasekara, A.; Wiredu, B. Acidic Ionic Liquid Catalyzed One-Pot Conversion of Cellulose to Ethyl Levulinate and Levulinic Acid in Ethanol-Water Solvent System. *BioEnergy Res.* **2014**, *7*. https://doi.org/10.1007/s12155-014-9459-z.

(22) Liu, C.; Lu, X.; Yu, Z.; Xiong, J.; Bai, H.; Zhang, R. Production of Levulinic Acid from Cellulose and Cellulosic Biomass in Different Catalytic Systems. *Catalysts* **2020**, *10* (9), 1–22. https://doi.org/10.3390/catal10091006.

(23) Ramli, N. A. S.; Hidayah, N.; Saidina Amin, N. A. Esterification of Renewable Levulinic Acid to Levulinate Esters Using Amberlyst-15 as a Solid Acid Catalyst. *J. Teknol.* **2016**, *79*.

https://doi.org/10.11113/jt.v79.8095.

(24) Ramli, N. A. S.; Hisham, N.; Saidina Amin, N. A. Esterification of Levulinic Acid to Levulinate Esters in the Presence of Sulfated Silica Catalyst. *Sains Malaysiana* **2018**, *47*, 1131–1138. https://doi.org/10.17576/jsm-2018-4706-08.

(25) Pasquale, G.; Vázquez, P.; Romanelli, G.; Baronetti, G. Catalytic Upgrading of Levulinic Acid to Ethyl Levulinate Using Reusable Silica-Included Wells-Dawson Heteropolyacid as Catalyst. *Catal. Commun.* **2012**, *18*, 115–120. https://doi.org/https://doi.org/10.1016/j.catcom.2011.12.004.

(26) Fernandes, D. R.; Rocha, A. S.; Mai, E. F.; Mota, C. J. A.; Teixeira da Silva, V. Levulinic Acid Esterification with Ethanol to Ethyl Levulinate Production over Solid Acid Catalysts. *Appl. Catal. A Gen.* **2012**, *425–426*, 199–204. https://doi.org/https://doi.org/10.1016/j.apcata.2012.03.020.

(27) Leal Silva, J.; Grekin, R.; Mariano, A.; Filho, R. Making Levulinic Acid and Ethyl Levulinate Economically Viable: A Worldwide Technoeconomic and Environmental Assessment of Possible Routes. *Energy Technol.* **2017**, *6*. https://doi.org/10.1002/ente.201700594.

(28) Conrad, M. X. Ueber Acetsuccinsäureester Und Dessen Derivate. *Justus Liebigs Ann. Chem.* **1877**, *188*, 217–226.

(29) Michael, A. Zur Kenntniss Der Lävulinsäure Und Des Acetondiessigsäuredilaktons. *J. Prakt. Chem.* **1891**, *44*, 113–129.

(30) Sah, P. P. T.; Ma, S.-Y. LEVULINIC ACID AND ITS ESTERS. *J. Am. Chem. Soc.* **1930**, *52* (12), 4880–4883. https://doi.org/10.1021/ja01375a033.

(31) Schuette, H. A.; Cowley, M. A. LEVULINIC ACID. II. THE VAPOR PRESSURES OF ITS ALKYL ESTERS (C1--C6. *J. Am. Chem. Soc.* **1931**, *53* (9), 3485–3489. https://doi.org/10.1021/ja01360a039.

(32) Tejero, M. A.; Ramírez, E.; Fité, C.; Tejero, J.; Cunill, F. Esterification of Levulinic Acid with Butanol over Ion Exchange Resins. *Appl. Catal. A Gen.* **2016**, *517*, 56–66. https://doi.org/https://doi.org/10.1016/j.apcata.2016.02.032.

(33) Brown, D. W.; Floyd, A. J.; Kinsman, R. G.; Roshan-ali, Y. Dehydration Reactions of Fructose in Non-Aqueous Media. **1982**, No. July, 920–924.

(34) Bart, H. J.; Reidetschlager, J.; Schatka, K.; Lehmann, A. Kinetics of Esterification of Levulinic Acid with N-Butanol by Homogeneous Catalysis. *Ind. Eng. Chem. Res.* **1994**, *33* (1), 21–25. https://doi.org/10.1021/ie00025a004.

(35) Rönnback, R.; Salmi, T.; Vuori, A.; Haario, H.; Lehtonen, J.; Sundqvist, A.; Tirronen, E. Development of a Kinetic Model for the Esterification of Acetic Acid with Methanol in the Presence of a Homogeneous Acid Catalyst. *Chem. Eng. Sci.* **1997**, *52* (19), 3369–3381. https://doi.org/https://doi.org/10.1016/S0009-2509(97)00139-5.

(36) Yang, F.; Tang, J. Catalytic Upgrading of Renewable Levulinic Acid to Levulinate Esters Using Perchloric Acid Decorated Nanoporous Silica Gels. *ChemistrySelect* **2019**, *4* (4), 1403–1409. https://doi.org/10.1002/slct.201803608.

(37) Enumula, S. S.; Gurram, V. R. B.; Chada, R. R.; Burri, D. R.; Kamaraju, S. R. R. Clean Synthesis of Alkyl Levulinates from Levulinic Acid over One Pot Synthesized WO3-SBA-16 Catalyst. *J. Mol. Catal. A Chem.* **2017**, *426*, 30–38. https://doi.org/https://doi.org/10.1016/j.molcata.2016.10.032.

(38) Trombettoni, V.; Bianchi, L.; Zupanic, A.; Porciello, A.; Cuomo, M.; Piermatti, O.; Marrocchi, A.; Vaccaro, L. Efficient Catalytic Upgrading of Levulinic Acid into Alkyl Levulinates by Resin-Supported Acids and Flow Reactors. *Catalysts* **2017**, *7* (8). https://doi.org/10.3390/catal7080235.

(39) Maheria, K. C.; Kozinski, J.; Dalai, A. Esterification of Levulinic Acid to N-Butyl Levulinate Over Various Acidic Zeolites. *Catal. Letters* **2013**, *143* (11), 1220–1225. https://doi.org/10.1007/s10562-013-1041-3.

(40) Nandiwale, K. Y.; Bokade, V. V. Environmentally Benign Catalytic Process for Esterification of Renewable Levulinic Acid to Various Alkyl Levulinates Biodiesel. *Environ. Prog. Sustain. Energy* **2015**, *34* (3), 795–801. https://doi.org/10.1002/ep.12042.

(41) Cirujano, F. G.; Corma, A.; Llabrés i Xamena, F. X. Conversion of Levulinic Acid into Chemicals: Synthesis of Biomass Derived Levulinate Esters over Zr-Containing MOFs. *Chem. Eng. Sci.* **2015**, *124*, 52–60. https://doi.org/https://doi.org/10.1016/j.ces.2014.09.047.

(42) Berger, R. J.; Stitt, E. H.; Marin, G. B.; Kapteijn, F.; Moulijn, J. A. Eurokin. Chemical Reaction Kinetics in Practice. *CATTECH* **2001**, *5* (1), 36–60. https://doi.org/10.1023/A:1011928218694.

(43) Nandiwale, K. Y.; Sonar, S. K.; Niphadkar, P. S.; Joshi, P. N.; Deshpande, S. S.; Patil, V. S.; Bokade, V. V. Catalytic Upgrading of Renewable Levulinic Acid to Ethyl Levulinate Biodiesel Using Dodecatungstophosphoric Acid Supported on Desilicated H-ZSM-5 as Catalyst. *Appl. Catal. A Gen.* **2013**, *460–461*, 90–98. https://doi.org/https://doi.org/10.1016/j.apcata.2013.04.024.

CHAPTER III

Esterification of levulinic acid with ethanol promoted by ion-exchange resins as catalysts

Preamble

In this chapter the use of ion exchange resins as catalysts for the synthesis of ethyl levulinate is detailed. At the purpose to find new cheapest catalyst for an eventual industrial application, batch experiments with different resins are studied: four commercial sulfonic resins were tested (Amberlyst-15 dp=600µm, Amberlyst-15 dp=300µm, Amberlite IR-120 and Dowex 50Wx8). Amberlyst-15, a macroreticular structure type and Amberlite IR120 and Dowex 50W-8 as gel-type structure. Comparing the activities of them, the kinetics of the reaction, changing the operation conditions (i.e., stirring rate, temperature, catalyst loading and reactants ratio) was investigated and a reliable kinetic model for the description of the experimental data is proposed. As a consequence, it will be possible to optimize the production of the ethyl levulinate (EL).

3.1. Introduction

As discusses in chapter II, heterogeneous catalysts are now preferred to the homogeneous one. The heterogeneous approach leads to various advantages, not only to safeguard the equipment, otherwise corroded by mineral acids, but also to the process design and plant costs. In the last few years, researchers have investigated the use of resins as catalysts in the levulinic acid esterification reaction. [1–4]

To get a deeper insight into the origin of the performance in the catalytic process, it is necessary to know that the structure of the catalyst seems to be a major factor.

The ion exchange resin catalysts are commercially available in spherical resin beads and can be of two categories: macroreticular and gel type, based on its pore structure. This porous nature directly influences the rate of the catalyzed reaction. Besides differing in structure, gelular and macroreticular type differ also in their ability to swell when in contact with the reaction media that depend in turn on the affinity among their and the capacity to adsorb part of the liquid according to the crosslinking degree of the resin. Since different component take part in the esterification reaction (acid, alcohol, ester, and water), the catalyst will sorbs selectively each of them in different amount. So, in order the reaction proceed it is necessary that the reagents diffuse inside the catalyst and obviously swelling process makes the active adsorption sites more accessible. [5]

The rate by which the reagents diffuse into the pore, directly influence the overall rate of chemical reaction, for this reason it is important to study the swelling phenomena and the eventual pore diffusion limitations.

The macroreticular resins have permanent mesopores that is the results of partial agglomeration of small, dense, and highly cross-linked polymer particles. When the resin swells, additional "true" pores open up within a thin layer of polymer gel, just beneath the pore walls, and thus only a portion of the polymer structure is implicated to form the accessible gel-phase.

Gel-type resins in dry state does not have any type of porosity and only a few catalytic active sites are appreciable on the surface. But, in swollen state, an appropriate liquid can pass through the whole polymer structure, due to the lower crosslinking degree. A completely accessible gel-phase extends to the whole volume of the resin particle.[6,7]

The swelling process is shown in figure 3.1.

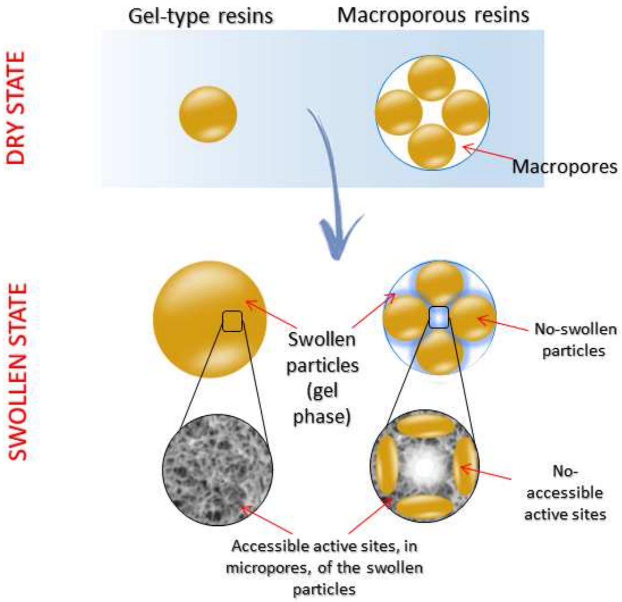

Figure 3.1. Morphological changes in dry state and in swelling state of a gel-type and macroreticular catalyst particle.

Consequently, gel-type resins have potentially in catalytic activity much higher than their macroreticular counterparts, due to the highest accessible acidic groups per unit of volume. Hence, the accessibility to the activated centres is always somewhat limited, depending on the swelling of the polymer matrix and the steric hindrance of the molecule that take part to the reaction.

To optimize the production of EL, the reaction kinetics catalyzed by sulfuric acid was study to evaluate the dependency of the kinetics on Brønsted concentration. Then, the performance of the two catalysts groups through in-dept kinetic study were investigated. The kinetic experiments were conducted varying different reaction conditions (i.e., temperature, LA: EtOH molar ratio, catalyst amount, stirring rate). Take-up and partition tests were performed on the resins in order to evaluate parameters such as the swelling ratio and the partition coefficients. A reliable model has been developed to describe the experimental data including kinetic and mass transfer phenomena, paying attention on both fluid–solid external and internal diffusion limitations. In this way, once determinate the realistic kinetic parameters, in perspective will allow to design more accurately dedicated pilot plants and among the catalysts studied, were chosen the best (in term of activity and commercial cost) to test in continuous operation and in reactive chromatography.

3.2. Experimental section

3.2.1. Materials

The following chemicals were used in the experiments without further purification: levulinic acid 98 wt% was purchased by Merck, ethanol 99 wt %, by Alfa Aesar. Following ion exchange resin was used as catalysts: Amberlite® IR-120 (H) was obtained by Room and Haas; Dowex 50WX-8, was obtained by Sigma Aldrich. Amberlyst-15 of two different size was used. Amberlyst-15 of 600 µm particle size (A15-1); Amberlyst-15 of 300 µm particle size (A15-2). A15-1 was purchased from Acros Organics, while A15-2 was obtained from Sigma Aldrich. The main characteristics of all the tested resins catalysts are reported in Table 3.1. For the analysis of the products, by titration were used: ethanol (96 wt%, by Carlo Erba) and phenolphthalein (by Merck) as indicator.

Table 3.1. Physical properties of the used ion exchange resin used as catalysts.

	Particle size [µm]	Active sites concentration [meq/g]	Crosslinking degree [%]	Surface area [m^2/g]	Density ρ_{Int} [g/cm^3]
A15-1	600	4.95	20	53	0.6
A15-2	300	4.53	20	45	0.6
Amberlite IR120	620-830	4.40	8	1.53	1.5
Dowex 50WX-8	150-300	4.83	8	0.23	0.8

3.2.2. Methods

Esterification of levulinic acid with ethanol in presence of different catalyst groups has been carried out in a batch reactor, showed in Figure 2 that consists of:

- Stainless steel reactor (Parr Instrument Company, Series 4560), with a capacity of 300 cm^3, equipped with an external heating jacket.
- Thermocouple connected to a controller system, which allows to regulate the temperature inside the reactor through the heating jacket.
- Magnetic stirrer on the top of the reactor allowed stirring the reaction mixture at the desired rate (100–600 rpm), it is connected to a controller system.
- Controller system, which can regulate the stirring velocity, temperature of the heating jacket and can also detect pressure level inside the reactor.
- Nitrogen tank.
- Manometer, to regulate N_2 pressure inside the reactor.
- Pin valve for sampling. A stainless-steel filter of 50 µm mesh it is installed on the sampling line to prevent catalyst loss during the sampling procedure.
- Pin valve for depressurization of the system.

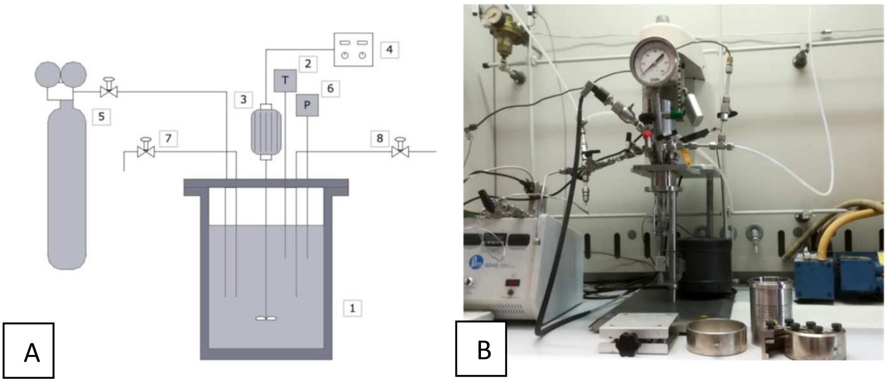

Figure 3.2. Scheme of the batch system setup (A) and laboratory batch system (B).

The classical experimental procedure consists in a pre-treatment of the catalyst in an oven at 333 K for 6-8 h, at the aim to remove water, since the resins are hygroscopic. This enables to avoiding the shift of the chemical equilibrium in the ethyl levulinate synthesis. Then the dried resin is weighted in the desired amount along with LA and ethanol and mixed inside the batch reactor for a total of 200 g. After the reactor is loaded, it is well sealed and exposed to nitrogen pressure. Nitrogen was used as an inert gas to maintain constant pressure (5 bar), preventing the evaporation of the lower boiling components (ethanol 351 K) at the operating temperatures. Once the operating temperature is reached, the first sample is taken through the sampling valve. Each sample is analyzed by acid-base titration using standardized 0.1 M NaOH as titrating agent and phenolphthalein as indicator, whereas the concentration of ethyl levulinate is determined by GC (HP 6890 Series) using a column ZB-Wax and an FI detector. To estimate the error on the experimental data, expressed as the standard deviation, each sample was analyzed three times.

3.2.3. Take-up and partition experiments

The experimental tests to evaluate the swelling degree were conducted following the steps of Bodamer and Kunin[8]. The experiments were conducted using a graduated cylinder of 10 mL, where an aliquot of 2 mL of dry resin was added and weighted. Each compound involved in the reaction was added separately. The solutions were mixed from time to time with a rod to improve contact between the chemical species and the resin and let increasing for about one hour. The absence of change in catalyst wet volume with time indicates the attainment of equilibrium. Finally, the catalyst, separated from the solution was weighed to obtain the total amount of the liquid incorporated by swelling and then it was possible to calculate the take-up factor.

To determine the real concentration of each reactant/product in the catalyst pores, a set of partition tests were conducted. Partition coefficients were measured by preparing solutions of reactants/products at different molar ratio, simulating samples characterized by different levulinic acid conversions. The tests were conducted at room temperature in a single-necked glass flask, in which about 2.5 g of dry catalyst was placed in contact with 20 mL of liquid solution for 30 min. Samples were withdrawn to check when the system reached the equilibrium conditions, analyzed via GC-FID method. The details of the method are reported here: column Zebron ZB-WAX, stationary phase: 100% polyethylene glycol, L = 60m, ID = 0.32 mm, film thickness = 0.25 µm, detector: FID, carrier He, injector temperature: 250 °C, detector temperature 250 °C, column pressure 14psi, temperature ramp: 150 °C for 0 min, heating at 20 °C/min up to 250 °C, temperature isotherm for 25 min. Measured retention times: levulinic acid 11.3 min, ethanol 5.6 min, ethyl levulinate 6.9 min. The water content in the samples was determined by Karl-Fischer titration using Hydranal KetoSolver Hydranal Composite 5 K as a titration reagent.

3.3. Results and discussion

3.3.1 Blank tests

Experiments are performed firstly in the absence of catalysts to evaluate the effect of non-catalytic reaction (Table 3.2). The results are reported in Fig. 3.3 in terms of levulinic acid conversion vs reaction time.

Table 3.2. Summary of experiments performed without catalyst.

Test	ν [rpm]	$c_{LA0}\cdot10^3$ [mol/m^3]	$c_{EtOH0}\cdot10^3$ [mol/m^3]	n_{EtOH}/n_{LA} [mol/mol]	T [K]	Time [h]
1	400	2.54	12.7	5/1	303.15	7
2	400	2.54	12.7	5/1	323.15	7
3	400	2.54	12.7	5/1	343.15	7
4	400	2.54	12.7	5/1	363.15	7
5	400	6.24	6.24	1/1	343.15	7

A maximum conversion of about 7% at 7h was observed at 363K with alcohol/LA molar ratio 5:1, since levulinic acid itself is able to act as a catalyst.

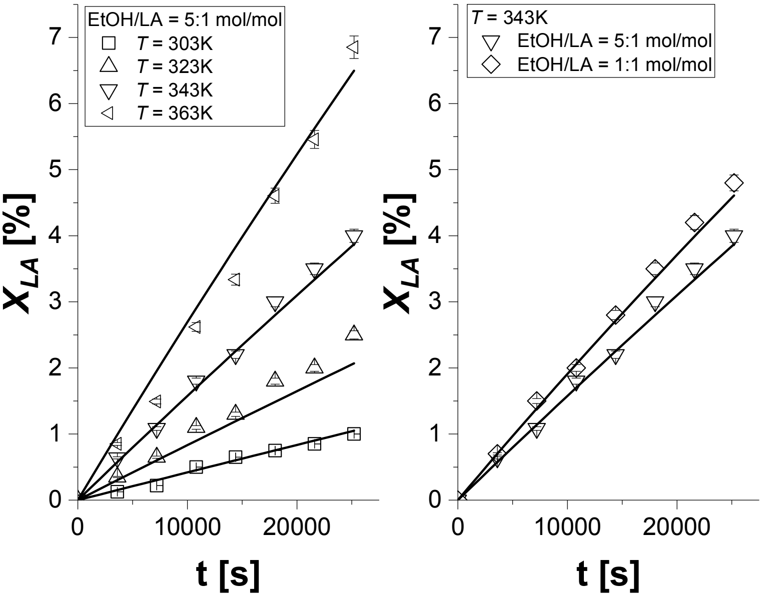

Figure 3.3. Blank test experiments at different temperature on the left and at different molar ration on the right. symbols are the experimental data; lines are the model predictions.

The activation energy of the non-catalyzed reaction was subsequently evaluated through the linearized Arrhenius equation:

$$k = A\,exp\left(-\frac{E_A}{RT}\right) \quad ; \quad \ln(k) = \ln(A) - \frac{E_A}{R}\cdot\frac{1}{T} \qquad (1)$$

From the slope of the linearized Arrhenius equation, obtained by linear fit, it was possible to determine a first experimental evaluation of the activation energy of the non-catalyzed reaction.

$E_{a\,BLANK}$ = 29.3 kJ/ mol

3.3.2 Kinetic study with H_2SO_4 as catalyst

Further experiments were carried out with sulfuric acid as catalyst (Table 3.3) investigating some operation conditions (i.e., temperature, catalyst load and reactant ratio). Despite the homogeneous catalyst are not now preferred, for the reasons explained in the Chapter 2, paragraph 2. The goal of these experiments was also to obtain the enthalpy and activation energy values useful as initial values in the parameters estimation (see below, paragraph 3.3.4.1).

Table 3.3. Summary of experiments performed without catalyst and with H_2SO_4 as homogeneous catalyst.

Test	v [rpm]	c_{LA0}·10^3 [mol/m^3]	c_{EtOH0}·10^3 [mol/m^3]	n_{EtOH}/n_{LA} [mol/mol]	*T* [K]	H_2SO_4 load [mol/m^3]	Time [h]
1	400	2.53	12.7	5/1	303.15	80	23
2	400	2.53	12.7	5/1	323.15	80	8
3	400	2.53	12.7	5/1	343.15	80	7
4	400	2.53	12.7	5/1	363.15	80	5
5	400	2.54	12.7	5/1	323.15	40	23
6	400	2.52	12.6	5/1	323.15	160	6
7	400	3.60	10.80	3/1	323.15	80	23
8	400	5.91	6.02	1/1	323.15	20	6
9	400	6.15	6.20	1/1	333.15	20	6
10	400	5.91	5.56	1/1	343.15	20	6

As we expected, increasing the temperature, an increase of the reaction rate was observed, and shorter reaction times were enough to reach the chemical equilibrium. The opposite occurs at lower temperature, where more than 24h were necessary. Furthermore, a maximum equilibrium conversion of 90% with an ethanol/levulinic acid (EtOH/LA) molar ratio of 5:1 at 363.15K was observed in the presence of sulfuric acid with a reaction rate higher than the blank tests. The results are reported in Figures 3.4 in terms of levulinic acid conversion vs reaction time.

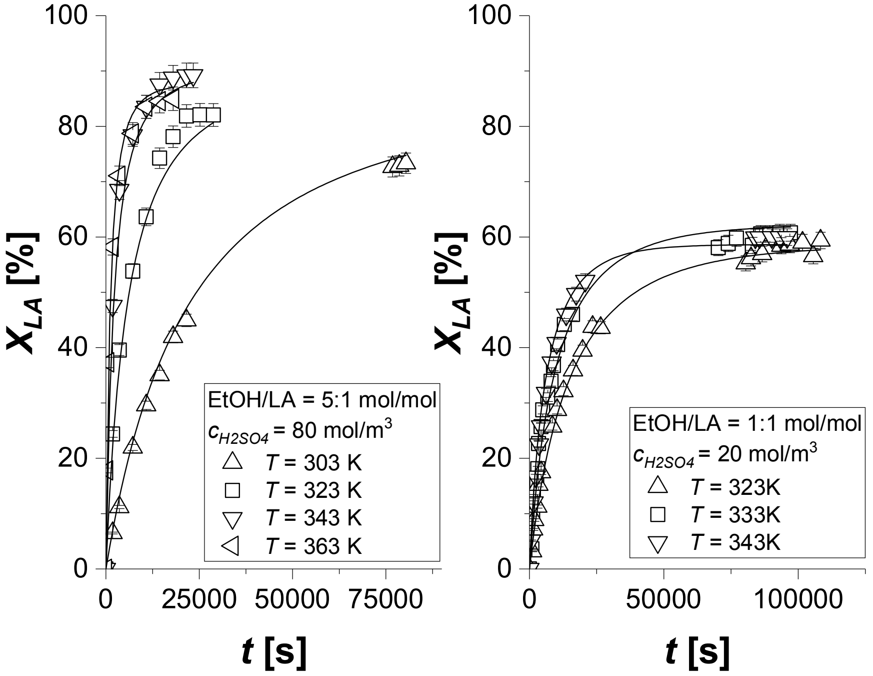

Figure 3.4. Effect of temperature (left) and molar ratio (right) on the levulinic acid esterification catalyzed by sulphuric acid. Symbols are the experimental data; lines are the model predictions.

On this set of data, a first experimental evaluation of the activation energy and the enthalpy of the reaction catalyzed with sulfuric acid respectively was performed obtaining the following values:

$Ea_{H_2SO_4}$ = 20.5 kJ/ mol

$\Delta H_{H_2SO_4}$ = 26.2 kJ/ mol

The enthalpy of the esterification reaction catalyzed by sulfuric acid was evaluated through the linearized van't Hoff equation.

$$\left(\frac{\partial(lnK_{eq})}{\partial T}\right)_P = -\frac{\Delta_r H^0}{T^2}\ ;\ \ln(K_{eq}) = -\frac{\Delta_r H^0}{R}\cdot\frac{1}{T}+\frac{\Delta S^0}{R} \quad (2)$$

While ln(K_{eq}) was obtained according to the following equation:

$$\ln(K_{eq}) = \ln\left(\frac{c_{ELeq}\cdot c_{H2Oeq}}{c_{LAeq}\cdot c_{EtOHeq}}\right) \quad (3)$$

Figure 3.5 (left) showed that increasing the catalyst concentration, the reaction rate increases as well and as a consequence shorter time is necessary to reach the equilibrium composition. These results demonstrated the potential of the homogeneous mineral acid, as Brønsted acid catalyst.

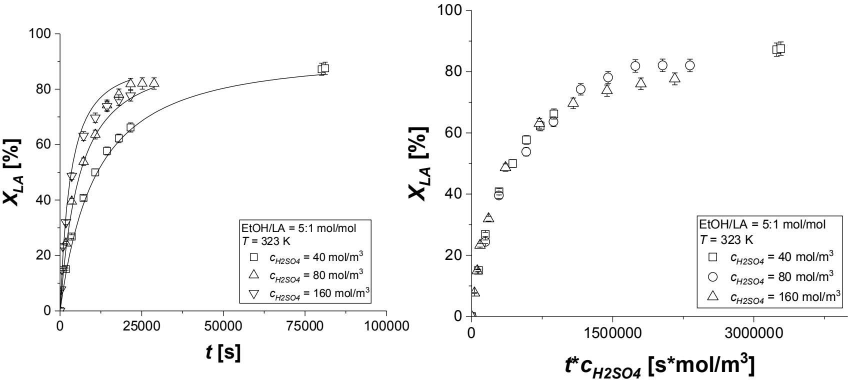

Figure 3.5. Effect of catalyst concentration on the levulinic acid esterification, on the left. Levulinic acid conversion plotted versus normalized experimental time by the catalyst bulk density, on the right. Symbols are the experimental data; lines are the model predictions.

A maximum equilibrium conversion of 83% with 1%mol (160 mol/m^3) of catalyst and an EtOH/LA molar ratio of 5:1 at 323.15K.

An interesting result is observable in Figures 3.5 (right), in which multiplying the reaction time per the sulfuric acid concentration, the experimental data overlap. As demonstrated in the literature[9], this plot is very useful as gives direct information: (i) the reaction order with respect to the catalyst load is equal to one; (ii) the absence of the external mass transfer resistance is confirmed.

The result which can be extracted from these data is that the reaction kinetics is of the first order respect to the sulfuric acid concentration and a single dissociation of sulfuric acid takes place.[10] Generally the dissociation of an acid depends on the medium, the dissociation of sulfuric acid in water is very high; since in this case the medium is ethanol and levulinic acid, different ethanol-to-levulinic acid molar ratios experiments were carried out showing that by increasing the ethanol content, higher ethyl levulinate concentrations are obtained.

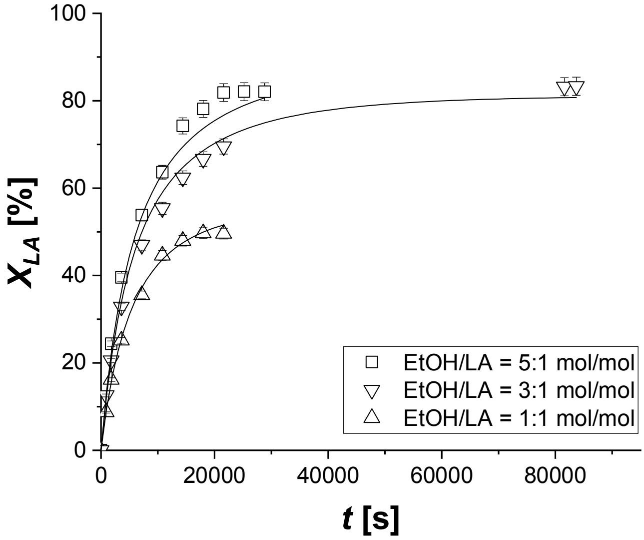

Figure 3.6. Effect of the molar ratio on the levulinic acid esterification catalyzed by H_2SO_4. Symbols are the experimental data; lines are the model predictions

A maximum equilibrium conversion of 85% with an EtOH/LA molar ratio of 5:1 at 323.15K. The results are reported in Figure 3.6 in terms of levulinic acid conversion vs reaction time.

3.3.3. Kinetic study with ion exchange resins as catalyst

The four resins were tested in EtOH molar excess (EtOH:LA= 5) at 333K and fixing the catalyst amount at 1.5 wt%. All tested commercial sulfonic resins were able to catalyse such reaction, the Figure 3.7 shows the effect of the different morphological structure of all the resins tested in this study. The catalytic activities of the resins decrease in the order: Amberlite IR120>Dowex 50Wx8> A15-2≈A15-1.

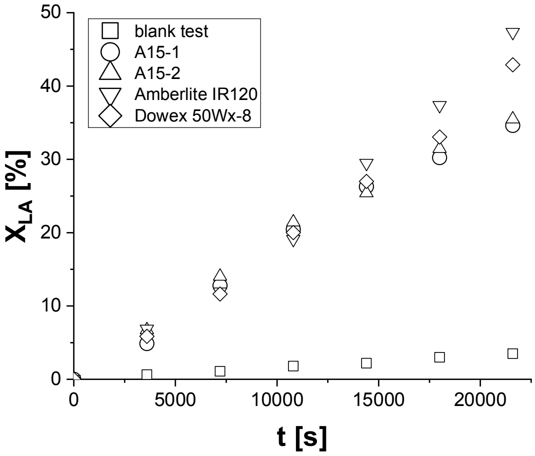

Figure 3.7. Levulinic acid conversion for blank test and the experiments catalyzed by A15-1, A15-2, Amberlite IR120 and Dowex 50Wx8. The temperature was fixed at 333K, the levulinic acid/alcohol molar ratio is equal to 5 mol/mol.

The behavior among the two classes of structure, macroreticular and gel-type, is similar and some differences are appreciable after 6 hours of reaction. Gel-type resins have been found to be more active than macroreticular ones. This is somewhat intuitive if it looks at the structure. As mentioned before, the macroreticular resins have higher crosslinking degree and as a consequence they have more rigid structure, probably this increases the resistance against the diffusion lowering their efficiency and activity. [6, 11] The best performance of the gel-type resins investigated in this thesis can be ascribed to their higher swelling degree. To confirm this hypothesis, take-up and partition experiments were conducted. These experiments were useful both to relate the behavior of the resin activity with the structure and to predict the kinetic behavior.

3.3.3.1. Take- up experiments

In the following section as a procedure example the take-up factor experiments of the two catalyst's type, i.e., Amberlyst-15 and Dowex 50Wx8 (see Table 3.2) were reported and determined at varying of the molar fractions of the components (1, 0.8, 0.5, 0.2, 0) preparing binary solution (LA/EtOH, LA/EL, LA/H2O, EtOH/EL, EtOH/H2O, EL/H2O). After obtaining the initial weight of the dry resin, note the intrinsic density (Table 3.2), the initial dry volume was obtained. After the addition of the solution and the subsequent swelling of the resin, it was possible to obtain the weight of the adsorbed solution and therefore the adsorbed volume given the density of the used binary mixture.

$$\varepsilon = \frac{V_{dryAmb}}{V_{dryAmb} + V_{ads}} \tag{4}$$

where the take-up (ε) factor is defined by the ratio between the volume of the dry resin (V_{dryAmb}) divided divided by total volume of the resin after the swelling, thus the sum of the volumes of the dry catalyst (V_{dryAmb}) and the liquid retained by the resin itself (Vads).

Table 3.4. Summary of Amberlyst-15 (A15-1 and A15-2) Take-up experiments.

x_{EtOH} [-]	$\varepsilon_{EtOH/LA}$ [-]	$\varepsilon_{EtOH/EL}$ [-]	$\varepsilon_{EtOH/H2O}$ [-]	x_{H2O} [-]	$\varepsilon_{H2O/EL}$ [-]	$\varepsilon_{H2O/LA}$ [-]	x_{LA} [-]	$\varepsilon_{LA/EL}$ [-]
0	0.50	0.49	0.54	0	0.49	0.50	0	0.49
0.2	0.51	0.50	0.54	0.2	0.51	0.44	0.2	0.49
0.4	0.50	0.51	0.54	0.4	0.52	0.43	0.4	0.49
0.6	0.53	0.53	0.55	0.6	0.53	0.45	0.6	0.51
0.8	0.52	0.53	0.54	0.8	0.54	0.43	0.8	0.50
1	0.53	0.53	0.53	1	0.54	0.54	1	0.50
Average	0.51	0.52	0.54	Average	0.52	0.47	Average	0.50

*The take- up factor are the same for A15-1 and A15-2 being the same the chemical structure type

As can be seen, the resin retained more H_2O and LA compared to EtOH and LE. Amberlyst-15 demonstrates a very high affinity with water in the presence of any other component. The results of the take-up experiments on Amberlyst-15 shown an average swelling for all the investigated binary solutions of 0.5.

Table 3.5. Summary of Dowex 50Wx-8 Take-up experiments.

x_{EtOH} [-]	$\varepsilon_{EtOH/LA}$ [-]	$\varepsilon_{EtOH/EL}$ [-]	$\varepsilon_{EtOH/H2O}$ [-]	x_{H2O} [-]	$\varepsilon_{H2O/EL}$ [-]	$\varepsilon_{H2O/LA}$ [-]	x_{LA} [-]	$\varepsilon_{LA/EL}$ [-]
0	0.52	0.46	0.57	0	0.46	0.52	0	0.46
0.2	0.46	0.48	0.58	0.2	0.45	0.49	0.2	0.45
0.5	0.49	0.44	0.53	0.5	0.51	0.51	0.5	0.36
0.8	0.53	0.52	0.55	0.8	0.57	0.56	0.8	0.45
1	0.58	0.58	0.58	1	0.57	0.57	1	0.52
Average	0.52	0.50	0.56	Average	0.51	0.53	Average	0.45

In this case, the resin retained more H_2O and EtOH compared to LA and LE. The results of the take-up experiments of Dowex 50Wx-8 shown an average for all the investigated binary solutions of 0.52.

At least, the take up factor of each mixture components that is retained by Amberlite IR120 shown the following results: 0.67 for ethanol, 0.23 for levulinic acid, 0.65 for water and 0.66 EtOH/LA 5:1

3.3.3.2. Partition experiments

The partition tests were useful to determinate the real concentration of each reactant/product in the catalyst pores. The partition coefficients were calculated in according to the following equation:

$$m_i = \frac{c_f}{c_i - c_f} \tag{5}$$

where c_i is the concentration of the component before the partition test and c_f is the concentration of the same component after the treatment. Different solutions were prepared by simulating different levulinic acid conversions. The average values of the partition coefficients were determined and listed in Table 3.6.

Table 3.6. Average value of the partition coefficients.

	m_{LA} [-]	m_{EtOH} [-]	m_{EtLA} [-]
Amberlyst-15	1.04	1.38	1.60
Amberlite IR120	1.00	1.00	1.00
Dowex 50Wx-8	1.06	1.17	0.97

3.3.4. Kinetic study with Amberlyst-15 as catalyst (I)

Several experiments were conducted with Amberlyst-15 as the catalyst, investigating a wide range of operation conditions (i.e., stirring rate, temperature, catalyst load, reactant ratio, listed in the **Publication I**) and the catalyst stability as well. It was decided to present only some examples of the obtained results, to make clearer the paragraph. By the evaluation of the stirring rate effect it was possible to conclude that, as expected, as the stirring rate increases, the thickness of the stagnant film of the catalyst particle decreases, on the other hand, if the stirring rate is sufficiently high, the external diffusion of the reagents to the catalyst particle is no longer limiting. The results are reported in Fig. 3.8 in terms of the initial reaction rate vs the stirring rate. It was observed that the reaction rate increases with increasing stirring rate and for both the ion exchange resins, external diffusion limitation is not observed at stirring rates exceeding 600 rpm.

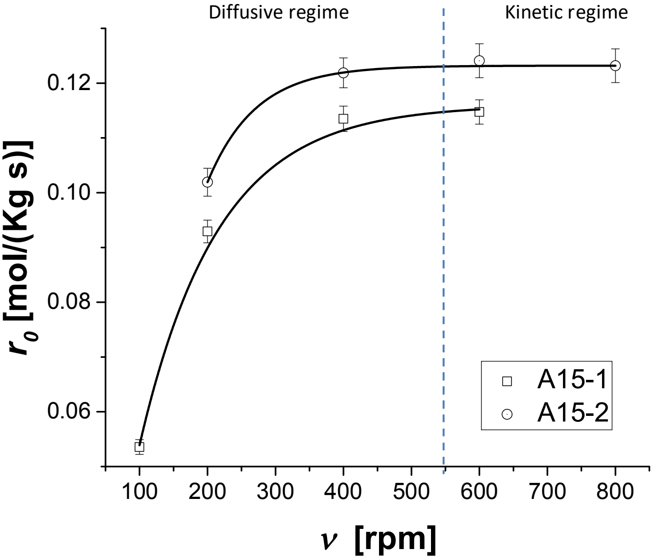

Figure 3.8. Effect of stirring rate on the levulinic acid esterification initial rate, catalyzed by A15-1 and A15-2, by fixing the ethanol-to-levulinic acid molar ratio of 5:1 at T = 343.15 K and at ρB = 22 kg/m3. Symbols are the experimental data, lines the calculated data.

This fact clearly indicates that the thickness of the stagnant liquid film surrounding the particles becomes negligible and the concentration of both reactants and products on the solid surface is equal to the one in the liquid bulk. Moreover, by using the two catalysts, different plateaus are observed (i.e., lower for higher particle radius), suggesting the occurrence of intraparticle mass transfer limitations for at least the catalyst characterized by the highest value of the radius (A15-1). The presence of different plateau values is a clear indication of intraparticle concentration profiles, as for bigger particle the diffusive path that the molecules should run across is longer compared to the one available for smaller particles.

The experiments conducted varying the temperature have showed a similar equilibrium conversion, with identical operation conditions, for both resins. A maximum equilibrium conversion of 91% was obtained when working at 600 rpm, T = 363.15 K with ρB = 22.02 kg/m^3 and an EtOH:LA molar ratio of 5:1.

Furthermore it was necessary to prolong the experiment overnight to determine the equilibrium constant at each temperature since the chemical equilibrium was reached at long reaction times (usually more than 24 h). As we expected by increasing the temperature, the reaction rate increases as well (Fig. 3.9).

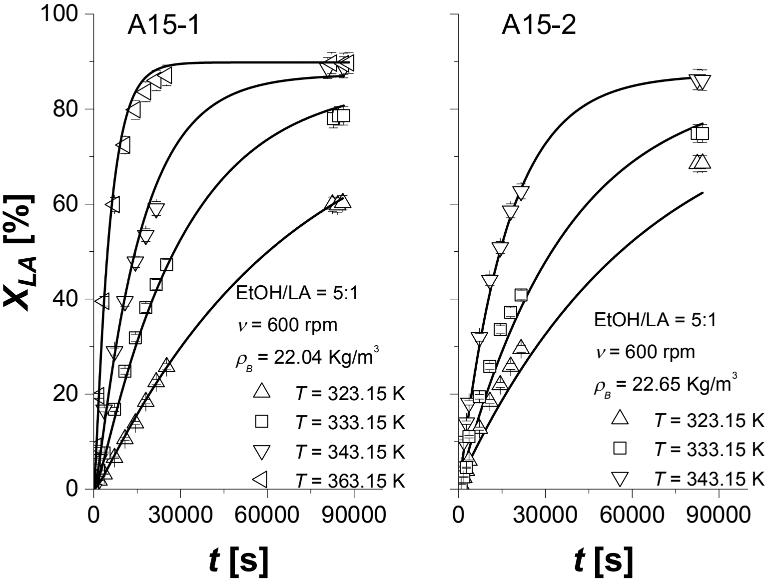

Figure 3.9. Effect of temperature on the levulinic acid esterification catalyzed by A15-1 (left) and A15-2 (right) by fixing the ethanol-to-levulinic acid molar ratio of 5:1, ρB = 22 kg/m3 and v = 600 rpm. Symbols are the experimental data, lines the model calculated profiles.

The activation energy of the heterogeneous catalyzed reaction was evaluated through the linearized Arrhenius equation (1), while the enthalpy through the linearized van't Hoff equation (2).

$Ea_{A15\text{-}1}$=45.2 kJ/mol $Ea_{A15\text{-}2}$=49.4 kJ/mol
$\Delta H_{A15\text{-}1}$=35.6 kJ/mol $\Delta H_{A15\text{-}2}$=62.2 kJ/mol

The experimental values of enthalpy and activation energy were used as initial values in the parametric estimation carried out on the whole experimental data set, in order to determinate an optimal value (section 3.3.4.1). Further results on the effect of the catalyst load and the ethanol-to-levulinic acid molar ratio on the levulinic acid esterification can be found in the **Publications I.**

The experiments shown that increasing the catalyst bulk density in the reactor, the reaction rate increased and by increasing the ethanol content, higher ethyl levulinate concentrations were obtained.

3.3.4.1. Mathematical model

The classic esterification reaction mechanism consists of two steps, protonation of the carboxylic group (RCOOH) and nucleophilic attack of alcohol (R-OH), namely Fisher esterification, is obviously also applicable in case of Amberlyst-15 for the esterification of levulinic acid. Applying the hypothesis of quasi-equilibrium to the first rapid reaction phase and considering the reversibility of the reaction, the reaction rates for the self-catalyzed reaction (R_1) in the liquid phase and for the reaction catalyzed by the Amberlyst-15 (R_2) were defined. The reaction rate expressions are given by the Eqs. (6) and (7) respectively.

$$R_1 = k_1 \cdot c_{LA_L}\left(c_{LA_L} c_{EtOH_L} - \frac{1}{K} \cdot c_{H_2O_L} c_{EL_L}\right) \tag{6}$$

$$R_2 = k_2 \left(c_{LA_S} c_{EtOH_S} - \frac{1}{K} \cdot c_{H_2O_S} c_{EL_S}\right) \tag{7}$$

A first order behavior with respect to the concentration of levulinic acid for the auto-catalytic reaction was hypothesized and verified, at this aim blank experiments (in absence of catalyst) were conducted (paragraph 3.3.2) and interpreted to retrieve kinetic parameters and rate law to describe the contribution of autocatalysis, showing that in every case a levulinic acid conversion lower than 10% was obtained in the adopted range of reaction conditions.

Even if the effect of autocatalysis is not remarkable high, it is necessary to take it in consideration to obtain more precise kinetic parameters for the reaction catalyzed by Amberlyst-15. Moreover, it will be of high importance when extrapolating the results at higher temperatures.

Two mass balance equations, liquid side and solid side were used:

$$\varepsilon_P \cdot \frac{\partial c_{i_S}}{\partial t} = \frac{D_{e_i}}{(x \cdot R_P)^2} \cdot \frac{\partial}{\partial x}\left(x^2 \frac{\partial c_{i_S}}{\partial x}\right) + \rho_P \cdot r_{2i} \tag{8}$$

$$\frac{1}{V_L} \cdot \frac{dn_{i_L}}{dt} = r_{1i} - J_{i_S} \cdot \varepsilon_1 \tag{9}$$

The fluid–solid mass transfer rate is given by Eq. (9), indicating a linear dependence between the mass transfer rate and the concentration gradients in the stagnant liquid film surrounding the catalyst particle. The transport rate of the component inside the resins (J_{i_S}) was evaluated in the liquid phase mass balance and concentrations are adjusted by the partition coefficients (mi):

$$J_{i_S} = k_S \cdot a_{Sp} \left(c_{i_L} - m_i c_{i_S} \big|_{x=1} \right) \tag{10}$$

The software gPROMS ModelBuilder v. 4.0 was used to conduct all the simulations and parameter estimation activities in the present study. The results of the parameter estimation are shown in Table 3.7, in which are shown that all the parameters errors and the correlations between them were reasonably low as it ca be see in Figures 3.8-3.9.

Table 3.7. Summary of the estimated parameters and correlations matrix.

	Value	95% C.I.	Units	Ea_C	k_{cref}
Ea_C	83.5	3.7	kJ/mol	1	
k_{ref}	$9.0 \cdot 10^{-11}$	$0.2 \cdot 10^{-11}$	$(m^3/mol) \cdot (m^3/kg) \cdot s^{-1}$	-0.16	1

The activation energy obtained from the parametric estimation was higher than those evaluated through the linearized Arrhenius equation (1) (45.2 kJ/mol for A15-1 and 49.4 kJ/mol for A15-2), this is due to the mass transport phenomena of the system. For both resins, the evaluation of the reaction efficiency was obtained in according to the Eq. 11,

$$\eta = \frac{\int_0^1 (r_2(x) \cdot R_P \cdot x)\, dx}{r_2|_{x=1} \cdot \int_0^1 (R_P \cdot x)\, dx} \tag{11}$$

where *x* represents the radial coordinate. The results are displayed in Figure 3.10, confirming that the efficiency of A15-2 is higher than the ones of A15-1 due to the lower diffusion path of the fluid elements in the resin.

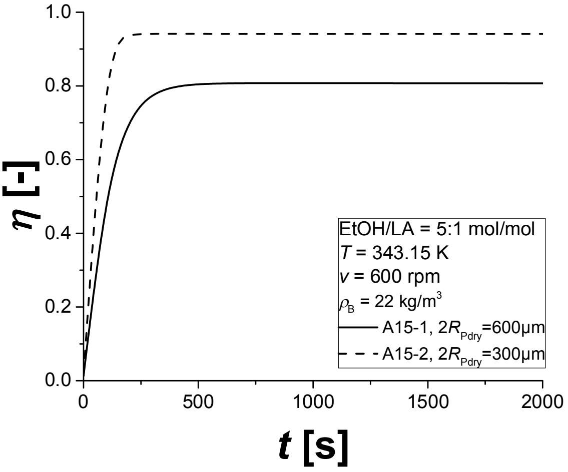

Figure 3.10. Reaction efficiency plot for A15-1 and A15-2.

The agreement between the experimental data and the model with all the simulated curves can be found with further detail in the corresponding paper (**Publication I**).

3.3.5 Kinetic study with Amberlite IR120 as catalyst (II)

Amberlite IR120 was also tested to evaluate the kinetics of the LA esterification with ethanol. The experiments were the same as Amberlyst-15 and all the adopted conditions tests and the compositions of the time zero sample are shown detail in **Publication II**.

Influence of external mass transfer resistance during kinetic tests was evaluated varying the velocity of the rotating impeller in the reactor vessel from 200 to 800 rpm; the catalyst mass and the molar ratio of levulinic acid to ethanol ratio was also evaluated. The obtained results for the observed reaction rate plot versus the stirring rate (Fig. 3.11) showed that at stirring speeds greater than 400 rpm the reaction rate profile becomes flat, allowing to conclude that from 400 rpm on the absence of external mass transfer limitation is evident.

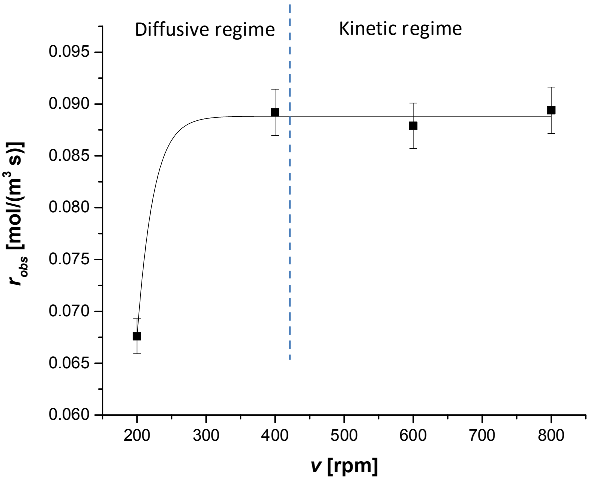

Figure 3.11. Effect of stirring rates on the reaction rate by fixing the EtOH to LA molar ratio of 5:1, at ρB=19.7 kg/m3 of catalyst and at temperature of 343K. The symbols are the experimental data collected at the four stirring rates; continuous lines represent the simulations.

Experiments were conducted varying the amount of the catalyst. The results reported in Figure 3.12A clearly indicate that by increasing the catalyst load, reaction rate increases as well. The equilibrium plateau is independent on the catalyst load as expected. The collected data were plotted as a function of normalized abscissa (i.e. catalyst density multiplied by reaction time), observing a good overlap of the experimental data (Fig. 3.12B).

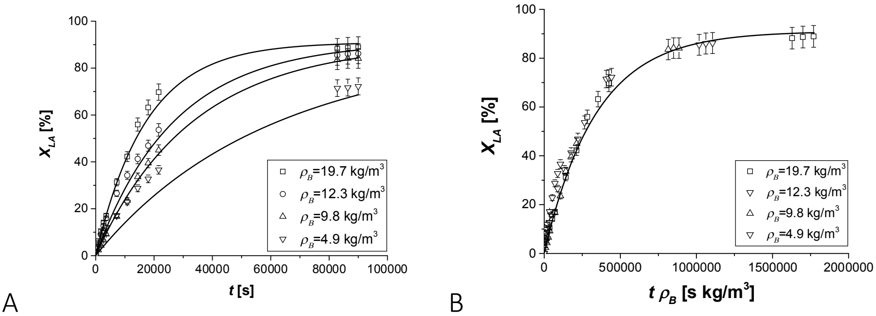

Figure 3.12. The effect of Amberlite IR120 bulk density on the levulinic acid esterification, fixing EtOH to LA 5:1 molar ratio at 800 rpm and at temperature of 343K. Raw data on levulinic acid conversion versus time (right); symbols are the experimental data; lines are the model predictions.

The effect of the molar ratio of levulinic acid to ethanol and temperature were and the results showed in **Publication II** indicated that by increasing the molar ratio, the highest yield in ethyl levulinate was obtained and an increase in temperature value lead to a higher reaction rate.

A first experimental activation energy and reaction enthalpy values was evaluated through the linearized Arrhenius equation (1) and the linearized van't Hoff equation (2) respectively. The results obtained are the follows:

E_a = 38.61 kJ/mol ΔH= 54.18 kJ/mol

The latter values will be used as initial values in the mathematical model developed with gPROMS Model builder (see below, section 3.3.5.1).

3.3.5.1. Mathematical model

A fluid-solid intraparticle model was used for the interpretation of experimental data collected with Amberlite IR120 H as catalyst in the batch reactor. All the equations used for the development of the mathematical model are readily available in **Publication II**. Even in this case, the model was developed considering the diffusion in the whole solid particle to verify the intra-particle mass transfer limitation, see equations reported before 8-10.

A parameter estimation was conducted simultaneously on all the collected experimental data. The results of the parameters estimation are shown in the Table 3.8, together with statistic information, and the simulated data are compared with the experimental data in Figures 3.11 and 3.12 and in more details in all the Figures reported in the **Publication II**.

Table 3.8. Results of parameter. CI: confidence interval. T_{ref}*=333 K.*

	Value	95% C.I.	Units	Ea_C	ks_0	k_{ref}
Ea_C	$68.83 \cdot 10^{3}$	$56.22 \cdot 10^{2}$	J/mol	1		
ks_0	$1.91 \cdot 10^{-7}$	$8.33 \cdot 10^{-8}$	m/s	-0.7	1	
$K_{c,ref}$	$2.86 \cdot 10^{-10}$	$2.73 \cdot 10^{-11}$	$(m^3/mol)\cdot(m^3/kg)\cdot s^{-1}$	0.6	-0.6	1

The parameters are consistent, and the standard error of the parameters were typically less than 4%, showing only a slight correlation.

High limitation in the intra-particle diffusion is confirmed by the Weisz-Prater criterion (W—P), Eq. 12:

$$C_{W-P} = \frac{-r_{obs}{R_p}^2}{D_e C_{LA(t=0)}} \qquad (12)$$

The result obtained from the W-P criterion is about 10^3, and this confirm the presence of intra-particle diffusion limitation. This result is opposite to the expected one, because the gel-type catalyst should involve a low intra-particle diffusion limitation, probably the high limitation of the diffusion inside the particle is due to the dimension of the molecules of the studied system.

The effectiveness factor of the system was calculated adopting the definition reported in Eq. 11. The results reported in Figure 3.13 confirm a rather high intraparticle diffusion limitation, leading to a plateau value of 0.7, lower than that obtained with A15-1 and A15-2.

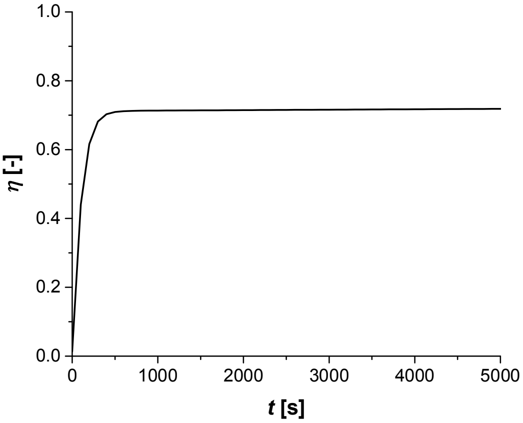

Figure 3.13. Reaction efficiency plot for Amberlite IR 120.

3.3.6 Kinetic study with Dowex 50Wx8 as catalyst

Batch experiments were performed changing the impeller rate, temperature, catalyst load and reactants' molar ratio to evaluate the Dowex 50WX-8 resin performance under various conditions.

Table 3.9. Experimental conditions adopted for the experiments conducted in batch reactor.

Test	v [rpm]	T [K]	ρ_{cat} [kg/m^3]	c_{EtOH} [mol/m^3]	c_{LA} [mol/m^3]	EtOH/LA ratio [mol/mol]
1	200	343	19.84	$14.3 \cdot 10^3$	$2.8 \cdot 10^3$	5:1
2	400	343	19.84	$14.3 \cdot 10^3$	$2.8 \cdot 10^3$	5:1
3	600	343	19.84	$14.3 \cdot 10^3$	$2.8 \cdot 10^3$	5:1
4	600	323	19.84	$14.3 \cdot 10^3$	$2.8 \cdot 10^3$	5:1
5	600	353	19.84	$14.2 \cdot 10^3$	$2.8 \cdot 10^3$	5:1
6	600	333	19.84	$14.3 \cdot 10^3$	$2.8 \cdot 10^3$	5:1
7	600	343	9.92	$14.3 \cdot 10^3$	$2.8 \cdot 10^3$	5:1
8	600	343	4.96	$14.3 \cdot 10^3$	$2.8 \cdot 10^3$	5:1
9	600	343	19.84	$1.0 \cdot 10^3$	$4.0 \cdot 10^3$	2.5:1
10	600	343	19.84	$5.3 \cdot 10^3$	$5.3 \cdot 10^3$	1:1

The first experiments were carried out to evaluate the effect of the stirring on the reaction rate (experiments 1-3, Table 3.9). The external film diffusion limitation is negligible due to the film thickness being reduced by the agitation, at high stirring rate (400-600 rpm). At 200 rpm the agitation is too slow and diffusion in the stagnant film layer limits the reaction rate. This obtained results are evident in figure 3.14 in which the observed reaction rate plot versus the stirring rate is reported.

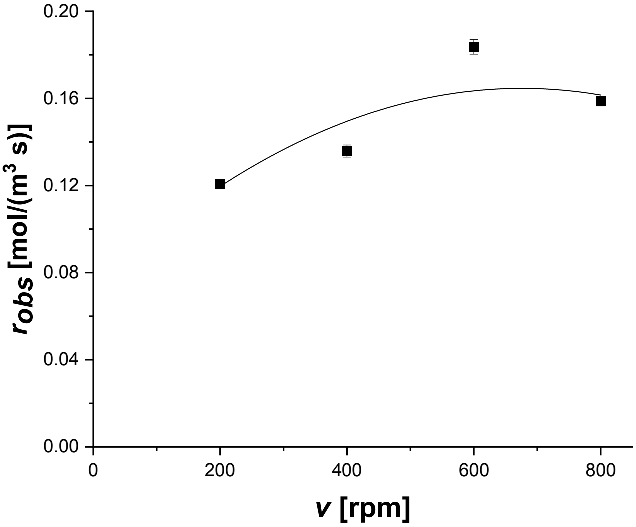

Figure 3.14. Effect of the stirring rates on the reaction rate by fixing the EtOH to LA molar ratio of 5:1, at 19.84 kg/cm3 of catalyst and at temperature of 343 K. The symbols are the experimental data collected at the three stirring rates; continuous line represents the simulation.

The LA conversion reached after 24 *h* of reaction is independent of impeller rate, resulting in 89*%* for all three tests. This was to be expected, as agitation does not affect the thermodynamics of the reaction. The results are reported in Figure 3.15.

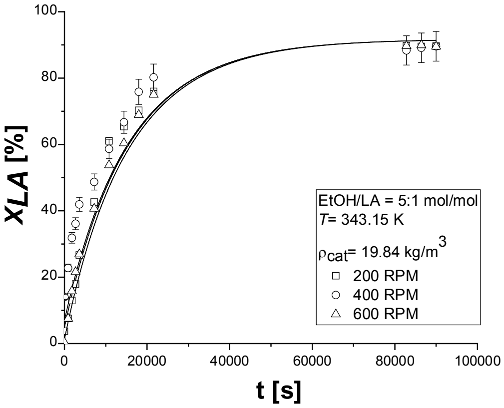

Figure 3.15. LA conversion vs. time for different impeller rates by fixing the EtOH:LA molar ratio of 5:1, the catalyst amount at bulk density of 19.84 kg/m3 and the temperature of 343 K.

Experiments were conducted to investigate the effect of the temperature (tests 3 to 6, Table 3.9). As expected, the higher the reaction temperature, the higher the observed reaction rate, as showed in figure 3.16 and in accordance with the Arrhenius law

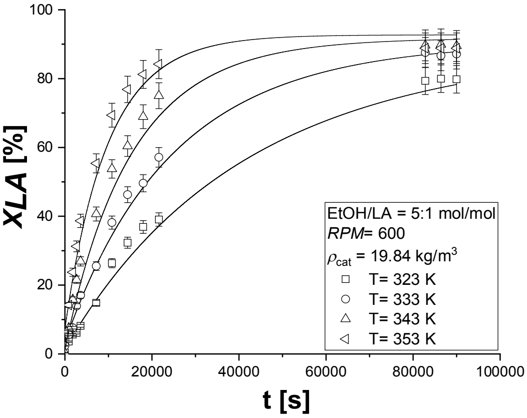

Figure 3.16. The effect of temperature on the levulinic acid esterification, fixing EtOH to LA 5:1 molar ratio at 600 rpm and with bulk density of 19.84 kg/m3 of catalyst. Symbols are the experimental data; lines are the model predictions.

From the linearization of the Arrhenius (1) and Van't Hoff equations (2) it was possible to extrapolate a first approximative values of the activation energy and the reaction enthalpy. The results obtained are:

E_a = 54.7 ± 6.0 kJ/mol

ΔH = 48.4 ± 9.5 kJ/mol

Better estimation of these parameters will be performed through the mathematical model developed.

Other set of experiments was conducted varying the catalyst amount and fixing the temperature, the EtOH:LA molar ratio and the rpm as shown in Table 3.9 (tests 3, 7 and 8). The results reported in figure 3.17 indicate that the quantity of Dowex 50 WX-8 in the reactive system affect both the reaction rate and the LA equilibrium conversion, as the percentage of resin determines the concentration of sulphonic groups that catalyze the esterification reaction. The highest LA conversion (89*%*) and reaction rate were obtained with the highest catalyst load (2*% wt.*) of the tests. Using 1 and 0.5 *% wt.* of catalyst load gave us 81.5 and 68 *%* LA conversion respectively. It is obvious that higher catalyst loads allow for the reaction to have more available active sites for reaction catalysis. Another interesting result can be deducted plotting the LA conversion rate as a function of normalized abscissa, i.e., the product between time of reaction and catalyst bulk density. The data collected in the first hours of reaction shown a good overlap (Fig. 3.17 right). This can be interpreted as the reaction kinetics being of the first order respect to the catalyst load.

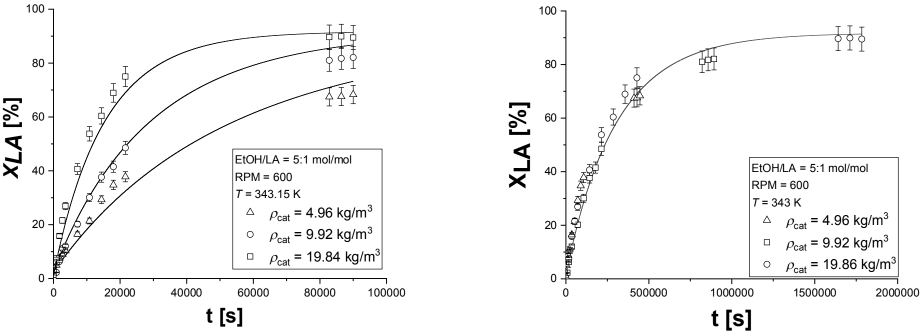

Figure 3.17. The effect of Dowex 50Wx8 amount on the levulinic acid esterification, fixing EtOH to LA 5:1 molar ratio at 600 rpm and at a temperature of 343 K, on the left. LA conversion vs. reaction time per catalyst bulk density, on the right. Symbols are the experimental data, lines are the model predictions.

Finally, the effect of the molar ratio of levulinic acid to ethanol was at least studied at 343 K (Fig. 3.18), see Table 3.9 tests 3, 9 and 10. The results showed that the highest molar ratio (5:1) resulted in the best LA conversion (89%) and rate reactions.

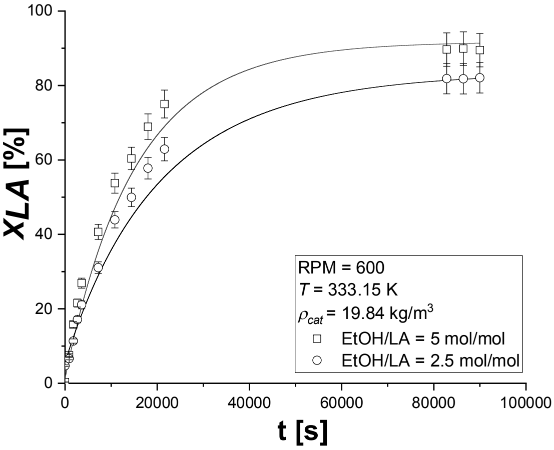

Figure 3.18. The effect of the ethanol to levulinic acid molar ratio on the levulinic acid esterification, fixing the temperature at 343 K, the stirring rate at 600 rpm and the catalyst density equals to 19.84 kg/m3. Symbols are the experimental data; lines are the model predictions.

3.3.6.1. Mathematical model

All the chemical and physical implication of the fluid-solid system were takin into account in a developed model that described the kinetics of the esterification of levulinic acid with Dowex 50Wx8 in the batch system. The model was developed follow the equation reported in **Publication II** with some differences reported below. The association factors for example depend on the nature of the component and in this case the values of Φi have been recovered from literature[12] and are reported in Table 3.10.

Table 3.10. Association factors of the four chemical components of our system.

Component	*Φ[-]*
LA	1
EtOH	1.5
EL	1
W	2.6

Molar volumes at normal boiling point have been determined through the Tin and Calus correlation[12] (Eq. 13):

$$V_i = 0.285\, V_{c,i}^{1.048} \tag{13}$$

Where $V_{c,i}$, the critical volume of component i, has been recovered from literature for EtOH and water while the Marrero and Pardillo group interaction contribution method has been used for LA and EL[12]. Table 3.11 reports the values for $V_{c,i}$ and Vi .

Table 3.11. Critical volumes and molar volumes at normal boiling points.

	Vc,i [cm^3/mol]	Vi [cm^3/mol]
LA	346.9	130.91
EtOH	168	61.23
EL	461.3	176.48
W	56	19.36

The viscosity of the mixture has been evaluated with the aid of the Grunberg-Nissan method (Eq. 14) and has been considered independent of temperature in the temperature range of our experiments:

$$\ln(\eta_M) = \sum_i x_i \ln(\eta_i) + \frac{1}{2}\sum_{i=1}^{n}\sum_{j=1}^{n} x_i x_j G_{ij} \tag{14}$$

Where ηi is the viscosity of the pure component i and Gij is an interaction parameter which is a function of composition and temperature. Table 3.12 shows the parameters used for the estimation of the viscosity of the mix.

Table 3.12. Correlation parameters and viscosity of pure components at 343.15 K.

Parameter	Unit Measure	Value
$G_{EtOH/LA}$	-	-1.0577
$G_{EtOH/EL}$	-	-1.1749
$G_{LA/EL}$	-	-0.1172
η_{LA}	cP	1.228
η_{EtOH}	cP	0.524
η_{EL}	cP	0.853
ηW	cP	0.4035

The two-mass balance for the bulk and solid phase can be find in the previous section, equation 8-10.

A parameter estimation was conducted simultaneously on all the collected experimental data. The results of the parameters estimation are shown in the Table 3.13, together with statistic information.

Table 3.13 Parameter estimation results.

	Estimated Value	95 % CI	Correlation Matrix		Units
			$E_{a,c}$	$k_{c,ref}$	
$E_{a,c}$	51387	2545	1		J/mol
$k_{c,ref}$	1.68×10^{-10}	4.69×10^{-12}	-0.34	1	$(m^3/mol)\cdot(m^3/kg)/s$

The agreements between experimental and calculated data are very good, as revealed in Figs. 3.16–3.18 and in the parity-plot reported in Fig. 3.19, showing that most of the data fall in a window of error of ±20%.

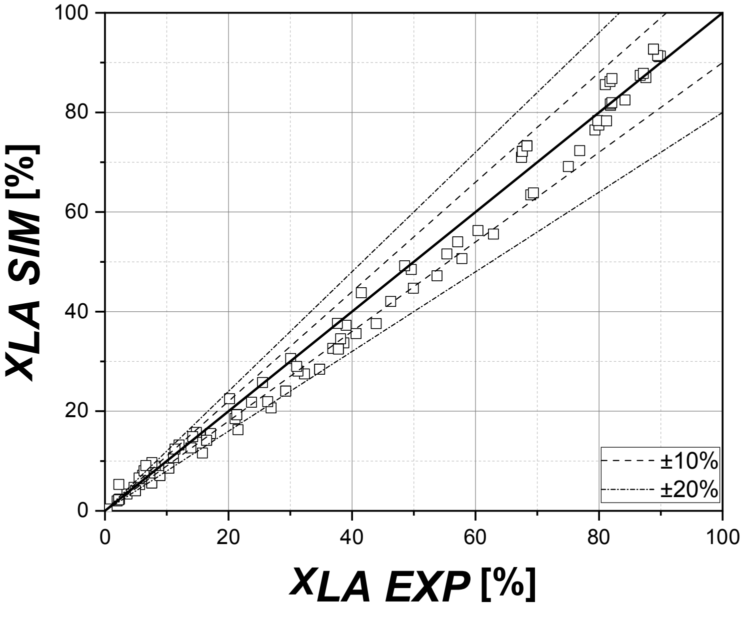

Figure 3.19. Parity plot comprising all the available experimental data collected in the batch reactor.

3.4. Conclusions

In conclusion, the screening study revealed that all the catalysts tested are able to catalyze such reaction from levulinic acid to ethyl levulinate. Comparing the results of the batch experiments, they produced rather similar LA conversion values. Despite that, looking the results of the parameter estimation summarized in table 3.14, activation energy and mass-transfer coefficient values are the highest for Amberlite IR120 and Dowex 50Wx8, resulting to be the most suitable catalysts for LA esterification under mild reaction conditions.

Table 3.14 Parameter estimation results.

Catalyst	$E_{a,c}$ **[J/mol]**	$k_{c,ref}$ **[(m³/mol)·(m³/kg)/s]**
Amberlyst-15	83500	$0.9 \cdot 10^{-10}$
Amberlite IR120	$68.83 \cdot 10^{3}$	$2.86 \cdot 10^{-10}$
Dowex 50Wx8	51387	$1.68 \cdot 10^{-10}$

Amberlite IR120 was selected to conduct a continuous esterification in a fixed bed reactor (Chapter IV); while Dowex 50Wx8 was used in reactive chromatography (Chapter V).

In perspective, this screening and kinetic studies will allow to design accurately dedicated pilot plants of the levulinic acid esterification process, normally run in industry in batch using mineral acids as catalyst.

References

(1) Fernandes, D. R.; Rocha, A. S.; Mai, E. F.; Mota, C. J. A.; Teixeira da Silva, V. Levulinic Acid Esterification with Ethanol to Ethyl Levulinate Production over Solid Acid Catalysts. Appl. Catal. A Gen. 2012, 425–426, 199–204. https://doi.org/https://doi.org/10.1016/j.apcata.2012.03.020.

(2) Tejero, M. A.; Ramírez, E.; Fité, C.; Tejero, J.; Cunill, F. Esterification of Levulinic Acid with Butanol over Ion Exchange Resins. Appl. Catal. A Gen. 2016, 517, 56–66. https://doi.org/https://doi.org/10.1016/j.apcata.2016.02.032.

(3) Ali, S. H.; Tarakmah, A.; Merchant, S. Q.; Al-Sahhaf, T. Synthesis of Esters: Development of the Rate Expression for the Dowex 50 Wx8-400 Catalyzed Esterification of Propionic Acid with 1-Propanol. Chem. Eng. Sci. 2007, 62 (12), 3197–3217. https://doi.org/10.1016/j.ces.2007.03.017.

(4) Trombettoni, V.; Bianchi, L.; Zupanic, A.; Porciello, A.; Cuomo, M.; Piermatti, O.; Marrocchi, A.; Vaccaro, L. Efficient Catalytic Upgrading of Levulinic Acid into Alkyl Levulinates by Resin-Supported Acids and Flow Reactors. Catalysts 2017, 7 (8). https://doi.org/10.3390/catal7080235.

(5) Lilja, J.; Aumo, J.; Salmi, T.; Murzin, D. Y.; Mäki-Arvela, P.; Sundell, M.; Ekman, K.; Peltonen, R.; Vainio, H. Kinetics of Esterification of Propanoic Acid with Methanol over a Fibrous Polymer-Supported Sulphonic Acid Catalyst. Appl. Catal. A Gen. 2002, 228 (1), 253–267. https://doi.org/https://doi.org/10.1016/S0926-860X(01)00981-4.

(6) Lavarda, G.; Morales-Delarosa, S.; Centomo, P.; Campos-Martin, J. M.; Zecca, M.; Fierro, J. L. G. Gel-Type and Macroporous Cross-Linked Copolymers Functionalized with Acid Groups for the Hydrolysis of Wheat Straw Pretreated with an Ionic Liquid. Catalysts 2019, 9 (8). https://doi.org/10.3390/catal9080675.

(7) Jeřábek, K.; Hanková, L.; Holub, L. Working-State Morphologies of Ion Exchange Catalysts and Their Influence on Reaction Kinetics. J. Mol. Catal. A Chem. 2010, 333 (1–2), 109–113. https://doi.org/10.1016/j.molcata.2010.10.004.

(8) Bodamer, G. W.; Kunin, R. Behavior of Ion Exchange Resins in Solvents Other Than Water - Swelling and Exchange Characteristics. Ind. Eng. Chem. 1953, 45 (11), 2577–2580. https://doi.org/10.1021/ie50527a057.

(9) Russo, V.; Hrobar, V.; Mäki-Arvela, P.; Eränen, K.; Sandelin, F.; Di Serio, M.; Salmi, T. Kinetics and Modelling of Levulinic Acid Esterification in Batch and Continuous Reactors. Top. Catal. 2018, 61 (18), 1856–1865. https://doi.org/10.1007/s11244-018-0998-y.

(10) Levenspiel, O. Chemical Reaction Engineering. Ind. Eng. Chem. Res. 1999, 38 (11), 4140–4143. https://doi.org/10.1021/ie990488g.

(11) Leveneur, S.; Murzin, D. Y.; Salmi, T.; Mikkola, J. P.; Kumar, N.; Eränen, K.; Estel, L. Synthesis of Peroxypropionic Acid from Propionic Acid and Hydrogen Peroxide over Heterogeneous Catalysts. Chem. Eng. J. 2009, 147 (2–3), 323–329. https://doi.org/10.1016/j.cej.2008.11.045.

(12) Prausnitz, J.; Poling, B.; O'Connell, J. The Properties of Gases and Liquids 5th Edition (2000)

CHAPTER IV

Ethyl levulinate synthesis in a fixed bed reactor promoted by Amberlite IR120 (II)

Preamble

In this chapter the use of Amberlite IR120 as catalysts for the synthesis of ethyl levulinate in a fixed bed continuous reactor is reported.

The kinetics of the reaction was validated, based on the previous batch experiments (Chapter III), and the levulinic acid conversion was optimized. A fluid-dynamic characterization was conducted to understand the behavior of the flow reactor.

4.1. Introduction

The optimization of the ethyl levulinate production could be possible through the transfer from batch reactors (current technology) to continuous ones. To proceed to a scale-up of the reaction, the comprehension of the reaction mechanism (kinetic and diffusive) is needed.

Object of this chapter is to validate the mathematical model described in Chapter III, paragraph 3.3.5.1, on the LA esterification with ethanol and the use of Amberlite IR120 as catalyst, which has been shown to be the best among the catalysts studied. As continuous reactor a fixed bed reactor packed with the same catalyst (Amberlite IR120) was used. The detail of this work can be found in the **Publication II.**

4.2. Experimental section

4.2.1. Materials

The following chemicals were used in the experiments without further purification: levulinic acid (98 wt%, by Merck), ethanol (99 wt%, by Alfa Aesar), Amberlite® IR-120 (H) ion exchange resin (by Room and Haas) was used as a solid acid catalyst. For the analysis of the products, by titration were used: ethanol (96 wt%, by Carlo Erba) and phenolphthalein (by Merck) as indicator.

4.2.2. Methods

To ensure a constant and precise volumetric flow, an HPLC pump was used to feed the reaction mixture to the packed bed reactor. The reactor was made of a steel tube (L = 0.3 m, ID = 0.0078 m). After pre-treatment, the catalyst was readily packed in the reactor. The amount of catalyst needed to fill the reactor was calculated also considering the swelling phenomena, i.e., the degree of swelling of the catalyst particle, resulting that 7 g of dry catalyst was enough to fill the reactor. A heating jacket was placed outside the reactor to ensure constant temperature guaranteeing isothermal operation; the temperature was measured by a thermocouple and regulated with a PID controller. To keep the reaction mixture in the liquid phase, the system was connected to a nitrogen cylinder regulated by a manometer to guarantee 5 bar of absolute pressure. Samples were collected periodically to measure the steady-state conditions, through a dedicated pin valve. As done for the kinetic study in batch, each sample was analyzed three times to estimate the error on the experimental data, also in this case expressed as standard deviation, using the same analytical methods. The kinetic experiments were conducted at flow rate $1.7^{-8}.3\cdot10^{-8}$ m^3/s, for each temperature (323, 343 and 363K) with a given reactant's molar ratio of roughly ethanol/levulinic acid ratio of 6:1. The summary of the operating conditions is reported in Table 4.1, while flow sheet of the continuous system is shown in Fig. 4.1.

Table 4.1. Summary of the operation conditions adopted for the kinetic experiments conducted in the packed bed reactor.

Test	**T [K]**	$\dot{V}\,[m^3/s]$	$c_{EtOH,feed}\,[mol/m^3]$	$c_{LA,feed}\,[mol/m^3]$
1	323	$(1.7\text{-}8.3)\cdot10^{-8}$	$13.0\cdot10^3$	$2.2\cdot10^3$
2	343	$(1.7\text{-}8.3)\cdot10^{-8}$	$13.3\cdot10^3$	$2.5\cdot10^3$
3	363	$(1.7\text{-}8.3)\cdot10^{-8}$	$13.0\cdot10^3$	$2.2\cdot10^3$

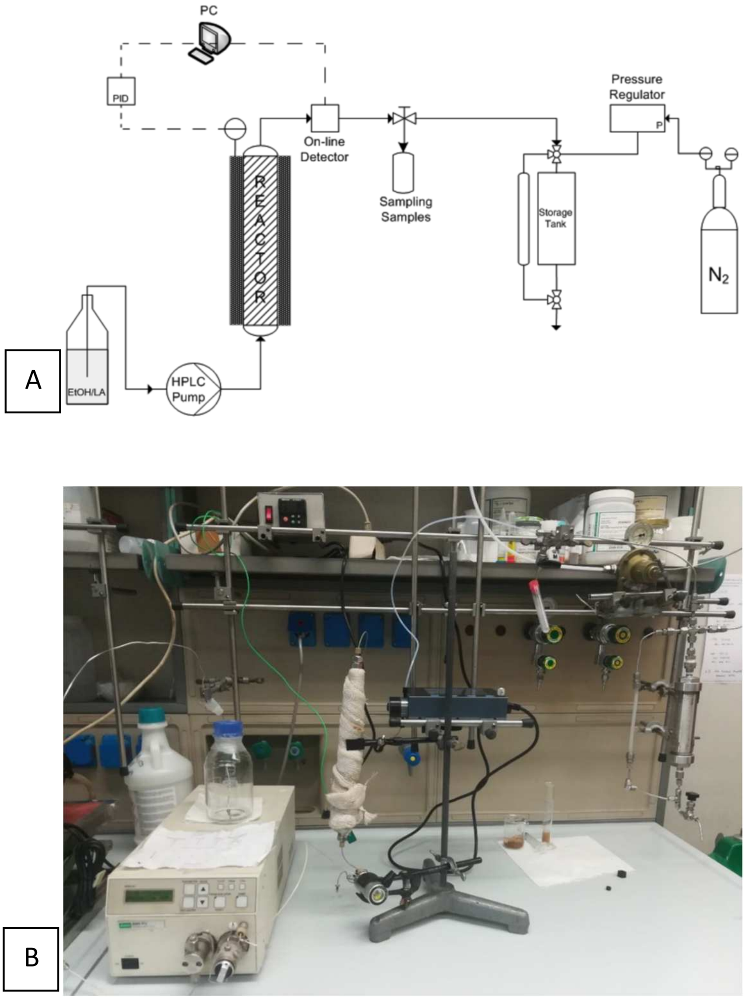

Figure 4.1. Continuous system flow sheet (A) and laboratory continuous system (B) adopted to conduct the kinetic experiments and the fluid-dynamic characterization.

Be aware that for the kinetic experiments, the on-line detector was not used. The test 1, experiment performed at T = 323 K and $\dot{V} = 1.7 \cdot 10^{-8}$ m^3/s, was prolonged for 50 h reaction time to check the catalyst stability.

4.2.2.1. Fluid-dynamic characterization

The fluid-dynamic study about real continuous system is one of the most important steps to understanding its behavior; in a real reactor there are mixing phenomena both in axial and radial direction that contribute to the dispersion of residence time into the reactor. In this case study the reactor is a tubular packed bed reactor, and its ideal pattern is a plug-flow, the fundamental hypothesis on which it is based is:

- Perfect radial mixing, whole fluid elements in the same axial coordinate have equal intensive properties along the radius;
- Perfect axial segregation, there are different intensive properties for each axial coordinate.

It is easy to note that these hypotheses are far from the real behavior and the equipment always deviates from the ideal pattern. The turbulent flow contributes to the deviation from laminar flow due to the existence of turbulent diffusivity, responsible both axial and radius mixing. It is important to underline that radius mixing approaching the turbulent flow to the plug flow, because contributing to flatten the concentration in axial direction, on the other hands it is responsible, in axial direction, from the ideal deviation. So, the mixing phenomena due to turbulent diffusivity acting both in axial and in radial direction, in the radius coordinate contributing to approaching the turbulent behavior to plug flow, but, at the same time, are totally responsible of the axial dispersion that contributing to the deviation from the ideal pattern (plug flow). On this basis the flow model used for the fluid-dynamic characterization is the axial dispersion model in which we take in account the contributing of turbulent diffusivity along axial dispersion. At first, is important introduce the residence time distribution (E) an equation utilized to know the age distribution of fluid elements. It is evident that elements of fluid taking different routes through the reactor needs different time to pass inside it. The distribution time for the fluid elements that leaving the reactor is called residence time distribution (RTD), and for the study case the equation is for an open vessel, derived by Levenspiel and Smith (1975).[2]

$$E(t) = \frac{u}{\sqrt{4\pi D_z t}} exp\left[-\frac{(L-ut)^2}{4D_z t}\right] \qquad (1)$$

Where u is the linear velocity [m/s], calculated as the ratio between the volumetric flow (Q) [m^3/s] and the product among surface area (A) [m^2] and bed void degree (εB) [/] as show in the following equation (Eq. 2). Dz is the axial dispersion coefficient [m^2/s], and its magnitude is indicative of the deviation from the ideal flow (plug flow). L is the reactor length [m].

$$u = \frac{Q}{A\varepsilon_B} \qquad (2)$$

The evaluation of E is possible with a tracer. Different methods are available, but in this case, we used the pulse experiment, more reliable and accurate with respect to step-pulse. The experiment consists to introduce an amount of tracer into the fluid entering the reactor and record the time of the tracer leaving the reactor. The tracer is injected in a short time, along the reactor start spreading caused by many things as velocity profile, turbulent mixing, molecular diffusion, etc., its shape curve is symmetrical and gaussian at any instant. At the reactor exit the detector detect the tracer and collect the data. Find the value of E is necessary to evaluate the magnitude of the axial dispersion coefficient (Dz) or the dimensionless group characterizing the spread in the whole vessel (Dz/(uL)), called vessel dispersion number (1/Pe), that measures the extent of axial dispersion.

The experiments were conducted in the same equipment used for the measurement of kinetic data in continuous, with the unique difference that an HPLC injector was installed between the HPLC pump and the packed bed reactor. Stimulus-response pulse experiments were conducted to evaluate the RTD (residence time distribution) with yellow naphthol as tracer, and the UV absorbance was recorded using an on-line detector (Reach Device RD4), using a HPLC injector to pulse the yellow naphthol solution to the reactor. Yellow naphthol was chosen for two main reasons: (i) a dye where sulfonic groups are present, thus exerting repulsive forces avoiding adsorption phenomena on the resin; (ii) it is a molecule big enough to exclude intraparticle diffusion. Thus, it is possible to directly obtain the bed void fraction using this tracer in pulse experiments. Each experiment was repeated three times to estimate the error on the axial dispersion coefficient (Dz). The operating conditions in the continuous reactor are listed in Table 4.2.

Table 4.2. Summary of the experimental conditions adopted for the fluid-dynamic characterization experiments.

Test	**T [K]**	$\dot{V}\,[m^3/s]$	***P* [Pa]**	**Δ*P* [Pa]**
1	298	$1.7\cdot10^{-8}$	$2\cdot10^{5}$	14
2	298	$2.5\cdot10^{-8}$	$2\cdot10^{5}$	20
3	298	$3.3\cdot10^{-8}$	$2\cdot10^{5}$	25
4	298	$5.0\cdot10^{-8}$	$2\cdot10^{5}$	33
5	298	$6.7\cdot10^{-8}$	$2\cdot10^{5}$	52
6	298	$10\cdot10^{-8}$	$2\cdot10^{5}$	76
7	298	$13\cdot10^{-8}$	$2\cdot10^{5}$	101
8	298	$17\cdot10^{-8}$	$2\cdot10^{5}$	122
9	343	$5.0\cdot10^{-8}$	$2\cdot10^{5}$	37
10	343	$8.3\cdot10^{-8}$	$2\cdot10^{5}$	68
11	343	$12\cdot10^{-8}$	$2\cdot10^{5}$	91

The collected data were subsequently processed with OriginPro®, each gaussian curve for each volumetric flow is separated on its injection time and overlapped with the others to evaluate the experimental reproducibility of the test (fig. 4.2).

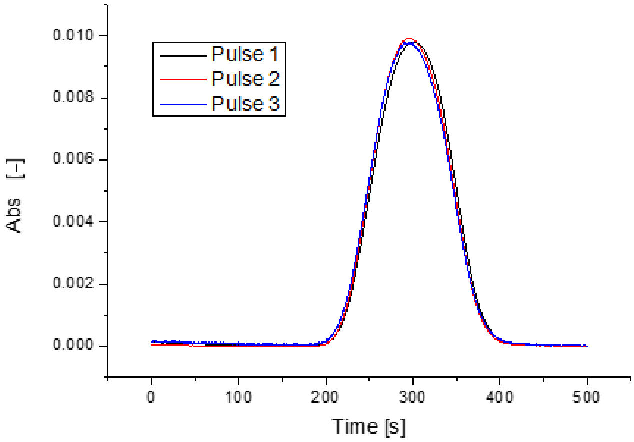

Figure 4.2. Pulse experiment reproducibility

If the test is reproducible, each gaussian curve is normalized, that is the area under the curve is unity, and the RTD is:

$$\int_0^{\infty} E(t)\,dt = 1 \tag{3}$$

In this way both the experimental residence time distribution and the average residential time (τ) were evaluated. Finally, the experimental RTD was compared with the calculated RTD, proposed by Levenspiel and Smith (eq. 1), and the value of the axial dispersion coefficient and the bed void degree are estimated. The following two images show the normalized experimental RTD and the comparing of this last one with the calculated RTD (figure 4.3).

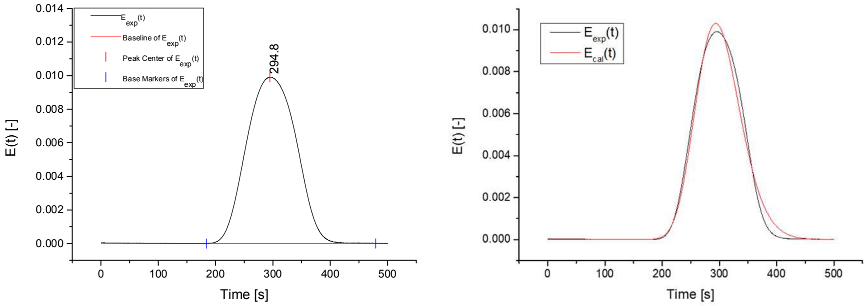

Figure 4.3. Normalized experimental RTD (left); Comparison among experimental and calculate RTD (right).

As is possible to see the calculated RTD describes accurately the experimental RTD allowing us to obtain the parameters.

The results from the RTD experiments were used to determine the axial dispersion coefficient (Dz) and thus, obtain the Peclet number. The axial dispersion model is often used to describe the fluid-dynamics in tubular reactors, describing the turbulence in the longitudinal direction with an axial dispersion term. The axial dispersion coefficient accounts for both molecular diffusion and convection mechanisms in the axial direction. Dz gives an idea of the performance of the reactor, e.i., when Dz = 0, it means that the reactor is a plug flow and when Dz→+∞, the reactor behaves as a continuous stirred tank reactor.

The main assumptions of the adopted reactor model are reported below:

- Uniform velocity and concentration profiles along the radius of the pipe
- No radial dispersion is considered

The collected data were interpreted using the mass balance equation reported in Eq. (4), that is a typical axial dispersion model for a nonreactive system.

$$\frac{dc_t}{dt} = -u\frac{\partial c_t}{\partial z} + D_z\frac{\partial^2 c_t}{\partial z^2} \qquad (4)$$

where, u is the velocity (m/s), Dz is the axial dispersion coefficient (m^2/s).

Two boundary conditions were defined to solve numerically the PDE system:

$$c_t|_{z=0} = c_{t,feed}(0 \le t \le t_{injection});\ c_t|_{z=0} = 0\ (t > t_{injection}) \qquad (5)$$

$$\left.\frac{\partial c_t}{\partial z}\right|_{z=L} = 0 \qquad (6)$$

Closed-closed vessel Boundary Condition (BC) were chosen as the Peclet numbers were expected to be high for the studied system; the mentioned BCs consider that no axial dispersion occurs both at the inlet and outlet of the reactor. The first BC is referred to the inlet of the reactor, considering the feed concentration, that for a pulse-experiment shows a classical pulse function, where the tracer concentration at the inlet of the reactor is equal to zero when the experimental time is greater than the injection time, while it is equal to a finite value for experimental time comprised between zero and the injection time.

The injection time is given by the volume of the HPLC injector loop (20 µL) divided by the flowrate of the experiment.

4.2.2.2. Mathematical model

The kinetic models for the esterification of levulinic acid developed for continuous reactors was written using gPROMS ModelBuilder v.4.0 software. The numerical method of lines, using a finite difference approach, was used to solve the partial differential equations systems, i.e., the mass balance equations of the continuous models. A first order backwards finite difference method was applied for the packed bed axial coordinate in the continuous model, adopting 200 discretization points.

4.3. Results and discussions

4.3.1. Fluid-dynamic characterization

The results of the experiments conducted in pulse modality using as a tracer yellow naphthol are reported in Table 4.3.

Table 4.3. Results of the fluid-dynamic characterization experiments in continuous packed bed reactor.

Test	$\dot{V}$ [m^3/s]	*T* [K]	*τ* [s]	D_Z [m^2/s]	ε_B [-]	*Pe* [-]	Re_p [-]
1	$1.7\cdot10^{-8}$	298	295	$(2.6\pm0.2)\cdot10^{-6}$	0.34±0.02	110	2.5
2	$2.5\cdot10^{-8}$	298	201	$(3.9\pm0.2)\cdot10^{-6}$	0.35±0.02	105	1.6
3	$3.3\cdot10^{-8}$	298	153	$(5.6\pm0.2)\cdot10^{-6}$	0.35±0.01	114	1.2
4	$5.0\cdot10^{-8}$	298	101	$(8.1\pm0.3)\cdot10^{-6}$	0.35±0.03	116	0.8
5	$6.7\cdot10^{-8}$	298	77	$(1.2\pm0.1)\cdot10^{-5}$	0.35±0.02	115	4.8
6	$10\cdot10^{-8}$	298	52	$(1.5\pm0.1)\cdot10^{-5}$	0.36±0.02	101	3.3
7	$13\cdot10^{-8}$	298	40	$(1.7\pm0.2)\cdot10^{-5}$	0.37±0.03	120	6.3
8	$17\cdot10^{-8}$	298	35	$(2.2\pm0.2)\cdot10^{-5}$	0.37±0.03	107	7.2
9	$5.0\cdot10^{-8}$	343	103	$(1.2\pm0.1)\cdot10^{-5}$	0.35±0.02	87	2.5
10	$8.3\cdot10^{-8}$	343	61	$(1.7\pm0.2)\cdot10^{-5}$	0.34±0.02	88	4.1
11	$12\cdot10^{-8}$	343	50	$(2.1\pm0.1)\cdot10^{-5}$	0.35±0.02	96	5.7

As revealed, the axial dispersion coefficient (D_z) increases with the volumetric flow rate, due to the increase in turbulent mixing which can't be neglected. Another parameter obtained was the reactor void degree (ε_B) is change between 0.34 and 0.37 with an average value of 0.36±0.02. The Péclet number, defined as in Eq. 7.

$$Pe = \frac{uL}{D_z} \tag{7}$$

Where u is the velocity magnitude (m/s), L is a characteristic length of the reactor (m), and D_z is a characteristic diffusion coefficient (m^2/s). As it is possible to note the Péclet number is equal to the inverse of axial dispersion coefficient. The Reynolds particle number is the ratio between the inertial forces against the viscous forces, in a packed bed such as our case it is define (Eq. 8):

$$Re_p = \frac{d_p \rho_f u}{\mu_f} \tag{8}$$

Where d_p is the particle diameter (m), ρ_f is the density of fluid (kg/m^3), u is the linear velocity of mixture through (m/s), and μ_f is the fluid viscosity (cP). The values obtained for each test are report in Table 4.3.

Considering that D_z (the reverse of Pèclet) is always <0.01, it can be confirmed that the deviation to the plug flow of our reactor configuration is small. Contrarily at 343 K the slope is more pronounced, then at this temperature the reactor behavior changes with the volumetric flow and, even considering the vessel dispersion number, its values are always >0.01 so the deviation of our reactor is large from the plug flow. The obtained *Pe* were fitted vs *Re$_p$*, obtaining the plot reported in Figure 4.4, showing a slight invariance in the investigated range.

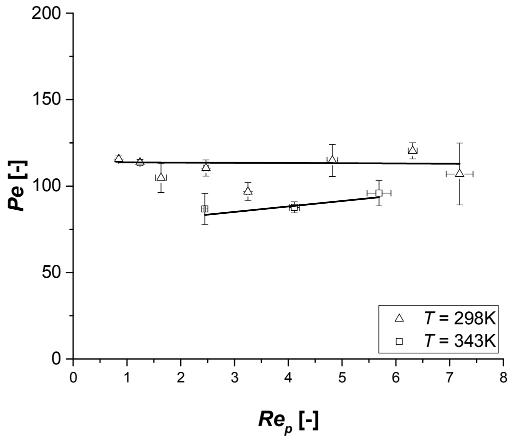

Figure 4.4. Péclet number plot vs Reynolds particle number.

4.3.2. Kinetic experiments in packed bed reactor

The first experiment was conducted to check the stability on stream of the catalyst. The experiment was performed at *T* = 323 K and $\dot{V}$ = 1.7·10^{-8} m^3/s flowrate. The results are reported in Fig. 4.5A. As revealed, the catalyst shows good stability in the adopted conditions, confirming its applicability in a continuous device. Experiments were conducted in a fixed bed reactor packed with Amberlite IR120, with the aim to validate the kinetic model developed in batch conditions.

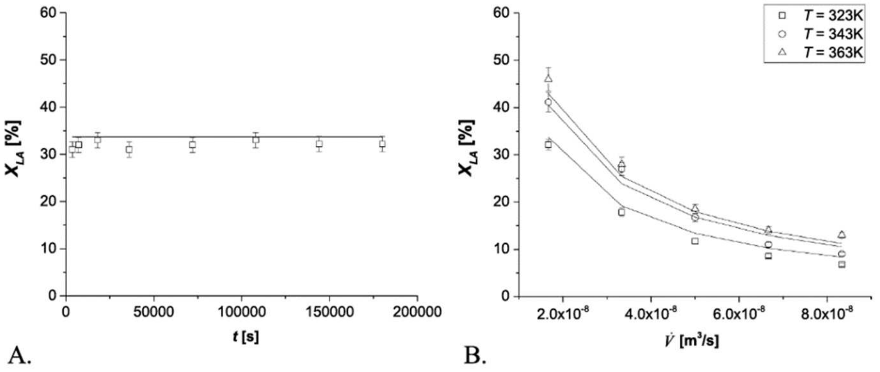

Figure 4.5. ***A.*** *Levulinic acid conversion vs time on stream for the experiment conducted at T = 323 K and a volumetric flowrate of 1.7·10−8 m^3/s.* ***B.*** *Simulated and experimental data comparison for the kinetic experiments conducted in the packed bed reactor. Symbols: Experimental data; Lines: Simulated values.*

Each test was conducted changing the volumetric flowrate and temperature. The experimental results are reported in Fig. 4.5B, showing the trend of the levulinic acid conversion degree that decreases with the volumetric flow, parametric with temperature. The highest conversions for the lower volumetric flow are due to a higher contact time between the reactants and the catalyst. Another important thing to underline is the temperature effect on the reaction: the conversion is high for the highest temperature adopted in the reactor, as expected.

The experimental data collected in the continuous system were simulated developing a dedicated model. In a heterogeneous system, with a porous solid as catalyst, three limiting regimes can be found: i) external fluid-solid mass-transfer, due to the diffusion of reactants from the liquid bulk to the solid surface; ii) internal mass-transfer, due to the diffusion of the reactant from the solid surface to the core of the particle and vice versa for the products; iii) kinetic regime, due only to the reaction rate. At first, the external mass transfer coefficient (*ks*) was estimated with the Dwivedi & Upadhyay correlation[3], applicable for Reynolds particle number <10, Eq. 9

$$k_s = 1.108\, u\, \varepsilon_B^{-1} \left(\frac{u\, d_p \rho}{\mu}\right)^{-0.72} \left(\frac{\mu}{\rho D}\right)^{-0.67} \tag{9}$$

where, D is the levulinic acid molecular diffusivity in ethanol (m^2/s), μ is the ethanol dynamic viscosity (cP) and ρ the ethanol density (kg/m^3). The result obtained from Dwidevi & Upadhyay correlation give a low external mass-transfer coefficient value ($ks = 2.3 \cdot 10^{-7}$ m/s). As, the reactants molecule would, with this assumption, diffuse slowly in the stagnant film surrounding the catalyst particle, it is reasonable to assume that the reaction occurs only on the catalyst surface. Thus, we excluded the intra-particle mass transfer limitations in the packed bed reactor. On this basis the continuous model was developed considering only external mass-transfer limitation and the surface reaction. The value of the external mass-transfer coefficient was calculated from Eq. 9. The summary of the modelling assumptions is reported below:

- Uniform velocity and concentration profiles along the radius of the pipe
- No radial dispersion is considered
- The autocatalytic reaction occurs in the liquid bulk phase
- The catalytic reaction occurs on the catalyst surface
- The reactor is considered isothermal
- Fluid-solid mass transfer resistance is dominant compared with intraparticle diffusion limitation

By adopting the mentioned assumptions, the bulk phase mass balance equation reported in Eq. 9 can be written, where *z* is the axial coordinate:

$$\frac{dc_i}{dt} = -u\frac{\partial c_i}{\partial z} + D_z\frac{\partial^2 c_i}{\partial z^2} - k_s a_{sp}\left(c_i - m_i c_{i(s)}\right) + \nu_i r_{NC} \quad (10)$$

where, *u* is the velocity (m/s), *Dz* is the axial dispersion coefficient (m^2/s) evaluated with the fluid-dynamic characterization and *ks* the fluid-solid external mass transfer (m/s) and a_{sp} the specific surface area (m^2/m^3). The reaction rate expression with related parameters is applied as can be found in the batch model and the physical quantities adopted are the same too. Two boundary conditions were defined to solve numerically the PDE system:

$$c_i|_{z=0} = c_i^0 \quad (11)$$

$$\left.\frac{\partial c_i}{\partial z}\right|_{z=L} = 0 \quad (12)$$

Closed-closed vessel Boundary Condition (BC) were chosen as the Peclet numbers are high for the studied system; the mentioned BCs consider that no axial dispersion occurs both at the inlet and outlet of the reactor. The first BC is referred to the inlet of the reactor, considering the feed concentration of each component. The second BC is referred at the outlet of the reactor. The mass balance on the solid phase considered in the model was evaluated as in Eq. (13).

$$k_s a_{sp}\left(c_i - m_i c_{i(s)}\right) = +\nu_i r_C \rho_B \quad (13)$$

Each experiment was simulated with no additional parameter estimation activity. The results of the simulation and the comparison with the experimental data are shown in Fig. 5 in terms of LA conversion against the volumetric flow, varying the temperature. As revealed, the model predictions are very good, simulating the trends accurately both with temperature and flowrate, allowing to conclude that the model was successfully validated.

Furthers information are reported in the **Publication II.**

4.4. Conclusions

The developed model was validated by conducting experiments in continuous packed bed reactor. The continuous unit was first characterized in terms of fluid-dynamics, showing a behavior not far from the plug-flow, then was used to conduct a set of experiments, varying temperature, and residence time. The data were interpreted by a fluid-solid mass transfer limited packed bed reactor model, as by using existing correlations it is possible to conclude that fluid-solid external mass transfer limitation is surely the rate-determining step of the reaction network. The collected data were simulated, with no additional parameter estimation allowing the validation of the developed kinetic model.

In conclusion, this study puts the basis for the scale-up of the levulinic acid esterification process, normally run-in industry in batch using mineral acids as catalyst.

References

(1) Levenspiel, O. Chemical Reaction Engineering. *Ind. Eng. Chem. Res.* **1999**, *38* (11), 4140–4143. https://doi.org/10.1021/ie990488g.

(2) Dwivedi, P. N.; Upadhyay, S. N. Particle-Fluid Mass Transfer in Fixed and Fluidized Beds. *Ind. Eng. Chem. Process Des. Dev.* **1977**, *16* (2), 157–165. https://doi.org/10.1021/i260062a001

CHAPTER V

Reactive chromatography applied to ethyl levulinate synthesis (III-IV)

Preamble

In this chapter a proof of concept of the reactive chromatography to ethyl levulinate synthesis from levulinic acid was given.

5.1. Introduction

The sustainable growth in the chemical industry implies a continue innovation with a transformation of the old way of seeing the chemical engineering, as converting the raw material into products through process at lower consumption of starting material and energy, zero waste and zero pollution. Obviously, this transformation requires a novel combination of science and technology, provided by process intensification techniques, i.e., multifunctional reactors in which the chemical reaction and the chromatographic separation are integrated into the same unit, such as reactive chromatography.[1]

Reactive chromatography has gained considerable attention for different reasons:

- For equilibrium limited reactions, continuous removal of the reaction products shifts the equilibrium and increase the conversion also reducing by-product formation.
- Using catalyst as packing material of column it is no longer necessary to remove the catalyst from the reaction product.
- It is possible to separate complex mixtures with great precision.
- The integration of both reaction and separation units reduces capital and operating costs.

Thus, the obtained reaction product is separated through the adsorption on the resin and in accordance with the adsorptive separation process principle, the difference in affinity between the sorbent and reaction products is the main reason for efficient separation.[2]

Cation exchange resins find employment as packing materials for ion exchange chromatography columns, in which the negatively charged analytes interact with the positive portion of the stationary phase and get separated depending on how strong the interaction is.

Good performance shown by the ion exchange resins studied in this thesis work as catalysts along with the adsorption capacity of these resins suggest that LA esterification with ethanol could be conducted in a chromatographic reactor in which the potential for catalysis and separation is carry out in a single reactor. To support this, in literature are reported the studies of Mazzotti[3], Rodrigues[1], Vu et al. [4] and Russo et al.[5] that used ion exchange resins for reactive chromatography experiments, conducting reactions such as acetic acid esterification and acetals synthesis, ethyl lactate production and xylene isomerization/separation, or esters hydrolysis.

In this chapter the realization of the chromatographic reactor experimental setup was delineated. To show the effectiveness of this concept, a chromatographic column (Resex ROA-Organic Acid H+ (8%)) was tested. Then, experiments in the fixed-bed chromatographic reactor packed with Dowex 50WX-8, among the resins previously studied in this thesis work, are conducted with the aim to demonstrate that the method ensures reaching full conversion of the system.

5.2. Experimental section

5.2.1 Materials

The following reagents were purchased from well-known companies and used without any further purification: levulinic acid (99 wt%) and ethyl levulinate (99 wt%) were supplied by Sigma Aldrich, ethanol (99 wt%) supplied by Carlo Erba Reagents. Rezex ROA-Organic Acid H+ (8%) HPLC ion-exclusion columns (8%) 300 x 7.8 mm was purchased by Phenomenex. Amberlyst-15 (A15-1, see Chapter III) and Dowex 50WX-8 ion exchange resin were purchased by Acros Organics and were used as solid acid catalysts. The main properties of the resins are reported in Table 3.2 (see Chapter III) and taken from the material data sheet of the catalyst itself.

5.2.2 Methods

The setup for the chromatographic reactor is shown in Figure 1. Ethanol is stored in the tank (1) and pumped into the system by an HPLC pump (2) that allows for flow rate setting and pressure drops reading. The ethanol flux passes through a Rheodyne injector valve (3) where an injector combined with a 20 µL loop allows to pulse the other reactant (LA) into the ethanol stream. The stream is then sent to the chromatographic reactor (4), consisting of a steel tube of 0.3 m length and

0.0078 m diameter jacketed with a heater regulated by a PID system (5). An online detector (Reach Device RD4, (6)) reveals the presence of solutes in the ethanol flux through UV (250 nm and 280 nm), IR and conductivity detectors. A pin valve (7) is placed after the detector, for samples withdrawal. The accumulation tank (8) is provided with a pin valve for decumulation of the liquid stream. The pressure in the chromatographic reactor system is applied through a reductor (9) linked to a N2 bottle (10). Packing of the tubular reactor (supplied by Phenomenex) was obtained after drying the resin and calculating the amount needed, considering the degree of swelling of the catalysts' particle (see Chapter III, section 3.3.1). About 6 g of A15-1 and about 6.5 g of Dowex 50 WX-8 were necessary to fill the tubular reactor. Ethanol was then streamed continuously for 6 h with a flow of 1.0 cm3/min into the reactor to let the resin swell and pack the tube completely.

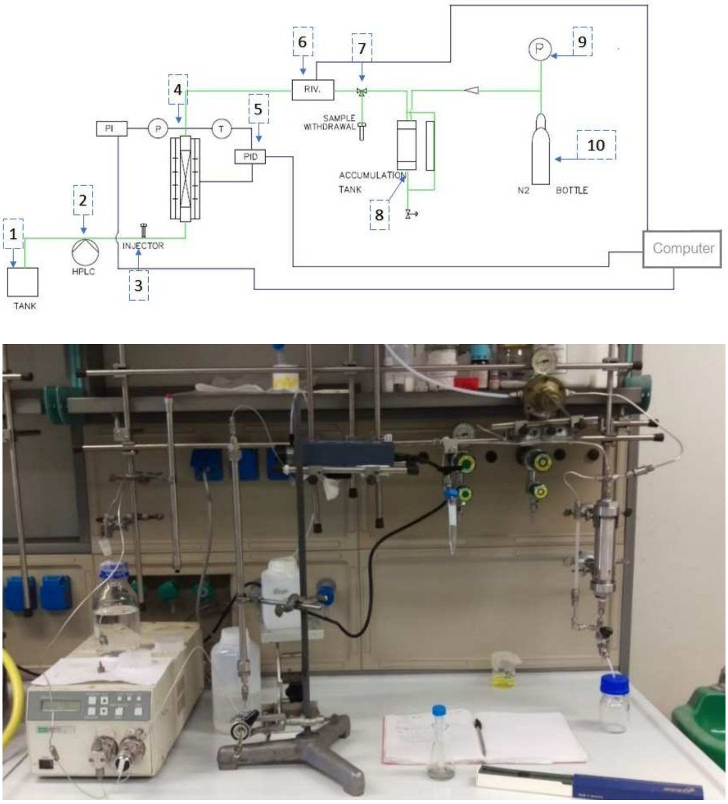

Figure 5.1. Chromatographic reactor setup scheme and laboratory system. (1) Tank; (2) HPLC pump; (3) Injector; (4) Chromatographic reactor; (5) PID; (6) Online detector; (7) Sample withdrawal valve; (8) Accumulation tank; (9) Reductor; (10) N_2 bottle.

The performance of the chromatographic reactor was evaluated with tests in which levulinic acid was pulsed into a stream of ethanol and collecting data from the online detector. To determine if the resins successfully separated the components of the system, tests pulsing EL were conducted and a comparison between the UV (250 nm) spectra was made. The summary of the experimental conditions with the use of Amberlyst-15, HPLC column Rezex ROA and Dowex 50Wx8, is illustrated in Table 5.1, Table 5.2, and Table 5.3 respectively. Rezex ROA column properties are listed in Table 5.3.

Table 5.1. Experimental conditions for the chromatographic reactor runs performed with ***Amberlyst-15*** *at P = 2 bar;* C_{LA} *= 0.5 mol/L.*

Test	T [K]	Q [cm^3/min]	ΔP [MPa]
1	303	1	5-6
2	303	2	12
3	303	3	18
4	303	4	24
5	303	5	30
6	303	6	38
7	303	7	46
8	303	8	51
9	303	9	59
10	303	10	67
11	323	1	5-6
12	343	1	5-6
13	363	1	5-6

Table 5.2. Experimental conditions for the chromatographic reactor runs performed with ***Rezex ROA*** *at P = 2 bar; CLA = 0.5 mol/L, ΔP= 5-6 MPa and T=273 K.*

Test	Q [cm^3/min]
R1	0.6
R2	0.7
R3	0.8
R4	0.9

It was not possible to fix the flow rates higher than 0.9 mL/min due to problems concerning excessive pressure drops.

Table 5.3. Rezex ROA- Organic acid properties.

Ionic form	Hydrogen
Standard Dimensions	300x7.8 mm
Matrix	Sulfonated styrene-divinylbenzene
Cross linking degree	8%
Particle size	8µ
Max flow rate	1.0 mL/min

Table 5.4. Experimental conditions for the chromatographic reactor runs performed with ***Dowex 50wx8****.*

Test	c_{LA} [mol/L]	c_{EL} [mol/L]	T [K]	Q [cm^3/min]	P [bar]	ΔP [MPa]
C1	6	-	303	0.8	2	9
C2	6	-	303	0.9	2	10
C3	6	-	303	1.1	2	13
C4	6	-	303	2.5	2	30
C5	6	-	303	5	2	54
C6	-	6	303	0.8	2	9
C7	-	6	303	0.9	2	10
C8	-	6	303	1.1	2	13
C9	-	6	303	2.5	2	30
C10	-	6	303	5	2	54
C11	6	-	313	1.1	2	13
C12	6	-	313	1.7	2	21
C13	6	-	313	1.8	2	23
C14	6	-	313	1.9	2	24
C15	6	-	313	2.5	2	30
C16	-	6	313	1.1	2	13
C17	-	6	313	1.7	2	21
C18	-	6	313	1.8	2	23
C19	-	6	313	1.9	2	24
C20	-	6	313	2.5	2	30
C21	6	-	323	1.8	2	23
C22	6	-	323	2.0	2	26
C23	6	-	323	2.5	2	30
C24	6	-	323	5.0	2	54
C25	-	6	323	1.8	2	23
C26	-	6	323	2.0	2	26
C27	-	6	323	2.5	2	30
C28	-	6	323	5.0	2	54

Take-up tests were performed to investigate how our reactive system affects the catalysts. Indeed, the evaluation of the swelling phenomenon is fundamental when a resin is to be used as a packing material for a reactor to avoid complete plugging of the system. The experimental procedure was reported in Chapter III, section 3.2.3 whereas the results were shown in section 3.3.3.1 of the same Chapter III.

5.3.Results and discussions

5.3.1 Reactive chromatography with Amberlyst-15

A first evaluation set of experiments were performed with the use of Amberlyst-15 (Table 1). The results of each experiments are reported in figure 2-4.

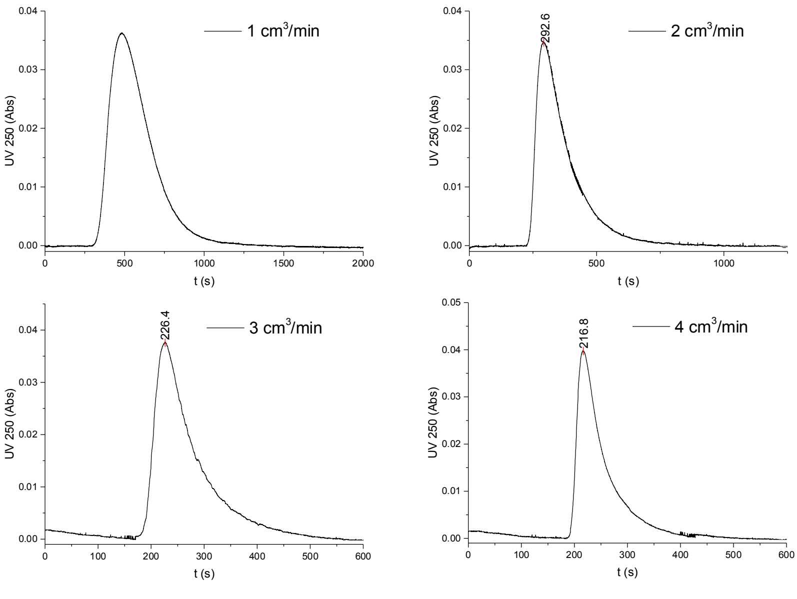

Figure 5.2. UV spectra of LA 0.5M injected in the chromatographic reactor packed with Amberlyst-15 and working at 303 K and at different flow rates.

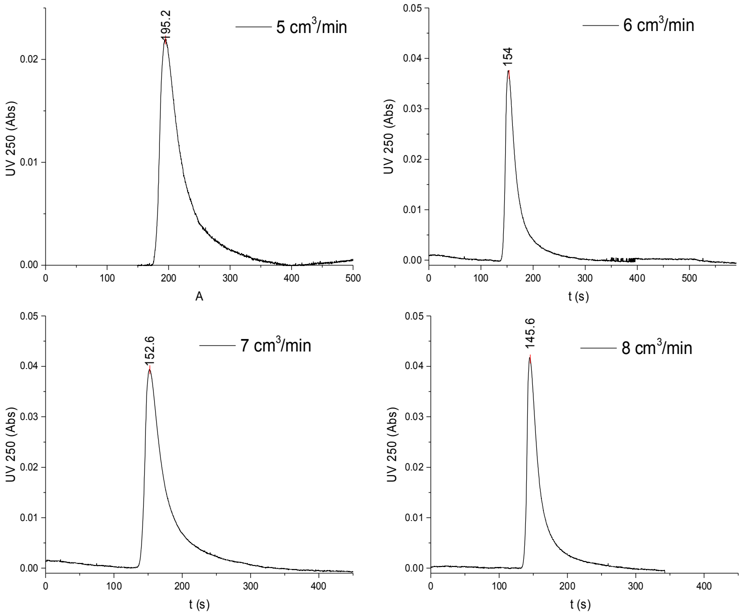

Figure 5.3. UV spectra of LA 0.5M injected in the chromatographic reactor packed with Amberlyst-15 and working at 303 K and at different flow rates.

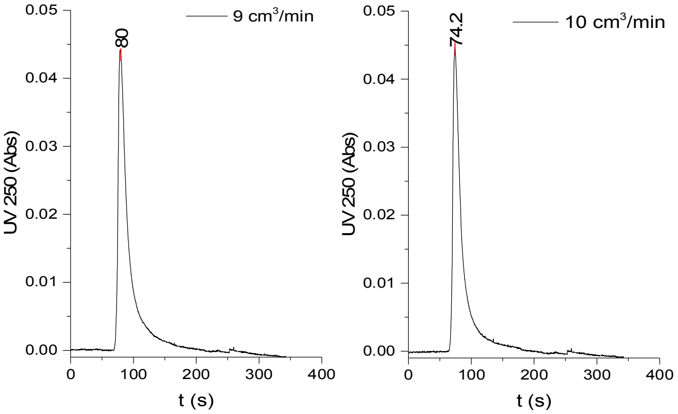

Figure 5.4. UV spectra of LA 0.5M injected in the chromatographic reactor packed with Amberlyst-15 and working at 303 K and at different flow rates.

It can be seen from the results, only one peak appears. After GC analysis both ethyl-levulinate and levulinic acid are presents in the reaction products and they have the same retention time. This can be easily evaluated comparing the results obtained pulsing ethyl-levulinate and levulinic acid separately, at the same volumetric flow rate of 1 cm^3/min, Figure 5.5.

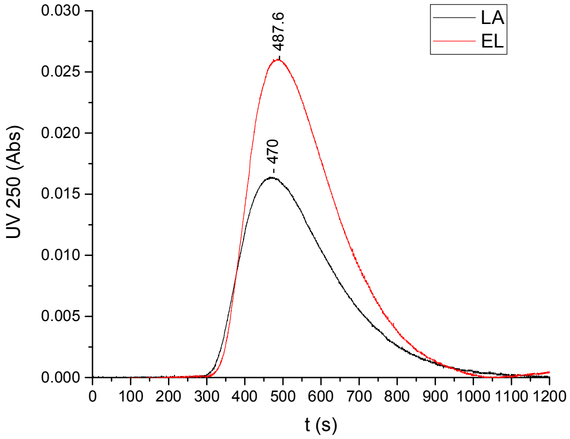

Figure 5.5. UV spectra of LA and EL 0.5 M at 303K and at flow rates of 1 cm³/min.

This is what we expected because at higher flow rates the time required to flow through the reactor is lower. LA is only partially converted, it has not got the time to interact with the resin and thus the UV analyzer only detects one peak, the chemical species exit the reactor at the same time.

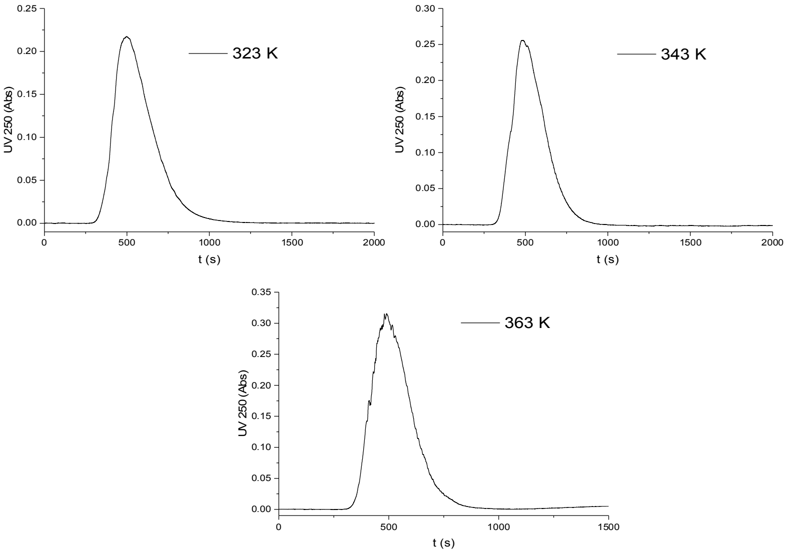

Figure 5.65. Figure 5. UV spectra of LA pulse at different temperatures and at flow rates of 1 cm^3/min.

Tests performed changing the temperature showed one peak that correspond, after GC analysis, to ethyl levulinate. It is possible to confirm that, enhancing the temperature a complete LA conversion occurs. Therefore, the reaction suffers from limitations due to external mass transfer, causing LA completely conversion but failing to separate it from the product. Probably this is due to the fact that LA is unable to enter inside Amberlyst-15 particle, and it is not adsorbed by the solid, while already in the external liquid film it has the favorable conditions to react.

5.3.2 HPLC column for reactive chromatography

To demonstrate the efficiency of this concept a set of experiments was done with an HPLC column, Rezex ROA, with sulfonated Styrene-divinylbenzene matrix, because the properties of the column allow to neglect the transfer limitations. In Table 5.3 the properties of the column are reported; among them the HPLC column has the limit to work at a maximum flow rate of 1 mL / min. In figure 5.7, the result obtained at 0.6 mL/min shown only one peak that correspond, after GC analysis, to ethyl levulinate. So, at this flow rate there are the complete LA conversion.

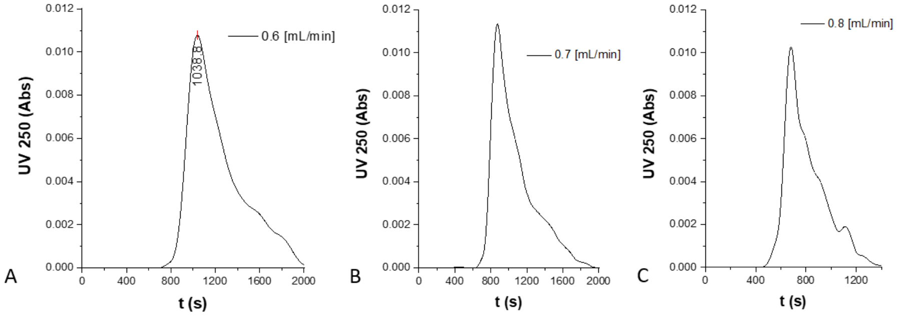

Figure 5.7. UV spectra of LA 0.5 M at 273K and 0.6 mL/min (A) 0.7 mL/min (B) and 0.8 mL/min (C).

In order to appreciate the goodness of the separation of the chromatographic reactor, tests increasing the flow rate were carried out up to a maximum of 0.9 mL /min.

An excellent result in terms of separation is obtained at 0.8 mL / min in which we have two peaks and GC analysis reveal the presence of levulinic acid too, more pronounced at 0.9 mL/ min (Fig. 5.8), demonstrating that it is possible to conduct a reaction with excellent conversion and selectivity also having an accetaple degree of separation.

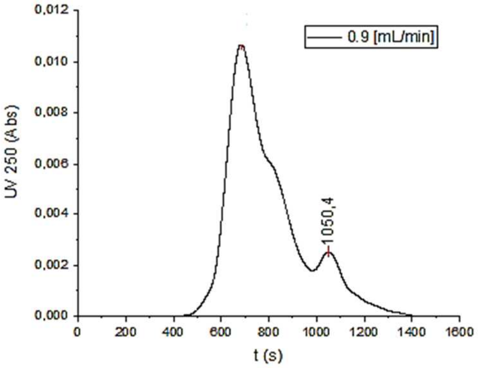

Figure 5.8. UV spectra of LA 0.5 M at 273K and 0.9 cm^3/min.

5.3.3 Reactive chromatography with Dowex 50Wx8

Having found that the concept can be applied there is no better choice than Dowex 50Wx8 in chromatographic separations, and for the highest levels of selectivity, consistency, and reliability in column separations, it is select among the catalysts studied in the previous chapter (see Chapter III).

- Effect of the stream flow rate

The first set of experiments consisted in pulsing LA at 303 K at different flow rates (Table 5.4, C1-C5). The UV spectra results are reported in figure 5.9.

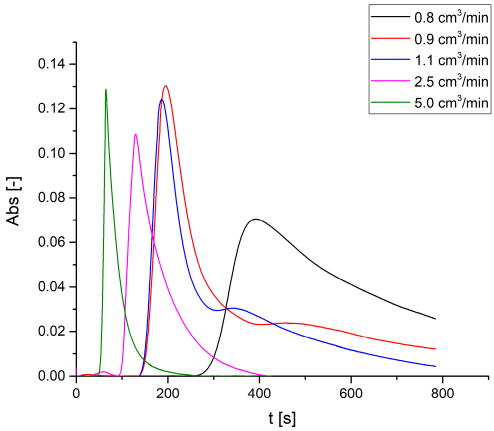

Figure 5.9. UV spectra of LA 6M injected in the chromatographic reactor working at 303 K and at different flow rates.

As revealed, the LA retention time decrease when the flow rate increase. This is what we expected because at higher flow rates the time required to flow through the reactor is lower. In more detail, looking at the curves shape at the intermediate flow rate (0.9 and 1.1 cm^3/min tests) it can be noted the formation of a second peak. Instead, the test at 0.8 cm^3/min flow rate shows a single, broad peak detected at a retention time similar to the second peak shown in the two tests at intermediate flow rates.

An explanation of this behavior can be ascribed to the time of interaction of the reagents with the resin that makes the reaction happen.

At lower flow rates, 0.8 cm^3/min, the entire quantity of LA pulsed into the reactor has enough time to interact with Dowex 50 WX-8 and it is totally converted, resulting in a single EL peak at the detection point. At intermediate flow rate values, LA is only partially converted, and both the carboxylic acid and the ester are detected by the UV analyzer with detection times that are in line with their affinity values. To confirm this hypothesis, a solution of EL 6M in ethanol was pulsed into the chromatographic reactor at the same operative conditions and the UV spectra were compared with the corresponding LA spectra (Table 5.4, C6-C10). Obtained curves are reported in detail in the relative **Publications IV**. At high flow rates, like 5.0 and 2.5 cm^3/min, the LA has not got the time to interact with the resin and thus the UV analyzer only detects one peak, the chemical species exit the reactor at the same time. Thus, Dowex 50 WX-8 performs a good separation of the product and the reagent, allowing theoretical recover of the pure product from the reactor outlet.

- Effect of the reactor temperature

The effect of temperature was evaluated performing tests at 313K data was collected pulsing LA at 1.1 and 2.5 cm^3/min flow rates (Table 5.4, C3 and C11; C4 and C15). In figure 5.10, a comparison of the experiments at the same flow rates and different temperatures are shown.

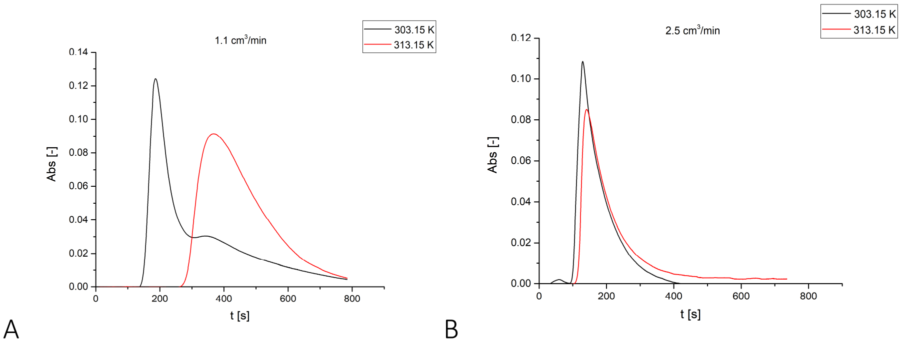

Figure 5.10. UV spectra for LA 6 M injections at 1.1 cm³/min (A) and 2.5 cm³/min (B) flow rate at different temperatures.

At 2.5 cm^3/min flow rate, as expected, the raise in temperature does not make a significant difference since LA has no time to interact with the resin. At 1.1 cm^3/min flow rate, it can be note that the conversion to EL is complete. The reaction kinetics is positively affected by higher temperatures, obtaining complete conversion of the carboxylic acid at higher flow rates.

Since we obtained two opposite outcomes (0 and 100% conversion), further tests were conducted to pinpoint the flow rate values that would give partial LA conversion at the same temperature, so that it could be verified that good separation would occur.

Figure 5.11 show the results of test at 313 K and 1.7, 1.8 and 1.9 cm^3/min flow rates.

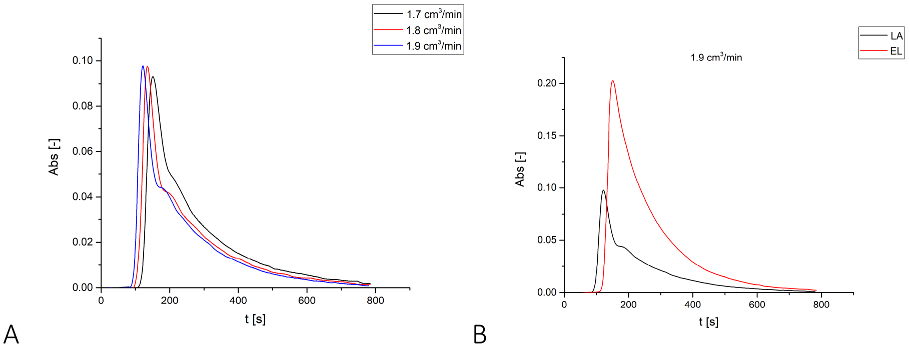

Figure 5.11. (A) UV spectra of LA 6 M pulses at 313 K and different flow rates. (B) UV spectra at 1.9 cm³/min of LA and EtOH.

All three tests display the formation of two peaks, one is to attribute to LA and the other, which is kind of embedded into the first, to EL.

To prove that the conversion is not complete and that there is the presence of both LA and EL, a solution of EL 6 M was prepared and injected at the same operative conditions. In **Publication IV**, are shown the results and the correspondence confirm that the second peak in the LA injections spectra can be attributed to EL formation.

Through peaks deconvolution the approximate LA conversion was determined. The conversion values were not much different for the tests at 1.7, 1.8 and 1.9 cm^3/min flow rate (65, 67 and 68% respectively) and given the difficulty in peaks fitting due to the EL peaks being broad these values are only indicative.

From this data it can be possible to confirm that the separation of EL from LA occurs at these operative conditions and that the range of conversion values is narrower than the one obtained with tests at 303 K and 0.9 and 1.1 cm^3/min flow rates.

Another set of experiments was carried out raising up the temperature to 323 K to further evaluate the performance of our chromatographic reactor setup. This time no second peak appeared in any of our tests at different flow rates (1.8, 2, 2.5, 5 cm^3/min) when LA 6 M pulses were sent through the resin-packed tubular reactor (Figure 5.7). If this was to be expected for the higher flow rates based on previous collected data, it remained to be demonstrated the nature of the single peaks at the lower flow rates.

EL 6 M injections at the same temperature and flow rate values demonstrate that at lower flow rates LA is completely converted to EL.

Further proof for the injection test at 1.8 cm^3/min (Figure 5.12) is given by the LA injection test with the same flow rate at lower temperature: the EL peak of that spectrum perfectly corresponds to the only peak in the LA injection spectrum at 323 K.

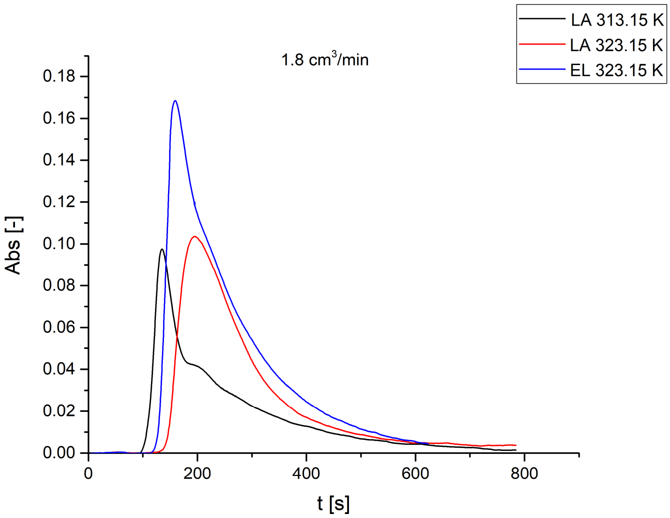

Figure 5.12. UV spectra of LA and EL 6 M at 313 and 323 K at 1.8 cm^3/min flow rate.

At 323 K the reaction kinetics and the quantity of catalyst that completely packs the column allow for complete conversion of LA to EL with flow rate values that give the organic acid enough time to interact with the ion-exchange resin.

Water produced by the esterification reaction is mostly kept inside the solid. This should not affect LA conversion largely, but too much water adsorbed in the resin could in fact reduce the quantity of EL obtained at the reactor outlet due to the EL hydrolysis taking place.

After many tests run with the chromatographic reactor setup, the resin showed that it was indeed starting to accumulate water. EL pulses started showing two peaks at the UV analyzer, which would only be explained by the presence of water in the system reacting with the ester and forming LA.

To remove water from the Dowex 50 WX-8 resin, a 0.05 cm^3/min flow of methanol was sent through the packed reactor for 24 h.

Finally, the LA conversion achieved by the chromatographic reactor setup at the different operative conditions employed is summarized Figure 5.13.

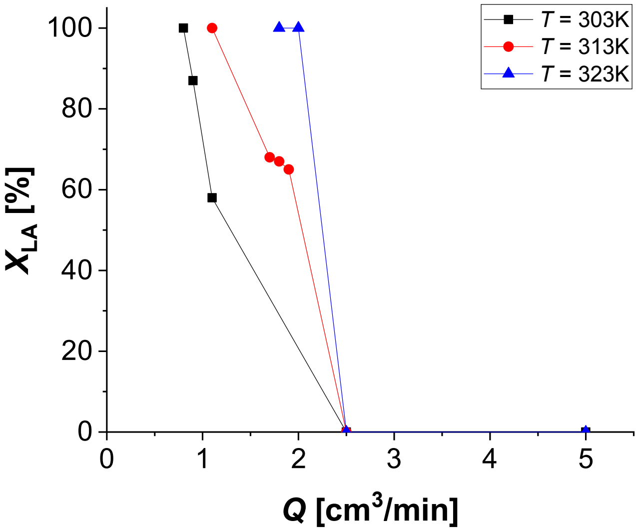

Figure 5.13. LA conversion achieved at different operative conditions during the chromatographic reactor tests with LA 6M pulses. XLA values were determined by comparison with EL 6M injections and with peaks deconvolution.

As revealed, the trends are rather logical, as conversion decreases by increasing the flowrate, as lower residence times are achieved. The quantification of the data reported in this paper can give a real impact in the optimization of the chromatographic reactor operation conditions.

5.4 Conclusions

The possibility of conducting LA esterification with ethanol for production of EL in a chromatographic reactor setup was successfully verified using Dowex 50 WX-8, demonstrating that in some cases it is possible to achieve full LA conversion.

A tubular reactor was packed with Dowex 50 WX-8 to build a chromatographic reactor setup. Tests at different temperatures and flow rates were done to evaluate the catalytic and the separation efficiency of the resin itself.

The chromatographic separation method proved to work for LA esterification, as with sufficiently low flow rates the LA pulses were completely converted to EL, while with moderate flow rates the partially unconverted LA was well separated from the ester. While, at flow rates higher than 2.5 cm^3/min LA do not have time to interact with the resin surface. At temperatures near to room temperature (303 K) LA was completely converted to EL. This is a very encouraging result considering that this is not possible in a batch system due to the thermodynamic equilibrium. It was also proved that if the resin should trap too much water, as a by-product of the esterification, it is possible to clean it with a methanol treatment. In a future perspective this promising reactive setup could be further investigated with a fluid-dynamic characterization and the development of a model that could describe the qualitative data obtained with the chromatographic reactor. Certainly, a higher experimental effort must be conducted to retrieve separately information about the kinetics of the reaction, point that it will be surely investigated in our future works.

References

(1) Rodrigues, A. E.; Pereira, C. S. M.; Santos, J. C. Chromatographic Reactors. *Chem. Eng. Technol.* **2012**, *35* (7), 1171–1183. https://doi.org/https://doi.org/10.1002/ceat.201100696.

(2) Srivastava, N.; Kuddus, M. Use of Ion-Exchange Resin in Reactive Separation. In *Applications of Ion Exchange Materials in Chemical and Food Industries*; Inamuddin, Rangreez, T. A., M. Asiri, A., Eds.; Springer International Publishing: Cham, 2019; pp 125–137. https://doi.org/10.1007/978-3-030-06085-5_6.

(3) Mazzotti, M.; Kruglov, A.; Neri, B.; Gelosa, D.; Morbidelli, M. A Continuous Chromatographic Reactor: SMBR. *Chem. Eng. Sci.* **1996**, *51* (10), 1827–1836. https://doi.org/https://doi.org/10.1016/0009-2509(96)00041-3.

(4) Vu, T. D.; Seidel-Morgenstern, A. Quantifying Temperature and Flow Rate Effects on the Performance of a Fixed-Bed Chromatographic Reactor. *J. Chromatogr. A* **2011**, *1218* (44), 8097–8109. https://doi.org/https://doi.org/10.1016/j.chroma.2011.09.018.

(5) Russo, V.; Tesser, R.; Rossano, C.; Vitiello, R.; Turco, R.; Salmi, T.; Di Serio, M. Chromatographic Reactor Modelling. *Chem. Eng. J.* **2019**, *377*, 119692. https://doi.org/https://doi.org/10.1016/j.cej.2018.08.078.

CHAPTER VI

Levulinic acid hydrogenation to γ-valerolactone

State of the art

Preamble

A brief state of the art on the γ-valerolactone (GVL) and the importance as intermediate chemical with a wide range of applications as fuel, fuel additive and as a green solvent are outlined (paragraph 6.1). The synthesis mechanism of GVL production from levulinic acid and the catalysts used are outlined in this chapter (paragraph 6.2).

6.1. Introduction

To highlight the value of LA, the most promising reaction is the hydrogenation to GVL, a platform molecule that has gained considerable attention in the last decade, as manifested by the high number of publications, about 1.210 in the last 10 years.[116]

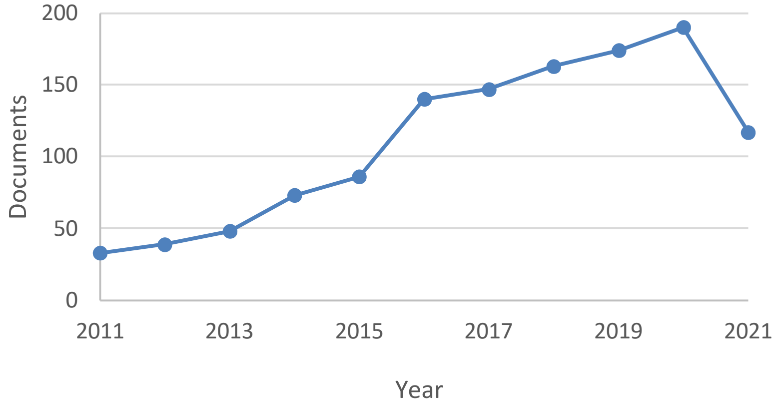

Figure 6.1. Statistical data over the last ten years from SCOPUS.[1]

GVL is a heterocyclic five carbon ester ($C_5H_8O_2$) with one methyl group in γ-position, has a sweet, herbaceous odor, that makes it perfect for application in perfumes and food additives.[2,3]

For its attractive physicochemical properties, GVL can be used as a solvent for various processes, for the synthesis of biomass derived chemicals; a precursor for more high value-added chemicals (like 1,4-pentanediol, 2-methyltetrahydrofuran) and in the fuel sector.[4-6]

GVL can be blended in gasoline and it performs comparably to ethanol/gasoline mixtures, since it retains 97% of the energy content of glucose and GVL combustion energy is similar to that of ethanol (29.7 MJ/Kg). Moreover, GVL has a lower vapor pressure (Table 6.1) and it is a fundamental parameter in fuel sector in order to control the emission of volatile organic compounds (VOCs). [7]

Table 6.1. Physicochemical properties of GVL.[8]

Molecular weight (g/mol)	100.112
Density (g/mL)	1.05
Flash point (°C)	96
Melting point (°C)	-31
Boiling point (°C)	207-208
Solubility in water (%)	100
ΔH_{vap} (kJ/mol)	54.8±0.4
$\Delta_c H°_{liq}$ (kJ/mol)	-2649.6±0.8
$\Delta_f H°_{298}$ (kJ/mol)	-461.3
Cetane number	<10
Vapor pressure (kPa)	3.5 at 80°C

Although GVL also possesses a stereogenic carbon center, the major application in the fuel sector or as solvent do not require a specific enantiomeric form and GVL is usually synthetized and used in the racemic form. However, the enantiomeric form of GVL find applications as a chiral chemicals in the synthesis of PhACs (pharmaceutically active molecules). [9]

6.2. Hydrogenation reaction mechanism

According to the literature the production of GVL from LA hydrogenation over a catalyst would be perhaps the most efficient and economic method reported to date[124], and GVL synthesis follow the reaction pathways shown in a schematic diagram (figure 2), based on the literature. [11-13]

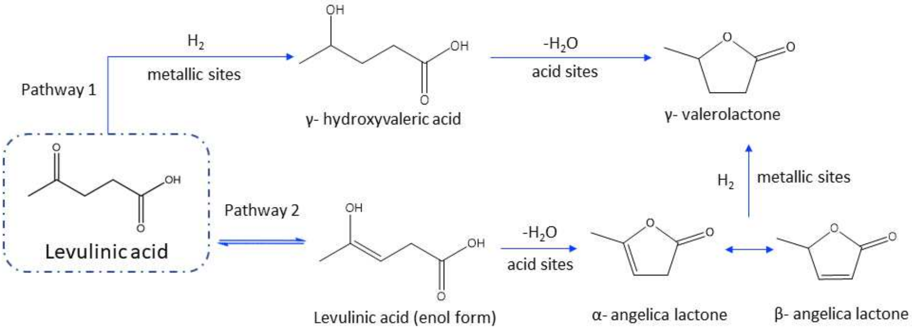

Figure 6.2. Schematic diagram on the hydrogenation of levulinic acid to γ-valerolactone. Figure adapted from Malu et al. [13]

Pathway 1, under mild conditions:

- hydrogenation of LA with H_2 attacks on the carbonyl group and the formation of an intermediate, γ-hydroxyvaleric acid;
- intramolecular dehydration and lactonization to form GVL.

Pathway 2, at high temperature:

- esterification of the enolic form of LA which leads to the formation of the angelica lactone;
- hydrogenation of the double bond in the α-angelic and β-angelic lactone to obtain GVL.

Thus, both reaction pathways carried out through the hydrogenation step and the dehydration step and in order to provide good yields it is necessary that are ensure both acid and metallic sites. [7,14,15]
The metallic sites activity influences the hydrogenation step while the acidic catalyst strength has an influence on the other reaction step.[16]
Either way, these two steps will always take place with the difference that changes the sequence in which occurs that in turn, depends on the conditions adopted.
Different researchers have demonstrated the presence of the γ-hydroxyvaleric acid as intermediate during the experiments proving that, the first pathway is the thermodynamically and kinetically preferred at low temperature. [17]
It was also demonstrated by Lomate et al. [18] that in vapor phase the reaction first proceeds to the formation of α-angelica lactone, so at high temperature the second pathway is preferred. Despite traditionally the reaction occurs with a direct hydrogenation (H_2), new better and safe methods to guarantee the

hydrogen supply are now constantly explored. In literature, formic acid and alcohols are at moment the best H_2 donors for the GVL production.[18-21]

6.3. Catalysts for GVL synthesis

Both homogeneous and heterogeneous catalysts have been studied over the past decades for this reaction. Typically, precious metals such as iridium (Ir)[22], palladium (Pd)[23], platinum (Pt)[24] and ruthenium (Ru)[25,26] are the most catalysts used. In particular, Ru-based catalysts are by now classified as benchmark catalysts for this reaction, since high GVL yield can be reached (> 97%) under relatively mild condition. [27] As well know the high boiling point of GVL (207–208°C) makes product/catalyst separation by means of distillation uneconomical so the catalyst recovery is very difficult in the case of homogeneous catalysts application, even if it is possible to obtain a high yield of GVL under relatively mild conditions. The latest more comprehensive review about homogeneous catalyst have been done in the 2016 by Omoruyi et al.[28] and covers all the advances until that moment. As far as the current research literature reports, Ru-chelating tridentate phosphine complexes, shows the best performance in promoting the efficiency of the reaction with better catalytic activity. Performing the reduction of LA with $[RuCl_2(PPh_3)_3]$ as catalyst, give rise to a yield of up 99% GVL and good catalytic performance were also achieved using the water-soluble ligand triphenylphosphine-trisulfonic acid (TPPTS) with $[Ru(acac)_3]$ (Table 6.2). [21,29]

,

Table 6.2. Overview of homogeneous Ru-based catalysts mostly used in LA hydrogenation reaction.

Catalyst	T(°C)	p_{H2} (bar)	Time (h)	GVL yield (%)	Ref.
$[RuCl_2(PPh_3)_3]$	180	12	24	99	[28]
$RuCl_3$ + TPPTS	90	45	1.33	>99	[28]
$[Ru(acac)_3]$	140	50	5	98	[30]
$[Ru(acac)_3]$ + TPPTS	140	50	5	97	[30]
$[Ru(acac)_3]$ + TPPTS	140	50	21	92	[30]

Given the above-mentioned shortcoming of homogeneous systems, heterogeneous catalytic systems have many advantages (low cost and recyclability) and have by now completely replace the homogeneous ones. Even for solid catalysts, significant progresses have been made in the GVL synthesis from LA with the application of ruthenium-based catalytic system by than the catalytic counterparts based on other transition metals. The great commitment in enhancing more and more the ruthenium-based catalysts is due to the inherent and unique ability of ruthenium itself, under mild reaction conditions, to hydrogenate the carbonyl moiety of LA selectively into an alcohol functionality to form 4-hydroxyvaleric acid intermediate which spontaneously yields GVL after dehydration and cyclization step. The potential of the ruthenium-based catalysts, also for the heterogeneous catalysts, was already showed by Manzer et al.[27] in 2004, comparing the activities of 5% of different metal catalysts (i.e., Ir, Rh, Pd, Ru, Pt, Re and N) supported on the same carrier (activated carbon) and using 1,4-dioxane as solvent. The 5% Ru/C catalyst was the best with ~ 100% conversion and >97% selectivity of GVL after 4 h hydrogenation. In 2011, Ru/C was again found to have a higher catalytic performance than the other catalysts by Upare et al.[25] that carried out the reaction over carbon supported Ru, Pt and Pd.

Despite, Ru/C is by now considered as a benchmark catalyst for this reaction it suffers of leaching issue and of slow and irreversible deactivation. The latter is probably due to the sintering of the ruthenium particles and at deposition of the carbonaceous deposits on the catalyst surface.[31]

Thus, very important in the studies of ruthenium-based catalysts is the proper regulation of the carrier acidity by which it could be enhance the activity of the catalyst. Stronger is the interaction between Ru and the carrier, more is the stability of Ru and so the cyclability performance. Moreover, as mentioned before it has been demonstrated that the supports have an effect on the coke deposition, active metal leaching and sintering so researchers have turned their attention to developing new highly efficient solid catalysts which greatly determine the catalytic stability, placing attention on the support type.[32]

Al-Shaal et al. [33] investigated other inorganic supports, other carbon, such as TiO_2, Al_2O_3, and SiO_2 at aim to compare the activity of the catalysts demonstrating that the highest LA conversion (99.2%) and GVL selectivity (89.8%) were achieving by Ru/C catalyst (entry 2, Table 6.3).

Seretis et al. [26] and Maumela et al.[34] have very lately published two reviews on the recent advances in the field of ruthenium-catalyzed hydrogenation reactions of LA. Both reviews are focused on the effect of different solid supports since its choice has a strong influence on the catalyst performance, as the stability. The first review is focused on TiO_2 and carbon supported catalysts; while the other one is very complete and ranging from a comparison of Ru with other metals, examining the effect of the support, the solvent and the effect of bimetallic catalyst on the catalyst performance.

Yu and coworkers[32], in their detailed review have classified and critically discusses the effect of different solid acid supports on the overall catalytic performance of the bifunctional systems: metal oxides, molecular sieves, metal organic frameworks (MOFs), acid functionalized carbons, acidic resins and others (i.e. hydroxyapatite (HAP) and sulfonated polyether sulfone (SPES)) are also developed as a novel support. Some examples of Ru-based catalysts are listed in Table 6.3.

Table 6.3. Overview of heterogeneous Ru-based catalysts mostly used in LA hydrogenation reaction

Entry	**Catalyst**	***T*** **(°C)**	p_{H_2} **(MPa)**	**Time (h)**	**Catalytic performance**	**Ref.**
1	5% Ru/C	150	3.5	4	90% GVL yield	[35]
2	5% Ru/C	130	1.2	2.7	89.8% GVL sel.	[33]
3	5% Ru/Al_2O_3	130	1.2	2.7	80.4% GVL sel.	[33]
4	5% Ru/TiO_2	130	1.2	2.7	87.8% GVL sel.	[33]
5	5% Ru/SiO_2	130	1.2	2.7	76.5% GVL sel.	[33]
6	1% Ru/TiO_2	130	4	0.5	>99% GVL sel.	[36]
7	Ru/SMS	70	0.5	4	95.6% GVL yield	[37]
8	Ru/MCM-41	70	0.5	4	84.1% GVL yield	[37]
9	Ru/MIL-101(Cr)	70	1	5	99% GVL yield	[38]
10	Ru/OMC-S	70	0.7	3	97% GVL sel.	[39]
11	Ru/SiO_2	70	3	2	98% GVL sel.	[40]
12	Ru/C	70	3	2	98% GVL sel.	[40]
13	Ru/SPES	70	3	2	100% GVL sel.	[40]
14	Ru/C+NBO	70	0.5	3	98.6% GVL sel.	[12]
15	Ru/C+NBP	70	0.5	3	98.3% GVL sel.	[12]
16	Ru/C+A15	70	0.5	3	98.9% GVL sel.	[12]
17	Ru/C+ A70	70	0.5	3	99.9% GVL sel.	[12]
18	Ru@Dowex	70	0.5	7	>99% GVL sel.	[41]
19	$Ru_{0.9}$-$Ni_{0.1}$/OMC	150	4.5	2	97% GVL sel.	[42]
20	$Ru_{0.9}$-$Ni_{0.1}$/C	150	4.5	2	15% GVL sel.	[42]

Molecular sieve: spherical mesoporous silica (SMS), mesoporous molecular sieve (MCM-41); metal organic framework: Chromium terephthalate metal–organic framework (MIL-101 (Cr)); Acid functionalized carbons: ordered mesoporous carbon with sulfuric groups (OMC-S); ion-exchange resin: Amberlyst-15 (A15), Amberlyst-70 (A70)

From this study is evident the importance and the fundamental role of both the support choice and the addition of the metals .[34,42,43]

As it is evident by the catalyst performance results show in Table 6.3, the use of acidic supports on which Ru metal nanoparticles are dispersed is a good strategy to prepare new catalysts act as a bifunctional catalyst for the hydrogenation of LA because offer a simultaneous access of both sites (acid and metal) useful to the dehydration and hydrogenation of LA to GVL.

A very interesting approach was studied by Raspolli-Galletti [12] that showed the enhancing effect that is could be obtained combining an heterogeneous acid, such as cationic exchange resins (Amberlyst 70, Amberlyst 15), niobium phosphate (NBP) or oxide (NBO), and the commercial ruthenium supported catalysts (Table 6.3, entry 14-17).

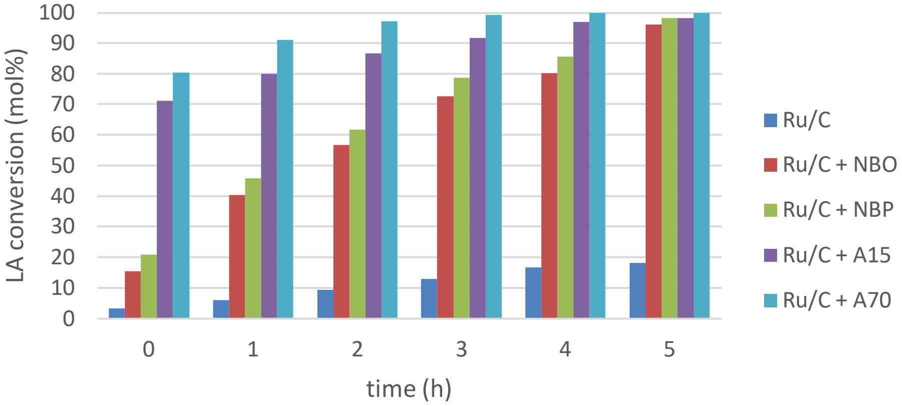

Figure 6.3. Effect of different bifunctional catalysts on the levulinic acid conversion (mol%). Adapted from [12]

A similar enhancement was obtained by Moreno-Marrodan and Barbaro [41] achieving 99.8% LA conversion and 99% GVL selectivity using Ruthenium nanoparticles supported on Dowex, as sulfonic acid ion exchange resin, through impregnation method.

To further improve the performance of Ruthenium catalysts' family, researchers have turned their attention on the combination of bi-metals by exploiting their complementary properties to achieve better catalytic activity and stability obtaining *bi-metallic catalysts*. One example is the addition of Re to the benchmark Ru/C for which was obtained an enhancement of the activity with a GVL selectivity higher than 95%. [44] Another example is given for the catalyst $Ru_{0.9}$-$Ni_{0.1}$/OMC, for which was reached a LA conversion of 99% and 97% of GVL selectivity. Comparing these results with those obtained in the case of $Ru_{0.9}$-$Ni_{0.1}$ on carbon as a support (LA conversion 34% and GVL yield 15%) a drastic drop was observed (Table 6.3, entry 19-20). It was demonstrating that adding Sn to the Ru/C catalyst, the stability of the catalyst increases although the initial catalytic activity was higher with Ru/C respect Sn-Ru/C. The above discussion, along with references cited, help the reader to appreciate and to further investigate the evolution of Ru-based catalysts. The efficiency of the latter catalysts is evaluated also in comparison with the use of non-noble metals (i.e., Ni, Zr, Co, Cu) and Ni-based catalysts have attracted a lot of attention to their high catalytic activity.[7,34,45,46]

Another important factor which must be taken into account in the GVL synthesis is the choice of the solvent. As reported in the literature, there is a direct influence among the solvent and the performance of the catalyst, in term of stability and selectivity towards the product. There are only few published studies that attempt to clarify the specifical role of solvent and they are agree that H_2O is the ideal solvent, other than the other (dioxane, THF, ethanol, toluene), for the hydrogenation reaction of LA to GLV. The enhancement in activity obtained with water is due to the hydrogen bond effect transporting H atoms to the catalysts surface, participating into reaction as hydrogen source. [36,47]

6.4. One-pot catalysts preparation: sol- gel method

Inspired by the results obtained with bifunctional catalysts, in the perspective to develop a new efficient ones and explore new preparation method, an interesting synthesis reported in literature is surely the one-pot sol-gel method. Sol-gel chemistry collect many strategies to prepare materials from solution precursors and the importance of this procedure is due to the possibility to regulate the physico-chemical properties of the materials through the manipulation of the operative conditions. High yield, low operation temperatures, and low production costs are only some of the advantages of the sol-gel method. This method potentially replaces the traditional preparation via that expected to obtain mixed-oxide catalysts or supported metal oxide by post synthesis methods: impregnation, coprecipitation and deposition procedures. In the following figure are summarized the main step of the procedure:

- Solution of the precursors.
- Condensation and hydrolysis to form a SOL.
- Polycondensation of hydrolyzed precursors with formation of GEL (gelation step).

- Drying & aging steps with formation of dense “XEROGEL” (evaporation of solvent and collapse of the porous network).
- Calcination at selected temperature to stabilize the materials.

The aging step can be added to ensure a growth of particles or a change in the composition and properties of the gel since chemical reactions continue long after the gel formation. [48]

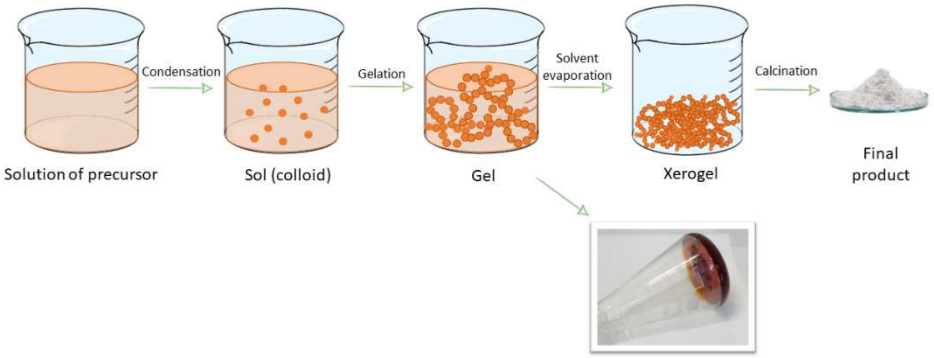

Figure 6.4. Main steps of the synthetic procedure via sol-gel method.

6.5. Greener alternative to H_2 as hydrogen source

In addition to the non-safety use of H_2 as hydrogen source in the LA reaction to GVL, another way it is possible which involves the use of inexpensive and accessible H-donor molecules, as alcohols. This reaction is recognized as catalytic transfer hydrogenation (CTH) and is considered to have bright application prospect. Xue et al. [45] recently, in their work about valorization of levulinic acid over non-noble metal catalysts, have dedicated a section on transfer hydrogenation with alcohols showing the performance of various catalysts. Among the metal-based catalysts (e.g., Ni, Cu, Zr), zirconium-based catalysts were comprehensively reported giving high LA conversion and selectivity toward GVL. For example, Chia and Dumesic [49] in their work have reported the CTH of LA and its esters to GVL over ZrO_2 using 2-butanol as hydrogen donor and they obtained 99.9% LA conversion with a GVL selectivity of 71% working at 220°C for 16-hour reaction.

The activity of ZrO_2, among a number of different metal oxides, resulted from the fact that possess both acid and base characteristics (Zr^{4+} and O^{2-}, respectively).

Recently, first Enumula et al. [50] and then Kuwahara et al. [19] found that ZrO_2 supported on mesoporous SBA-15 catalyze very efficiently the LA conversion.

Enumula et al. studied the reaction in with different secondary alcohols in continuous hydrogenation, obtaining the best results with 2-butanol (100% LA conversion with 96% GVL selectivity at 250°C). Kuwahara et al., achieved 99.9% LA conversion and 90% GVL selectivity in 2-propanol under mild reaction conditions (150°C for 3h).

References

(1) SCOPUS data analysis TITLE-ABS-KEY (gamma AND valerolactone) https://www.scopus.com/term/analyzer.uri?sid=15174a84e4419447e5641e7284e80abf&origin=resultslist&src=s&s=TITLE-ABS-KEY%28gamma+valerolactone%29&sort=plf-f&sdt=b&sot=b&sl=34&count=1593&analyzeResults=Analyze+results&txGid=d04ca4de1fa6d875e39a25c253e93506 (accessed Jul 6, 2021).

(2) Liu, M.; Li, S.; Fan, G.; Yang, L.; Li, F. Hierarchical Flower-like Bimetallic NiCu Catalysts for Catalytic Transfer Hydrogenation of Ethyl Levulinate into γ-Valerolactone. *Ind. Eng. Chem. Res.* **2019**, *58* (24), 10317–10327. https://doi.org/10.1021/acs.iecr.9b01774.

(3) Yan, K.; Yang, Y.; Chai, J.; Lu, Y. Catalytic Reactions of Gamma-Valerolactone: A Platform to Fuels and Value-Added Chemicals. *Appl. Catal. B Environ.* **2015**, *179*, 292–304. https://doi.org/https://doi.org/10.1016/j.apcatb.2015.04.030.

(4) Alonso, D. M.; Gallo, J. M. R.; Mellmer, M. A.; Wettstein, S. G.; Dumesic, J. A. Direct Conversion of Cellulose to Levulinic Acid and Gamma-Valerolactone Using Solid Acid Catalysts. *Catal. Sci. Technol.* **2013**, *3* (4), 927–931. https://doi.org/10.1039/c2cy20689g.

(5) Al-Shaal, M. G.; Dzierbinski, A.; Palkovits, R. Solvent-Free γ-Valerolactone Hydrogenation to 2-Methyltetrahydrofuran Catalysed by Ru/C: A Reaction Network Analysis. *Green Chem.* **2014**, *16* (3), 1358–1364. https://doi.org/10.1039/C3GC41803K.

(6) Wang, H.; Yang, B.; Zhang, Q.; Zhu, W. Catalytic Routes for the Conversion of Lignocellulosic Biomass to Aviation Fuel Range Hydrocarbons. *Renew. Sustain. Energy Rev.* **2019**, No. November, 109612. https://doi.org/10.1016/j.rser.2019.109612.

(7) Dutta, S.; Yu, I. K. M.; Tsang, D. C. W.; Ng, Y. H.; Ok, Y. S.; Sherwood, J.; Clark, J. H. Green Synthesis of Gamma-Valerolactone (GVL) through Hydrogenation of Biomass-Derived Levulinic Acid Using Non-Noble Metal Catalysts: A Critical Review. *Chem. Eng. J.* **2019**, *372* (April), 992–1006. https://doi.org/10.1016/j.cej.2019.04.199.

(8) Tang, X.; Sun, Y.; Zeng, X.; Lei, T.; Li, H.; Lin, L. Γ-Valerolactone-an Excellent Solvent and a Promising Building Block. *Biomass, Biofuels, Biochem. Recent Adv. Dev. Platf. Chem.* **2019**, 199–226. https://doi.org/10.1016/B978-0-444-64307-0.00007-X.

(9) Götz, K.; Liese, A.; Ansorge-Schumacher, M.; Hilterhaus, L. A Chemo-Enzymatic Route to Synthesize (S)-γ-Valerolactone from Levulinic Acid. *Appl. Microbiol. Biotechnol.* **2013**, *97* (9), 3865–3873. https://doi.org/10.1007/s00253-012-4652-5.

(10) Orlowski, I.; Douthwaite, M.; Iqbal, S.; Hayward, J. S.; Davies, T. E.; Bartley, J. K.; Miedziak, P. J.; Hirayama, J.; Morgan, D. J.; Willock, D. J.; Hutchings, G. J. The Hydrogenation of Levulinic Acid to γ-Valerolactone over Cu–ZrO2 Catalysts Prepared by a PH-Gradient Methodology. *J. Energy Chem.* **2019**, *36*, 15–24. https://doi.org/https://doi.org/10.1016/j.jechem.2019.01.015.

(11) Manzer, L. E. Preparation of Levulinic Acid Esters from α- Angelica Lactone and Alcohols.

(12) Galletti, A. M. R.; Antonetti, C.; De Luise, V.; Martinelli, M. A Sustainable Process for the Production of γ-Valerolactone by Hydrogenation of Biomass-Derived Levulinic Acid. *Green Chem.* **2012**, *14* (3), 688–694. https://doi.org/10.1039/c2gc15872h.

(13) Malu, T. J.; Manikandan, K.; Cheralathan, K. K. *Levulinic Acid-a Potential Keto Acid for Producing Biofuels and Chemicals*; Elsevier B.V., 2019. https://doi.org/10.1016/B978-0-444-64307-0.00006-8.

(14) Varkolu, M.; Bathula, H. B.; Suh, Y.-W.; Burri, D. R.; Kamaraju, S. R. R. Hydrogenation of Levulinic Acid with and without External Hydrogen over Ni/SBA-15 Catalyst. *Appl. Petrochemical Res.* **2018**, *8* (3), 153–162. https://doi.org/10.1007/s13203-018-0203-z.

(15) Guo, Y.; Yang, Q.; Guo, P.; Yao, G.; Jin, F. Recent Progress in Conversion of Carbohydrate Biomass and Their Derivatives to γ-Valerolactone. *IOP Conf. Ser. Earth Environ. Sci.* **2020**, *446* (2). https://doi.org/10.1088/1755-1315/446/2/022035.

(16) Lomate, S.; Sultana, A.; Fujitani, T. Vapor Phase Catalytic Transfer Hydrogenation (CTH) of Levulinic Acid to γ-Valerolactone Over Copper Supported Catalysts Using Formic Acid as Hydrogen Source. *Catal. Letters* **2018**, *148* (1), 348–358. https://doi.org/10.1007/s10562-017-2241-z.

(17) Abdelrahman, O. A.; Heyden, A.; Bond, J. Q. Analysis of Kinetics and Reaction Pathways in the Aqueous-Phase Hydrogenation of Levulinic Acid To Form γ-Valerolactone over Ru/C. *ACS Catal.* **2014**, *4* (4), 1171–1181. https://doi.org/10.1021/cs401177p.

(18) Lomate, S.; Sultana, A.; Fujitani, T. Effect of SiO2 Support Properties on the Performance of Cu–SiO2 Catalysts for the Hydrogenation of Levulinic Acid to Gamma Valerolactone Using Formic Acid as a Hydrogen Source. *Catal. Sci. Technol.* **2017**, *7* (14), 3073–3083. https://doi.org/10.1039/C7CY00902J.

(19) Kuwahara, Y.; Kaburagi, W.; Fujitani, T. Catalytic Transfer Hydrogenation of Levulinate Esters to γ-Valerolactone over Supported Ruthenium Hydroxide Catalysts. *RSC Adv.* **2014**, *4* (86), 45848–45855. https://doi.org/10.1039/C4RA08074B.

(20) Amarasekara, A. S.; Hasan, M. A. Short Communication. *Catal. Commun.* **2015**, *60* (Complete), 5–7. https://doi.org/10.1016/j.catcom.2014.11.009.

(21) Yu, Z.; Lu, X.; Liu, C.; Han, Y.; Ji, N. Synthesis of Γ-Valerolactone from Different Biomass-Derived Feedstocks: Recent Advances on Reaction Mechanisms and Catalytic Systems. *Renew. Sustain. Energy Rev.* **2019**, *112* (April), 140–157. https://doi.org/10.1016/j.rser.2019.05.039.

(22) Wang, J.; Wang, Y.; Tong, X.; Wang, Y.; Jin, G.; Guo, X. Highly Active Ir/SiC Catalyst for Aqueous Hydrogenation of Levulinic Acid to γ-Valerolactone. *Catal. Commun.* **2020**, *139*, 105971. https://doi.org/https://doi.org/10.1016/j.catcom.2020.105971.

(23) Amarasekara, A. S.; Hasan, M. A. Pd/C Catalyzed Conversion of Levulinic Acid to γ-Valerolactone Using Alcohol as a Hydrogen Donor under Microwave Conditions. *Catal. Commun.* **2015**, *60*, 5–7. https://doi.org/https://doi.org/10.1016/j.catcom.2014.11.009.

(24) Parapat, R. Y.; Yudatama, F. A.; Musadi, M. R.; Schwarze, M.; Schomäcker, R. Antioxidant as Structure Directing Agent in Nanocatalyst Preparation. Case Study: Catalytic Activity of Supported Pt Nanocatalyst in Levulinic Acid Hydrogenation. *Ind. Eng. Chem. Res.* **2019**, *58* (7), 2460–2470. https://doi.org/10.1021/acs.iecr.8b03555.

(25) Upare, P. P.; Lee, J.-M.; Hwang, D. W.; Halligudi, S. B.; Hwang, Y. K.; Chang, J.-S. Selective Hydrogenation of Levulinic Acid to γ-Valerolactone over Carbon-Supported Noble Metal Catalysts. *J. Ind. Eng. Chem.* **2011**, *17* (2), 287–292. https://doi.org/https://doi.org/10.1016/j.jiec.2011.02.025.

(26) Seretis, A.; Diamantopoulou, P.; Thanou, I.; Tzevelekidis, P.; Fakas, C.; Lilas, P.; Papadogianakis, G. Recent Advances in Ruthenium-Catalyzed Hydrogenation Reactions of Renewable Biomass-Derived Levulinic Acid in Aqueous Media. *Front. Chem.* **2020**, *8*, 221. https://doi.org/10.3389/fchem.2020.00221.

(27) Manzer, L. E. Catalytic Synthesis of α-Methylene-γ-Valerolactone: A Biomass-Derived Acrylic Monomer. *Appl. Catal. A, Gen.* **2004**, *272* (1–2), 249–256. https://doi.org/10.1016/j.apcata.2004.05.048.

(28) Omoruyi, U.; Page, S.; Hallett, J.; Miller, P. W. Homogeneous Catalyzed Reactions of Levulinic Acid: To Γ-Valerolactone and Beyond. *ChemSusChem* **2016**, *9* (16), 2037–2047. https://doi.org/10.1002/cssc.201600517.

(29) Ye, L.; Han, Y.; Feng, J.; Lu, X. A Review about GVL Production from Lignocellulose: Focusing on the Full Components Utilization. *Ind. Crops Prod.* **2020**, *144* (December 2019), 112031. https://doi.org/10.1016/j.indcrop.2019.112031.

(30) Delhomme, C.; Schaper, L.-A.; Zhang-Preße, M.; Raudaschl-Sieber, G.; Weuster-Botz, D.; Kühn, F. E. Catalytic Hydrogenation of Levulinic Acid in Aqueous Phase. *J. Organomet. Chem.* **2013**, *724*, 297–299. https://doi.org/https://doi.org/10.1016/j.jorganchem.2012.10.030.

(31) Li, S.; Wang, Y.; Yang, Y.; Chen, B.; Tai, J.; Liu, H.; Han, B. Conversion of Levulinic Acid to γ-Valerolactone over Ultra-Thin TiO2 Nanosheets Decorated with Ultrasmall Ru Nanoparticle Catalysts under Mild Conditions. *Green Chem.* **2019**, *21* (4), 770–774. https://doi.org/10.1039/C8GC03529F.

(32) Yu, Z.; Lu, X.; Bai, H.; Xiong, J.; Feng, W.; Ji, N. Effects of Solid Acid Supports on the Bifunctional Catalysis of Levulinic Acid to γ-Valerolactone: Catalytic Activity and Stability. *Chem. - An Asian J.* **2020**, *15* (8), 1182–1201. https://doi.org/10.1002/asia.202000006.

(33) Al-Shaal, M. G.; Wright, W. R. H.; Palkovits, R. Exploring the Ruthenium Catalysed Synthesis of γ-Valerolactone in Alcohols and Utilisation of Mild Solvent-Free Reaction Conditions. *Green Chem.* **2012**, *14* (5), 1260–1263. https://doi.org/10.1039/C2GC16631C.

(34) Maumela, Mulisa; Marx, Sanette; Meijboom, R. *Heterogeneous Ru Catalysts as the Emerging Potential Superior Catalysts in the Selective Hydrogenation of Bio-Derived Levulinic Acid to γ -Valerolactone : Effect of Particle Size ,*; 2021.

(35) Primo, A.; Concepción, P.; Corma, A. Synergy between the Metal Nanoparticles and the Support for the Hydrogenation of Functionalized Carboxylic Acids to Diols on Ru/TiO2. *Chem. Commun.* **2011**, *47* (12), 3613–3615. https://doi.org/10.1039/C0CC05206J.

(36) Tan, J.; Cui, J.; Deng, T.; Cui, X.; Ding, G.; Zhu, Y.; Li, Y. Water-Promoted Hydrogenation of Levulinic Acid to γ-Valerolactone on Supported Ruthenium Catalyst. *ChemCatChem* **2015**, *7* (3), 508–512. https://doi.org/https://doi.org/10.1002/cctc.201402834.

(37) Kuwahara, Y.; Magatani, Y.; Yamashita, H. Ru Nanoparticles Confined in Zr-Containing Spherical Mesoporous Silica Containers for Hydrogenation of Levulinic Acid and Its Esters into γ-Valerolactone

at Ambient Conditions. *Catal. Today* **2015**, *258*, 262–269. https://doi.org/https://doi.org/10.1016/j.cattod.2015.01.015.

(38) Guo, Y.; Li, Y.; Chen, J.; Chen, L. Hydrogenation of Levulinic Acid into γ-Valerolactone Over Ruthenium Catalysts Supported on Metal–Organic Frameworks in Aqueous Medium. *Catal. Letters* **2016**, *146* (10), 2041–2052. https://doi.org/10.1007/s10562-016-1819-1.

(39) Villa, A.; Schiavoni, M.; Chan-thaw, C. E.; Fulvio, P. F.; Mayes, R. T.; Dai, S.; More, K. L.; Veith, G. M.; Prati, L. Acid-Functionalized Mesoporous Carbon : An Efficient Support for Ruthenium-Catalyzed g - Valerolactone Production. 1–9. https://doi.org/10.1002/cssc.201500331.

(40) Yao, Y.; Wang, Z.; Zhao, S.; Wang, D.; Wu, Z.; Zhang, M. A Stable and Effective Ru/Polyethersulfone Catalyst for Levulinic Acid Hydrogenation to γ-Valerolactone in Aqueous Solution. *Catal. Today* **2014**, *234*, 245–250. https://doi.org/10.1016/j.cattod.2014.01.020.

(41) Moreno-Marrodan, C.; Barbaro, P. Energy Efficient Continuous Production of γ-Valerolactone by Bifunctional Metal/Acid Catalysis in One Pot. *Green Chem.* **2014**, *16* (7), 3434–3438. https://doi.org/10.1039/C4GC00298A.

(42) Yang, Y.; Gao, G.; Zhang, X.; Li, F. Facile Fabrication of Composition-Tuned Ru–Ni Bimetallics in Ordered Mesoporous Carbon for Levulinic Acid Hydrogenation. *ACS Catal.* **2014**, *4* (5), 1419–1425. https://doi.org/10.1021/cs401030u.

(43) Yu, Z.; Lu, X.; Bai, H.; Xiong, J.; Feng, W.; Ji, N. Effects of Solid Acid Supports on the Bifunctional Catalysis of Levulinic Acid to γ -Valerolactone : Catalytic Activity and Stability. **2020**, 1182–1201. https://doi.org/10.1002/asia.202000006.

(44) Braden, D. J.; Henao, C. A.; Heltzel, J.; Maravelias, C. C.; Dumesic, J. A. Production of Liquid Hydrocarbon Fuels by Catalytic Conversion of Biomass-Derived Levulinic Acid. *Green Chem.* **2011**, *13* (7), 1755–1765. https://doi.org/10.1039/C1GC15047B.

(45) Xue, Z.; Liu, Q.; Wang, J.; Mu, T. Valorization of Levulinic Acid over Non-Noble Metal Catalysts: Challenges and Opportunities. *Green Chem.* **2018**, *20* (19), 4391–4408. https://doi.org/10.1039/c8gc02001a.

(46) Mohan, V.; Raghavendra, C.; Pramod, C. V.; Raju, B. D.; Rama Rao, K. S. Ni/H-ZSM-5 as a Promising Catalyst for Vapour Phase Hydrogenation of Levulinic Acid at Atmospheric Pressure. *RSC Adv.* **2014**, *4* (19), 9660–9668. https://doi.org/10.1039/c3ra46485g.

(47) Sudhakar, D. M.; lakshmi Kantam, M.; Jaya, V.; Ramineni, K.; Ramanujachary, K.; Akula, V. Hydroxyapatite as a Novel Support for Ru in the Hydrogenation of Levulinic Acid to γ-Valerolactone. *Catal. Commun.* **2014**, *50*. https://doi.org/10.1016/j.catcom.2014.03.005.

(48) Esposito, S. “Traditional” Sol-Gel Chemistry as a Powerful Tool for the Preparation of Supported Metal and Metal Oxide Catalysts. Materials 2019, 12, 668; doi:10.3390/ma12040668

(49) Chia, M.; Dumesic, J. A. Liquid-Phase Catalytic Transfer Hydrogenation and Cyclization of Levulinic Acid and Its Esters to γ-Valerolactone over Metal Oxide Catalysts. *Chem. Commun.* **2011**, *47* (44), 12233–12235. https://doi.org/10.1039/c1cc14748j.

(50) Enumula, S. S.; Gurram, V. R. B.; Chada, R. R.; Burri, D. R.; Kamaraju, S. R. R. Clean Synthesis of Alkyl Levulinates from Levulinic Acid over One Pot Synthesized WO3-SBA-16 Catalyst. *J. Mol. Catal. A Chem.* **2017**, *426*, 30–38. https://doi.org/https://doi.org/10.1016/j.molcata.2016.10.032.

CHAPTER VII

Investigation on metallic and acid sites of Ru/Nb/Si catalysts to efficiently produce γ-Valerolactone from Levulinic Acid Hydrogenation

7.1 Introduction

The synthesis reaction of γ-valerolactone (GVL) is carried out by the hydrogenation of levulinic acid (LA) using heterogeneous catalysts, which have the advantage of being relatively easy to separate and recycle. An important aspect that emerges from the studies in the literature, reported in the previous section, is that classical hydrogenation catalysts, such as Ru/C, seem to work better in the presence of an acidic co-catalyst. To optimize the process, it is necessary to design bifunctional catalysts able to favor both the hydrogenation and the acid-catalyzed step of the reaction. In a recent review Yu et al.[1] , examined the effects of the acid characteristic of the support in which the metallic phase is dispersed on the performance of bifunctional catalysts for the heterogeneous transformation LA to GVL. They conclude that the acidity of the support plays a key role in this transformation affecting both the metal dispersion and the stability of the catalyst in mild reaction conditions.[1]

This observation represents the starting point of this study in which it has been demonstrated that gels deriving from mixed oxides of niobium, silicon and ruthenium made possible the hydrogenation reaction of LA with good yields.

In this part of work, the effect the chemical composition of different Ru-Nb-Si gel-derived nanomaterials on the catalytic performance in the LA hydrogenation reaction was explored with special attention to the acid surface characteristics of the matrix in which the Ru nanoparticles are dispersed. Keeping the RuO_2 amount at 3.8 mol% the Nb_2O_5 content was changed from 0 to 6.9 mol% in the RuO_2 - Nb_2O_5-SiO_2 (Ru-Nb-Si) mixed-oxide system with the aim to clarify the role played by the two components (the metallic phase and the acid matrix) in determining the reaction pathway and then the GVL yields. It should be noted that modulating the composition of the support and then its acid characteristics HPA or GVL were isolated as the only product of the reaction.

7.2 Experimental section

7.2.1 Sol-gel synthesis

Mixed-oxide materials, whose nominal molar composition is reported in Table 7.1, were prepared by a one-pot sol-gel route in collaboration with Prof. Aronne group at the Department of Chemical, Materials and Production Engineering.

The following reagents by Sigma–Aldrich were used. Tetraethoxysilane (TEOS, $Si(OC_2H_5)_4$ 99%), niobium(V) chloride, ($NbCl_5$ 99%), anhydrous ethanol (EtOH), ruthenium(III) chloride-3-hydrate ($RuCl_3{\cdot}3H_2O$ 99.98%), tetramethylsilane (TMS, $Si(CH_3)_4 \geq 99.0\%$).

A solution of $NbCl_5$ in anhydrous EtOH with a molar ratio $NbCl_5$/EtOH = 1:6 was prepared in a dry box at room temperature. The solution was stirred for 20 minutes to allow the formation of partially substituted $Nb(OEt)_{5-X}(Cl)_X$ species and the removal of HCl produced. An alcoholic solution of TEOS with molar ratio TEOS/EtOH = 1:4 was prepared to which a proper amount of $RuCl_3{\cdot}3H_2O$ (0.613 mmol) was added: the latter solution was then mixed with the former solution. The resulting clear reddish solution was hydrolysed at room temperature by using deionized water, finally obtaining a hydro-alcoholic solution with the molar ratio TEOS/H_2O = 1:4. From this final solution, a transparent dark-red gel was obtained within two days. The gelled system was kept for 3 days at room temperature before drying, and afterwards it was fully dried in air at 110 °C in an electric oven until a constant weight was reached. After such treatments, amorphous hardened dry gels were obtained. The dried gels (xerogels) were annealed for 2 h at 500 °C in air to obtain stable powdered materials (Table 7.1).

The catalysts used in the reaction were obtained from these materials by a reduction treatment under a 0.1 L min^{-1} H_2 flow, 1 bar, 300 °C for 3 h and finally cooled at room temperature (r.t.) under H_2 flow.

Table 7.1. Textural properties of samples

Sample	Molar Composition	N_2 physisorption[a]	NH_3-TPD[a]	Nb/Ru[e]		D_{Ru}[g]
		S_{BET}[b] (m^{2}g^{-1})	Acid sites[d] (mmol/g)	Ox[a]	Red[f]	
4Ru0Nb	$RuO_{2(0.038)}SiO_{2(0.962)}$	523*	>0.01	-	-	12
4Ru2.5Nb	$RuO_{2(0.038)}Nb_2O_{5(0.024)}SiO_{2(0.938)}$	398	0.08	0.56	1.62	5
4Ru5Nb	$RuO_{2(0.038)}Nb_2O_{5(0.047)}SiO_{2(0.915)}$	472	2.39	1.15	3.58	5
4Ru7.5Nb	$RuO_{2(0.038)}Nb_2O_{5(0.069)}SiO_{2(0.893)}$	412	2.00	1.93	10.99	4

[a] annealed sample at 500°C for 2 h

[b] specific surface area calculated by BET method from N_2 adsorption data in 0.1 – 0.3 P/P^0 range

[c] micropore volume estimated using t-plot analysis in the 0.35 – 0.5 nm range.

[d] amount of NH_3 chemisorbed per gram of sample

[e] Nb/Ru ratio calculated on the basis of EDS maps

[f] reduced sample in H_2 (1 bar, 0.1 ml/min) at 300°C for 3 h

[g] ruthenium dispersion obtained by CO chemisorption

7.2.2 Structural, morphological and surface acidity characterization

X-ray diffraction patterns were recorded with a Bruker D8 X-ray diffractometer, operating in the reflection mode with Cu-Kα radiation (λ = 1.5418 Å, 40 kV, 30 mA). The data were collected in the 5 - 80° range ($2\theta B$) with steps of 0.015°.

FTIR (Fourier Transform Infrared) spectra were collected in the ATR (Attenuated Total Reflection) mode using a Bruker Equinox 55 spectrometer equipped with a Platinum ATR cell, in which diamond (refractive index = 2.41) is used as ATR crystal. The spectra were recorded between 4000 and 500 cm^{-1} with a resolution of 4 cm^{-1}. DR UV–vis (Diffuse Reflectance UV-Visible) spectra were recorded in the range of 200 – 800 nm on a Shimadzu UV-3600 Plus spectrophotometer. A Spectralon® Diffuse Reflectance Standard was used to measure the background spectra. The measured intensity was expressed as the value of the Kubelka–Munk function F(R). N2 adsorption and desorption isotherms of the samples were recorded at -196 °C using a Micromeritics Tristar 3000 apparatus. Samples were previously outgassed at 250 °C under vacuum for minimum 6 h. The BET (Brunauer-Emmett-Teller) method was used to calculate the samples specific surface area, *SBET*, in the 0.1 – 0.3 P/P^0 range. The micropores volume was estimated using *t*-plot analysis in the 0.35 – 0.5 nm statistical thickness range.

FTIR spectroscopy measurements of NH_3 adsorption were carried out at room temperature (r.t.). FTIR spectra of self-supporting wafers were collected on an Equinox 55 (Bruker) spectrophotometer equipped with MCT (Mercury – Cadmium- Telluride) cryodetector. The powders were pressed into thin self-supporting wafers (optical density of about 20 mg cm^{-2}) and treated under high vacuum (residual pressure $<10^{-3}$ mbar) at 300 °C in a standard vacuum frame, to remove water and other atmospheric contaminants. Afterwards, increasing pressures of $NH_{3(g)}$ were dosed on the outgassed samples (equilibrium pressure range: 0 – 15 mbar). Afterwards, the samples were outgassed for 1 h at r.t. and at 300 °C, to check adsorption reversibility.

NH_3-TPD (Temperature Programmed Desorption) measurements were carried out using a CATLAB-PCS (Hiden Analytical), a quartz microreactor coupled to a Mass Spectrometer. About 0.1 g fresh sample was preheated in argon flow (50 mL min^{-1}) at 300 °C for 60 min (ramp 10 °C min^{-1}). Adsorption of NH_3 (5 vol. % in helium; flow rate 30 mL min^{-1}) was done at 70 °C. The TPD measurement, under an argon flow of 30 mL min^{-1}, was conducted by heating the sample from 70 to 600 °C at a 10°C min^{-1} rate.

FESEM (Field Emission Scanning Electron) measurements were performed using a Tescan S9000G FESEM 3010 microscope (30 kV) equipped with a high brightness Schottky emitter and fitted with Energy Dispersive X-ray Spectroscopy (EDS) analysis by an Ultim Max Silicon Drift Detector (SDD, Oxford). For analyses, the samples, in the form of powders, were deposited on a stub coated with a conducting adhesive and inserted in the chamber by a fully motorized procedure.

Carbon monoxide chemisorption was performed in a Micromeritics Pulse Chemisorb 2705 equipment. The catalyst (0.15 g), placed in a U-shaped sample tube, was heated at a rate of 10 °C min^{-1}, under a pure flow of H_2, to perform a reduction pretreatment at 300 °C for 3 hours. The sample was cooled down to 35 °C. The CO chemisorption was performed sending pulses of 0.037 mL of CO in helium, to the sample and recording the corresponding peak value of the non adsorbed CO. This process was repeated until saturation, namely when no more CO was adsorbed when an additional pulse is given. The total amount of CO adsorbed is found by summing the amount adsorbed at each pulse.

7.2.3 Catalytic tests

The synthesis of GVL from LA hydrogenation was performed in a fed-batch reactor, where H_2 is fed at constant pressure to a vessel charged with about 4.0 g of LA, 200 g of water and 0.5 g of catalyst. The catalyst was pre-treated, before loading, performing a reduction in a dedicated system under a 0.1 L min^{-1} H_2 flow, 1 bar and 300 °C for 3 h. The so-reduced catalyst was cooled at room temperature under H_2 flow and then quickly charged to the vessel.

The reaction mixture, containing the catalyst, was flushed with N_2 at 5 bar, to evacuate the dissolved O_2 before feeding H_2. In this step, the temperature was increased to the desired value (70 °C) using a heating jacket, and the solution is kept under constant stirring at 300 rpm. After approximately 10 N_2 washes, H_2 was fed to the reactor at 20 bar and the reaction was started. Samples were periodically withdrawn from the reaction vessel, to evaluate the evolution with time of both LA conversion and GVL yield. An AISI 316 stainless steel net was installed at the bottom of the withdrawn pipe to avoid any catalyst loss. Temperature and H_2 flow were measured by a National Instruments DAQ device, equipped with a homemade acquisition script written in LabView 2013. During the reaction, reagents/intermediates/products were analysed by GC every 30 min, according to a procedure described in the following. All the experimental tests were performed at 300 rpm, at temperature of 70 °C and with a hydrogen pressure of 20 bar, while N_2 pressure was fixed at 1.0 bar.

The samples were analysed by GC, using ethylene glycol as an external standard. In a sample volume of approximately 2-3 cm^3, a 100 mL volume of the standard was dissolved. The so-prepared sample (1µL) was injected in a PerkinElmer Clarus 580 GC (equipped with a 30mx0.32mmx0.26µm Supelco SLB-IL60 column) with a FID detector. The injector was a PSSI, working at 300 °C, with a carrier (He) pressure of 14 psi and working in on-column mode. The temperature ramp was set as follows: 100 °C heating to 300 °C with a rate of 10 °C min^{-1}; the temperature was kept at the final value for 25 min. The retention times were the following: ethylene glycol: 4.7 min; γ-valerolactone: 6.2 min; γ-hydroxyvaleric acid: 7.11 min; levulinic acid: 10.4 min.

7.3 Results and discussion

7.3.1Structural, textural, and electronic properties

All dried gels are amorphous (data not shown) while the XRD profiles of the annealed samples (2h at 500 °C) are shown in Figure 7.1. The peaks of RuIV oxide, RuO_2, (JCPDS Card No. 40-1290) can be noticed in all profile together with a broad halo centred at approximately $2\theta = 24°$, typical of amorphous silica.[2-4] This indicates that the annealing causes the precipitation in the amorphous matrix of RuO_2 crystals. On the other hand, the lack of typical peaks of Nb_2O_5 crystalline aggregates corroborate the hypothesis of a very high dispersion of niobium in the siloxane matrix.

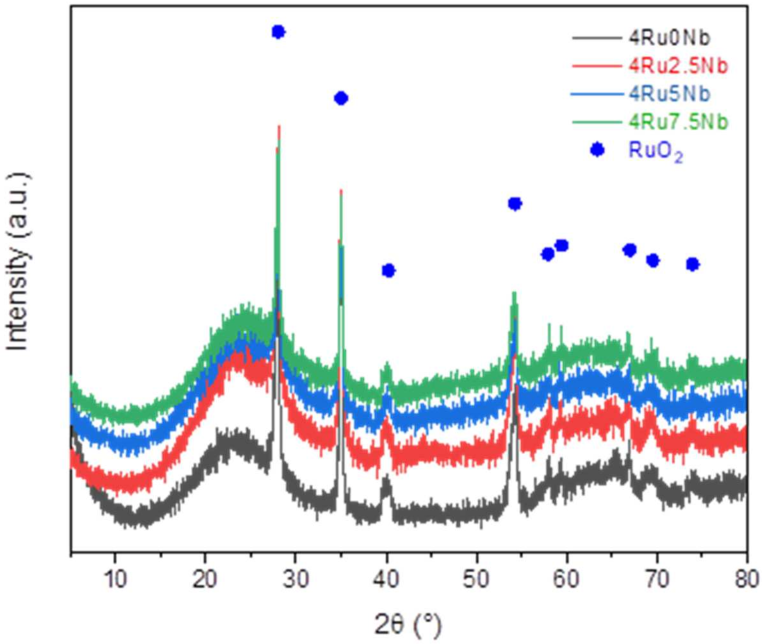

Figure 7.1. XRD patterns of gel-derived materials annealed at 500 °C for 2 h. The pattern of the corresponding 4Ru0Nb sample is also reported as a reference.

In the FTIR-ATR spectra of the annealed samples the main absorption bands at 1055 and 1200 cm^{-1} (Figure S1) are related to vibration modes of siloxanes (Si-O-Si) groups[166]. The bands at 795 and 1630 cm^{-1} are assigned to the symmetric stretch of Si-O-Si groups (vSi-O-Si) and to the bending mode of molecular water ($\delta_{O\text{-}H}$), respectively. Interestingly, the spectra of the samples containing niobium show a band at 950 cm^{-1} related to Si-O^{-}(Nb) bonds at the silica-niobia interface[167] indicating the enhanced interaction between SiO_4 tetrahedra and NbO_6 octahedra, which results into high niobium dispersion, in agreement with the XRD findings.. In the range 2850-3650 cm^{-1}, the spectra of all the samples exhibit a broad absorption band due to the O-H stretching mode of hydroxy groups involved in H bonding. The presence of OH-related bands indicates that the annealed samples adsorb water during cooling as a result of their porous nature. The DR UV-vis spectra (FigureS2) of the annealed samples containing niobium are dominated by the ligand-to-metal-charge-transfer transition band (LMCT from O^{2-} to Nb^{5+}) centred at about 245 nm. As the niobium content increases, the peaks position shift to slightly higher wavelengths and the absorption bands become a little wider indicating the presence of a wide distribution of NbO_6 octahedra (less or more distorted).

The surface areas, evaluated by the BET, together with micropore volumes are reported in Table 7.1.

The isotherms of all the annealed samples show an initial step increase at low P/P_0 values, owing to the presence of micropores, followed by a continuous increase of the adsorbed volume with increasing P/P^0 and a small hysteresis loop (especially evident in the isotherms of 4Ru0Nb and 4Ru2.5Nb), likely caused by the presence of some disordered mesopores.

According to the results, among the samples with the same content of ruthenium, the 4Ru0Nb catalyst displays the highest specific surface area (300 m^2g^{-1}) while a decrease can be observed in the samples containing niobium. Such behaviour can be related to the amount of Nb_2O_5 dispersed in silica, nevertheless at low Nb–Si ratio the niobium dispersion is very high and markedly decreases when the Nb loading is 6.9 wt%. Micropore volume is merely by niobium content.

7.3.2 Surface acidity properties

To assess the nature of acid sites on the surface of the synthesized materials a spectroscopic IR investigation was performed using NH_3 as probe molecule, because it can interact with both Brønsted acidic sites (by forming NH_4^+ ions) and Lewis acidic sites (by forming acidic–basic adducts). Its small size allows quantitatively probing of almost all acid sites inmicro-, meso-, and macro-porous oxides. The protonated species (NH_4^+ ions) and the coordinatively bonded NH_3 in Lewis adducts have different NH vibrations. In particular, the deformation vibrations (bending modes) at ca. 1450 and 1610-1630 cm^{-1} provide reliable indicators for the presence of protonated and coordinatively bonded NH_3, respectively.

Figure 7.2 reports difference spectra (after subtraction of the spectra of the bare samples, i.e., outgassed at 300 °C) concerning NH_3 adsorption (equilibrium pressure ca. 5.0 mbar) at r.t. on the annealed samples previously outgassed at 300 °C. To allow comparison, the spectra in Fig. 7.2 were normalized to sample unit weight, in such a way that the bands intensity of different samples can be compared. These spectra show that, in the absence of Nb a single band is observed at 1633 cm^{-1} (4Ru0Nb sample), readily ascribed to NH_3 molecules interacting with surface Si-OH species via H-bond, such OH groups being weakly acidic and, thus, unable to transfer a proton to NH_3, but able to H-bond the molecule at r.t..

Addition of Nb brings about the appearance of other two bands at ca. 1610 and 1456-1465 cm^{-1}. The former is assigned to the bending mode of NH_3 molecules adsorbed on coordinatively unsaturated Lewis (L) sites (e.g. Nb^{5+} ions), the latter to the bending mode of NH_4^+ species, formed upon interaction between NH_3 and (Nb-related) acidic -OH groups acting as Brønsted sites (B). Such bands were not removed by prolonged evacuation at r.t., but by outgassing the samples at 300 °C (spectra not shown). Since the spectra have been normalized to sample unit weight, a comparison of the relative intensity of the bands is allowed, showing that both intensities follow this trend: 4Ru2.5Nb < 4Ru7.5Nb < 4Ru5Nb. This trend also agrees with the total desorbed amounts of NH_3 measured by TPD later reported. Both L and B bands are less intense with 4Ru2.5Nb, showing that at low Nb loading the surface acidic sites are less abundant; moreover, the band due to the bending mode of the NH_4^+ species is seen at 1465 cm^{-1}, i.e. at lower wavenumbers than with the other two samples (4Ru5Nb and 4Ru7.5Nb), giving rise to a bending mode at 1456 cm^{-1}. The position of the bending mode is related to the strength of the interaction of NH_3 with surface OH groups, i.e. to their acidic strength showing that the 4Ru2.5Nb has weaker B sites. Considering the spectra in Fig. 7.2, the 4Ru5Nb catalysts seems to be the one containing more acidic sites, whereas at higher Nb loadings (4Ru7.5Nb) some Nb-related phenomena occur, which bring about an overall decrease of acidity. Further information can be found in the **Publication V.**

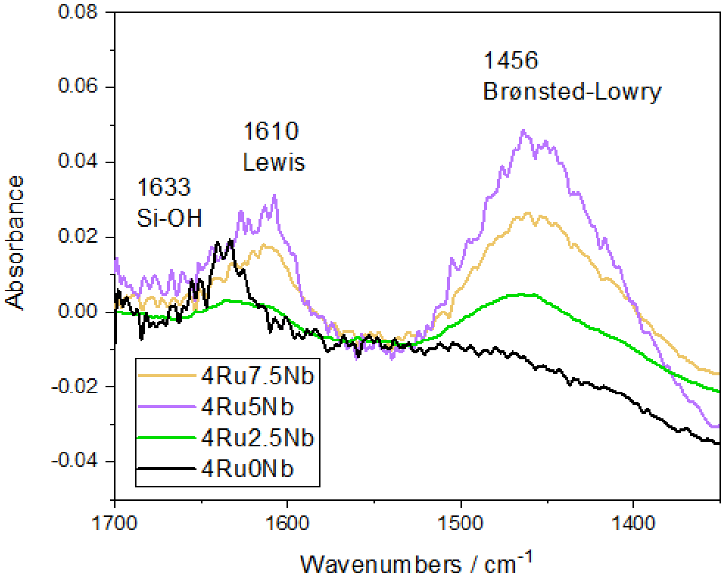

Figure 7.2. Difference FTIR spectra concerning the room temperature. adsorption of NH_3 (equilibrium partial pressure ca 5.0 mbar) on the samples previously outgassed at 300 °C. Spectra have been normalized to sample unit weight, in order to allow comparison.

The surface acidic properties of the synthesized materials were also analysed by NH_3 temperature-programmed desorption (TPD) experiments. The obtained values of the total amount of NH_3 desorbed are reported in Tab. 7.1. As can be seen, the trend of these values well agrees with the above IR analysis. As matter of fact, the acidity of 4Rb0Nb is very low, then we observe an increase of acidity with the increase of Nb content until a nominal concentration of 4.7%. The acidity then decreases for a further increase in Nb mount.

NH_3 TPD and FTIR spectroscopy studies point out that the composition, i.e. the Nb/Ru ratio, strongly influences the surface acidity of the catalysts, which suggest that a synergic interaction between Ru and Nb is established within the silica matrix.

7.3.3 Morphology and elemental distribution of both annealed and reduced materials

Both morphology and element distribution of both annealed (500 °C for 2 h) and reduced (300 °C under H_2 flow for 3 h) materials were investigated by FESEM. The aim was to obtain information on the dispersion of Ru and Nb as well as on their respective arrangements within the materials to disclose the interaction between the two elements.

FESEM representative images of the 4Ru2.5Nb catalyst (reduced sample) are shown in panels a and b of Figure 7.3, revealing Ru flower-like morphology in the presence of Nb. EDS maps of Si, O, Ru and Nb showed homogeneous distribution of the different elements at nanometric scale within the 4Ru2.5Nb catalyst, panel c of Figure 3.

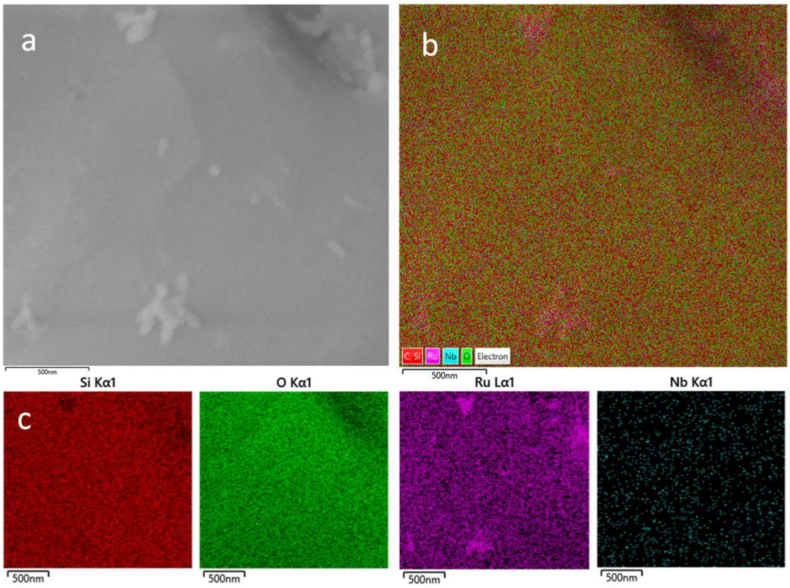

Figure 7.3. FESEM image (a) and EDS layered image (b) of the 4Ru2.5Nb catalyst. EDS maps of the region shown in a) for Si, O, Ru and Nb (c). Image collected at 25 kV with the standard SE detector. Instrumental magnification: 34000x

These findings were corroborated by measurements carried out at higher magnification (Figure 7.4), that highlighted the Nb dispersion at atomic level, whereas Ru is in the form of very small nanoparticles. These features put in evidence a close contact between the highly dispersed Nb and Ru species.

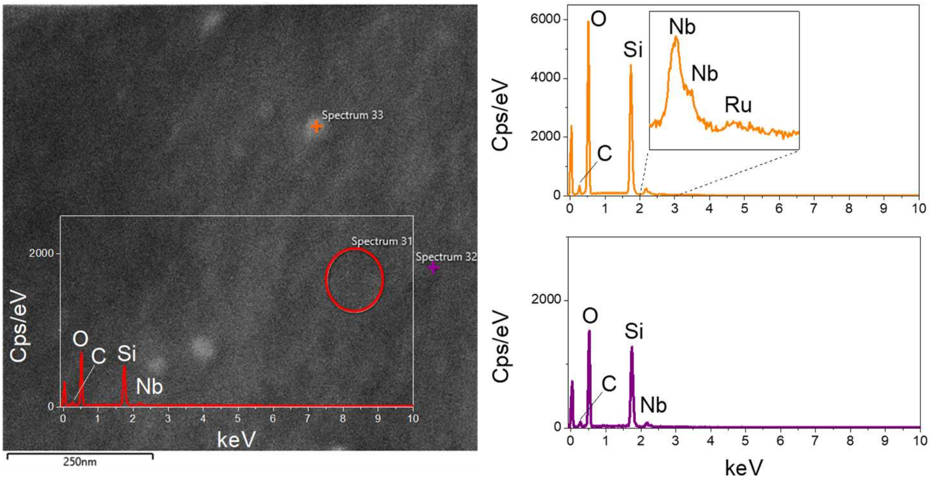

Figure 7.4. FESEM representative image of 4Ru2.5Nb catalyst and EDS spectra of selected points/regions. Image collected at 25 kV with the standard SE detector. Instrumental magnification: 261000x.

Morphology and element distribution were checked also in the case of both annealed and reduced 4Ru5Nb and 4Ru7.5Nb samples. Similar features were observed, as shown in Figure 7.5 and Figure 7.6, confirming that also in these cases, Ru is located in regions where the flower-like morphology is not present and that Nb is homogeneously dispersed within the materials, independently from the Ru amount in the catalysts. Further information can be found in the **Publication V.**

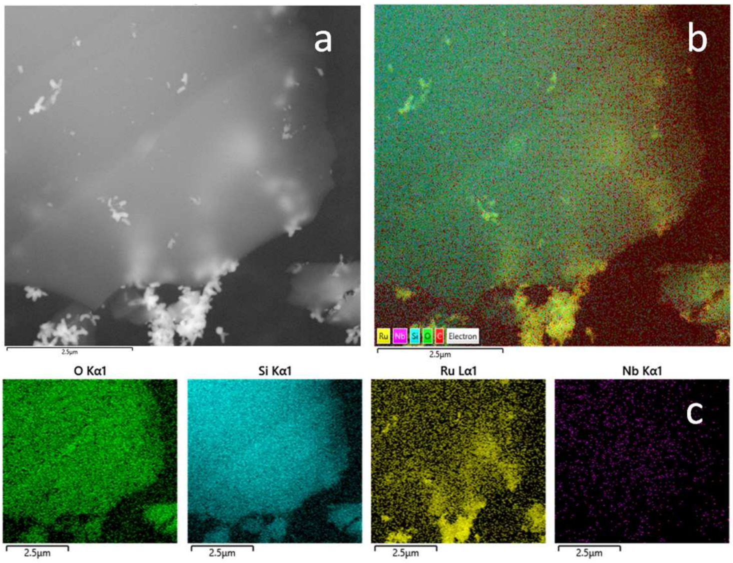

Figure 7.5. FESEM image of the 4Ru5Nb catalyst (a), EDS layered image (b) with the corresponding EDS maps O, Si, Ru and Nb (c). Image collected at 25 kV with the standard SE detector. Instrumental magnification: 30000x

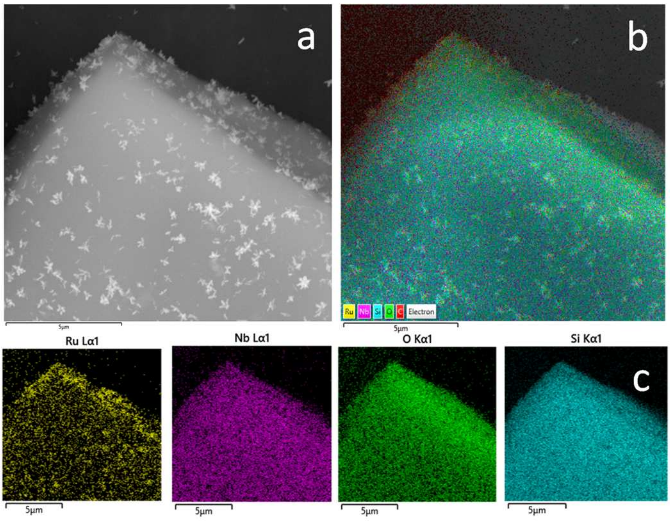

Figure 7.6. FESEM image of the 4Ru7.5Nb catalyst (a), EDS layered image (b) with the corresponding EDS maps of Ru, Nb, O, and Si (c). Image collected at 25 kV with the standard SE detector. Instrumental magnification: 15000x

In Table 7.1 the Nb/Ru ratios calculated on the basis of EDS maps (obtained as wt % of the different elements) are summarised for all ternary materials containing Nb. The ratios have been determined for both annealed and reduced catalysts.

Overall, the Nb/Ru increased with increasing the Nb loading and it is shown that, among the annealed samples, 4Ru2.5Nb has the lowest Nb/Ru ratio, meaning that in this case the lowest amount of Nb is located at the surface and/or close to the surface of the material.

Upon reduction at 300 °C, an increased Nb/Ru ratio was observed for all the catalysts, which could be an indication that Nb migrates toward the surface of the catalyst under reducing conditions, possibly affecting the dispersion of the highly dispersed Ru phase. Moreover, such enhancement was minimum for 4Ru2.5Nb and it was particularly evident for 4Ru7.5Nb. These features corroborated that the Nb species are highly and homogeneously dispersed on the 4Ru2.5Nb material either after oxidation at 500 °C or after reduction at 300 °C, in agreement with XRD and FTIR-ATR results. In addition, the ruthenium dispersion in the reduced materials was estimated by CO chemisorption and the results are summarized in Table 7.1.

The 4Ru0Nb catalyst, without niobium, shows the best ruthenium dispersion, whilst the ruthenium dispersion gets worse as the amount of Nb increases, in agreement with the characterization results showing the occurrence of strong mutual influence between the two elements. In conclusion, the observed interaction between Nb and Ru is depending on the composition and affects both metal dispersion and acidity of the bifunctional Ru-Nb-Si catalysts.

Further information can be found in the **Publication V.**

7.3.4 Catalyst screening for LA hydrogenation to GVL

The Ru-Nb-Si catalysts were tested in the hydrogenation of LA to GVL, under mild conditions and in aqueous environment. In Figure 7.7, the intermediate γ-hydroxypentanoic acid (HPA) and product (GVL) final concentrations (after 2 h) for each catalyst are displayed.

Using the 4Ru0Nb catalyst at the end of the reaction LA is completely converted into HPA and only traces of GVL was observed.

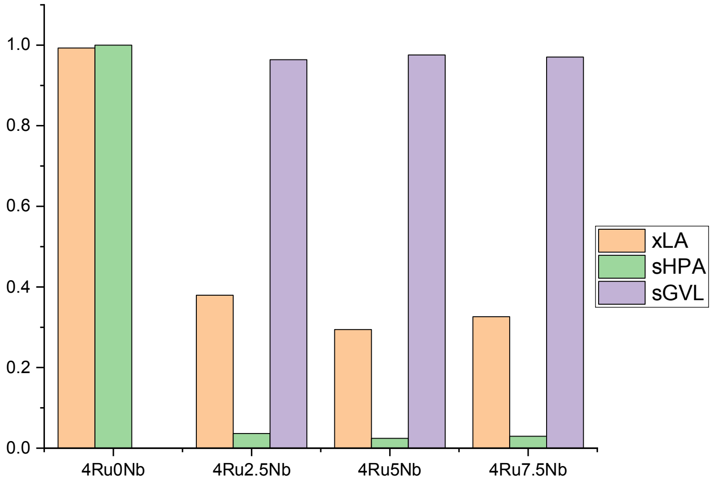

Figure 7.7. Conversion of LA and selectivity to GVL and HPA obtained for each catalyst.at 2h reaction (70 °C, P_{H2}= 20 bar, 200g water, 4.0 g LA, 0.5 g catalyst)

In the case of catalysts containing niobium the lactonization reaction of HPA to GVL was favoured with almost complete selectivity to GVL whereas different final LA conversion values were obtained with the increase of niobium content indicating that the yield to GVL is strongly influenced by the acid characteristics of the matrix.

The turnover frequency (TOF) per mole of ruthenium was calculated as the LA consumption rate referred to the number of moles of ruthenium, as shown in the following equation:

$$TOF_{Ru} = \frac{1}{n_{Ru}}\frac{dn_{LA}}{dt}$$

and the results obtained are shown in Table 7.2.

Table 7.2. TOF_{Ru} values and Kinetic constants calculated on the experimental data.

Catalyst	TOF_{Ru} (s^{-1})	k_1 [h^{-1}]	k_2 [h^{-1}]
4Ru0Nb	5.85×10^{-2}	2.20	0.01
4Ru2.5Nb	1.24×10^{-2}	0.26	8.76
4Ru5Nb	0.98×10^{-2}	0.25	29.40
4Ru7.5Nb	0.95×10^{-2}	0.25	29.90

The TOF_{Ru} values calculated on the LA reveal the influence of catalyst composition on LA conversation. However, to investigate quantitively the influence of morphology on both LA conversion and selectivity to GVL or HPA, deeper kinetic analysis of the data was performed. The kinetic data collected using the different Ru-Nb-Si catalysts were elaborated using a pseudo-homogeneous kinetic model, which considers that the reaction is in series, the reagent LA produces the intermediate HPA in the first step, and HPA is converted into the product GVL in the second step:

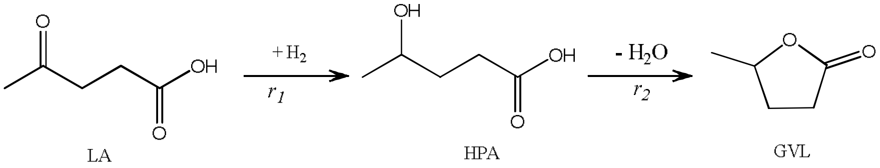

The rate of LA disappearance, r_1, is given by the equation:

$$r_1 = k_1 C_{LA} \tag{2}$$

The rate of disappearance of the intermediate HPA, r_2, is given by the equation:

$$r_2 = k_2 C_{HPA} \tag{3}$$

It is assumed that the kinetics are of the first order both in the first and in the second reaction step since the experiments were conducted in excess of hydrogen and both kinetic constants have physical dimensions equal to [h^{-1}]. The mass balance equation are as follows:

$$\frac{dC_{LA}}{dt} = -k_1 C_{LA} \tag{4}$$

$$\frac{dC_{HPA}}{dt} = +k_1 C_{LA} - k_2 C_{HPA} \tag{5}$$

$$\frac{dC_{GVL}}{dt} = + k_2 C_{HPA} \tag{6}$$

The two kinetic constants of the reactions, k_1 and k_2, were estimated and their values are displayed in Table 5.

In Figure 7.8, as an example, the comparison between experimental data and the concentration profiles obtained by the model is displayed for 4Ru2.5Nb.

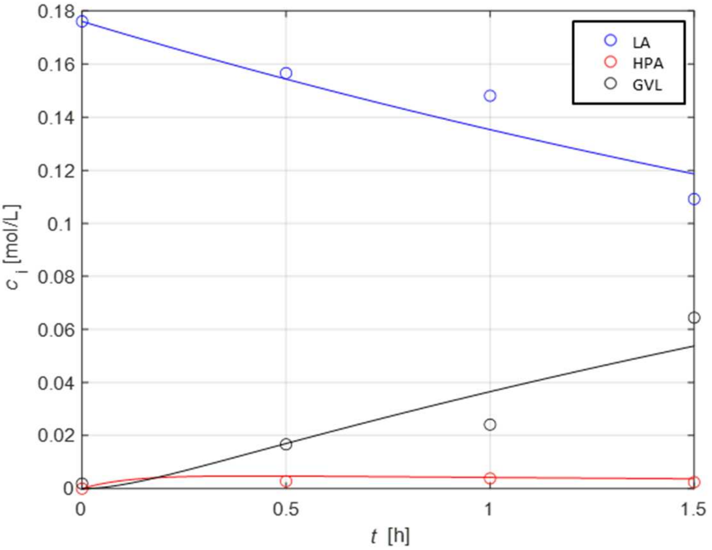

Figure 7.8. Experimental data and calculated concentration profile for 4Ru2.5Nb as catalyst. (70 °C, PH2= 20 bar, 200 g water, 4.0 g LA, 0.5 g catalyst)

The values of k_1 calculated well agree with both TOF_{Ru} ones (Table 7.2) confirming that the hydrogenation is mainly controlled by Ru dispersion. The hydrogenation activity is maximum for 4Ru0Nb catalyst and became lower with the decrease of dispersion (see also Table 7.1). An opposite trend is seen for the lactonization kinetic constant k_2 that is mainly favoured by the increasing niobium content and so by the increasing of the acidity of the surface.

It has to point out, the observed 100% selectivity of 4Ru0Nb catalyst to HPA with the complete conversion of LA. At our knowledge this is the first case where such results have been reported.

The silica support for ruthenium in the LA hydrogenation is not extensively used because ruthenium catalysts on silica prepared by impregnation are subject to irreversible deactivation for the sintering phenomena[5]. However, in addition to the acidity of the support, selectivity can also be inflected by reaction conditions. For example, Kuwahara et al, working at 70°C (as in this work) with a ruthenium catalyst supported by impregnation on silica, achieved a selectivity of 4% at HPA for a conversion of 88% LA. [6]

However, one must consider that in addition to the possible difference in acidity of the support, they used about 15 times higher concentration of LA and about 2.5 times higher concentration of catalyst. This certainly increases the acidity of the reaction environment.

Based on the above results, we explored the possibility to perform the whole transformation of LA to GVL by means of two separate and consecutive steps. In the former the LA hydrogenation to HPA takes place using the 4Ru0Nb catalyst and in the successive step the HPA dehydration to GVL occurs using a catalyst with suitable distribution of acid sites. For the latter step we used the $2.5Nb_2O_5 \cdot 97.5SiO_2$ catalyst.

A preliminary test was performed adopting the same reaction conditions described in section 7.2.3 for the first step, obtaining a liquid solution rich of HPA. This solution, in the consecutive step, was put in contact with the $2.5Nb_2O_5 \cdot 97.5SiO_2$ catalyst, obtaining very encouraging results: after 2h of reaction, HPA was fully converted in GVL, leading to no side product.

7.4 Conclusions

Bifunctional Ruthenium-Niobium-Silicon (RNS) mixed oxides-based catalysts, with different contents of ruthenium and niobium, were studied for LA hydrogenation to γ-valerolactone. With the aim of comparing the performance of the different RNS catalysts, tests were conducted in a fed-batch reactor under H_2 flow and the results were coupled with a multi technique characterization, in order to establish structure-activity relationships. The pre-reduced Ru containing catalysts demonstrated to be effective in the hydrogenation of LA to HPA, whereas for the successive lactonization reaction the presence of niobium is necessary as it is responsible of the increase of acidity of the catalyst. A competition between the two metals takes place at the material surface due to the migration of Ru and Nb species upon the reduction treatment before catalysis. This phenomenon is strongly connected with the different Nb/Ru ratios of the catalysts and therefore affects in different extent the Ruthenium dispersion, ruling as a consequence the hydrogenation activity. For the first time a catalyst and related conditions have been found to obtain 100% selectivity to HPA at complete conversion of LA.

References

[1] Yu, Z.; Lu, X.; Bai, H.; Xiong, J.; Feng, W.; Ji, N. Effects of Solid Acid Supports on the Bifunctional Catalysis of Levulinic Acid to γ -Valerolactone : Catalytic Activity and Stability. 2020, 1182–1201

[2] Turco, R.; Aronne, A.; Carniti, P.; Gervasini, A.; Minieri, L.; Pernice, P.; Tesser, R.; Vitiello, R.; M, D.S. Influence of preparation methods and structure of niobium oxide-based catalysts in the epoxidation reaction. *Catal. Today* **2015**, *254*, 99–103

[3] Velmurugan, P.; Shim, J.; Lee, K.-J.; Cho, M.; Lim, S.-S.; Seo, S.-K.; Cho, K.-M.; Bang, K.-S.; Oh, B.-T. Extraction, characterization, and catalytic potential of amorphous silica from corn cobs by sol-gel method. J. Ind. Eng. Chem. 2015, 29, 298–303

[4] Rossetti, I.; Bonelli, B.; Ramis, G.; Bahadori, E.; Nasi, R.; Aronne, A.; Esposito, S. New Insights into the Role of the Synthesis Procedure on the Performance of Co-Based Catalysts for Ethanol Steam Reforming. *Top. Catal.* **2018**, *61*, 1734–1745

[5] Abdelrahman, O.A.; Luo, H.Y.; Heyden, A.; Román-Leshkov, Y.; Bond, J.Q. Toward rational design of stable, supported metal catalysts for aqueous-phase processing: Insights from the hydrogenation of levulinic acid. *J. Catal.* **2015**, *329*, 10–21

[6] Kuwahara, Y.; Magatani, Y.; Yamashita, H. Ru nanoparticles confined in Zr-containing spherical mesoporous silica containers for hydrogenation of levulinic acid and its esters into γ-valerolactone at ambient conditions. *Catal. Today* **2015**, *258*, 262–269.

Conclusions

Starting from levulinic acid, it is possible to obtain bio-chemicals of high industrial interest: ethyl levulinate obtained by esterification reaction and γ-valerolactone, by hydrogenation reaction. The aim of this PhD thesis project was the study of the kinetic, catalytic and reactor aspects of the reactions mentioned above.

Some general conclusions can be drawn from the obtained results.

In the ***part A***, the esterification reaction was optimized by performing a catalyst screening, in batch reactor, of four ion exchange resins with different structure.

A kinetic study was conducted at the aim to evaluate the effect of the mass-transfer phenomena, developing a mathematical model that is in good agreement with the experimental data collected.

A general conclusion is that the developed model shown high flexibility and it was possible to simulate a large set of experiments, very useful for researchers in both academia and industry to design laboratory-scale and industrial-scale reactors.

Among the group of catalysts studied, two of them have showed the highest activity and they have been chosen for two different purposes of process intensification: a continuous operation in a fixed bed reactor and a reactive chromatography application; both successfully validate for LA esterification.

In the ***part B*** of this thesis work, bifunctional Ruthenium-Niobium-Silicon (RNS) mixed oxides-based catalysts, synthesized by sol-gel route, with different contents of ruthenium and niobium, were studied for LA hydrogenation to γ-valerolactone.

The aim was to clarify the role of both redox (Ru) and acid (Nb) sites in the reaction and the catalytic performances of the materials are related to a morphologic and structural characterization. The results confirm the hydrogenation-dehydration consecutive reaction network and evidence the possibility to selectively produce either GVL or the intermediate γ-hydroxypentanoic acid by an accurate choice of the catalyst composition.

Abbreviations

5-Cl-SHPAOs	5-chloro-sulfonated hyper branched poly-(arylene oxindole)s
5-HMF	5-hydroxymethylfurfural
A15-1	Amberlyst-15 (600 µm)
A15-2	Amberlyst-15 (300 µm)
BPA	Bisphenol A
$([BSmim]HSO_4)_4$	1-(4-sulfonic acid) butyl-3-methylimidazolium hydrogen sulphat
CTH	Catalytic transfer hydrogenation
DALA	δ-aminolevulinic acid
DOE/NREL	Department of Energy of the National Renewable Energy Laboratory Documents
DPA	Diphenolic acid
EL	Ethyl levulinate
EtOH	Ethanol
FID	Flame ionization detector
GVL	Gamma Valero lactone
H_2O	Water
HPLC	High Performance Liquid Chromatography
ILs	Ionic liquid
L	Liquid phase
LA	Levulinic acid
LAEs	Levulinic acid esters
MOF	Metal organic frameworks
MTHF	2-methyltetrahydrofuran
NREL	National Renewable Energy Laboratory
PID	Proportional Integral Derivative
PDE	Particle differential equation
RTD	Residence time distribution
S	Solid phase
SA	Succinic acid

List of symbols

A_μ, B_μ, C_μ, D_μ, E_μ	Viscosity coefficients of component *i*
A_ρ, B_ρ, C_ρ, D_ρ	Density coefficients of component *i*
a_{sp}	Specific surface area [m^2/m^3]
c_L	Concentration in liquid phase [mol/m^3]
c_S	Concentration in solid phase [mol/m^3]
$C_{W\text{-}P}$	Weisz-Prater criterion (W—P)
D	Molecular diffusivity [m^2/s]
D_e	Effective molecular diffusivity [m^2/s]
Dz	Axial dispersion coefficient [m^2/s]
ID	Internal diameter [m]
Ea	Activation energy [J/mol]
Gij	Interaction parameter [-]
J_S	Transport rate [$mol/(m^3\ s)$]
K	Equilibrium constant [–]

k_1	Self-catalyzed rate constant [(m^3/mol)^2/s]
k_2	Amberlyst-15 catalyzed rate constant [(m^3/mol)·(m^3/kg)·s^{-1}]
k_s	Fluid–solid mass transfer coefficient [m/s]
m	Partition coefficient [–]
$<m>$	Average value of the partition coefficient [–]
MW	Molecular weight [g/mol]
n_L	Amount of species in liquid phase [mol]
Pe	Péclet number [-]
R_1	Self-catalyzed reaction rate [mol/(m^3 s)]
R_2	Catalytic reaction rate [mol/(kg s)]
$r_{1,i}$	Component self-catalyzed generation rate [mol/(m^3 s)]
$r_{2,i}$	Component catalytic generation rate [mol/(kg s)]
Re	Reynolds number [-]
Rg	Ideal gas constant [J/(K mol)]
R_P	Particle radius [m]
R_{Pdry}	Dry particle radius [m]
T	Temperature [K]
t	Time [s]
v	Stirring rate [rpm]
$\dot{\mathrm{V}}$	Flow rate [m^3/s]
Vads	Volume of liquid retained by the resins [m^3]
$\mathrm{V}_{\mathrm{dryAmb}}$	Volume of the dry resin [m^3]
V_L	Liquid volume [m^3]
x	Dimensionless radial coordinate of the spherical particle [–]
x_i	Molar fraction [–]
X_{LA}	Conversion of levulinic acid [–]
w_{cat}	Catalyst mass [kg]
ΔH	Reaction enthalpy [J/mol]
ΔP	Pressure difference [Pa]
α_{sw}	Swelling coefficient [%]
ε	Take-up factor [–]
ε_1	Volumetric ratio between the solid and the liquid phases [–]
μ	Viscosity [cP]
μ_{mix}	Viscosity of the reaction mixture [cP]
v_i	Stoichiometric coefficient [–]
ρ_i	Density [kg/m^3]
ρ_B	Catalyst bulk density (mass of catalyst/ volume) [kg/m^3]
ρ_P	Amberlyst-15 density [kg/m^3]
τ	Tortuosity of the Amberlyst-15 particle [–]
ϕ	Association factor [–]
η	Reaction efficiency [–]

Publications

Chemical Engineering Science 228 (2020) 115974

Contents lists available at ScienceDirect

Chemical Engineering Science

journal homepage: www.elsevier.com/locate/ces

Intraparticle diffusion model to determine the intrinsic kinetics of ethyl levulinate synthesis promoted by Amberlyst-15

Vincenzo Russo [a,b,*], Carmelina Rossano [a], Emiliano Salucci [a], Riccardo Tesser [a], Tapio Salmi [b], Martino Di Serio [a,c]

[a] Università degli Studi di Napoli Federico II, Complesso Universitario M.S. Angelo, IT-80126 Napoli, Italy
[b] Johan Gadolin Process Chemistry Centre, Laboratory of Industrial Chemistry and Reaction Engineering, Åbo Akademi University, FI-20500 Turku/Åbo, Finland
[c] IROAST, Kumamoto University, JP-43201-6 Kumamoto, Japan

HIGHLIGHTS

- Ethyl levulinate formation kinetics promoted by Amberlyst-15.
- Kinetics and mass transfer phenomena were considered.
- Liquid take-up and fluid–solid partition were measured.
- Intraparticle modelling was adopted.
- Intrinsic reaction kinetics was revealed.

GRAPHICAL ABSTRACT

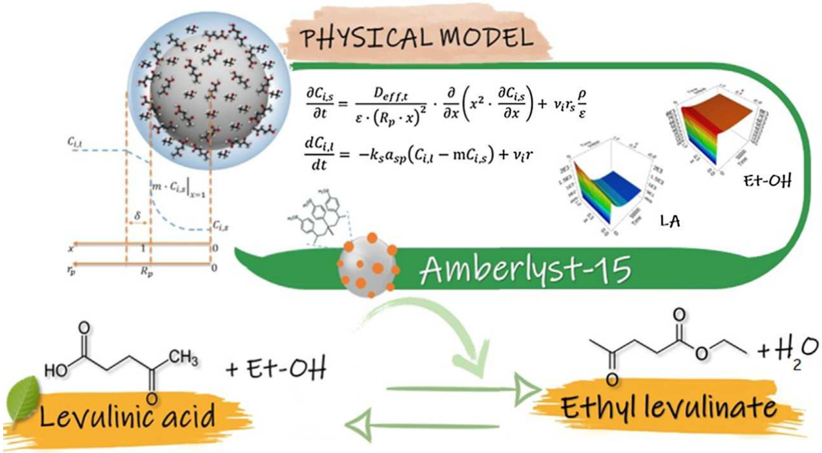

ARTICLE INFO

Article history:
Received 10 April 2020
Received in revised form 8 June 2020
Accepted 12 July 2020
Available online 15 July 2020

Keywords:
Levulinic acid
Ethyl levulinate
Amberlyst-15
Modelling
Kinetics
Mass transfer

ABSTRACT

Levulinic acid and its esters are considered very versatile chemical compounds used for a wide range of derivatives. Traditionally ethyl levulinate is synthesized in batch reactors, using homogeneous catalysts (H_2SO_4, H_3PO_4). Several investigations were reported on solid acid catalysts, as zeolites, sulfated oxides, sulfonic ion-exchange resins. Amberlyst-15 showed high potentials: to design a continuous reactor, it is necessary to investigate the stability of the catalyst and the kinetics of the reaction. In the present work, we demonstrated that the resin is stable for more than 5 days. Kinetic and mass transfer phenomena were studied, evaluating the partition and take-up of the used resin when put in contact with reactants and products. Two different samples of Amberlyst-15 were used, characterized by different size, demonstrating that bigger particles lead to higher intraparticle diffusion limitations.

1. Introduction

The continuous consumption of fossil fuel resources and increasing energy demand worldwide has led to considerable

---

* Corresponding author at: Università degli Studi di Napoli Federico II, Complesso Universitario M.S. Angelo, IT-80126 Napoli, Italy.
E-mail address: v.russo@unina.it (V. Russo).

https://doi.org/10.1016/j.ces.2020.115974
0009-2509/

Nomenclature

Abbreviations

A15-1	Amberlyst-15 (600 μm)
A15-2	Amberlyst-15 (300 μm)
EtLA	Ethyl levulinate
EtOH	Ethanol
FID	Flame ionization detector
H_2O	Water
L	Liquid phase
LA	Levulinic acid
S	Solid phase

List of symbols

A_μ, B_μ, C_μ, D_μ, E_μ	Viscosity coefficients of component *i*
A_ρ, B_ρ, C_ρ, D_ρ	Density coefficients of component *i*
a_{sp}	Specific surface area [m^2/m^3]
c_L	Concentration in liquid phase [mol/m^3]
c_S	Concentration in solid phase [mol/m^3]
D	Molecular diffusivity [m^2/s]
D_e	Effective molecular diffusivity [m^2/s]
Ea_j	Activation energy of reaction *j* [J/mol]
f	Objective function
J_S	Transport rate [mol/(m^3 s)]
K	Equilibrium constant [–]
k_1	Self-catalyzed rate constant [$(m^3/mol)^2/s$]
k_2	Amberlyst-15 catalyzed rate constant [$(m^3/mol)\cdot(m^3/kg)\cdot s^{-1}$]
$k_{1,ref}$	Self-catalyzed reference rate constant [$(m^3/mol)^2/s$]
$k_{2,ref}$	Amberlyst-15 catalyzed reference rate constant [$(m^3/mol)\cdot(m^3/kg)\cdot s^{-1}$]
k_s	Fluid–solid mass transfer coefficient [m/s]
m	Partition coefficient [–]
$<m>$	Average value of the partition coefficient [–]
MW	Molecular weight [g/mol]
N_e	Number of experiments [-]
$N_{data,l}$	Number of experimental data in experiment *l* [-]
n_L	Amount of species in liquid phase [mol]
R_1	Self-catalyzed reaction rate [mol/(m^3 s)]
R_2	Catalytic reaction rate [mol/(kg s)]
$r_{1,i}$	Component self-catalyzed generation rate [mol/(m^3 s)]
$r_{2,i}$	Component catalytic generation rate [mol/(kg s)]
R	Ideal gas constant [J/(K mol)]
R_P	Particle radius [m]
R_{Pdry}	Dry particle radius [m]
T	Temperature [K]
T_{ref}	Reference temperature [K]
t	Time [s]
v	Stirring rate [rpm]
V_{ads}	Liquid volume retained by the catalyst [m^3]
V_{dryAmb}	Volume of dry catalyst [m^3]
V_L	Liquid volume [m^3]
V_{tot}	Total volume of the resin after swelling [m^3]
x	Dimensionless radial coordinate of the spherical particle [–]
x_i	Molar fraction [–]
X_{LA}	Conversion of levulinic acid [–]
w_{cat}	Catalyst mass [kg]
ΔH	Reaction enthalpy [J/mol]
ε	Take-up factor [–]
ε_1	Volumetric ratio between the solid and the liquid phases [–]
ε_p	Catalyst porosity [–]
μ	Viscosity [cP]
μ_{mix}	Viscosity of the reaction mixture [cP]
ν_i	Stoichiometric coefficient [–]
ρ_i	Density [kg/m^3]
ρ_B	Catalyst bulk density (mass of catalyst/ volume) [kg/m^3]
ρ_P	Amberlyst-15 density [kg/m^3]
τ	Tortuosity of the Amberlyst-15 particle [–]
ϕ	Association factor [–]
η	Reaction efficiency [–]

Subscripts and superscripts

cat	Catalyst
EXP	Experimental data
i	Component
j	Reaction
l	Experiment
p	Experimental data
ref	Reference
SIM	Simulation

attention the conversion of biomass and its derivatives due to the possibility of becoming an alternative source for the sustainable production of chemicals and fuels (Cirujano et al., 2015). Lignocelluloses, the most abundant biomass in the world (Chun et al., 2009), can be depolymerized to monosaccharide and converted into various platform chemicals, such as 5-hydroxymethyl furfural, formic acid, and levulinic acid (LA) (Yabushita et al., 2014). LA is one of the top platform chemicals, for its versatile chemistry (Zavozin et al., 2010). The technology to produce bio-based levulinic acid is straightforward, as it can be obtained by hydrolysis of cellulose in the presence of acid catalysts (Lourvanij and Rorrer, 1994). Recently, a process called Biorefine was developed, where diluted sulfuric acid is utilized in the fractionation of lignocellulosic material (Hayes et al., 2006). Alkyl levulinates, such as ethyl levulinate (EtLA), are of particular interest due to their specific physicochemical properties. They find applications as specialty chemicals and in petrochemical industries (Yadav and Yadav, 2014). Addition of EtLA to diesel fuel modifies the fuel properties such as a clean burning fuel with high lubricity, stability in flash-point, improvement in viscosity (Yadav and Yadav, 2014). Levulinic acid esters can be obtained by esterification in the presence of mineral homogenous acid catalysts, such as sulfuric or phosphoric acids (Liu et al., 2006; Bart et al., 1994). The use of homogeneous acid catalyst implies several drawbacks, e.g. corrosion and separation issues. The use of solid acid catalysts is more desirable as they are easier to be recovered and reuse, there is no need for neutralization, and corrosion is limited. Among the solid acid catalysts heteropoly acids (HPAs) (Nandiwale et al., 2013; Pasquale et al., 2012; Yan et al., 2013), zeolites (Patil et al., 2014), sulfated oxides (Fernandes et al., 2012) and ion exchange have been tested (Fernandes et al., 2012; Ramli and Amin, 2017). Despite the industrial interest, few kinetic investigations have been published in the literature on the ethyl levulinate synthesis. In our previous work, a detailed kinetic study was conducted in the presence of homogeneous (H_2SO_4) and heterogeneous catalysts (Smopex-101), underlying also the influence of the autocatalytic extent of the reaction, i.e. in the absence of the catalyst. A kinetic model for both types of catalysts was proposed (Russo et al., 2018) and it was successfully applied to describe experiments conducted both in batch and in continuous reactors. Smopex-101 showed a good activity in the ethyl levulinate synthesis, but the commercial price of such a catalyst is rather high and, currently, it is not available anymore. For this reason, an industrial application of such catalyst is not feasible. Zeolites are low cost materials (prize for laboratory application 0.1€/g (https://www.sigmaaldrich.com/) but Fernandes et al (Fernandes et al., 2012) showed that all of the zeolites tested for ethyl levulinate synthesis (HZSM-5, HUSY, HMCM-22) showed low activity (levulinic acid conversion lower than 15%). Amberlyst-15, an available commercial low-cost ion exchange-resin, is a good candidate as catalyst for the levulinic acid esterification reaction, due to the strong acidity provided by -SO_3H functional groups and as it is cheapest available commercial ion exchange-resin (prize for laboratory application 0.1€/g compared with 0.2€/g for Amberlite IR120 (https://www.sigmaaldrich.com/).

The growing interest of Amberlyst-15 is due to the acidic properties and find various application in different chemical transformations in, for example, transesterification, Friedel-Crafts alkylation, halogenation, hydroalkylation. Previous studies demonstrated that Amberlyst-15 was successfully used to conduct the esterification of several carboxylic acids, both short and long chained (Shahid et al., 2018; Banchero and Gozzellino, 2018; Nguyen et al., 2018; Lamba et al., 2018; Hykkerud and Marchetti, 2016), also tested to produce ethyl levulinate (Fernandes et al., 2012; Ramli and Amin, 2017; Su et al., 2014). Furthermore, it was demonstrated that the activity of Amberlyst-15 was practically constant after four reaction cycles (Ramli and Amin, 2017).

For the mentioned reasons, Amberlyst-15 is a good candidate for an eventual industrial application, that would require a dedicated kinetic investigation. Despite the high potential of this catalyst and the availability of pseudohomogeneous and LHHW heterogeneous kinetic models for esterification reactions using Amberlyst-15 as catalyst (Banchero and Gozzellino, 2018; Lamba et al., 2018), intrinsic rate expressions for the esterification reaction between levulinic acid and ethanol catalyzed by Amberlyst-15 are inexistent. Therefore, when trying to reveal the intrinsic kinetics of a reaction, attention must be paid on the occurrence of mass transfer limitations, i.e. fluid–solid and intraparticle, with a more sophisticated approach (Di Serio et al., 2017).

The endeavour of this work was to study in depth the esterification kinetics of levulinic acid with ethanol in the presence of Amberlyst-15 as the solid catalyst. Experiments were carried out in an isothermal batch reactor, varying the operating conditions (i.e. stirring rate, temperature, catalyst loading, molar ratio of the reagents). Take-up and partition tests were conducted on Amberlyst-15 in order to evaluate parameters such as the swelling ratio and the partition coefficients. A reactive model was developed including both kinetic and mass transfer phenomena, paying attention on both fluid–solid external and internal diffusion limitations, using two types of Amberlyst-15, characterized by different mean size, in order to have a better control on the intraparticle diffusion limitation. With this approach, the intrinsic kinetics of ethyl levulinate synthesis promoted by Amberlyst-15 was obtained, determining realistic kinetic parameters, that in perspective will allow to design more accurately dedicated pilot plants.

2. Materials and methods

2.1. Materials

All the used reactants were purchased from Sigma Aldrich at the highest purity available. Two different samples of Amberlyst-15 commercially available were tested to investigate the ethyl levulinate synthesis. The two catalysts differ in size (A15-1: 600 μm; A15-2: 300 μm). A15-1 was purchased from Acros Organics, while A15-2 was obtained from Sigma Aldrich. The main properties of both catalysts are reported in Table 1.

2.2. Methods

2.2.1. Esterification

The esterification reactions were carried out in a Hastelloy reactor with a capacity of 200 mL, equipped with an external heating jacket connected to a thermoregulator to keep the reaction temperature at the value desired. A magnetic stirrer on the top of the reactor allowed stirring the reaction mixture at the desired rate (100–600 rpm). Nitrogen was used as an inert gas to maintain constant pressure (5 bar), preventing the evaporation of the lower boiling components (i.e. ethanol 351.15 K) at the operating temperatures. Samples were withdrawal by using a pin valve. A stainless-steel filter of 50 μm mesh was installed on the sampling line to prevent catalyst loss during the sampling procedure. Different experiments were conducted by varying the most important variables to investigate both kinetic and mass transfer effects occurring in the reaction network. The summary of the adopted experimental conditions for each kinetic experiment is given in Table 2. The initial concentrations were measured as the reaction already progressed during the pre-heating time, thus a certain amount of ethyl levulinate was present as the set temperature was reached.

The classical experimental procedure to conduct the esterification experiments is described here. The heterogenous catalyst was pretreated in an oven at 333.15 K (6–8 h), to eliminate water, avoiding the shift of the chemical equilibrium in the ethyl levulinate synthesis. The reactor vessel was loaded with a fixed amount of ethanol and levulinic acid at a given molar ratio (5:1, 3:1 or 1:1), to which the catalyst was added. The system was therefore well sealed and exposed to nitrogen pressure. The impeller was switched on, and the temperature of the reactor was regulated through a thermoregulator at the desired level. Once the operating temperature was reached, the first sample was taken through the sampling valve, thus starting to investigate the esterification kinetics. The next sample was withdrawal after the first 15 or 30 min and at regular intervals of one hour after the first. The amount of liquid withdrawn for each sample was less than 0.5 cm^3, thus the sampling procedure did not affect the liquid-catalyst ratio inside the reactor. Each sample was analyzed by acid-base titration using standardized 0.1 M NaOH as titrating agent and phenolphthalein as indicator, whereas the concentration of ethyl levulinate was determined by GC (HP 6890 Series) using a column ZB-Wax and an FI detector. The determined relative response factors for each component were: 0.18 for ethanol, 0.13 for ethyl levulinate and 1.00 for levulinic acid. The retention times for each component were: 5.6 min for ethanol, 7.0 min for ethyl levulinate and 11.3 min for levulinic acid. Both titration and GC analysis were conducted on each sample to confirm the obtained results. Two re-use experiment sets were conducted adopting the experimental conditions as Tests 4 and 15. Each experiment was repeated 5 times recovering the catalyst at the end of the reaction and reusing it as such after filtration, to verify the stability of the catalyst.

2.2.2. Take-up and partition experiments

Take-up experiments were conducted by putting in contact in a graduated cylinder of 10 mL (±0.1 mL) 3 mL of dry Amberlyst-15 with 5 mL of one of the four reactants comprising the chemical system. From the volume increase of the catalyst packing it was possible to calculate the take-up factor.

Partition coefficients were measured by preparing solutions of reactants/products at different molar ratio, simulating samples characterized by different levulinic acid conversions. The tests

Table 1
Physical properties of the used Amberlyst-15 catalysts.

	Particle size [µm]	Ionic form	Active sites concentration [eq/L]	Crosslinking degree [%]	Surface area [m^2/g]	Pore diameter [Å]	Pore volume [mL/g]	ρ_{Int}[kg/m^3]
A15-1	600	Hydrogen	1.7	20	53	300	0.4	600
A15-2	300	Hydrogen	1.6	20	45	300	0.4	600

Table 2
Operation conditions adopted to conduct the kinetic study. *Re-use experiments.

Test	ν [rpm]	$c_{LA,0}\cdot10^3$[mol/m^3]	$c_{EtOH,0}\cdot10^3$[mol/m^3]	$c_{EtLA,0}\cdot10^3$[mol/m^3]	$c_{H2O,0}\cdot10^3$[mol/m^3]	T[K]	Amberlyst-15	ρ_B[kg/m^3]
1	100	2.43	12.60	0.11	0.11	343.15	A15-1	22.04
2	200	2.38	12.55	0.16	0.16	343.15	A15-1	22.04
3	400	2.37	12.54	0.17	0.17	343.15	A15-1	22.05
4*	600	2.39	12.56	0.15	0.15	343.15	A15-1	22.04
5	600	2.44	12.61	0.10	0.10	323.15	A15-1	22.03
6	600	2.41	12.58	0.13	0.13	333.15	A15-1	22.03
7	600	2.29	12.46	0.25	0.25	363.15	A15-1	22.02
8	600	2.41	12.58	0.13	0.13	343.15	A15-1	11.04
9	600	2.38	12.55	0.16	0.16	343.15	A15-1	16.53
10	600	2.34	12.51	0.20	0.20	343.15	A15-1	44.07
11	600	6.0	6.01	0.23	0.23	343.15	A15-1	25.34
12	600	3.43	10.66	0.18	0.18	343.15	A15-1	23.01
13	200	2.49	12.66	0.05	0.05	343.15	A15-2	22.65
14	400	2.45	12.59	0.10	0.10	343.15	A15-2	22.69
15*	600	2.35	12.52	0.19	0.19	343.15	A15-2	22.65
16	800	2.38	12.54	0.17	0.17	343.15	A15-2	22.69
17	600	2.46	12.63	0.08	0.08	323.15	A15-2	22.66
18	600	2.36	12.53	0.18	0.18	333.15	A15-2	22.62
19	600	2.54	12.71	0.00	0.00	333.15	A15-2	13.63
20	600	2.35	12.53	0.19	0.19	333.15	A15-2	14.00
21	600	3.44	10.64	0.18	0.18	333.15	A15-2	22.94
22	600	5.22	5.22	1.02	1.02	333.15	A15-2	22.77

were conducted at room temperature in a single-necked glass flask, in which they about 2.5 g of dry catalyst was placed in contact with 20 mL of liquid solution for 30 min. Samples were withdrawn to check when the system reached the equilibrium conditions, analyzed via GC-FID method. The details of the method are here reported: column Zebron ZB-WAX, stationary phase: 100% polyethylene glycol, L = 60 m, ID = 0.32 mm, film thickness = 0.25 µm, detector: FID, carrier He, injector temperature: 250 °C, detector temperature 250 °C, column pressure 14psi, temperature ramp: 150 °C for 0 min, heating at 20 °C/min up to 250 °C, temperature isotherm for 25 min. Measured retention times: levulinic acid 11.3 min, ethanol 5.6 min, ethyl levulinate 6.9 min. The water content in the samples was determined by Karl-Fischer titration using Hydranal KetoSolver Hydranal Composite 5 K as a titration reagent.

3. Results and discussion

3.1. Kinetic experiments

Several experiments were conducted with Amberlyst-15 as the catalyst, investigating a wide range of operation conditions (i.e. stirring rate, temperature, catalyst load, reactant ratio) and the catalyst stability as well. In every case, it was demonstrated by GC analysis that the unique product obtained from the reaction is ethyl levulinate, thus no side reactions take place in the adopted reaction conditions.

The first kinetic experiments were carried out to evaluate the effect of stirring on the reaction rate (experiments 1–4 and 13–16 of Table 2). It is expected that, as the stirring rate increases, the thickness of the stagnant film of the catalyst particle decreases, on the other hand, if the stirring rate is sufficiently high, the external diffusion of the reagents to the catalyst particle is no longer limiting. The results are reported in Fig. 1 in terms of the initial reaction rate vs the stirring rate. It was observed that the reaction rate increases with increasing stirring rate and for both the ion exchange resins, external diffusion limitation is not observed at stirring rates exceeding 600 rpm. This fact clearly indicates that the thickness of the stagnant liquid film surrounding the particle becomes negligible and the concentration of both reactants and products on the solid surface is equal to the one in the liquid bulk

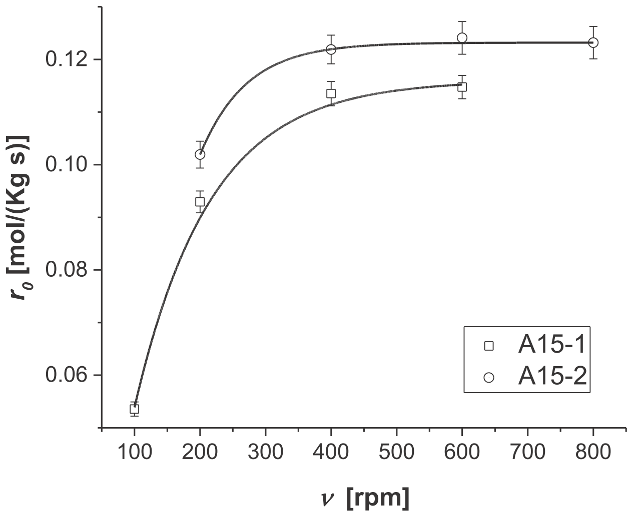

Fig. 1. Effect of stirring rate on the levulinic acid esterification initial rate, catalyzed by A15-1 and A15-2, by fixing the ethanol-to-levulinic acid molar ratio of: 5:1 at T = 343.15 K and at ρ_B = 22 kg/m^3. Symbols are the experimental data, lines the calculated profiles.

phase. Moreover, by using the two catalysts, different plateaus are observed (i.e. lower for higher particle radius), suggesting the occurrence of intraparticle mass transfer limitations for at least the catalyst characterized by the highest value of the radius (A15-1). The presence of different plateau values is a clear indication of intraparticle concentration profiles, as for bigger particle the diffusive path that the molecules should run across is longer compared to the one available for smaller particles. For bigger particles, the average concentrations of reactants become naturally lower than the ones obtainable for smaller particles, due to the parabolic trend of the concentration profiles inside the catalyst, leading to the smaller observed reaction rate plateau that can be observed in Fig. 1.

Two sets of re-use experiments were conducted at the optimal stirring rate, using the two available resins, to investigate the stability of the catalysts. In particular, the experimental conditions were fixed as for Test 4 and 15 of Table 2. The results are reported in Fig. 2, showing that both resins are stable for 5 days of operation as the curves are practically overlapped. Of course, in perspective the catalyst should be tested in a continuous device to check the real stability for long time on stream.

Kinetic experiments were conducted varying the temperature (experiments 2, 5–7 and 16–18 of Table 2). At each temperature, the chemical equilibrium was reached at long reaction times (usually more than 24 h), thus it was necessary to prolong the experiment overnight to determine the equilibrium constant at each temperature. For both ion exchange resins, a similar equilibrium conversion was observed with identical operation conditions; a maximum equilibrium conversion of 91% was obtained when working at 600 rpm, T = 363.15 K with ρ_B = 22.02 kg/m^3 and an EtOH:LA molar ratio of 5:1. By increasing the temperature, an enhancement of the reaction rate was always observed (Fig. 3). Furthermore, experiments were carried out to evaluate the effect of the Amberlyst-15 load on the esterification rate (experiments 2, 8–10 and 18, 19 of Table 2). Fig. 4 reveals that by increasing the catalyst bulk density in the reactor, the reaction rate increased. An interesting result is displayed in Fig. 5. As it can be seen from the figure, by multiplying the reaction time per the Amberlyst-15 bulk density, the experimental data overlap. This implies that the reaction kinetics is linearly dependent respect to the Amberlyst-15 amount for both catalysts. This plot also confirms the absence of external mass transfer limitations around the particle, as confirmed also by the results reported in Fig. 1.

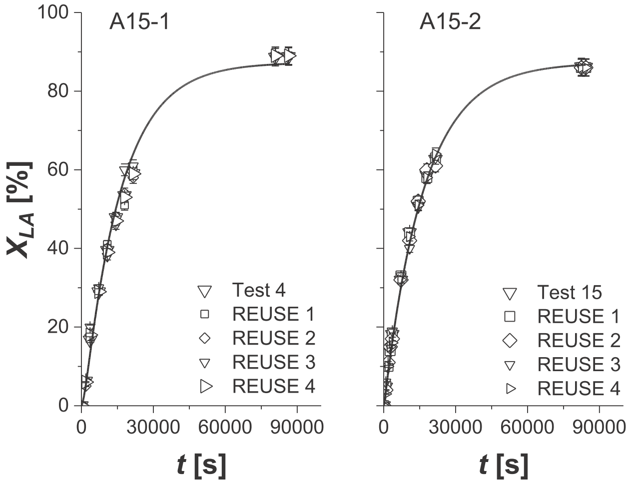

Fig. 2. Reuse experiments on both A15-1 (left) and A15-2 (right). Experimental conditions: ethanol-to-levulinic acid molar ratio 5:1, T = 343.15 K, ρ_B = 22 kg/m^3 and v = 600 rpm.

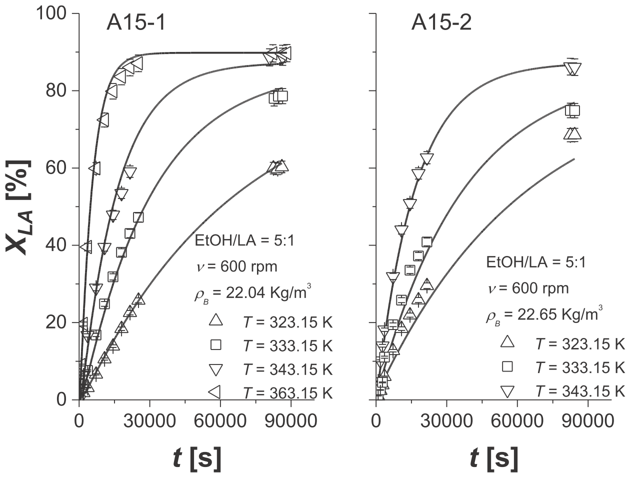

Fig. 3. Effect of temperature on the levulinic acid esterification catalyzed by A15-1 (left) and A15-2 (right) by fixing the ethanol-to-levulinic acid molar ratio of: 5:1, ρ_B = 22 kg/m^3 and v = 600 rpm. Symbols are the experimental data, lines the calculated profiles.

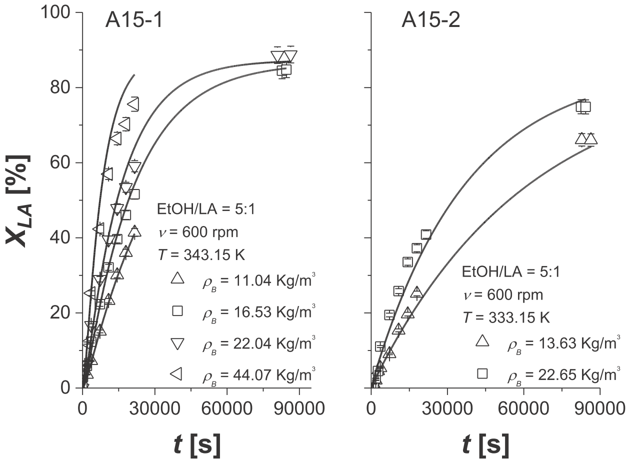

Fig. 4. The effect of the Amberlyst-15 density on the levulinic acid esterification by fixing the ethanol to-levulinic acid molar ratio of: 5:1, v = 600 rpm and (left) at T = 343.15 K; (right) at T = 333.15 K. Symbols are the experimental data, while lines the calculated values.

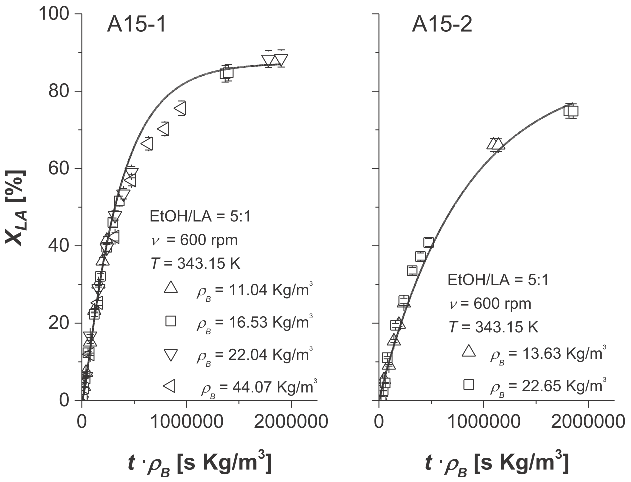

Fig. 5. Fig. 4 redrawn normalizing the reaction time per the Amberlyst-15 bulk density. Symbols correspond to the experimental data, lines to the calculated values.

The molar ratio effect on the reagents was evaluated on the reaction rate by conducting dedicated experiments (experiments 2, 11, 12 and 18, 21, 22 of Table 2). The experiments carried out by fixing the different ethanol-to-levulinic acid molar ratios demonstrated that by increasing the ethanol content, higher ethyl levulinate concentrations were obtained as shown in Fig. 6.

3.2. Take-up and partition experiments

The take-up experiments were useful to determine the take-up factor (ε), necessary for the description of the experimental data. The take-up factor of the Amberlyst-15 was determined at varying of the molar fractions of the components, in according to Eq. (1).

$$\varepsilon = \frac{V_{dryAmb}}{V_{dryAmb} + V_{ads}} \tag{1}$$

where the take-up (ε) factor is defined by the ratio between the volume of the dry resin (V_{dryAmb}) divided by total volume of the resin after the swelling, thus the sum of the volumes of the dry catalyst (V_{dryAmb}) and the liquid retained by the resin itself (V_{ads}).

The results of the take-up experiments of Amberlyst-15 shown an average for all the investigated binary solutions of 0.5.

The partition tests were useful for the determination of the partition coefficients for LA and EtOH, i.e. the parameters necessary to determinate the real concentration of each reactant/product in the catalyst pores. The partition coefficients were calculated according to Eq. (2).

$$m_i = \frac{c_i}{c_{i,A15}} \tag{2}$$

where c_i is the concentration of the component before the partition test and $c_{i,A15}$ is the concentration of the same component after the treatment. The determined partition coefficients are collected in Table 3, for different solutions prepared by simulating different levulinic acid conversions. The average values of the partition coefficients were determined.

3.3. Modelling

3.3.1. Chemical-physical properties

The dependence on the liquid density of the temperature for each single component was evaluated, according to the empirical expression retrieved from CHEMCAD database (CHEMCAD);

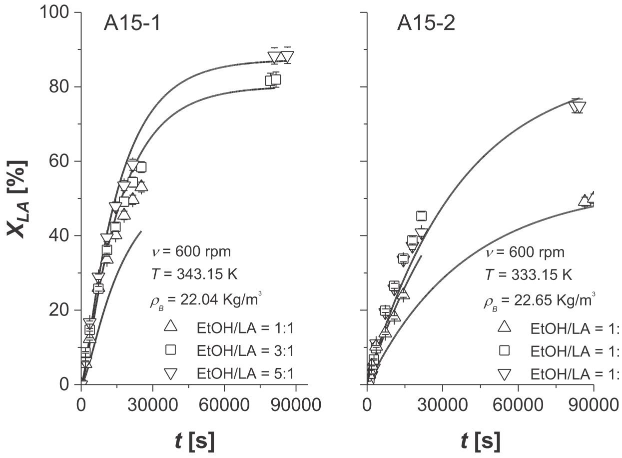

Fig. 6. The effect of the ethanol-to-levulinic acid molar ratio on the levulinic acid esterification by fixing the other variables: ρ_B = 22 kg/m^3, at ν = 600 rpm and (left) at T = 343.15 k; (right) at T = 333.15 K. Symbols are the experimental data, while lines the calculated values.

$$\rho_i = MW_i \frac{A_{\rho i}}{B_{\rho i}^{\left[1+\left(1-\frac{T}{C_{\rho i}}\right)^{D_{\rho i}}\right]}} \tag{3}$$

the coefficients of the Eq. (8), for each component, are reported in Table 4.

The catalyzed reaction takes place inside the catalyst resin, so it was necessary to differentiate, according to the phase considered, the volumes involved (L = liquid phase and S = solid phase).

$$V_L = \sum_i^n \frac{n_{i_L} MW_i}{\rho_i 1000} (n = 4) \tag{4}$$

where MW_i is the molecular weight. The bulk density and the ratio between the bulk and overall catalyst volumes were obtained in according to the Eqs. (5) and (6).

$$\rho_B = \frac{w_{cat}}{V_L} \tag{5}$$

$$\varepsilon_1 = \frac{\rho_{int}}{\rho_B} \tag{6}$$

where w_{cat} is the mass of catalyst and ρ_{int} is the intrinsic density of Amberlyst-15.

The evaluation of the diffusion coefficient (D_i) of the various components was carried out in accordance with the Wilke and Chang equation for liquid systems (Wilke and Chang, 1995):

$$D_i = \frac{7.4\ 10^{-8} (\phi M_i)^{1/2} T}{\mu_{mix}\ V_i^{0.6}} \tag{7}$$

where V_i represents the molar volume at the normal boiling point (cm^3/mol) calculated through the inverse of Eq. (3) and μ_{mix} the viscosity of the reaction mixture (cP). The term ϕ is defined as association factor and depends on the nature of the chemical component ($\phi_{LA} = \phi_{EtLA} = 1.0$, $\phi_{EtOH} = 1.5$ and $\phi_{H2O} = 2.6$), while ϕM_i was therefore obtained, for each component, according to Eq. (8).

$$\phi M_i = \sum_j^{n-1} x_i^j \phi_i MW_i (n = 4; j \neq i) \tag{8}$$

where x_i^j is a molar fraction, determined only on three of the four components, always using the i-th component and varying the others. The dependence on the viscosity of the temperature was therefore evaluated for each single component present in the reaction system, based on the empirical expression retrieved from CHEMCAD database (CHEMCAD):

$$\mu_i = exp\left(A_{\mu i} + \frac{B_{\mu i}}{T} + C_{\mu i} ln(T) + D_{\mu i} T^{E_{\mu i}}\right) \tag{9}$$

The coefficients of the equation, for each component, are reported in Table 5.

3.3.2. Kinetics

The classic esterification reaction mechanism consisting of two steps, protonation of the carboxylic group (RCOOH) and nucleophilic attack of alcohol (R'COH), namely Fisher esterification, is obviously also applicable in case of Amberlyst-15 for the esterification of levulinic acid. Applying the hypothesis of quasi-equilibrium to the first rapid reaction phase and considering the reversibility of the reaction, the reaction rates for the self-catalyzed reaction (R_1) in the liquid phase and for the reaction catalyzed by the Amberlyst-15 (R_2) were defined. The reaction rate expressions are given by the Eqs. (10) and (11) respectively.

$$R_1 = k_1 c_{LA_L}\left(c_{LA_L} c_{EtOH_L} - \frac{1}{K} c_{H_2O_L} c_{EtLA_L}\right) \tag{10}$$

Table 3
Summary partition coefficients for each solution prepared simulating different levulinic acid conversions.

X_{LA} [%]	0	10	20	40	60	80	100	$<m_i>$ [-]
m_{LA} [-]	1.13	1.05	1.01	1.03	1.04	1.03	1.01	1.04
m_{EtOH} [-]	1.26	1.32	1.28	1.11	1.19	1.22	2.02	1.38
m_{LE} [-]	1.59	1.58	1.63	1.62	1.57	1.58	1.6	1.60
m_{H2O} [-]	0.23	0.22	0.26	0.28	0.27	0.25	0.23	0.25

Table 4
Numerical values of the coefficients used to calculate the density of each component with temperature.

	LA	EtOH	EtLA	H_2O
$A_{\rho i}$	0.754	1.65	0.528	5.46
$B_{\rho i}$	0.258	0.276	0.246	0.305
$C_{\rho i}$	738	514	666	647
$D_{\rho i}$	0.220	0.233	0.286	0.081

Table 5
Numerical values of the coefficients used to calculate the viscosity of each component with temperature.

	LA	EtOH	EtLA	H_2O
$A_{\mu i}$	−12.873	7.874	−1.3913	−51.964
$B_{\mu i}$	2295.7	781.98	1034.8	3670.6
$C_{\mu i}$	−0.043631	−3.0418	−1.4837	5.7331
$D_{\mu i}$	0	0	0	$-5.3495 \cdot 10^{-29}$
$E_{\mu i}$	0	0	0	10

$$R_2 = k_2\left(c_{LA_S}c_{EtOH_S} - \frac{1}{K}c_{H_2O_S}c_{EtLA_S}\right) \tag{11}$$

For the catalyzed reaction we assumed that the sulfonic groups present on the ion exchange resin catalyze the reaction without any kind of physical adsorption.

The reaction stoichiometry is very simple; the generation rates for each component are obtained from Eq. (12).

$$r_i = \nu_i R \tag{12}$$

where ν_i is $\nu_{LA} = \nu_{EtOH} = -1$ and $\nu_{EtLA} = \nu_{H2O} = +1$.

A first order behavior with respect to the concentration of levulinic acid for the auto-catalytic reaction was hypothesized and verified in our previous work, where blank experiments (in absence of catalyst) were conducted and interpreted to retrieve kinetic parameters and rate law to describe the contribution of autocatalysis, showing that in every case a levulinic acid conversion lower than 10% was obtained in the adopted range of reaction conditions (Russo et al., 2018). Even if the effect of autocatalysis is not remarkable high, it is necessary to take it in consideration to obtain more precise kinetic parameters for the reaction catalyzed by Amberlyst-15. Moreover, it will be of high importance when extrapolating the results at higher temperatures.

The temperature dependence of the kinetic and equilibrium constants was evaluated using the modified Arrhenius law and the van't Hoff equation, using as reference temperature, T_{ref} = 333 K (Eqs. (13) and (14)).

$$k_j = k_{j,ref}exp\left[-\frac{Ea_j}{R}\left(\frac{1}{T} - \frac{1}{T_{ref}}\right)\right] \tag{13}$$

$$K = K_{ref}exp\left[-\frac{\Delta H}{R}\left(\frac{1}{T} - \frac{1}{T_{ref}}\right)\right] \tag{14}$$

3.3.3. Mass balances and mass transfer

The experimental data were interpreted using a reactor model that follows the assumptions reported below:

- Isotropic system: the liquid bulk phase is homogeneous in temperature and composition
- The partition of the components between vapor and liquid phases is neglected, as the system work under nitrogen pressure
- Sample withdrawal is considered negligible
- The size of the catalyst is considered uniform (average value reported in Table 1)

Two mass balance equations, liquid side and solid side were developed,

$$\varepsilon_P\frac{\partial c_{i_S}}{\partial t} = \frac{D_{e_i}}{(x\,R_p)^2}\frac{\partial}{\partial x}\left(x^2\frac{\partial c_{i_S}}{\partial x}\right) + \rho_P r_{2i} \tag{15}$$

Eq. (15) represent a classical dimensionless intraparticle mass balance equation written for a spherical particle, where only the catalyzed reaction occurs. Here, x represents the radial coordinate of the spherical particle of Amberlyst-15 ($x = r/R_p$), ε_p represents the particle porosity.

The liquid bulk phase mass balance includes both the fluid–solid mass transfer rate, responsible of the diffusion of reactants/products to the catalyst surface, and the term related to the auto-catalytic reaction, Eq. (16).

$$\frac{1}{V_L}\frac{dn_{i_L}}{dt} = r_{1i} - J_{i_S}\varepsilon_1 \tag{16}$$

The fluid–solid mass transfer rate is given by Eq. (17), indicating a linear dependence between the mass transfer rate and the concentration gradients in the stagnant liquid film surrounding the catalyst particle. Concentrations are adjusted by the partition coefficients (m_i):

$$J_{i_S} = k_S a_{Sp}\left(c_{i_L} - m_i c_{i_S}|_{x=1}\right) \tag{17}$$

where, ε_1 the volumetric ratio between the solid and the liquid phases, as the ratio between the catalyst bulk density and the particle density ($\varepsilon_1 = \rho_B/\rho_P$).

The R_p value was obtained starting from the take-up experiments, evaluating the take-up factor, from geometric considerations:

$$\frac{V_{dryAmb}+V_{ads}}{V_{dryAmb}} = \frac{1}{\varepsilon} \rightarrow \frac{V_{tot}}{V_{dryAmb}} = \frac{1}{\varepsilon} \rightarrow \frac{(4/3)\pi R_P^3}{(4/3)\pi R_{Pdry}^3} = \frac{1}{\varepsilon} \rightarrow R_P = \frac{R_{P_{dry}}}{\sqrt[3]{\varepsilon}} \tag{18}$$

The transport rate of the components inside the resin (J_{iLS}) was defined in the liquid phase mass balance. The mass transfer coefficient (k_s) and the specific surface area of the Amberlyst-15 particle (a_{sp}), were obtained from Eqs. (19) and (20),

$$k_S = k_{S0}\nu^{0.5} \tag{19}$$

$$a_{Sp} = \frac{3}{R_P} \tag{20}$$

where ν is the stirring rate used in the reaction. The expression (19) was defined starting from the Kolmogorov theory, for stirred tank reactors (Kolrnogorov et al., 1937). Two boundary conditions were defined to solve the partial differential equation system (15). The boundary conditions representing the center of the Amberlyst-15 particle ($x = 0$) and its outer surface ($x = 1$),

$$\frac{1}{R_P}\frac{\partial c_{i_S}}{\partial x}\bigg|_{x=0} = 0 \tag{21}$$

$$\frac{D_{e_i}}{R_P}\frac{\partial c_{i_S}}{\partial x}\bigg|_{x=1} = k_S\left(c_{i_L} - m_i c_{i_S}\big|_{x=1}\right) \tag{22}$$

Eq. (21) represents the symmetry condition in the particle centre, due to the parabolic profile of the concentrations inside the particle, while at the catalyst surface a continuity equation is adopted, Eq. (22).

The effective diffusivity of each component was calculated from

$$D_{e_i} = D_i\frac{\varepsilon}{\tau} \tag{23}$$

where τ and ε represent respectively the tortuosity and porosity of the Amberlyst-15 particle.

3.3.4. Parameter estimation

The developed model, comprising the mass balance equations reported in Eqs. (15) and (16), and the rate expression for the catalyzed reaction, Eq. (11), was used to estimate the kinetic parameters of the catalyzed reaction, namely the activation energy (Ea_2) and kinetic constant at the reference temperature of T_{ref} = 333 K ($k_{2,ref}$). gPROMS ModelBuilder v. 4.0 was used to conduct all the simulations and parameter estimation activities in the present work. The enthalpy and equilibrium constant values were fixed as the ones obtained in our previous work from the parameter estimation carried out on the experimental data collected using sulfuric acid as catalyst (Russo et al., 2018). The same for the autocatalysis rate laws and related parameters (Russo et al., 2018). The experimentally determined partition coefficients were used as fixed parameters. The value of the tortuosity was set in order to obtain an effective diffusivity of about one tenth of the diffusivity obtained for each component through the Wilke-Chang correlation (τ = 5). All the catalytic experimental data (Table 2, 2–12 and 15–22) were evaluated together, using the objective function reported in Eq. (24).

$$f(Ea_2, k_{ref,2}) = \sum_{l=1}^{N_e}\sum_{p=1}^{N_{data,l}}\sqrt{\frac{\left(X_{LA,EXP,l,p} - X_{LA,SIM,l,p}\right)^2}{X^2_{LA,EXP,l,p}}} \tag{24}$$

The results of the parameter estimation are shown in Table 6.

All the parameters errors and the correlations between them were reasonably low. The activation energy obtained from the parameter estimation is higher than those evaluated experimentally through the linearization of the Arrhenius equation (45.2 kJ/mol for A15-1 and 49.4 kJ/mol for A15-2). The activation energy obtained by linear fit is lower due to the intraparticle mass transfer limitations occurring in the system. As can be seen in Figs. 1–6, most of the simulated kinetic curves follow the experimental trends correctly, describing the equilibrium conversion and the temperature dependence of the reaction. The overall fitting can be better appreciated in the parity plot shown in Fig. 7, which reveals that most of the data fall into an error window of ± 20%.

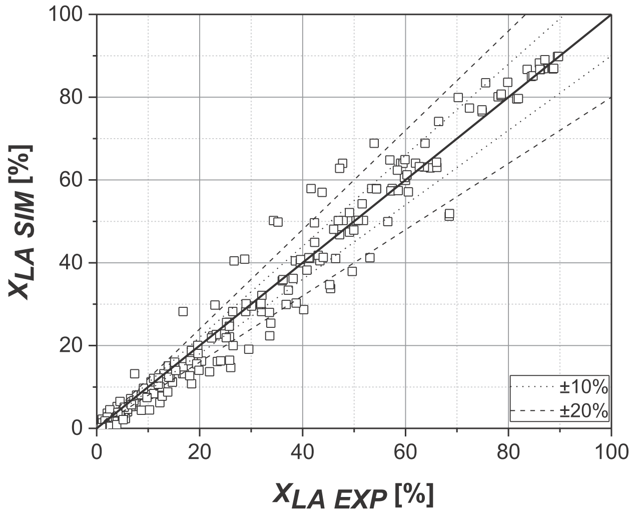

Fig. 7. Parity plot comprising all the available experimental data collected in the batch reactor.

The presence of internal diffusion limitation at the varying of intraparticle concentration with respect to the radial coordinate of the particle was evaluated. For each Amberlyst-15, a simulation was carried out on a single experiment (Table 2, test 4 and 15), using the estimated kinetic parameters. If the intraparticle concentration profile is flat, the internal diffusion limitation is negligible. The results of the simulations are displayed in Fig. 8 for both A15-1 and A15-2, fixing the experimental conditions for respectively Test 4 and 15.

As can be seen, levulinic acid showed non-flat profiles confirming the presence of internal diffusion limitation. Moreover, later the particle, higher concentration gradients were calculated as the diffusion path for each molecule is longer when the particle radius is higher. Analogous simulations were used for the evaluation of the reaction efficiency, for both resins, obtained in according to the Eq. (25),

$$\eta = \frac{\int_0^1 (r_2(x)R_P x)dx}{r_2|_{x=1}\int_0^1 (R_p x)dx} \tag{25}$$

where x represents the radial coordinate. The results are displayed in Fig. 9, confirming that the efficiency of A15-2 is higher than the ones of A15-1 due to the lower diffusion path of the fluid elements in the resin. The results of the computations are clearly in line with

Table 6
Summary of the estimated parameters and correlations matrix.

	Value	95% C.I.	Units	Ea_C	k_{cref}
Ea_2	83.5	3.7	kJ/mol	1	
$k_{2,ref}$ (T_{ref} = 333 K)	$9.0\cdot10^{-11}$	$0.2\cdot10^{-11}$	$(m^3/mol)\cdot(m^3/kg)\cdot s^{-1}$	−0.16	1

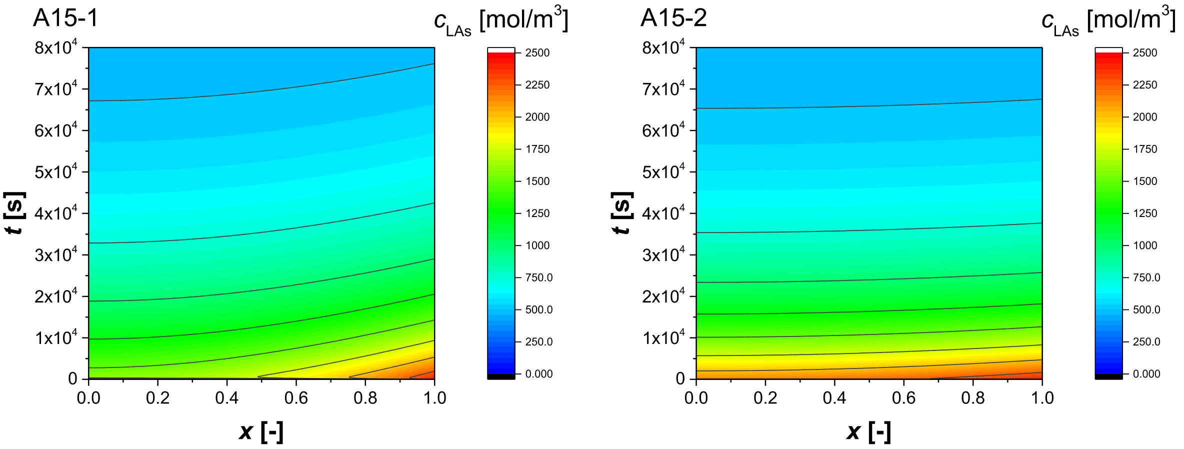

Fig. 8. Intraparticle diffusion effect of LA with respect to the reaction time and the radial coordinate. Simulation performed fixing the operation conditions for respectively Test 4 and 15: T = 343.15 K, ρ_B = 22 kg/m^3, v = 600 rpm, ethanol-to-levulinic acid molar ratio 5:1.

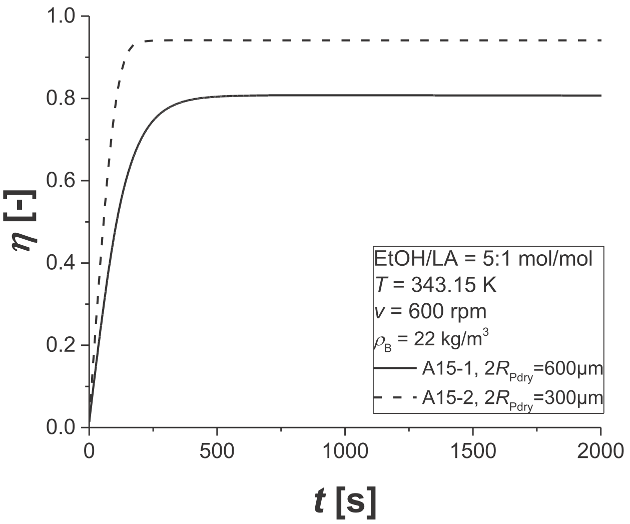

Fig. 9. Reaction efficiency plot for A15-1 and A15-2.

the experimental observations reported in Fig. 1, where a lower plateau was observed for larger particles.

4. Conclusions

In the present work, the kinetic and mass transfer aspects of the levulinic acid esterification with ethanol was investigated in the presence of ion-exchange resins as heterogenous catalysts. Two samples of Amberlyst-15 characterized by different acidity and particle size were adopted and a kinetic study was conducted varying the operating conditions.

The experimental results showed that Amberlyst-15 is an excellent heterogeneous catalyst for the esterification of levulinic acid, observing high activity. A linear dependence with respect to the catalyst bulk density was imposed. Depending on the catalyst particle size, the influence of the fluid–solid mass transfer limitation was investigated checking the minimum stirring rate to adopt to work in kinetic/intraparticle regime. By measuring the partition coefficients and take-up factors, a parameter estimation was conducted simultaneously on all the collected data, independently on the particle size, finding that the activation energy was equal to 83.5 kJ/mol.

It was demonstrated, that depending on the particle size, intraparticle diffusion limitation can be an important effect to be considered, as the effectiveness factor value becomes lower than one for large catalyst size.

The model shown high flexibility, as with only two parameters it was possible to simulate a large set of experiments. Thus, it is possible to be confident that the intrinsic kinetics of the levulinic acid esterification with ethanol was determined.

In perspective, the model could be used to simulate reactors in flow to switch the operation from batch to continuous. An effort could be made in designing the right type of reactor to conduct the operation, eg. packed bed reactor, loop reactor, fed-batch with water stripping.

CRediT authorship contribution statement

Vincenzo Russo: Conceptualization, Supervision, Writing - review & editing, Formal analysis, Software. **Carmelina Rossano:** Investigation, Writing - original draft. **Emiliano Salucci:** Investigation, Software, Writing - original draft. **Riccardo Tesser:** Formal analysis, Software. **Tapio Salmi:** Conceptualization, Writing - review & editing. **Martino Di Serio:** Conceptualization, Supervision.

Declaration of Competing Interest

The authors declare that they have no known competing financial interests or personal relationships that could have appeared to influence the work reported in this paper.

Acknowledgements

University of Naples Federico II is acknowledged for funding “The international agreement between University of Naples Federico II (IT) and Åbo Akademi University (FI)” that allowed the exchange between researchers of the two affiliations, making the realization of this work possible. Antonio Dello Stritto and Samuele Vito are acknowledged for the experimental support.

References

Banchero, M., Gozzellino, G., 2018. A simple pseudo-homogeneous reversible kinetic model for the esterification of different fatty acids with methanol in the presence of amberlyst-15. Energies 11, 1843. https://doi.org/10.3390/en11071843.

CHEMCAD v. 7.0, http://www.chemstations.com/.

Chun, C., Xiaojian, M., Peilin, C., 2009. Kinetics studies on wheat straw hydrolysis to levulinic acid. Chin. J. Chem. Eng. 17, 835–839. https://doi.org/10.1016/S1004-9541(08)60284-0.

Cirujano, F.G., Corma, A., Llabrés I Xamena, F.X., 2015. Conversion of levulinic acid into chemicals: synthesis of biomass derived levulinate esters over Zr-containing MOFs. Chem. Eng. Sci. 124, 52–60. https://doi.org/10.1016/j.ces.2014.09.047.

Di Serio, M., Russo, V., Santacesaria, E., Tesser, R., Turco, R., Vitiello, R., 2017. Liquid-liquid-solid model for the epoxidation of soybean oil catalyzed by Amberlyst-16. Ind. Eng. Chem. Res. 56, 12963–12971. https://doi.org/10.1021/acs.iecr.7b00881.

Fernandes, D.R., Rocha, A.S., Mai, E.F., Mota, C.J.A., Teixeira da Silva, V., 2012. Levulinic acid esterification with ethanol to ethyl levulinate production over solid acid catalysts. Appl. Catal. A-Gen. 425–426, 199–204. https://doi.org/10.1016/j.apcata.2012.03.020.

Hayes, D.J., Fitzpatrick, S., Hayes, M.H.B., Ross, J.R.H., 2006. The Biofine process – production of levulinic acid, furfural, and formic acid from lignocellulosic feedstocks. In: Kamm, B., Gruber, P.R., Kamm, M. (Eds.), Biorefineries-Industrial Processes and Products. Weinheim, Wiley-VCH Verlag GmbH, pp. 139–164.

https://www.sigmaaldrich.com/ (last visited 04/06/2020).

Hykkerud, A., Marchetti, J.M., 2016. Esterification of oleic acid with ethanol in the presence of Amberlyst 15. Biomass Bioeng. 95, 340–343. https://doi.org/10.1016/j.biombioe.2016.07.002.

Kolrnogorov, A., Petrovskii, I., Piskunov, N., 1937. Étude de l'équations de la chaleur, de la matiére et son application á un probleme biologique. Bull. Math. 1, 1–26.

Lamba, R., Kumar, S., Sarkar, S., 2018. Esterification of decanoic acid with methanol using Amberlyst 15: Reaction kinetics. Chem. Eng. Commun. 205, 281–294. https://doi.org/10.1080/00986445.2017.1387540.

Liu, Y., Lotero, E., Goodwin Jr, J.G., 2006. A comparison of the esterification of acetic acid with methanol using heterogeneous versus homogeneous acid catalysis. J. Catal. 242, 278–286. https://doi.org/10.1016/j.jcat.2006.05.026.

Lourvanij, K., Rorrer, G.L., 1994. Dehydration of glucose to organic acids in microporous pillared clay catalysts. Appl. Catal. A 109, 147–165. https://doi.org/10.1016/0926-860X(94)85008-9.

Nandiwale, K.Y., Sonar, S.K., Niphadkar, P.S., Joshi, P.N., Deshpande, S.S., Patil, V.S., Bokade, V.V., 2013. Catalytic upgrading of renewable levulinic acid to ethyl levulinate biodiesel using dodecatungstophosphoric acid supported on desilicated H-ZSM-5 as catalyst. Appl. Catal. A 460–461, 90–98. https://doi.org/10.1016/j.apcata.2013.04.024.

Nguyen, V.C., Bui, N.Q., Mascunan, P., HaVu, T.T., Fongarland, P., Essayem, N., 2018. Esterification of aqueous lactic acid solutions with ethanol using carbon solid acid catalysts: Amberlyst 15, sulfonated pyrolyzed wood and graphene oxide. Appl. Catal. A: General 552, 184–191. https://doi.org/10.1016/j.apcata.2017.12.024.

Pasquale, G., Vázquez, P., Romanelli, G., Baronetti, G., 2012. Catalytic upgrading of levulinic acid to ethyl levulinate using reusable silica included Wells–Dawson heteropolyacid as catalyst. Catal. Commun. 18, 115–120. https://doi.org/10.1016/j.catcom.2011.12.004.

Patil, C.R., Niphadkar, P.S., Bokade, V.V., Joshi, P.N., 2014. Esterification of levulinic acid to ethyl levulinate over bimodal micro-mesoporous H/BEA zeolite derivatives. Catal. Commun. 43, 188–191. https://doi.org/10.1016/j.catcom.2013.10.006.

Ramli, N.A.S., Amin, N.A.S., 2017. Esterification of renewable levulinic acid to levulinate esters using Amberlyst-15 as a solid acid catalyst. Jurnal Teknologi 79 (1), 137–142. https://doi.org/10.11113/jt.v79.8095.

Russo, V., Hrobar, V., Mäki-Arvela, P., Eränen, K., Sandelin, F., Di Serio, M., Salmi, T., 2018. Kinetics and modelling of levulinic acid esterification in batch and continuous reactors. Top. Catal. 61, 1856–1865. https://doi.org/10.1007/s11244-018-0998-y.

Shahid, A., Jamal, Y., Khan, S.J., Khan, J.A., 2018. Esterification reaction kinetics of acetic and oleic acids with ethanol in the presence of amberlyst 15. Arab. J. Sci. Eng. 43, 5701–5709. https://doi.org/10.1007/s13369-017-2927-y.

Su, F., An, S., Song, D., Zhang, X., Lu, B., Guo, Y., 2014. Heteropoly Acid and ZrO_2 bifunctionalized organosilica Hollow Nanospheres For Esterification and Transesterification. J. Mater. Chem. A. 2 (34), 14127–14138. https://doi.org/10.1039/C4TA02257B.

Wilke, C.R., Chang, P., 1995. Correlation of diffusion coefficient in dilute solutions. AIChE J. 1, 264–270. https://doi.org/10.1002/aic.690010222.

Yabushita, M., Kobayashi, H., Fukuoka, A., 2014. Catalytic transformation of cellulose into platform chemicals. Appl. Catal. B Environ. 145, 1–9. https://doi.org/10.1016/j.apcatb.2013.01.052.

Yadav, G.D., Yadav, A.R., 2014. Synthesis of ethyl levulinate as fuel additives using heterogeneous solid superacidic catalysts: Efficacy and kinetic modeling. Chem. Eng. J. 243 (1), 556–563. https://doi.org/10.1016/j.cej.2014.01.013.

Yan, K., Wu, G., Wen, J., Chen, A., 2013. One-step synthesis of mesoporous ${}_{H}4Si_{W1}2_{O4}0\text{-}Si_{O}2$ catalysts for the production of methyl and ethyl levulinate biodiesel. Catal. Commun. 34, 58–63. https://doi.org/10.1016/j.catcom.2013.01.010.

Zavozin, A.G., Kravchenko, N.E., Ignat'ev, N.V., Zlotin, S.G., 2010. Variation in the regioselectivity of levulinic acid bromination in ionic liquids. Tetrahedron Lett. 51 (2010) 545–547. https://doi.org/10.1016/j.tetlet.2009.11.097

II

Chemical Engineering Journal 401 (2020) 126126

Contents lists available at ScienceDirect

Chemical Engineering Journal

journal homepage: www.elsevier.com/locate/cej

Kinetic study of Amberlite IR120 catalyzed acid esterification of levulinic acid with ethanol: From batch to continuous operation

Vincenzo Russo[a,b,*], Riccardo Tesser[a,*], Carmelina Rossano[a], Tommaso Cogliano[a], Rosa Vitiello[a], Sébastien Leveneur[c], Martino Di Serio[a]

[a] University of Naples Federico II, Chemical Science Department, Via Cinthia, IT-80126 Naples, Italy
[b] Åbo Akademi, Laboratory of Industrial Chemistry and Reaction Engineering, Piispankatu, FI-20500 Åbo/Turku, Finland
[c] Laboratoire de Sécurité des Procédés Chimiques, Normandie Univ, INSA Rouen, UNIROUEN, LSPC, EA4704, 76000 Rouen, France

HIGHLIGHTS

- Ethyl levulinate synthesis kinetics promoted by Amberlite IR120.
- Kinetic model including external, internal and swelling effects.
- Diffusion limitations occur and are quantified.
- PBR was characterized and tested for model validation.
- From batch to continuous reactor.

GRAPHICAL ABSTRACT

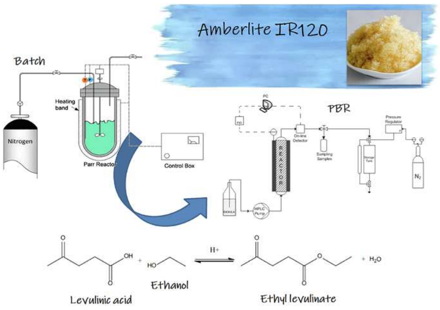

ARTICLE INFO

Keywords:
Esterification
Levulinic acid
Ion exchange resin
Batch to continuous
Modelling
Scale-up

ABSTRACT

Levulinic acid (LA) is one of the most important platform chemicals as it is a versatile building block for a variety of high value-added products, fine chemicals and pharmaceutical intermediates. Catalytic esterification of LA with alkyl alcohols leads to levulinate esters which can be used as fragrances, flavoring agents and fuel additives. In the present work, the kinetics of the levulinic acid esterification with ethanol in the presence of Amberlite IR120 was investigated in a batch reactor. The collected experimental data were interpreted with a reliable model taking into account also for the mass transfer phenomena involved in the reaction network. The kinetic model was further validated by conducting experiments in a fixed bed reactor. The reactor was characterized in terms of fluid-dynamics and the collected kinetic data were interpreted with a reliable reactor model, considering the extent of the reaction and fluid-solid mass transfer limitation.

1. Introduction

To satisfy the energy need, despite being in the 21st century, fossil resources such as oil, natural gas and coal are still used. Besides, many products used daily (i.e. polymers, fabrics, lubricants, etc.) are derived from fossil resources. Now, one of the major challenges facing industries is the transition to a renewable resource economy. For this reason, there is a strong need to search for renewable alternatives for the production of chemical building blocks [1].

Lignocellulosic biomass materials gained increasing attention due to their renewability and abundance. Among these renewable resources a target building block is levulinic acid (LA), that can be produced by acid

---

* Corresponding authors at: University of Naples Federico II, Chemical Science Department, Via Cinthia, IT-80126 Naples, Italy (V. Russo).
E-mail addresses: v.russo@unina.it (V. Russo), riccardo.tesser@unina.it (R. Tesser).

https://doi.org/10.1016/j.cej.2020.126126
Received 11 April 2020; Received in revised form 26 June 2020; Accepted 27 June 2020

Nomenclature

a_{sp}	Particle external surface area [m^2/m^3]
c_i	Concentration i-species [mol/m^3]
$c_{i,0}$	Concentration i-species at time zero [mol/m^3]
$c_{i,feed}$	Concentration of i-specie at the packed bed reactor inlet [mol/m^3]
$c_{i,s}$	Concentration of i-specie on solid [mol/m^3]
c_t	Tracer concentration [mol/m^3]
$c_{t,feed}$	Tracer concentration at the packed bed reactor inlet [mol/m^3]
$C_{W\text{-}P}$	Weisz-Prater criterion
D_i	Molecular diffusivity [m^2/s]
$D_{e,\ i}$	Effective diffusion coefficient [m^2/s]
d_p	Particle diameter [m]
D_Z	Axial dispersion coefficient [m^2/s]
E	Residence time distribution equation [–]
E_a	Activation energy [J/mol]
ID	Internal Diameter [m]
k_c	Equilibrium constant for catalyzed reaction [$(m^3/mol)(m^3/kg)s^{-1}$]
$k_{c,\ ref}$	Reference equilibrium constant for catalyzed reaction [$(m^3/mol)(m^3/kg)s^{-1}$]
K_{eq}	Equilibrium constant [–]
$K_{eq,\ ref}$	Reference equilibrium constant [–]
k_{NC}	Auto-catalyzed reaction rate constant [$(m^3/mol)^2/s$]
$k_{NC,\ ref}$	Reference equilibrium constant for auto-catalyzed reaction [$(m^3/mol)^2/s$]
k_s	Mass transfer coefficient [m/s]
k_{s0}	Mass transfer coefficient solid side [m/s]
L	Lenght [m]
M_i	Molecular weight of i-specie [g/mol]
Pe	Péclet number [–]
R	Ideal gas constant [J/(K·mol)]
r_c	Catalyzed reaction rate [mol/(kg·s)]
Re_p	Reynolds particle number [–]
r_{NC}	Auto-catalyzed reaction rate [$mol/(m^3 \cdot s)$]
r_{obs}	Observed reaction rate [$mol/(m^3 \cdot s)$]
r_{obs}	Observed reaction rate per mass of catalyst [mol/(kg·s)]
r_T	Overall reaction rate [$mol/(m^3 \cdot s)$]
R_p	Particle radius [m]
$R_{p,dry}$	Dry particle radius [m]
s	Shape factor [–]
T	Temperature [K]
t	Time [s]
$t_{injection}$	Injection time [s]
T_{ref}	Reference temperature [K]
u	Velocity [m/s]
$\dot{V}$	Flow rate [m^3/s]
V_{ads}	Liquid volume taken-up by Amberlite IR 120 [m^3]
V_i	Molar volume [m^3/mol]
V_{dry}	Amberlite IR 120 vol in dry state [m^3]
$V_{k,i}$	Molar volume coefficients of i-component
x_i^j	Molar fraction without one component [–]
X_{LA}	Levulinic acid conversion [%]

Greek Letters

α_{sw}	Swelling coefficient [–]
$\Delta_r H$	Reaction enthalpy [J/mol]
ε	Ratio between the particle density and bulk density [–]
ε_B	Bed void fraction [–]
ε_p	Particle void fraction [–]
μ_f	Fluid viscosity [cP]
μ_i	Viscosity of i-specie [cP]
$\mu_{k,i}$	Viscosity coefficients of i-component
μ_{mix}	Mixture viscosity [cP]
ν	Dynamic viscosity [m^2/s]
ν_i	Stoichiometric coefficient [–]
ρ_B	Bulk density [kg/m^3]
ρ_f	Fluid density [kg/m3]
ρ_p	Catalyst density [kg/m3]
τ	Average residence time [s]
τ_p	Particle tortuosity [–]
ϕ	Association parameter [–]
ω	Impeller rate [rpm]

Abbreviations

EtLA	Ethyl Levulinate
EtOH	Ethanol
HPLC	High Performance Liquid Chromatography
LA	Levulinic Acid
PID	Proportional Integral Derivative
PDE	Partial differential equation
RTD	Residence time distribution

catalysis from sugars and from waste materials.

Levulinic acid, also known as 4-oxovaleric acid or 4-oxopentanoic acid, is a short molecule with carboxylic acid and ketone functionality and the coexistence of these two functional groups makes it a very versatile compound with interesting reactivity pathways [2].

Thus, a wide variety of products can be obtained from LA using different types of chemical reactions, such as esterification, halogenation, hydrogenation, oxy dehydrogenation and condensation. Examples of important chemicals from LA include γ-valerolactone, levulinate esters, α-angelica lactone, ketals, diphenolic acid and δ-amino levulinic acid [3–6].

Levulinate esters are biobased chemicals having a strong potential to be used in various applications, e.g. in the flavoring industry as solvents and plasticizers, in biodiesel as cold flow improvers or diesel fuels due to its non-toxic, good lubricity and high flash point [7].

Esters of levulinic acid can be obtained according to the following acid-catalyzed reaction:

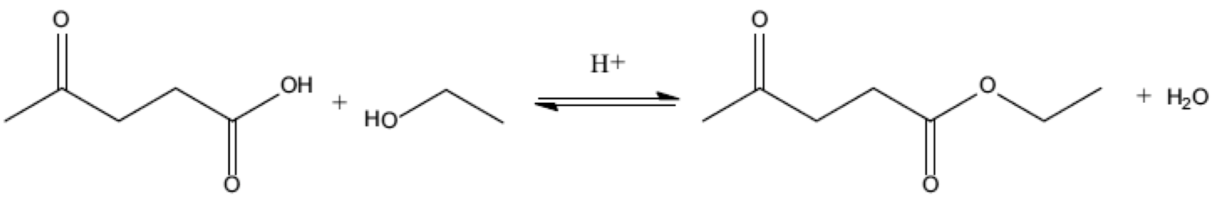

(1)

The esterification reactions are usually performed in the presence of homogeneous acid catalysts, such as H_2SO_4, H_3PO_4 or HCl [8,9].

Nowadays, heterogeneous catalysts are preferred due to their advantages that concern the recyclability, regeneration ability and reuse. Moreover, it is common knowledge that corrosion and disposal issues are due to the use of liquid mineral acids. For heterogeneously catalyzed esterification of levulinic acid, solids with Brønsted acidity are often used. Mechanism proposed for the formation of levulinate esters is clarified in many papers [10,11].

The esterification of levulinic acid has been investigated with zeolites [10], organo-silica or mesoporous silica incorporating –SO_3H groups [12,13], ion exchange resin [14,15], and heteropoly acids [16]. The most widely studied alkyl levulinate is ethyl levulinate (EL). Ethyl levulinate, made by esterifying LA with ethanol, can be used as an oxygenate additive and in the flavoring and fragrance industries. Some different heterogeneous catalysts were tested in the production of EL from LA; for example, Fernandes et al. [10] used different solid acid catalysts, demonstrating that Amberlyst-15 was the most active catalyst for the LA esterification.

We have already tested Amberlyst-15 [17] and another ion exchange resin (Smopex 101) [15] to determine the kinetic parameters of a such reaction. Smopex 101 is surely a good candidate to promote the reaction, as it is a non-porous ion exchange resin that avoids intraparticle diffusion limitations. Therefore, this resin is not available on the market anymore, and an alternative must be found.

Earlier studies [18,19] found that the cation exchange resins showed the highest catalytic efficiency and among these Amberlite IR120 has revealed as an affordable, green esterification catalyst capable of being used repeatedly without a significant decrease in its activity.

To the best of our knowledge the kinetics of ethyl levulinate is not reported over acidic ion-exchange resin as Amberlite IR120. Therefore, the present paper is devoted to filling this gap.

Experiments conducted in a batch reactor were performed changing the system operating conditions (i.e. temperature, stirring rate, alcohol/acid molar ratio and catalyst loading) and the effect of these conditions on the conversion degree was evaluated. The kinetic constants, the rate constant and the activation energies were also determined.

The collected experimental data were interpreted with a reliable model also considering the mass transfer phenomena involved in the reaction network, such as eventual fluid–solid and intraparticle mass-transfer limitations. Continuous esterification in a fixed bed reactor packed with the same catalyst (Amberlite IR120) was conducted.

The kinetics was further validated in a continuous packed bed reactor. A fluid-dynamic characterization was conducted to determine the axial dispersion coefficient. Kinetic experiments were conducted and successfully interpreted by using reliable reactor models.

2. Experimental section

2.1. Chemicals and reagents

The following chemicals were used in the experiments without further purification: levulinic acid (98 wt%, by Merck), ethanol (99 wt %, by Alfa Aesar), Amberlite® IR-120 (H) ion exchange resin (by Room and Haas) was used as a solid acid catalyst. For the analysis of the products, by titration were used: ethanol (96 wt%, by Carlo Erba) and phenolphthalein (by Merck) as indicator.

2.2. Kinetic experiments in batch reactor

The batch reactor consists of a storage tank reactor (capacity of 0.3L) with an integrated heating system. The reaction mixture was stirred using a mechanically driven impeller to suppress the external mass transfer limitations and homogenize the liquid phase. The system was equipped with a digital pressure transducer and a thermocouple to measure, respectively, pressure and temperature, a pin valve for samples withdrawal of the reaction mixture. The system was pressurized with nitrogen at 5 bar to limit gas–liquid partition of the liquid phase. For each experiment, the reactor was loaded with a fixed amount of ethanol and levulinic acid, at a given molar ratio (1.0, 2.5 or 5.0), adding to it the catalyst previously preheated to remove the adsorbed water. The system was preheated, and a first sample was collected once temperature was stable. A first sample was withdrawn once the system reached the set temperature, to quantify the extent of the reaction occurred during the heating procedure (time zero sample). Periodic withdrawals were conducted and analyzed to obtain kinetic data. Each sample was analyzed by acid-base titration using standardized 0.1 M NaOH as titrating agent and phenolphthalein as indicator, whereas the concentration of ethyl levulinate was determined by GC (HP 6890 Series) using a column DB5 and an FI detector. Each sample was analyzed three times to estimate the error on the experimental data, expressed as the standard deviation. Moreover, some experiments were repeated to calculate the error on the kinetic experiment reproducibility, obtaining an average value of 2.5%. All the adopted experimental conditions and the compositions of the time zero sample are shown in Table 1.

Table 1
Experimental conditions adopted for the experiments conducted in batch reactor. The concentrations are referred to as the time zero sample, withdrawal once that the temperature reached the set value.

Test	ω [rpm]	T [K]	ρ_B [kg/m^3]	$c_{EtOH,0}$ [mol/m^3]	$c_{LA,0}$ [mol/m^3]	$c_{EtLA,0}$ [mol/m^3]	$c_{H2O,0}$ [mol/m^3]
1	200	343	19.7	$13.9\cdot10^3$	$2.3\cdot10^3$	$0.5\cdot10^3$	$0.5\cdot10^3$
2	400	343	19.7	$14.3\cdot10^3$	$2.7\cdot10^3$	$0.1\cdot10^3$	$0.1\cdot10^3$
3	600	343	19.7	$14.3\cdot10^3$	$2.7\cdot10^3$	$0.2\cdot10^3$	$0.2\cdot10^3$
4	800	343	19.7	$14.3\cdot10^3$	$2.7\cdot10^3$	$0.2\cdot10^3$	$0.2\cdot10^3$
5	800	333	19.7	$14.2\cdot10^3$	$2.6\cdot10^3$	$0.2\cdot10^3$	$0.2\cdot10^3$
6	800	323	19.7	$14.3\cdot10^3$	$2.7\cdot10^3$	$0.1\cdot10^3$	$0.1\cdot10^3$
7	800	343	12.3	$14.3\cdot10^3$	$2.8\cdot10^3$	$0.1\cdot10^3$	$0.1\cdot10^3$
8	800	343	9.8	$14.2\cdot10^3$	$2.7\cdot10^3$	$0.2\cdot10^3$	$0.2\cdot10^3$
9	800	343	18.7	$9.9\cdot10^3$	$3.8\cdot10^3$	$0.3\cdot10^3$	$0.3\cdot10^3$
10	800	343	17.2	$5.3\cdot10^3$	$5.2\cdot10^3$	$0.1\cdot10^3$	$0.1\cdot10^3$
11	800	343	4.9	$14.2\cdot10^3$	$2.6\cdot10^3$	$0.3\cdot10^3$	$0.3\cdot10^3$

The experiments were conducted by defining a reference experiment; Test 4 of Table 1 conducted adopting the experimental conditions to have the maximum reaction rate in the selected range of investigation. In this way, by studying the effect of the stirring rate of the system, it is possible to find the best stirring rate to exclude fluid–solid mass transfer resistance. Starting from this experiment, the main operation conditions that would affect the kinetics of the reaction were systematically varied (i.e. temperature, catalyst loading, stirring rate and reactants molar ratio).

The ion-exchange resins constituted by cross-linked copolymers of the styrene–divinylbenzene type, show swelling in water or in a solvent that depends on the degree of cross-linking and on the nature and concentration of acid or basic groups. The experimental tests to evaluate the swelling degree were conducted following the footsteps of Bodamer and Kunin [20]. The experiments were conducted using a graduated cylinder of 10 mL, where an aliquot of 2 mL of dry Amberlite IR120 H was added and weighted. Each compound involved in the reaction was added separately. After adding the corresponding solvent, the mixture was mixed to improve contact, and let increasing for about an hour. Finally, the catalyst, separated from the solution was weighed in order to obtain the total amount of the liquid incorporated by swelling. The properties of the tested commercial ion exchange resin, directly taken from the material data sheet of Amberlite IR120, are summarized in Table 2.

2.3. Kinetic experiments in continuous reactor

To ensure a constant and precise volumetric flow, an HPLC pump was used to feed the reaction mixture to the packed bed reactor. The reactor was made of a steel tube (L = 0.3 m, ID = 0.0078 m).

After pre-treatment, the catalyst was readily packed in the reactor. The amount of catalyst needed to fill the reactor was calculated

Table 2
Physical properties of catalysts in dry state. Data are taken directly from the material data sheet of Amberlite IR 120.

Catalyst	Particle size [μm]	Structure	Crosslinking degree [%]	Porosity [vol.%]	Conc. of acid sites [m_{equiv}/g]	Surface area [m^2/g]
Amberlite IR120	620–830	Styrene-divinylbenzene (gel)	8	18	4.4	1.53

Table 3
Summary of the operation conditions adopted for the kinetic experiments conducted in the packed bed reactor by varying temperature (T), volumetric flowrate ($\dot{V}$) and the concentration of each reactant fed to the reactor.

Test	T [K]	$\dot{V}$ [m^3/s]	$c_{EtOH,feed}$ [mol/m^3]	$c_{LA,feed}$ [mol/m^3]
1	323	$(1.7–8.3)·10^{-8}$	$13.0·10^3$	$2.2·10^3$
2	343	$(1.7–8.3)·10^{-8}$	$13.3·10^3$	$2.5·10^3$
3	363	$(1.7–8.3)·10^{-8}$	$13.0·10^3$	$2.2·10^3$

considering also the swelling phenomena, i.e. the degree of swelling of the catalyst particle, resulting that 7 g of dry catalyst was enough to fill the reactor.

A heating jacket was placed outside the reactor to ensure constant temperature guaranteeing isothermal operation; the temperature was measured by a thermocouple and regulated with a PID controller. To keep the reaction mixture in the liquid phase, the system was connected to a nitrogen cylinder regulated by a manometer to guarantee 5 bar of absolute pressure. Samples were collected periodically to measure the steady-state conditions, through a dedicated pin valve. As done for the kinetic study in batch, each sample was analyzed three times to estimate the error on the experimental data, also in this case expressed as standard deviation, using the same analytical methods. Also in this case, some experiments were repeated to calculate the error on the experiment reproducibility, obtaining an average value of 2.5%.

The kinetic experiments were conducted at $1.7–8.3·10^{-8} m^3/s$, for each temperature (323, 343 and 363 K) with a given reactant's molar ratio of roughly ethanol/levulinic acid ratio of 6:1. The summary of the operating conditions is reported in Table 3, while flow sheet of the continuous system is shown in Fig. 1. Be aware that for the kinetic experiments, the on-line detector was not used.

Test 1, experiment performed at $T = 323$ K and $1.7·10^{-8} m^3/s$, was prolonged for 50 h reaction time to check the catalyst stability.

2.4. Fluid-dynamic characterization of the continuous reactor

The fluid-dynamic study is one of the most important steps to understand the behavior of a flow reactor. In a real reactor there are mixing phenomena in axial direction contributing to the dispersion phenomena into the reactor. The experiments were conducted in the same equipment used for the measurement of kinetic data in continuous, with the unique difference that an HPLC injector was installed between the HPLC pump and the packed bed reactor.

Stimulus-response pulse experiments were conducted to evaluate the RTD (residence time distribution) with yellow naphthol as tracer, and the UV absorbance was recorded using an on-line detector (Reach Device RD4), using a HPLC injector to pulse the yellow naphthol solution to the reactor. Yellow naphthol was chosen for two main reasons: (i) a dye where sulfonic groups are present, thus exerting repulsive forces avoiding adsorption phenomena on the resin; (ii) it is a molecule big enough to exclude intraparticle diffusion. Thus, it is possible to obtain directly the bed void fraction using this tracer in pulse experiments.

Each experiment was repeated three times to estimate the error on the axial dispersion coefficient (D_z). The operating conditions in the continuous reactor are listed in Table 4.

2.5. Modelling

The kinetic models for the esterification of levulinic acid developed for both batch and continuous reactors were written using gPROMS ModelBuilder v.4.0 software. The sketch of the modelling rationalization is reported in Fig. S1 of Supplementary Material. In particular, the numerical method of lines, using a finite difference approach, was used to solve the partial differential equations systems, i.e. the mass balance equations of the batch and continuous models. A second-order centered finite difference method was applied for the particle radial coordinate in the batch model, adopting 50 discretization points. A first-order backwards finite difference method was applied for the packed bed axial coordinate in the continuous model, adopting 200 discretization points.

3. Results and discussion

3.1. Esterification kinetics in batch reactor

Experiments were carried out with Amberlite IR120 as catalyst, investigating a wide range of operation conditions (i.e. impeller rate, temperature, catalyst amount and reactant ratio, see Table 1).

The eventual presence of by-products was checked in every case by GC analysis, verifying that ethyl levulinate was the unique product formed by the reaction, together with water.

The influence of external mass transfer resistance during kinetic tests was evaluated varying the velocity of the rotating impeller in the reactor vessel from 200 to 800 rpm; the catalyst mass and the molar ratio of levulinic acid to ethanol ratio was also evaluated.

The obtained results for the observed reaction rate plot, calculated by the initial slope of the conversion trends till 3600 s reaction time, versus the stirring rate (Fig. 2) showed that at stirring speeds greater than 400 rpm the reaction rate profile becomes flat, allowing to conclude that from 400 rpm on the absence of external mass transfer limitation is evident.

Experiments were conducted varying the bulk density of the catalyst. The results reported in Fig. 3A clearly indicate that by increasing the catalyst loading, a corresponding increase of the reaction rate is observed. The equilibrium plateau is independent on the catalyst loading as expected. The collected data were plotted as a function of normalized abscissa (i.e. catalyst density multiplied by reaction time), observing a good overlap of the experimental data (Fig. 3B). As demonstrated in the literature, this plot is very useful as it gives direct information: (i) the dependence with respect to the catalyst loading is linear; (ii) the absence of the external mass transfer resistance is confirmed [15]. The mathematical derivation of this assumption is reported in Supplementary Material.

The effect of the molar ratio of levulinic acid to ethanol was also studied at 343.15 K (Fig. 4). The results showed that by increasing the molar ratio, the highest yield in ethyl levulinate was obtained.

The effect of the temperature was investigated (Fig. 5). The observed trends are rather logical, as an increase in temperature value leads to a higher reaction rate, reaching a higher equilibrium plateau, confirming that the reaction is slightly endothermic.

The experimental work was then completed by conducting take-up experiments, evaluating the swelling of the resin when put in contact with a liquid, to measure the swelling factor of each component that is retained by Amberlite IR120. The results showed the following values:

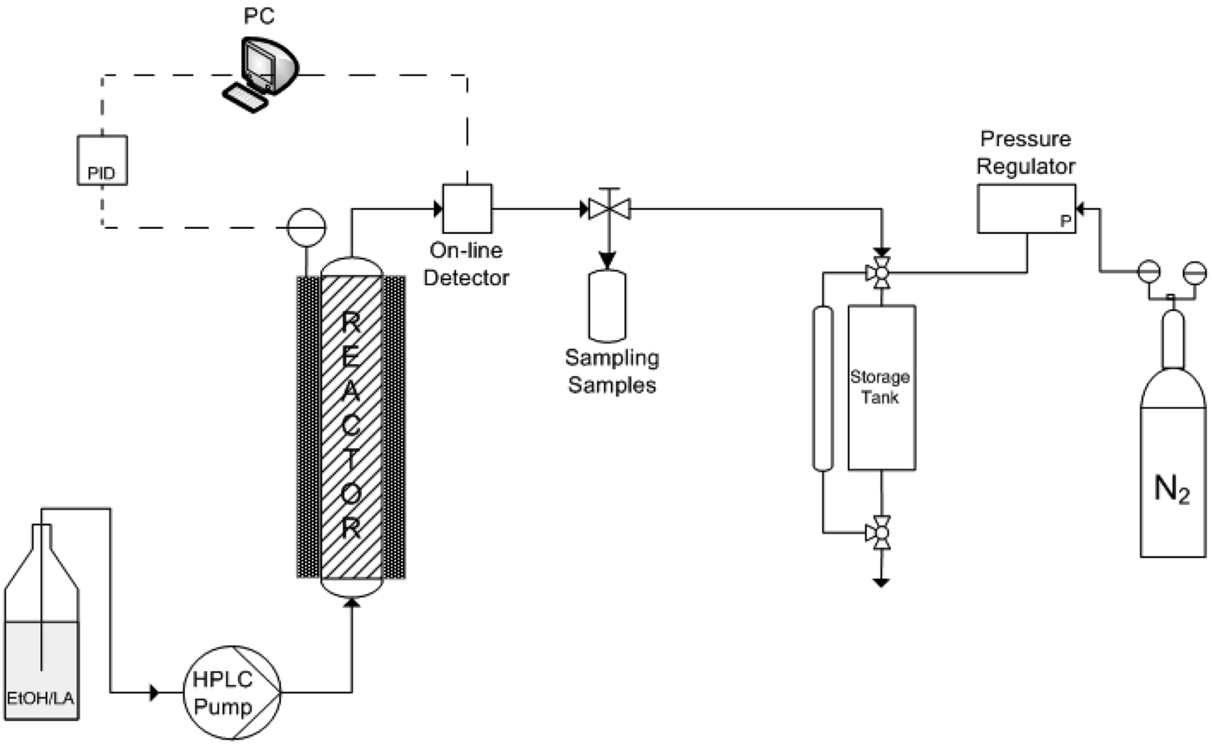

Fig. 1. Continuous system flow sheet adopted to conduct the kinetic experiments and the fluid-dynamic characterization. For the latest, an HPLC injector was installed between the HPLC pump and the packed bed reactor.

Table 4
Experimental conditions in continuous reactor adopted for the fluid-dynamic characterization experiments, varying volumetric flowrate ($\dot{V}$) and temperature (T).

Test	$\dot{V}$ [m³/s]	T [K]
1	$1.7 \cdot 10^{-8}$	298
2	$2.5 \cdot 10^{-8}$	298
3	$3.3 \cdot 10^{-8}$	298
4	$5.0 \cdot 10^{-8}$	298
5	$6.7 \cdot 10^{-8}$	298
6	$10 \cdot 10^{-8}$	298
7	$13 \cdot 10^{-8}$	298
8	$17 \cdot 10^{-8}$	298
9	$5.0 \cdot 10^{-8}$	343
10	$8.3 \cdot 10^{-8}$	343
11	$12 \cdot 10^{-8}$	343

70 ± 5 vol% for ethanol, 20 ± 1 vol% for levulinic acid and ethyl levulinate, 100 ± 5 vol% for water and 80 ± 5 vol% for the binary solution of ethanol and LA, in molar ratio to 5:1.

3.1.1. Kinetic modelling for the batch system

A fluid–solid intraparticle model was used for the interpretation of experimental data collected with Amberlite IR120 H as catalyst in the batch reactor. Whereas, we have already shown the results of the autocatalytic effect and the kinetic and thermodynamic parameters of the esterification reaction, conducting tests in homogeneous phase, in the absence of any additional homogeneous or heterogeneous catalyst [15]. The reaction rate expressions for auto-catalyzed reaction (r_{NC}) can be written as in Eq. (2).

$$r_{NC} = k_{NC}\, c_{LA\,(l)} \left(c_{LA\,(l)} c_{EtOH\,(l)} - \frac{1}{K_{eq}} c_{H2O\,(l)} c_{EL\,(l)} \right) \tag{2}$$

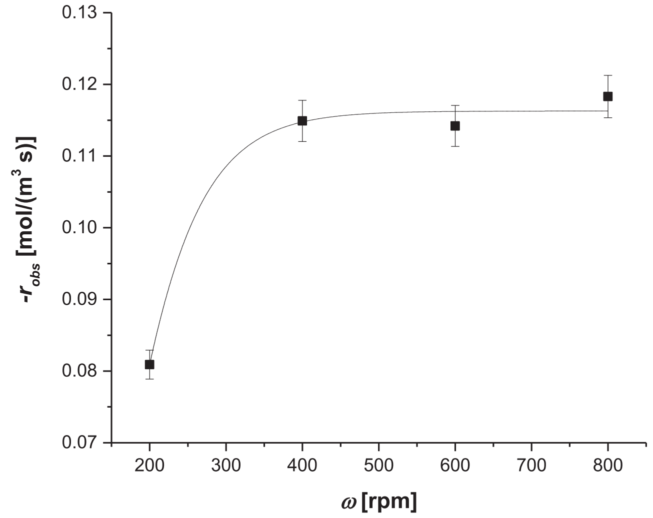

Fig. 2. Effect of stirring rates on the observed reaction rate by fixing the EtOH to LA molar ratio of 5:1, at ρ_B = 19.7 kg/m³ of catalyst and at temperature of 343 K. The symbols are the experimental data collected at the four stirring rates, fixing the reaction time at 3600 s; continuous lines represent the simulations.

where the kinetic parameters obtained in the mentioned study are reported in Table 5. As revealed, the thermodynamic parameters obtained in our previous study were fixed, as independent on the catalyst. Thus, the thermodynamic plateau measured in the present paper are just simulated by the model. No additional parameters are needed.

The autocatalytic rate expression, with related parameters, is fixed as reported in the present study. The reaction rate for the heterogeneously catalyzed system promoted by Amberlite IR120, was taken as a second order reversible rate expression, Eq. (3), assuming that the sulfonic groups present on the ion exchange resin catalyze the reaction without any kind of physical adsorption.

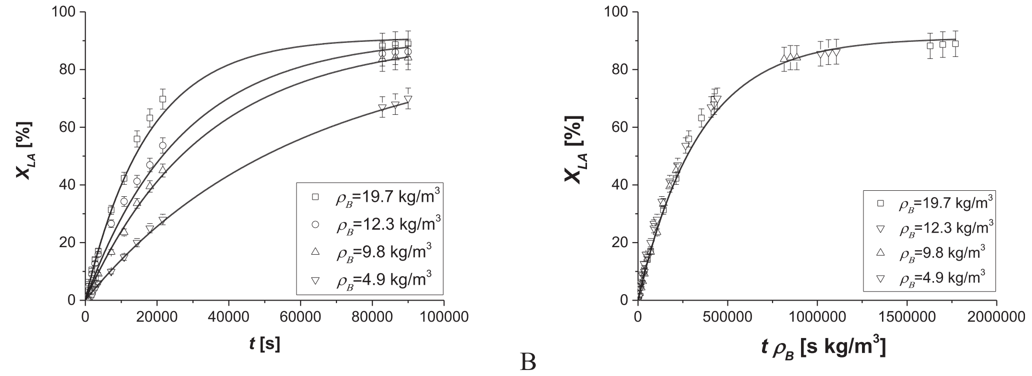

Fig. 3. A. The effect of Amberlite IR120 bulk density on the levulinic acid esterification, fixing EtOH to LA 5:1 M ratio at 800 rpm and at temperature of 343 K. Raw data on levulinic acid conversion versus time; symbols are the experimental data; lines are the model predictions. B. Levulinic acid conversion plotted versus the normalized experimental time by the catalyst bulk density.

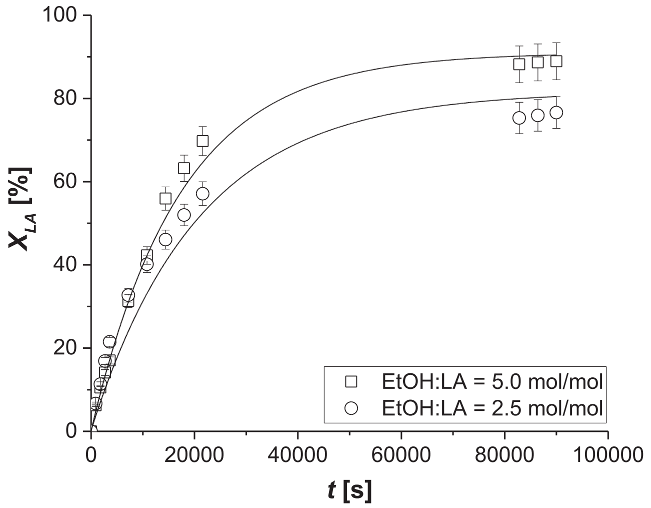

Fig. 4. The effect of the EtOH to LA ratio on the levulinic acid esterification catalyzed by Amberlite IR120 fixing the temperature at 343 K, the stirring rate at 800 rpm and the catalyst amount equals to $\rho_B = 18$ kg/m^3. Symbols are the experimental data, lines the calculated values.

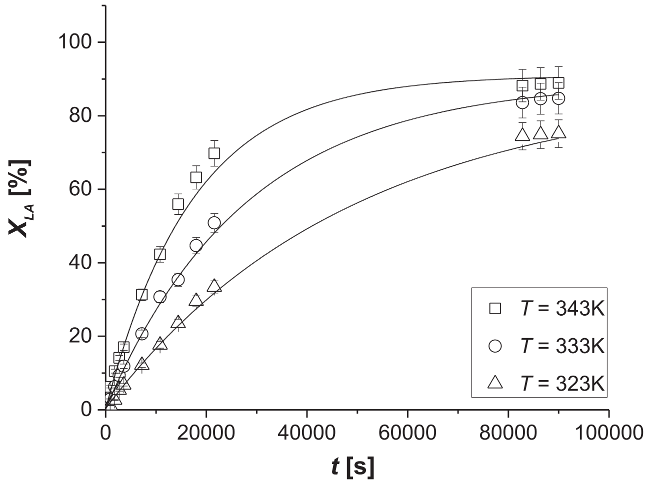

Fig. 5. Effect of temperature on the levulinic acid esterification catalyzed by Amberlite IR120 by fixing the ethanol to levulinic acid molar ratio of 5:1, an amount of catalyst equal to $\rho_B = 18$ kg/m^3 and 800 rpm. Symbols are the experimental data; lines are the predicted values.

Table 5
Results of parameter estimation reported by Russo et al [15].

Parameters	Value	95% CI	Units
$\Delta_r H$	$15.1\cdot10^3$	$5.6\cdot10^3$	J/mol
Ea_{NC}	$32.5\cdot10^3$	$0.3\cdot10^3$	J/mol
$K_{eq,ref}$ (T_{ref} = 333 K)	3.2	0.1	–
$k_{NC,ref}$ (T_{ref} = 333 K)	$5.7\cdot10^{-14}$	$0.5\cdot10^{-14}$	[(m^3/mol)^2/s]

$$r_c = k_c\left(c_{LA(s)}c_{EtOH(s)} - \frac{1}{K_{eq}}c_{H2O(s)}c_{EL(s)}\right) \tag{3}$$

The total rate of esterification (r_T) can be obtained by summing the catalytic and autocatalytic contributions, Eq. (4).

$$r_T = r_{NC} + r_C\rho_B \tag{4}$$

The reaction stoichiometry is very simple; the generation rates of each component is obtained from Eq. (5).

$$r_i = \nu_i r_T \tag{5}$$

where, ν_i is $\nu_{\mathrm{LA}} = \nu_{\mathrm{EtOH}} = -1$ and $\nu_{\mathrm{EtLA}} = \nu_{\mathrm{H2O}} = +1$.

The dependence of the kinetic and equilibrium constants from the temperature was evaluated using the modified Arrhenius equation (Eq. (6)) and van't Hoff law (Eq. (7)), respectively, using a reference temperature (T_{ref}) equal to 333 [K].

$$k_c = k_{c,ref}\,exp\left[-\frac{Ea_c}{R}\left(\frac{1}{T} - \frac{1}{T_{ref}}\right)\right] \tag{6}$$

$$K_{eq} = K_{eq,ref}\,exp\left[-\frac{\Delta_r H}{R}\left(\frac{1}{T} - \frac{1}{T_{ref}}\right)\right] \tag{7}$$

A linear dependence of the reaction rate with respects to the Amberlite IR120 H bulk density was assumed, in agreement with the collected experimental evidence (see Fig. 3B).

The experimental data were interpreted using a reactor model that follows the assumptions reported below:

- Isotropic system: the liquid bulk phase is homogeneous in temperature and concentrations
- The partition of the components between vapor and liquid phases is neglected, as the system work under nitrogen pressure
- Sample withdrawal can be considered negligible as only a small amount of liquid is collected for the analysis
- The particle size of the catalyst is considered uniform and equal to the average value reported in Table 2

The mass balance equation utilized for each component in the liquid phase can be written as in Eq. (8).

$$\frac{dc_{i(l)}}{dt} = \nu_i r_{NC} - k_s a_s \varepsilon (c_{i(l)} - c_{i(s)}) \tag{8}$$

where, ν_i is the stoichiometric coefficient for each component [–], r_{NC} is the autocatalytic reaction rate, k_s is the mass transfer coefficient [m/s], a_s is the particle specific surface area [m^2/m^3], ε is the ratio between the bulk density and the particle density [–]. The mass transfer coefficient (k_s) and the external surface (a_s) of Amberlite IR120 H were evaluated as follows.

$$k_s = k_{s0} \nu^{\frac{1}{2}} \tag{9}$$

$$a_s = \frac{3}{R_p} \tag{10}$$

The expression (Eq. (9)) was defined starting from the Kolmogorov theory [21], for stirred reactors.

Where, ν in the mass transfer coefficient equation represents the stirring rate of the system [rpm], and R_p in the specific surface area is the average radius of the catalyst particles, taking into account the take-up test and the swelling factor (α_{sw}) of the catalyst in the reaction mixture, Eq. (11).

$$R_p = R_{p,dry}\alpha_{sw} = \frac{R_{p,dry}}{\sqrt[3]{\frac{V_{dry}}{V_{dry} + V_{ads}}}} \tag{11}$$

where, $R_{p,dry}$ is the radius of the particle in dry state, V_{ads} is the liquid volume taken-up by Amberlite IR120 after swelling, V_{dry} the catalyst volume in dry state.

It is necessary to introduce the swelling factor as it affects the real radius of the particle, thus the diffusion path that reactants and products molecules must run across. Moreover, the particle radius also affects the specific surface area of the catalyst, having a direct influence on the fluid-solid external mass transfer rate.

The mass balance on the solid phase was evaluated considering the diffusion of the reactants inside the catalyst along the dimensionless radial coordinate. The obtained mass balance is reported in the following equation:

$$\varepsilon_p \frac{dc_{i(s)}}{dt} = \frac{D_{e,i}}{R_p^2}\left(\frac{s}{x}\frac{\partial c_{i(s)}}{\partial x} + \frac{\partial^2 c_{i(s)}}{\partial x^2}\right) + \nu_i r_C \rho_p \tag{12}$$

where, ε_p is the particle void fraction [–], s is the shape factor representing the shape form of the particle, in this case s is equal to 2 (spherical case), ρ_p is the catalyst density [kg/m^3], and r_c is the catalytic reaction rate [mol/(kg•s)]. Finally, $D_{e,i}$ is the effective diffusion coefficient for each reactive component [m^2/s] evaluated weighting the molecular diffusivity by the porosity and tortuosity of the catalyst, Eq. (13).

$$D_{e,i} = D_i \frac{\varepsilon_p}{\tau_p} \tag{13}$$

where, D_i [m^2/s] is the molecular diffusivity for the various component, and τ_p [–] is the particle tortuosity. The evaluation of the diffusivity (D_i) for each component was carried out in agreement with Wilke and Chang equation for liquid mixtures, Eq. (14).

$$D_i = \frac{7.4\ 10^{-8}(\phi M_i)^{1/2} T}{\mu_{mix} V_i^{0.6}} \tag{14}$$

where, the term ϕ [–] is the association parameter and depends of the nature of the chemical component, M_i is the molecular weight [g/mol], T is the operating temperature [K], μ_{mix} is the viscosity mixture [cP] and finally V_i is the molar volume at normal boiling point of the solute [cm^3/mol]. The association parameter was calculated as it follows:

Table 6

Viscosity and molar volume coefficients for each component comprising the reaction system.

	LA	EtOH	EL	H_2O
μ_A	−12.87	7.87	−1.39	−51.96
μ_B	0.23	7.82	0.10	0.37
μ_C	−0.04	−3.04	−1.48	5.73
V_A	0.75	1.65	0.53	5.46
V_B	0.26	0.28	0.25	0.31
V_C	0.74	0.51	0.67	0.65
V_D	0.22	0.23	0.29	0.08

$$\phi M_i = \sum_{j}^{n-1} x_i^j \phi_i M_i \tag{15}$$

where, x_i^j is the molar fraction [–], determined only on three of the four components, always using the i^{th} component and varying the others, moreover, $n = 4$ and $j \neq 1$. The association factor ϕ_i [–] depends on the nature of components, being 1 for both levulinic acid and ethyl levulinate, 1.5 for ethanol and 2.6 for water. Moreover, M_i is the molecular weight of the components [g/mol].

The viscosity mixture (μ_{mix}) was evaluated as in Eq. (16).

$$\ln(\mu_{mix}) = \sum_{i=1}^{n=4} x_i \ln(\mu_i) \tag{16}$$

where, x_i is the molar fraction and μ_i the viscosity of the i^{th} components. The dependence of the viscosity of the i^{th} component from the temperature was evaluated for each single component present in the reaction system with the empirical expression taken from ChemCAD v. 7.0 database [22], Eq. (17).

$$\mu_i = \exp\left[\mu_{A,i} + \frac{\mu_{B,i}}{T} + \mu_{C,i} ln(T)\right] \tag{17}$$

The coefficients of each component are reported in the Table 6.

The molar volume at normal boiling point (V_i) was obtained from ChemCAD v. 7.0 database [22], Eq. (18).

$$V_i = \left[\frac{V_{Ai}}{V_{Bi}^{\left[1+\left(1-\frac{T_{eb}}{V_{Ci}}\right)^{V_{Di}}\right]}}\right]^{-1} \tag{18}$$

The coefficients for each component are reported in Table 6.

To solve the intraparticle mass balance equation, two boundary conditions (BC) were defined, Eqs. (19) and (20).

$$\left.\frac{1}{R_p}\frac{\partial c_{i(s)}}{\partial x}\right|_{x=0} = 0 \tag{19}$$

$$\left.\frac{D_{e,i}}{R_p}\frac{\partial c_{i(s)}}{\partial x}\right|_{x=1} = k_s(c_{i(l)} - c_{i(s)}) \tag{20}$$

The first BC is consistent with the symmetry of the particle at its center. The second BC represents a continuity equation on the external surface of the catalyst particle.

A parameter estimation was conducted simultaneously on all the collected experimental data. In particular, the parameters related to the autocatalytic reaction, the equilibrium constant and the reaction enthalpy values were fixed as reported in Table 5, values obtained in our previous work using sulfuric acid as catalyst [15]. The only adjustable parameters in this paper are: (i) the reference kinetic constant of the reaction catalyzed by Amberlite IR120; (ii) the activation energy of the mentioned reaction; (iii) the k_{s0} value that is specific for the system. These parameters were estimated adopting all the experimental data available for the experiments listed in Table 1.

The results of the parameters estimation are shown in the Table 7,

Table 7

Results of parameter estimation based on all the experimental data collected in batch reactor. CI: confidence interval. $T_{ref} = 333$ [K].

	Value	95% CI	Correlation Matrix			Units
			Ea_c	k_{s0}	$k_{c,ref}$	
Ea_c	$68.83{\cdot}10^{3}$	$56.22{\cdot}10^{2}$	1			[J/mol]
k_{s0}	$1.91{\cdot}10^{-7}$	$8.33{\cdot}10^{-8}$	−0.7	1		[m/s]
$k_{c,ref}$	$2.86{\cdot}10^{-10}$	$2.73{\cdot}10^{-11}$	0.6	−0.6	1	[(m^3/mol)(m^3/kg)s^{-1}]

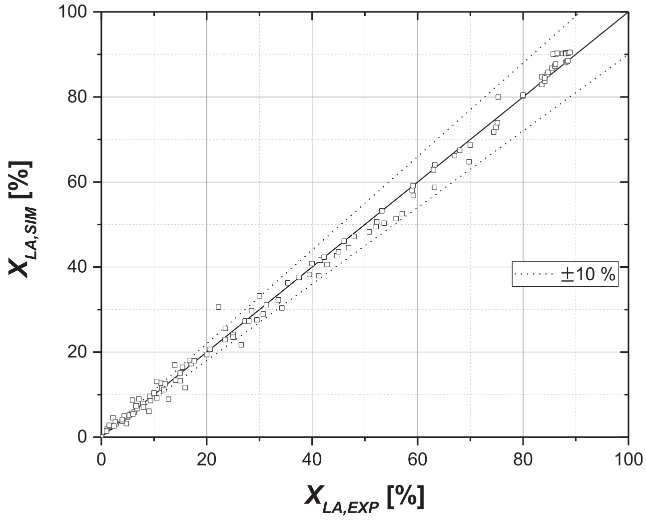

Fig. 6. Parity plot on all the collected data.

together with statistic information, and the simulated data are compared with the experimental data in Figs. 2–5.

The parameters are consistent, and the standard error of the parameters were typically less than 4%, showing only a slight correlation. The agreements between experimental and calculated data are very good, as revealed in Figs. 2–5 and in the parity plot reported in Fig. 6, showing that all the data fall in a window of error of ± 10%.

High limitation in the intra-particle diffusion is confirmed by the Weisz-Prater criterion, Eq. (21).

$$C_{W-P} = \frac{-r_{obs,p} R_p{}^2}{D_{e,LA} C_{LA,0}} = \frac{-r_{obs} \rho_p R_p{}^2}{D_{e,LA} \rho_B C_{LA,0}} \tag{21}$$

The results obtained from adopting the W-P criterion is always about 10, fact that confirms the presence of intra-particle diffusion limitation (please, see Supplementary Material for detailed information). This result is opposite to the expected one, because the gel-type catalyst should involve a low intra-particle diffusion limitation, probably the high limitation of the diffusion inside the particle is due to the dimension of the molecules of the studied system.

The effectiveness factor of the system was calculated for the reference experiment (Test 4 of Table 1), adopting the definition reported in Eq. (22). The results reported in Fig. 7 confirm a rather high intraparticle diffusion limitation, leading to a plateau value of 0.7.

$$\eta = \frac{\int_0^1 r_C(x) x^{s-1} dx}{r_C|_{x=1} \int_0^1 x^{s-1} dx} \tag{22}$$

3.2. Kinetics in continuous packed bed reactor

3.2.1. Fluid-dynamic characterization

The results from the RTD experiments were used to determine the axial dispersion coefficient (D_z) and thus, obtain the Péclet number. The axial dispersion model is often used to describe the fluid-dynamics in tubular reactors, describing the turbulence in the longitudinal direction with an axial dispersion term. The axial dispersion coefficient accounts for both molecular diffusion and convection mechanisms in the axial direction. D_z gives an idea of the performance of the reactor, e.g. when $D_z = 0$, it means that the reactor is a plug flow and when $D_z \rightarrow +\infty$, the reactor behaves as a continuous stirred tank reactor.

The main assumptions of the adopted reactor model are reported below:

- Uniform velocity and concentration profiles along the radius of the pipe
- No radial dispersion is considered

The collected data were interpreted using the mass balance equation reported in Eq. (23), that is a typical axial dispersion model for a non-reactive system.

$$\frac{\partial c_t}{\partial t} = -u\frac{\partial c_t}{\partial z} + D_z\frac{\partial^2 c_t}{\partial z^2} \tag{23}$$

where, u is the velocity [m/s], D_z is the axial dispersion coefficient [m^2/s].

Two boundary conditions were defined to solve numerically the PDE system:

$$c_t|_{z=0} = c_{t,feed}(0 \le t \le t_{injection}),\ c_t|_{z=0} = 0(t > t_{injection}) \tag{24}$$

$$\left.\frac{\partial c_t}{\partial z}\right|_{z=L} = 0 \tag{25}$$

Closed-closed vessel Boundary Condition (BC) were chosen as the Péclet numbers were expected to be high for the studied system; the mentioned BCs consider that no axial dispersion occurs both at the inlet and outlet of the reactor. The first BC is referred to the inlet of the reactor, considering the feed concentration, that for a pulse-experiment

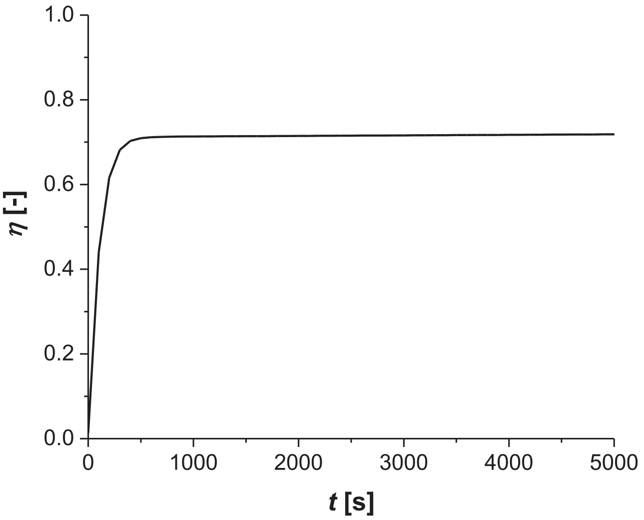

Fig. 7. Effectiveness factor trend vs the experimental time calculated for Test 4 of Table 1, conducted by fixing $T = 343$ K, 800 rpm stirring rate, $\rho_B = 19.7$ kg/m^3 and EtOH to LA 5:1 M ratio.

Table 8
Results of the fluid-dynamic characterization experiments in continuous packed bed reactor. The calculated values of the axial dispersion coefficient (D_z), bed void degree (ε_B), Péclet number (Pe) and Reynolds particle number (Re_p) are reported as a function of the experimental temperature (T) and volumetric flowrate ($\dot{V}$).

TEST	$\dot{V}$ [m^3/s]	T [K]	τ [s]	D_Z [m^2/s]	ε_B [–]	Pe [–]	Re_p [–]
1	$1.7{\cdot}10^{-8}$	298	295	$(2.6 \pm 0.2){\cdot}10^{-6}$	0.34 ± 0.02	110	2.5
2	$2.5{\cdot}10^{-8}$	298	201	$(3.9 \pm 0.2){\cdot}10^{-6}$	0.35 ± 0.02	105	1.6
3	$3.3{\cdot}10^{-8}$	298	153	$(5.6 \pm 0.2){\cdot}10^{-6}$	0.35 ± 0.01	114	1.2
4	$5.0{\cdot}10^{-8}$	298	101	$(8.1 \pm 0.3){\cdot}10^{-6}$	0.35 ± 0.03	116	0.8
5	$6.7{\cdot}10^{-8}$	298	77	$(1.2 \pm 0.1){\cdot}10^{-5}$	0.35 ± 0.02	115	4.8
6	$10{\cdot}10^{-8}$	298	52	$(1.5 \pm 0.1){\cdot}10^{-5}$	0.36 ± 0.02	101	3.3
7	$13{\cdot}10^{-8}$	298	40	$(1.7 \pm 0.2){\cdot}10^{-5}$	0.37 ± 0.03	120	6.3
8	$17{\cdot}10^{-8}$	298	35	$(2.2 \pm 0.2){\cdot}10^{-5}$	0.37 ± 0.03	107	7.2
9	$5.0{\cdot}10^{-8}$	343	103	$(1.2 \pm 0.1){\cdot}10^{-5}$	0.35 ± 0.02	87	2.5
10	$8.3{\cdot}10^{-8}$	343	61	$(1.7 \pm 0.2){\cdot}10^{-5}$	0.34 ± 0.02	88	4.1
11	$12{\cdot}10^{-8}$	343	50	$(2.1 \pm 0.1){\cdot}10^{-5}$	0.35 ± 0.02	96	5.7

shows a classical pulse function, where the tracer concentration at the inlet of the reactor is equal to zero when the experimental time is greater than the injection time, while it is equal to a finite value for experimental time comprised between zero and the injection time. The injection time is given by the volume of the HPLC injector loop (20 µL) divided by the flowrate of the experiment.

The results of the experiments conducted in pulse modality using as a tracer yellow naphthol are reported in Table 8.

As revealed, the axial dispersion coefficient (D_z) increases with the volumetric flow rate, due to the increase in turbulent mixing which cannot be neglected. Another parameter obtained was the reactor void fraction (ε_B) is change between 0.34 and 0.37 with an average value of 0.36 ± 0.02.

The Péclet number, defined as in Eq. (26).

$$Pe = \frac{uL}{D_z} \tag{26}$$

where, u is the velocity magnitude [m/s], L is a characteristic length of the reactor [m], and D_z is a characteristic diffusion coefficient [m^2/s]. As it is possible to note the Péclet number is proportional to the inverse of the axial dispersion coefficient. The Reynolds particle number is the ratio between the inertial forces against the viscous forces, in a packed bed such as our case it is define (Eq. (27)):

$$Re_p = \frac{d_p \rho_f u}{\mu_f} \tag{27}$$

where, d_p is the particle diameter [m], ρ_f is the density of fluid [kg/m^3], u is the interstitial velocity of the mixture through the packed bed [m/s], and μ_f is the fluid viscosity [cP]. The values obtained for each test are reported in Table 8.

Considering that D_z (proportional to the reverse of Péclet) is always < 0.01, it can be confirmed that the deviation to the plug flow of our reactor configuration is small. The obtained Pe were fitted vs Re_p, obtaining the plot reported in Fig. 8. As revealed, at T = 298 K, a clear invariance can be observed. At higher temperatures, the trend shows a slight increase of the Pe vs Re_p, whereas if the experimental error is considered, also in this case it is possible to assume that only a slight invariance in the investigated range can be observed. At this temperature, the reactor behavior changes slightly with the volumetric flow and, even considering the vessel dispersion number, its values are always > 0.01, thus the fluid-dynamics of our reactor is not far from the plug flow.

3.2.2. Kinetic experiments in packed bed reactor

The first experiment was conducted to check the stability onstream of the catalyst. The experiment was performed at T = 323 K and $1.7{\cdot}10^{-8}$m^3/s flowrate. The results are reported in Fig. 9A.

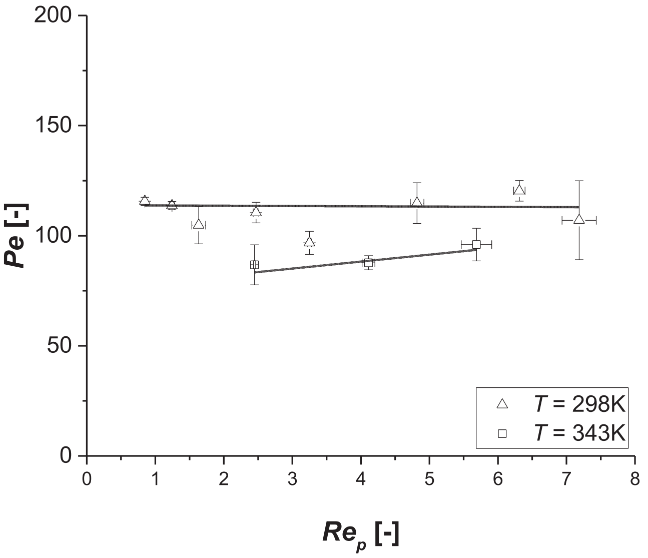

Fig. 8. Péclet number plot vs Reynolds particle number.

As revealed, the catalyst shows good stability in the adopted conditions, confirming its applicability in a continuous device.

Experiments were conducted in a fixed bed reactor packed with Amberlite IR120, with the aim to validate the kinetic model developed in batch conditions.

Each test was conducted changing the volumetric flowrate and temperature. The experimental results are reported in Fig. 9B, showing the trend of the levulinic acid conversion degree that decreases with the volumetric flow, parametric with temperature. The highest conversions for the lower volumetric flow are due to a higher contact time between the reactants and the catalyst.

Another important thing to underline is the temperature effect on the reaction: the conversion is high for the highest temperature adopted in the reactor, as expected.

The experimental data collected in the continuous system were simulated developing a dedicated model. In a heterogeneous system, with a porous solid as catalyst, three limiting regime can be found: i) external fluid-solid mass-transfer, due to the diffusion of reactants from the liquid bulk to the solid surface; ii) internal mass-transfer, due to the diffusion of the reactant from the solid surface to the core of the particle and vice versa for the products; iii) kinetic regime, due only to the reaction rate. At first, the external mass transfer coefficient (k_s) was estimated with the Dwivedi & Upadhyay correlation [23], applicable for Reynolds particle number < 10, Eq. (28).

$$k_s = 1.108 u \varepsilon_B^{-1} \left(\frac{u d_p \rho}{\mu}\right)^{-0.72} \left(\frac{\mu}{\rho D}\right)^{-0.67} \tag{28}$$

where, D is the levulinic acid molecular diffusivity in ethanol [m^2/s], μ is the ethanol dynamic viscosity [cP] and ρ the ethanol density [kg/m^3]. The result obtained from Dwidevi & Upadhyay correlation give a low external mass-transfer coefficient value ($k_s = 2.3{\cdot}10^{-7}$ [m/s]). As, the reactants molecule would, with this assumption, diffuse slowly in the stagnant film surrounding the catalyst particle, it is reasonable to assume that the reaction occurs only on the catalyst surface. Thus, we excluded the intra-particle mass transfer limitations in the packed bed reactor. On this basis the continuous model was developed considering only external mass-transfer limitation and the surface reaction. The value of the external mass-transfer coefficient was calculated from Eq. (28).

The summary of the modelling assumptions is reported below:

- Uniform velocity and concentration profiles along the radius of the pipe

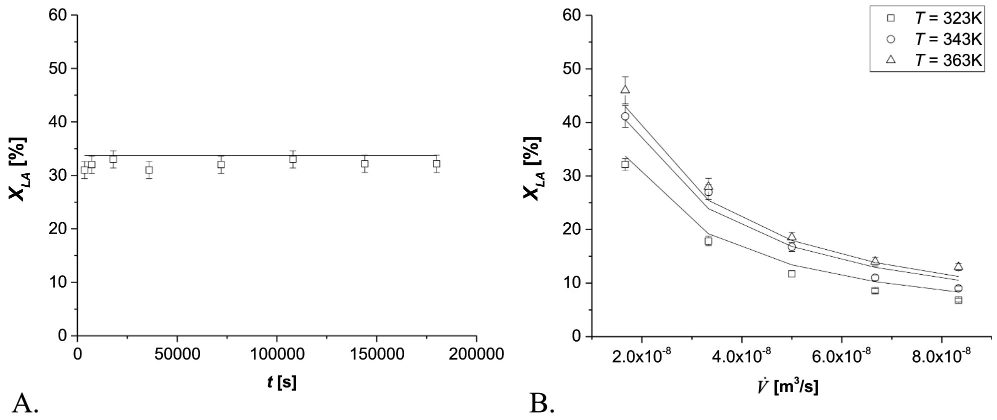

Fig. 9. A. Levulinic acid conversion vs time on stream for the experiment conducted at $T = 323$ K and a volumetric flowrate of $1.7 \cdot 10^{-8}$m^3/s. B. Simulated and experimental data comparison for the kinetic experiments conducted in the packed bed reactor. Symbols: Experimental data; Lines: Simulated values.

- No radial dispersion is considered
- The autocatalytic reaction occurs in the liquid bulk phase
- The catalytic reaction occurs on the catalyst surface
- The reactor is considered isothermal
- Fluid-solid mass transfer resistance is dominant compared with intraparticle diffusion limitation

By adopting the mentioned assumptions, the bulk phase mass balance equation reported in Eq. (29) can be written, where z is the axial coordinate:

$$\frac{\partial c_{i(l)}}{\partial t} = -u\frac{\partial c_{i(l)}}{\partial z} + D_z\frac{\partial^2 c_{i(l)}}{\partial z^2} - k_s a_{sp}(c_{i(l)} - c_{i(s)}) + \nu_i r_{NC} \tag{29}$$

where, u is the velocity [m/s], D_z is the axial dispersion [m^2/s] evaluated with the fluid-dynamic characterization and k_s the fluid-solid external mass transfer [m/s] and a_{sp} the specific surface area [m^2/m^3].

The reaction rate expression with related parameters is applied as can be found in the batch model and the physical quantities adopted are the same too.

Two boundary conditions were defined to solve numerically the PDE system:

$$c_i|_{z=0} = c_i^0 \tag{30}$$

$$\left.\frac{\partial c_i}{\partial z}\right|_{z=L} = 0 \tag{31}$$

Closed-closed vessel Boundary Condition (BC) were chosen as the Péclet numbers are high for the studied system; the mentioned BCs consider that no axial dispersion occurs both at the inlet and outlet of the reactor. The first BC is referred to the inlet of the reactor, considering the feed concentration of each component. The second BC is referred at the outlet of the reactor. The mass balance on the solid phase considered in the model was evaluated as in Eq. (32).

$$k_s a_{sp}(c_i - c_{i(s)}) = +\nu_i r_C \rho_B \tag{32}$$

Each experiment was simulated with no additional parameter estimation activity. The results of the simulation and the comparison with the experimental data are shown in Fig. 9 in terms of LA conversion against the volumetric flow, varying the temperature. As revealed, the model predictions are very good, simulating the trends accurately both with temperature and flowrate, allowing to conclude that the model was successfully validated.

4. Conclusions

The effects of the temperature, alcohol:levulinic acid molar ratio, catalyst loading and stirring rates have been investigated at the aim to study the kinetics of the system. Reliable kinetic models were proposed, and the experimental data were interpreted adopting an intraparticle mass balance model. The experimental data collected are in good agreement with the data calculated by the developed model allowing to obtain reliable kinetic parameters, while the thermodynamic ones were fixed from our previous investigations. The model predictions showed a rather high influence of intraparticle diffusion limitation. The developed model was validated by conducting experiments in continuous packed bed reactor. The continuous unit was first characterized in terms of fluid-dynamics, showing a behavior not far from the plug-flow, then was used to conduct a set of experiments, varying temperature and residence time. The data were interpreted by a fluid-solid mass transfer limited packed bed reactor model, as by using existing correlations we concluded that fluid-solid external mass transfer limitation is surely the rate-determining step of the reaction network. The collected data were simulated, with no additional parameter estimation allowing the validation of the developed kinetic model.

In conclusion, this study puts the basis for the scale-up of the levulinic acid esterification process, normally run in industry in batch using mineral acids as catalyst.

Declaration of Competing Interest

The authors declare that they have no known competing financial interests or personal relationships that could have appeared to influence the work reported in this paper.

Acknowledgement

Emmanuel De Gregorio and Anthony Smith are acknowledged for their experimental support in conducting the kinetic experiments in respectively batch and packed bed reactor.

Appendix A. Supplementary data

Supplementary data to this article can be found online at https://doi.org/10.1016/j.cej.2020.126126.

References

[1] B. Girisuta, Levulinic Acid from Lignocellulosic Biomass, phD Thesis, 2007.
[2] C. Antonetti, D. Licursi, S. Fulignati, G. Valentini, A.M. Raspolli Galletti, New frontiers in the catalytic synthesis of levulinic acid: from sugars to raw and waste biomass as starting feedstock, Catalysts 12 (2016) 196, https://doi.org/10.3390/catal6120196.
[3] Q.B. Broxterman, M.C.C. Janssen, M.M.P.W.M. Rijkers, The levulinic acid product tree: a versatile opportunity in the bio-based economy What does it take to establish such transition? Chem. Today 35 (2017) 6–18.
[4] C. Gong, J. Wei, X. Tang, X. Zeng, Y. Sun, L. Lin, Production of levulinic acid and

ethyl levulinate from cellulosic pulp derived from the cooking of lignocellulosic biomass with active oxygen and solid alkali, Korean J. Chem. Eng. 36 (2019) 740–752, https://doi.org/10.1007/s11814-019-0254-6.

[5] V. Umrigar, M. Chakraborty, P. Parikh, Esterification and ketalization of levulinic acid with desilicated zeolite β and pseudo-homogeneous model for reaction kinetics, Int. J. Chem. Kinet. 51 (2019) 299–308, https://doi.org/10.1002/kin.21253.

[6] J. Zhang, S. Wu, B. Li, H. Zhang, Advances in the catalytic production of valuable LevulinicAcid derivatives, ChemCatChem 4 (2012) 1230–1237, https://doi.org/10.1002/cctc.201200113.

[7] F. Yang, J. Tang, Catalytic Upgrading of Renewable Levulinic Acid to Levulinate Esters Using Perchloric Acid Decorated Nanoporous Silica Gels, Chemistry Select 4 (2019) 1403–1409, https://doi.org/10.1002/slct.201803608.

[8] H.J. Bart, J. Reidetschlager, K. Schatka, A. Lehmann, Kinetics of esterification of levulinic acid with n-butanol by homogeneous catalysis, Ind. Eng. Chem. Res. 33 (1994) 21–25, https://doi.org/10.1021/ie00025a004.

[9] Y. Liu, E. Lotero, J.G. Goodwin, A comparison of the esterification of acetic acid with methanol using heterogeneous versus homogeneous acid catalysis, Jr. J. Catal. 242 (2006) 278–286, https://doi.org/10.1016/j.jcat.2006.05.026.

[10] D.R. Fernandes, A.S. Rocha, E.F. Mai, C.J.A. Mota, V. Teixeira da Silva, Levulinic acid esterification with ethanol to ethyl levulinate production over solid acid catalysts, Appl. Catal. A 425–426 (2012) 199–204, https://doi.org/10.1016/j.apcata.2012.03.020.

[11] N.A.S. Ramli, N.H. Zaharudin, N.A.S. Saidina, Esterification of renewable levulinic acid to levulinate esters using amberlyst-15 as a solid acid catalyst, Jurnal Teknologi (Sciences & Engineering) 79 (2017) 137–142, https://doi.org/10.17576/jsm-2018-4706-08.

[12] J.A. Melero, G. Morales, J. Iglesias, M. Paniagua, B. Hernández, S. Penedo, Efficient conversion of levulinic acid into alkyl levulinates catalyzed by sulfonic mesostructured silicas, Appl. Catal. A 466 (2013) 116–122, https://doi.org/10.1016/j.apcata.2013.06.035.

[13] S. An, D. Song, B. Lu, X. Yang, Y.H. Guo, Morphology tailoring of sulfonic acid functionalized organosilica nanohybrids for the synthesis of biomass-derived alkyl levulinates, Chem. Eur. J. 21 (2015) 10786–10798, https://doi.org/10.1002/chem.201501219.

[14] M.A. Tejero, E. Ramírez, C. Fité, J. Tejero, F. Cunill, Esterification of levulinic acid with butanol over ion exchange resins, Appl. Catal. A 517 (2016) 56–66, https://doi.org/10.1016/j.apcata.2016.02.032.

[15] V. Russo, V. Hrobar, P. Mäki-Arvela, K. Eränen, F. Sandelin, M. Di Serio, T. Salmi, Kinetics and modelling of levulinic acid esterification in batch and continuous reactors, Top. Catal. 61 (2018) 1856–1865, https://doi.org/10.1007/s11244-018-0998-y.

[16] S.B. Onkarappa, M. Javoor, S.S. Mal, S. Dutta, Efficient and Scalable production of alkyl levulinates from cellulose-derived levulinic acid using heteropolyacid catalysts, ChemistrySelect 4 (2019) 2501–2504, https://doi.org/10.1002/slct.201803641.

[17] V. Russo, C. Rossano, E. Salucci, R. Tesser, T. Salmi, M. Di Serio, Intraparticle diffusion model to determine the intrinsic kinetics of ethyl levulinate synthesis promoted by Amberlyst-15, Chem. Eng. Sci. (Submitted 2020).

[18] M.R. Altıokka, A. Cıtak, Kinetics study of esterification of acetic acid with isobutanol in the presence of Amberlite catalyst, Appl. Catal. A 239 (2003) 141–148, https://doi.org/10.1016/S0926-860X(02)00381-2.

[19] O. Jogunola, T. Salmi, K. Eranen, J.P. Mikkola, Qualitative treatment of catalytic hydrolysis of alkyl formats, Appl. Catal. A 384 (2010) 36–44, https://doi.org/10.1016/j.apcata.2010.06.002.

[20] G.W. Bodamer, R. Kunin, Behavior of ion exchange resins solvents other than water, Ind. Eng. Chem. 45 (1953) 2577–2580, https://doi.org/10.1021/ie50527a057.

[21] A. Kolrnogorov, I. Petrovskii, N. Piskunov, Étude de l'équations de la chaleur, de la matiére et son application á un probleme biologique, Bull. Math. 1 (1937) 1–26.

[22] ChemCAD 7.0. https://www.chemstations.com/ (accessed 07.04.2020).

[23] P.N. Dwivedi, S.N. Upadhyay, Particle-Fluid Mass Transfer in Fixed and Fluidized Beds, Ind. Eng. Chem. Process Des. Dev. 16 (1977) 157–165, https://doi.org/10.1021/i260062a001.

III

Chemical Engineering Journal 377 (2019) 119692

Contents lists available at ScienceDirect

Chemical Engineering Journal

journal homepage: www.elsevier.com/locate/cej

Chromatographic reactor modelling

Vincenzo Russo[a,*], Riccardo Tesser[a], Carmelina Rossano[a], Rosa Vitiello[a], Rosa Turco[a], Tapio Salmi[b], Martino Di Serio[a]

[a] *Università di Napoli Federico II, Naples Industrial Chemistry Laboratory, Complesso Universitario Monte S. Angelo, via Cintia 4, IT-80126 Napoli, Italy*
[b] *Åbo Akademi, PCC/Chemical Engineering, Laboratory of Industrial Chemistry and Reaction Engineering, FI-20500 Turku/Åbo, Finland*

HIGHLIGHTS

- Dynamic Adsorptive Chromatographic Reactor model (DACR) was developed.
- External and intraparticle diffusion limitations were considered.
- gPROMS Model Builder was used to implement the model.
- The model was tested on literature data with satisfactory results.
- A sensitivity analysis shown the predictive power of the model.

GRAPHICAL ABSTRACT

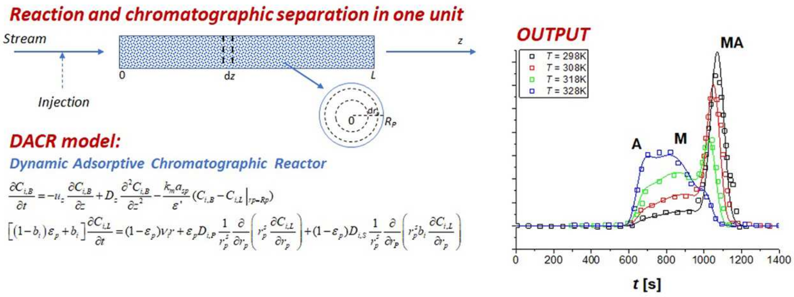

ARTICLE INFO

Keywords:
Chromatographic reactor
Ester hydrolysis
Modelling
Mass-transfer
Intraparticle diffusion

ABSTRACT

Reactive chromatography is a special topic in chemical reaction engineering, consisting of the combination of chemical reaction and chromatographic separation. The main idea is to avoid a further separation unit, by performing reaction and separation in one unique equipment, allowing process intensification. This technology is usually applied in hydrolysis (or esterification) reactions, that undergoes through the reaching of chemical equilibrium. The chromatographic reactor application would lead to complete conversion, by separating reactants and products as the reaction proceeds. Modelling is certainly a delicate issue for chromatographic reactor to optimize the operation conditions, thus different approaches were published. The aim of the present work is to show a novel chromatographic reactor model, were all the physical and chemical phenomena involved and described by a rigorous approach. The fluid-dynamics was treated by axial dispersion approach, and the Péclet number values were obtained from dedicated experiments. The external fluid-solid mass transfer was calculated from existing correlations, demonstrating to be negligible for the modelled chromatographic reactor. The intraparticle mass diffusion was assumed to be the sum of two parallel contributions, i.e. porous and surface diffusivity. The model was tested on literature data for methyl acetate hydrolysis experiments with satisfactory results, obtaining reliable values of the surface diffusivity. A sensitivity analysis was conducted highlighting that the model can predict complete ester conversion and product separation.

1. Introduction

Reactive chromatography is a very actual topic for chemical reaction engineering. The concept implies the combination of reaction and chromatographic separation in the same unit [1–4], allowing the intensification of chemical processes. The chromatographic reactor is a

---

[*] Corresponding author.
E-mail address: v.russo@unina.it (V. Russo).

https://doi.org/10.1016/j.cej.2018.08.078
Received 11 June 2018; Received in revised form 10 August 2018; Accepted 12 August 2018

Nomenclature

A_i, B_i, C_i, D_i	coefficients, -
a_{sp}	geometrical specific surface area, m^2/m^3
b	adsorption parameter, m^3_L/m^3_S
$C_{i,B}$	concentration of component i in the bulk phase, mol/m^3_{BULK}
$C_{i,L}$	concentration of component i in the liquid pore phase, mol/m^3_L
$C_{i,S}$	concentration of component i in the solid phase, mol/m^3_S
D_{mol}	molecular diffusivity, m^2/s
D_p	pore diffusivity, m^2/s
D_P	particle diameter, m
D_S	surface diffusivity, m^2/s
D_z	axial dispersion coefficient, m^2/s
E	residence time distribution function, -
Ea	activation energy, kJ/mol
E_S	surface energy, kJ/mol
J_D	external mass transfer factor, m^2/s
k	kinetic constant, $m^3/mol/s$
K	equilibrium constant, -
k_m	liquid-solid mass transfer coefficient, m/s
L	reactor length, m
Mw	molecular weight, g/mol
Pe	Péclet number, -
Q	volumetric flow-rate, mL/min
r	reaction rate, $mol/m^3_L/s$
R	gas ideal constant, kJ/mol/K
Re_p	Reynolds number of particle, -
r_p	radial coordinate of particle, m
R_p	particle radius, m
s	shape factor, -
Sc	Schmidt number, -
t	time, s
T	temperature, K
t_0	time for not-retained component, s
T_b	standard boiling point temperature, K
t_{inj}	injection time, s
t_{MAX}	time at the chromatographic peak maximum, s
V_{loop}	loop volume, m^3
$\dot{V}$	volumetric flow-rate, mL/min
V_{mol}	molar volume, cm^3/mol
u_z	free velocity, m/s
z	reactor axial coordinate, m

Greek symbols

α	mass transfer coefficient, -
ΔH_i	adsorption heat, kJ/mol
ΔH_r	reaction enthalpy, kJ/mol
ε	bed void fraction, -
ε'	volumetric ratio between the bulk volume and the overall particle volume, -
ε_p	solid particle porosity, -
μ	viscosity, cP
ν	stochiometric matrix, -
ρ	density, Kg/m^3
τ	tortuosity factor, -
φ	association factor, -

Abbreviations

A	acetic acid
B	liquid bulk
feed	feed
L	liquid inside porous particles
M	methanol
MA	methyl acetate
S	surface
W	water

packed bed unit where reaction and chromatographic separation occur in the same equipment, thus the solid phase must act both as catalyst and stationary phase. It is evident that the solid phase must be characterized by reactivity and selective adsorption to reactants/products.

The comparison between packed-bed reactors and chromatographic reactors shows that for equilibrium reactions, the separation of the products is responsible for the increase of the reactant conversion. The chromatographic reactor concept can offer several advantages: (i) the enhancement of conversion overcoming equilibrium limitations, (ii) the possibility of full separation of pure products, (iii) potential to influence the selectivity of complex reaction networks [5]. The concept finds interesting industrial applications, particularly when shifted to simulated moving bed chromatographic technology, which is used to increase conversion and separation of the products [6–12].

The modelling of chromatographic reactors is still an open issue, as the efforts published in the literature are simplified, thus characterized

Table 1
Literature survey on chromatographic reactor modelling.

Year	Refs.	Application/approach
1978	[13]	● **Application**: cyclohexane dehydrogenation. ● **Approach**: simplified model as semi-batch reactor; each component shows different flow velocity. ● **Drawbacks:** no fluid-dynamics, low predictivity.
1996–1999	[14,15]	● **Application**: acetic acid esterification with ethanol. ● **Approach**: liquid–solid model working under kinetic regime. ● **Drawbacks:** low predictive power. - No mass transfer limitation: fluid/solid, intraparticle. - No axial dispersion. - Solid phase pseudo-homogeneous.
2011	[17,18]	● **Application**: methyl formate and methyl acetate hydrolysis. ● **Approach**: liquid–solid model where axial dispersion fixed by the number of theoretical plates. ● **Drawbacks:** good predictive power only when the adopted operation conditions. - Different axial dispersion coefficient for each component: fluid/solid affinity and diffusion lumped in one parameter. - No mass transfer limitation: fluid/solid, intraparticle.
2011–2015	[19–21]	● **Application:** butyl acrylate, glycerol ethyl acetal, 1,1-dibutoxyethane synthesis. ● **Approach:** linear driving force approximation where internal and external mass transfer mechanisms were lumped. ● **Drawbacks:** high predictive power only in the adopted operation conditions. - Average concentration was considered in the particle: valid when intraparticle diffusion resistance is negligible.

by a low predictive power. A summary of the main modelling approaches to the reactive chromatography is reported in Table 1.

The first model, published in 1978, was applied to cyclohexane dehydrogenation, treating the reactor as a semi-batch reactor, in which each component was characterized by a different flow velocity [14]. This simplification leads to a low predicting power of the model. The breakthrough came in 1990s, where Mazzotti et al. [14,15] published a new liquid-solid model, operating in kinetic regime, for acetic acid esterification. The model showed a good performance, but it cannot be extended in predicting industrial reactors where mass-transfer phenomena can dominate the system. In this century, more advanced models were published in the literature, including heat transfer aspects, but simplifying the fluid-dynamics to plug flow model [16]. More advanced models were published including axial dispersion, defining an axial dispersion coefficient for each chemical compound involved in the reaction, calculating it from the number of theoretical plates. These models were a real breakthrough as it was possible to simulate peaks of different widths, depending on the interaction between the reactants, the products and the solid phase [17–21]. These models were characterized by a good predictive power only within the adopted range of operation conditions. No fluid/solid external mass transfer limitation was considered [17,18], and intraparticle diffusion effects were lumped in an apparent axial dispersion coefficient. Other approaches adopted a linear driving force approximation where external and internal mass transfer mechanisms were lumped, calculating an average concentration in the solid particle, thus no intraparticle profiles can be calculated [19–21], assumption valid only if intraparticle mass transfer limitation can be considered negligible (i.e. low viscous media, small particle size), leading to the absence of concentration gradients.

In the present work, a new Dynamic Adsorptive Chromatographic Reactor model (DACR) will be presented. The model is based on the description of the chemistry and physics in detail, focusing the attention on all the possible mass transfer steps appearing in the chromatographic reactor. Axial dispersion was measured with dedicated experiments; external mass transfer resistance was evaluated from existing correlations; intraparticle diffusivity was considered to comprise the sum of two contributions: (i) pore diffusivity; (ii) surface diffusivity. Intraparticle diffusivity was included to include the influence of concentration gradients inside the solid particles on the chromatographic reactor performance predictions. The model was tested on literature data and it was used to predict the behavior of the chromatographic reactor performance in a sensitivity study.

2. Materials and methods

2.1. Materials

All the reactants and catalysts used in the present work were purchased by Sigma Aldrich, at the highest purity level available.

2.2. Methods

A chromatographic reactor equipment was designed and tested to determine the axial dispersion coefficients. The device consisted of a HPLC pump (flowrate range < 10 mL/min) connected to a HPLC injector (loop volume $= 10$ μL). The reactor consisted of a jacketed pipe of 0.3 m length and 0.78 cm diameter. The detector was an RD4: 250-280-RI-Cond purchased by REACH Devices. The detector allowed the simultaneous of refractive index (RI), conductivity and UV (at both 250 and 280 nm). A sketch of the installed equipment is shown in Fig. 1. The experimental data were acquired via RS232 to a PC.

The PDE system describing the chromatographic reactor was solved with the method of lines already implemented in gPROMS Model Builder v. 4.0. The axial coordinate of the reactor was solved with an asymmetrical backward finite difference approximation, defining 150 grid points transformed by log10. The reason of the logarithm transformation was to achieve a better resolution of the chromatographic peaks in the initial part of the reactor where the peaks are approaching the δ function of Dirac due to the injection. The radial coordinate of the particle was approximated by a 2nd order central finite difference method (CFDM) with 20 discretization points.

3. Results and discussion

3.1. Chromatographic reactor model

The chromatographic reactor model, namely the Dynamic Adsorptive Chromatographic Reactor model (DACR), was developed to describe ester hydrolysis experiments in the presence of a solid phase acting both as a catalyst and a stationary phase. The model assumes that an excess of the reactant is continuously fed to the reactor inlet (i.e. water in hydrolysis reactions), while the second reactant (methyl acetate) is pulsed trough the injector. The reaction occurs in a liquid-solid system; hence it is necessary to write mass balance equations related to both phases. The balance schemes are reported in Fig. 2.

The model was written in a time-dependent form, to simulate the evolution of the concentration profiles along the reactor bed. The liquid

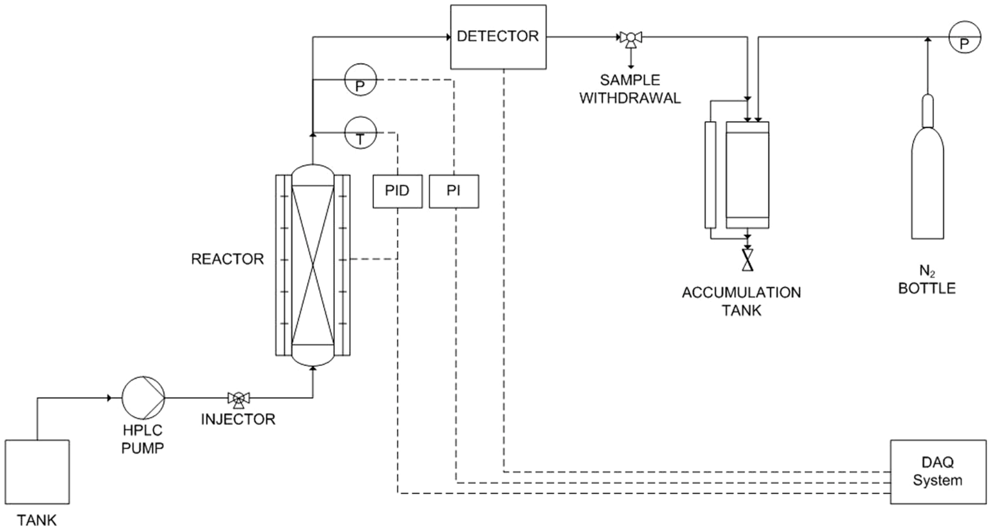

Fig. 1. Schematic flowsheet of the chromatographic reactor set-up. DET: detector. DAQ: Data acquisition module.

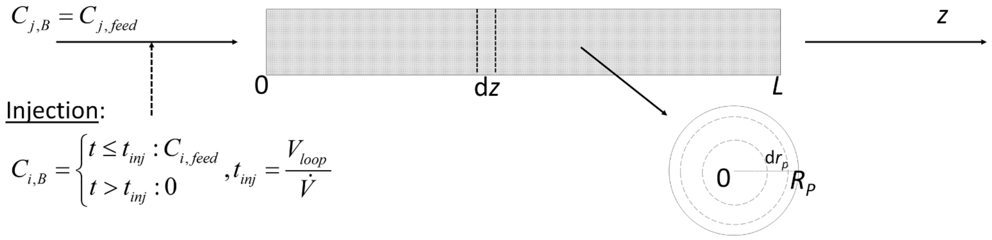

Fig. 2. Mass balance scheme of the chromatographic with related coordinates.

phase flows in the axial z coordinate. The fluid-dynamics was described by considering both axial dispersion and liquid film mass transfer, Eq. (1).

$$\frac{\partial C_{i,B}}{\partial t} = -u_z \frac{\partial C_{i,B}}{\partial z} + D_z \frac{\partial^2 C_{i,B}}{\partial z^2} - \frac{k_m a_{sp}}{\varepsilon'}(C_{i,B} - C_{i,L}|_{rp=Rp}) \tag{1}$$

As revealed by Eq. (1), fluid-velocity and total concentration were considered constants. This assumption is surely valid for a chromatographic reactor where one of the reactants is pulsed is small quantity to a stream of the other reactant, thus the change in the overall composition is not very influent on the fluid-velocity.

The solution of Eq. (1), requires two boundary conditions (BCs), defined at the reactor inlet and outlet for both the continuous stream and the pulse, Eq. (2)–(4).

$$C_{i,B}|_{z=0} = \begin{cases} t \leqslant t_{inj}: C_{i,feed} \\ t > t_{inj}: 0 \end{cases}, \quad t_{inj} = \frac{V_{loop}}{\dot{V}} \tag{2}$$

$$C_{j,B}|_{z=0} = C_{j,feed} \tag{3}$$

$$\left.\frac{\partial C_{i,B}}{\partial z}\right|_{z=L} = 0 \tag{4}$$

The pulsed-stream BCs take into account that a small quantity of a reactant (*i*) flows in the reactor with an injection time that is proportional to the volume of the injection loop and the volumetric flow-rate of the main stream (component *j*). The stream composition at the inlet of the reactor was considered constant with reactor radius. This assumption is valid for a fluid-dynamic characterized by high Péclet numbers, i.e. an assumption always realistic for beds packed by particles characterized by small dimension (i.e. 38.5 µm for Dowex 50 W-X8 catalyst), which act as static mixer elements. This will be demonstrated in the next paragraphs related to the axial dispersion determination. Finally, at the reactor outlet, a mass flux equal to zero was considered (Danckwerts' closed boundary condition).

The intraparticle mass balance equation was written to include both liquid inside pores and surface diffusion phenomena. As it was previously demonstrated by us [22–25], adsorption can be described by calculating the diffusion path in a solid particle as the sum of two parallel contributions: (i) the porous diffusion, depending on the porosity and tortuosity of the particle; (ii) surface diffusion, depending on the interaction between one component present in the fluid phase and the solid surface. It is possible to write the general intraparticle mass balance equation as follows, Eq. (5).

$$\begin{aligned} [(1-b_i)\varepsilon_p + b_i]\frac{\partial C_{i,L}}{\partial t} &= (1-\varepsilon_p)\nu_i r + \varepsilon_p D_{i,P}\frac{1}{r_p^s}\frac{\partial}{\partial r_p}\left(r_p^s \frac{\partial C_{i,L}}{\partial r_p}\right) \\ &+ (1-\varepsilon_p)D_{i,S}\frac{1}{r_p^s}\frac{\partial}{\partial r_P}\left(r_p^s b_i \frac{\partial C_{i,L}}{\partial r_p}\right) \\ C_{i,S} &= b_i C_{i,L} \end{aligned} \tag{5}$$

The two contributions to the intraparticle diffusion path are added and they are proportional to different diffusion parameters. To calculate the solid concentration, the adsorption isotherm must be considered. As the pulsed component becomes diluted in the continuous stream, the adsorption isotherm can be approximated to be linear. This assumption is certainly wrong in the case of a fixed-bed adsorptive reactor, where the two reactants are fed simultaneously at the inlet of the reactor, thus the system cannot be considered diluted and the implementation of a dedicated adsorption isotherm is needed. In our recent publications [24,25], we demonstrated how to model a continuous adsorption column. In this case, a Langmuir isotherm was included in modelling the methylene blue adsorption over silica. The readers are strongly suggested to refer to those papers, as a more general set of mass balance equations are reported for both bulk and intraparticle phases.

Four sets of boundary conditions are needed to calculate the evolution with both time and particle radius of both liquid and solid concentrations, Eqs. (6) and (7).

$$[\varepsilon_p D_p + (1-\varepsilon_p)b_i D_S]\left.\frac{\partial C_{i,L}}{\partial r_P}\right|_{z=0} = k_m(C_{i,B} - C_{i,L}|_{z=0}), \quad \left.\frac{\partial C_{i,L}}{\partial z}\right|_{z=L} = 0 \tag{6}$$

$$\left.\frac{\partial C_{i,L}}{\partial r_P}\right|_{rP=0} = 0, \quad [\varepsilon_p D_p + (1-\varepsilon_p)b_i D_S]\left.\frac{\partial C_{i,L}}{\partial r_P}\right|_{rP=RP} = k_m\left(C_{i,B} - C_{i,L}|_{rP=RP}\right) \tag{7}$$

As revealed, at the reactor inlet, steady state-conditions were assumed to prevail, thus the flux due to the fluid-solid mass transfer is equal to the intraparticle diffusion. The concentration derivative was set to zero for all the components at the reactor outlet. Symmetry conditions were imposed to the particle center, while a continuity equation was applied to the catalyst surface ($r_p = R_p$), where the flux coming from the liquid film is equal to the diffusion rate in the first elements of the solid phase.

3.2. Kinetics and adsorption

In the present work, literature data were simulated with the developed DACR model. The kinetic and adsorption parameters were obtained directly from literature [18] for the methyl acetate hydrolysis. The kinetic rate law was fixed as in Eq. (8).

$$r = kb_{MA}\left(C_{L,W}C_{L,MA} - \frac{C_{L,A}C_{L,M}}{K}\right) \tag{8}$$

As revealed, the authors used a simplified approach, where the liquid-phase concentration was used. Modified Arrhenius and van't Hoff equations were used to calculate the temperature dependencies of the kinetic and equilibrium constants, Eqs. (9) and (10).

$$k = k(298\,\mathrm{K})\exp\left[-\frac{Ea}{R}\left(\frac{1}{T} - \frac{1}{298}\right)\right] \tag{9}$$

$$K = K(298\,\mathrm{K})\exp\left[-\frac{\Delta H_r}{R}\left(\frac{1}{T} - \frac{1}{298}\right)\right] \tag{10}$$

The parameters, taken from the literature, are reported in Table 2.

The adsorption parameters were calculated by the authors from the retention time at the chromatographic peak maximum ($t_{MAX,i}$) in agreement with Eq. (11).

$$b_i = \frac{\varepsilon}{1-\varepsilon}\left(\frac{t_{MAX,i}}{t_0} - 1\right) \tag{11}$$

Table 2
Kinetic and adsorption parameters [18].

	Value	Units
k(298 K)	$6.24\cdot10^{-9}$	
Ea	67.58	kJ/mol
K(298 K)	0.14	–
ΔH_r	12.20	kJ/mol
b_{MA}	1.13	–
ΔH_{MA}	−2.70	kJ/mol
b_M	0.51	–
ΔH_M	1.50	kJ/mol
b_A	0.70	–
ΔH_A	−1.65	kJ/mol

From the obtained results, the temperature dependence with temperature can be calculated as in Eq. (12).

$$b_i = b_i(298K)\exp\left[-\frac{\Delta H_i}{R}\left(\frac{1}{T}-\frac{1}{298}\right)\right] \tag{12}$$

The parameters used in the present work are listed in Table 2.

3.3. Physical properties

Several physical properties were fixed to perform the simulation activities. The water density and viscosity changes temperature were calculated from Eqs. (13) and (14) [26].

$$\mu_W = 10^3\cdot\exp\left[-51.964+\frac{3670.6}{T}+5.7331\log(T)-5.3495\cdot10^{-29}T^{10}\right] \tag{13}$$

$$\rho_W = \left[\frac{2.459}{0.30542^{1+\left(1-\frac{T}{647.13}\right)^{0.081}}}\right]Mw_W \tag{14}$$

The molecular diffusivities were calculated from the Wilke-Chang correlation [27], as reported in Eq. (15), fixing the association factor $\varphi = 2.6$.

$$D_{mol,i} = 7.4\cdot10^{-12}\frac{(\varphi Mw_{H_2O})^{0.5}T}{\mu_{H_2O}V_{mol,i}^{0.6}} \tag{15}$$

where, molar volumes at the standard boiling points were calculated in agreement with Eq. (16) [26,28].

$$V_{mol,i} = \left[\frac{A_i\cdot10^{-3}}{B_i^{1+\left(1-\frac{T_{b,i}}{C_i}\right)^{D_i}}}\right]^{-1} \tag{16}$$

The coefficients and the boiling temperatures for each component are reported in Table 3.

Pore diffusivity was calculated with classical correlation, adjusting the molecular diffusivity by the porosity and tortuosity of the catalyst particle, Eq. (17).

$$D_p = D_{mol,W}\frac{\varepsilon_p}{\tau} \tag{17}$$

A porosity of $\varepsilon_p = 0.5$ was considered from literature findings [29] while the tortuosity factor was fixed to $\tau = 1$ being Dowex 50 W-X8 a macroreticular resin. The particle diameter was fixed at 38.5 µm [18] and shape factor at $s = 2$ (spherical particles).

The surface diffusivity was assumed to be dependent on temperature, Eq. (18) [23,30].

$$D_{S,i} = D_{S,i,0}e^{-\frac{E_{S,i}}{RT}} \tag{18}$$

This parameter indicates the affinity of the component to the solid phase. As the pre-exponential factor and the surface energy are not determinable a priori, they can be considered the unique adjustable parameters of the model.

3.4. Fluid-solid mass transfer

The fluid-solid mass transfer coefficient was calculated from Dweivedi and Upadhyay correlation, originally published and tested for values obtained using a packed-bed reactor, Eq. (19) [31].

$$\varepsilon_P J_D = 1.1062\mathrm{Re}_P^{\alpha} = 1.1062\left(\frac{D_P u_z \rho_W}{\mu_W}\right)^{\alpha},\quad \alpha = \begin{cases}-0.72, & \mathrm{Re}_P\leqslant 10\\ -0.4069, & \mathrm{Re}_P > 10\end{cases} \tag{19}$$

The exponent α depends on the value of Re_p. From this correlation, it is possible to calculate the fluid-solid mass transfer value substituting the J_D and Sc definitions, Eq. (20).

$$k_m = J_D u_z Sc^{-2/3} = \frac{1.1062}{\varepsilon_p}\left(\frac{D_P u_z \rho_W}{\mu_W}\right)^{\alpha}u_z\left(\frac{\mu_W}{\rho_W D_{mol,W}}\right)^{-2/3} \tag{20}$$

As the diameter of the solid particles is very small, the influence of the eventual fluid-solid mass transfer resistance was found to be negligible. However, to keep the model more general, the equation was implemented in the model.

3.5. Determination of axial dispersion

Axial dispersion values were determined with dedicated experiments conducted in a chromatographic reactor constructed as the one used in the literature for the methyl acetate hydrolysis experiments. Yellow naphthol was used as an inert tracer, being a sulfonated molecule, performing pulse-experiments. The presence of sulfonic groups warranties a low interaction between the tracer and the sulfonated solid surface of the Dowex 50 W-X8 catalyst, thus, axial dispersion can be determined with high precision neglecting eventual adsorption effects.

Several experiments were carried out by investigating the effect of both temperature and fluid velocity. A summary of the adopted experimental conditions is reported in Table 4, while an example of experimental output in Fig. 3A. The results were interpreted with the analytical solution of the residence time distribution function valid for high Péclet numbers, Eq. (21) [32].

$$E = \frac{u_z}{\sqrt{4\pi D_z t}}\exp\left[-\frac{(L-u_z t)^2}{4D_z t}\right] \tag{21}$$

The obtained fits were in every case satisfactory (see Fig. 3A). From the data elaboration, the numerical value of the axial dispersion coefficient (D_z) was determined. The Péclet numbers ($Pe = u_z L/D_z$) as a function of Re_p are reported in Fig. 3B. As revealed by the figure, Pe is highly influenced by the fluid velocity but practically invariant with temperature.

High Péclet numbers were determined even for low Re_p values, fact characteristic of static mixer reactors where small size particles are used as inert material. Such values are not predictable from classical correlations derived from packed bed reactors.

A correlation was derived by parameter estimation analysis on the Pe vs Re_p plot, Eq. (22), and implemented in chromatographic reactor model.

Table 3
Molar volume coefficients and boiling temperature for each component for the methyl acetate hydrolysis.

Component	A_i	B_i	C_i	D_i	$T_{b,\,i}$ [K]
Water (W)	−13.851	0.64038	0.0019	$1.82\cdot10^{-6}$	373.1
Methyl acetate (MA)	1.130	0.2593	506.55	0.2764	330.1
Acetic acid (A)	1.449	0.2589	591.95	0.2529	391.1
Methanol (M)	2.327	0.2707	512.50	0.2471	337.7

Table 4
Experimental conditions adopted to determine the axial dispersion coefficients in the chromatographic reactor. Axial dispersion values are reported along with the error.

Test	Q [mL/min]	T [K]	$D_z{\cdot}10^7$ [m^2/s]	
1	0.6	298	2.60	± 0.05
2	0.7	298	1.50	± 0.01
3	0.8	298	1.41	± 0.08
4	0.9	298	1.58	± 0.05
5	0.6	298	2.80	± 0.03
6	0.7	308	1.48	± 0.04
7	0.8	308	1.46	± 0.07
8	0.9	308	1.52	± 0.01
9	0.6	323	2.30	± 0.02
10	0.7	323	1.54	± 0.06
11	0.8	323	1.40	± 0.05
12	0.9	323	1.45	± 0.04

$$Pe = -1.0{\cdot}10^6\exp\left(\frac{-\mathrm{Re}_p}{0.00158}\right) + 2062.15 \qquad (22)$$

3.6. Description of literature data

The developed DACR model was applied to interpret existing literature data. Methyl acetate hydrolysis (to acetic acid and methanol) experiments were obtained from the literature [18]. The authors carried out different experiments by fixing the flow-rate at 0.75 mL/min and injecting pulses of 100 µL of a 0.5 mol/L solution of methyl acetate in water. The experiments were conducted at different temperatures (from 298 to 328 K), analyzing continuously the output stream. The results are reported in Fig. 4. The symbols, corresponding to the experimental data, were reduced in number for reading purposes. The signal output was calculated by measuring aside the detector's proportional factors for each component: 4 for MA, 2.4 for both methanol and acetic acid.

As revealed by the calculations, a temperature increase corresponds to an increase of the reaction conversion (the MA area decreases) with the related formation of the two products (methanol and acetic acid). Parameter estimation was carried out to obtain the surface diffusivity for each component. The surface diffusivity of water was considered equal to that of methanol for the sake of simplicity. This value could be obtained by reversing the reaction (esterification), thus feeding continuously methanol and pulsing water. Unfortunately, this information was not available. Therefore, after the parameter estimation, a sensitivity analysis was performed on this parameter, confirming that the results change only slightly. The agreements between the experimental and calculated data can be considered satisfactory, overall considering that kinetic and adsorption parameters are kept constants and taken directly from the literature. This would explain the slightly less accuracy fit in some cases, as the kinetic and adsorption parameters were calibrated in the literature with dedicated and separate experiments. In the present work, we decided to use the parameters such as reported in the literature, demonstrating that the model performance is satisfactory estimating only a very limited number of adjustable parameters.

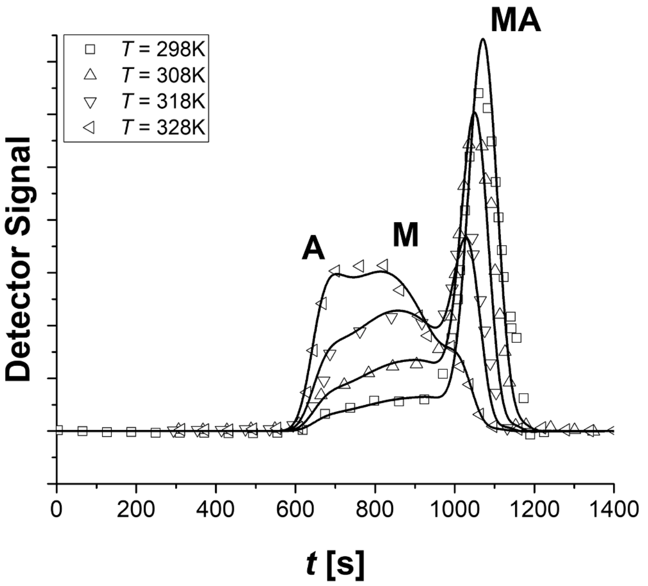

Fig. 4. Methyl acetate hydrolysis experiments performed in a chromatographic reactor loaded with Dowex 50W-X8 [15]. The symbols represent the experimental data, reduced in number for reading purposes, while continuous lines represent the calculated values. A: acetic acid, M: methanol, MA: methyl acetate.

The trend of D_S along temperature is displayed in Fig. 5A, while the corresponding logarithmic plot is shown in Fig. 5B.

The calculated values are consistent and show logical trends with temperature. From the plots reported in Fig. 5, it is possible to calculate the $D_{S,0}$ and E_S for each component. The values are reported in Table 5.

As revealed by modelling, methyl acetate shows the highest surface diffusivity, resulting by the fact that the chromatographic peaks are sharper. This fact is explainable by the low interaction that the ester group has with the sulfonic pendants on the catalyst surface. Methanol and acetic acid, instead, show lower surface diffusivities, being characterized by a certain acidity. As a matter of fact, acetic acid shows a lower D_S value than methanol, because acetic acid can interact with the resin by a proton exchange mechanism.

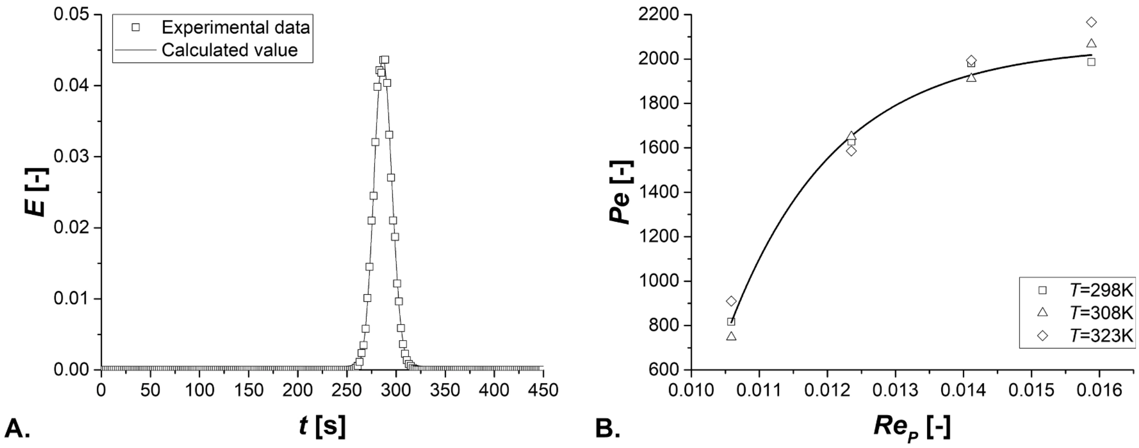

Fig. 3. A. Experimental results and data fit for the pulse-experiment performed at 298 K with a flow-rate of 0.9 mL/min. B. Pe vs Re_p plot.

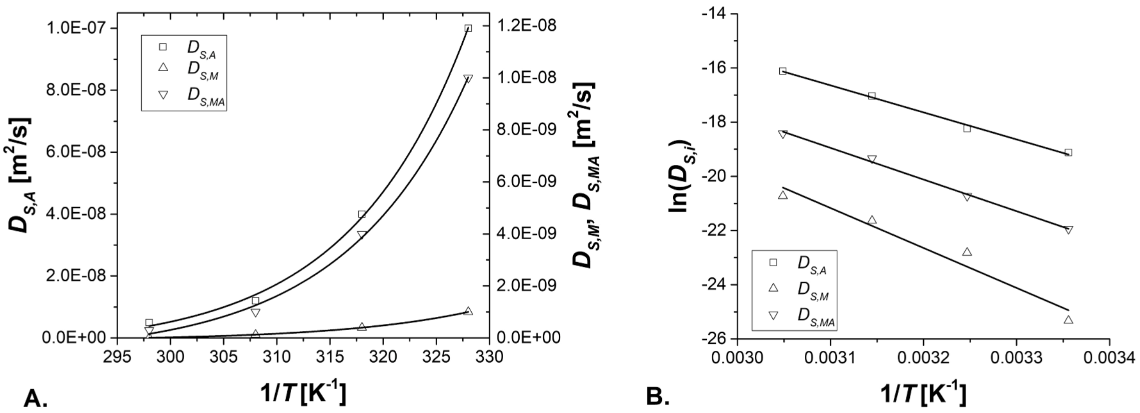

Fig. 5. A. The surface diffusivity trend with the reaction temperature for methyl acetate, methanol and acetic acid. B. Logarithmic D_S plot.

Table 5
Surface diffusivity parameter estimation output.

Component	$D_{S,i,o}$ [m^2/s]	$E_{S,i}$ [kJ/mol]
A	$1.64{\cdot}10^6$	83.01
M	$3.16{\cdot}10^7$	97.14
MA	$4.59{\cdot}10^{10}$	122.63

Table 6
Sensitivity study summary.

Simulation	Legend	Q [mL/min]	D_p [μm]	L [m]	T [K]
1	Reference simulation	0.75	38.5	0.25	298
2	Flow-rate effect	0.60	38.5	0.25	298
3		1.00	38.5	0.25	298
4		1.50	38.5	0.25	298
5		2.00	38.5	0.25	298
6	Particle diameter effect	0.75	77.0	0.25	298
7		0.75	192.5	0.25	298
8		0.75	288.8	0.25	298
9		0.75	385.0	0.25	298
10	Reactor length effect	0.75	38.5	0.50	298
11	(T = 298 K)	0.75	38.5	1.00	298
12		0.75	38.5	2.50	298
13	Reactor length effect	0.75	38.5	2.50	303
14	(T = 303 K)	0.75	38.5	1.00	303

3.7. Sensitivity study

A parametric investigation was conducted to check the sensitivity of the model. All the simulations were performed by fixing the shape factor to $s = 2$ (spherical particles). A summary of the study is provided in Table 6.

The influence of the volumetric flow-rate on the chromatographic reactor output is demonstrated in Fig. 6A. An increase of the flow-rate suppresses the axial dispersion, thus Pe increase, leading to sharper peaks. Moreover, the flow-rate increase corresponds to a decrease in the residence time, leading to two main effects: (i) shift of the chromatographic peaks at lower times; (ii) decrease of the overall conversion. These two phenomena are correctly interpreted by using the model developed.

The influence of the solid particle diameter is depicted in Fig. 6B. As expected, by increasing the catalyst diameter, an increase of the intraparticle diffusion path leads to wider peaks and in general lower product contents. It was checked that even when the largest particle diameter was used, the liquid-solid external mass transfer resistance can be considered negligible.

The influence of the reactor length on the column performance shows interesting results (Fig. 7A), as by increasing L the system is characterized by higher residence time, that brings to higher conversion and shifts of the chromatographic peaks, because the column is characterized by a higher number of theoretical plates.

Finally, two simulations were carried out by varying the reactor length at a higher temperature, T = 323 K (Fig. 7B). As revealed, by fixing the reactor length to L = 2.50 m, it is possible to achieve complete methyl acetate conversion and product separation. This result demonstrates that by using a chromatographic reactor, it is possible to obtain full conversion also for equilibrium reactions, as the reactants and products are separated in the column. Moreover, as demonstrated, because the products are separated, no other purification units are needed.

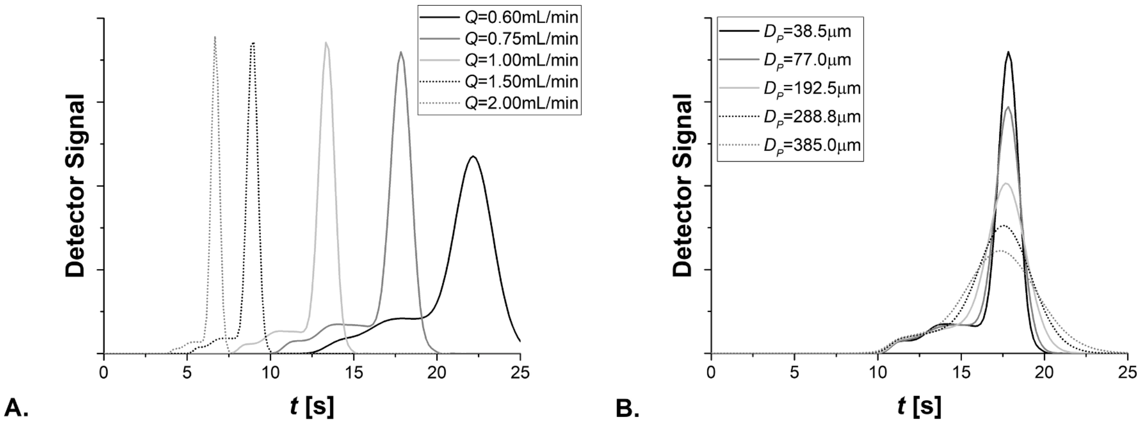

Fig. 6. Sensitivity study results: A. Volumetric flow-rate dependency. B. Influence of the particle diameter.

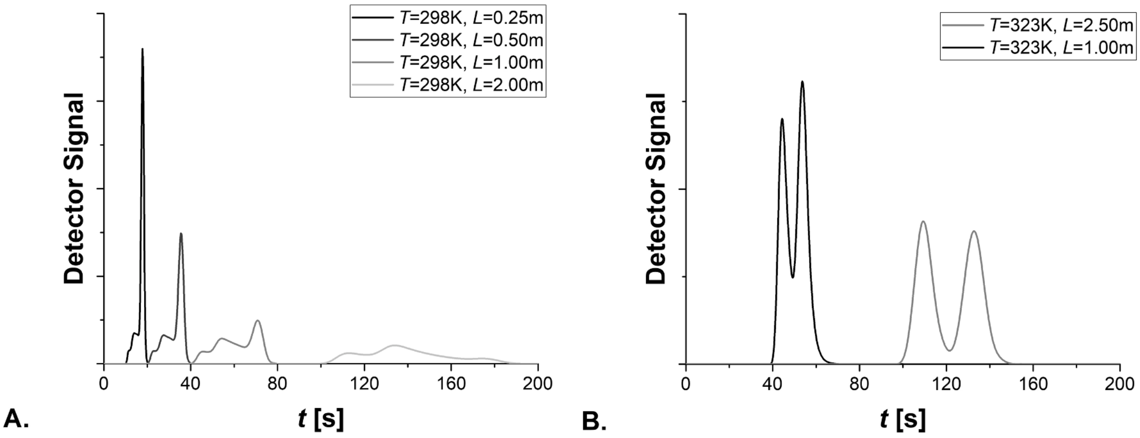

Fig. 7. Chromatographic reactor length effect on the final output: A. $T = 298\,K$ B. $T = 323\,K$.

4. Conclusions

In the present work, a novel chromatographic reactor model was developed (DACR). The modelling approach consists of the simultaneous solution of both liquid bulk and intraparticle mass balance equations. No rate-determining steps were considered, and fluid-dynamics was described in terms of the axial dispersion model.

Axial dispersion coefficients were determined with dedicated experiments collected from a chromatographic reactor equipment. The Péclet number showed high influence on the liquid velocity, but a negligible variation with temperature. A semi-empirical equation for the Péclet number was derived to be included in the chromatographic reactor model. The fluid-solid mass transfer resistance was estimated from literature correlations developed for packed bed reactors. Because the catalyst particles were relatively small ($D_p = 38.5\,\mu m$), it was concluded that the external mass transfer was negligible under the conditions studied.

The chromatographic reactor model was tested on literature data, namely methyl acetate hydrolysis. The kinetic and adsorption data were obtained from the literature. The adjustable parameters were the surface diffusivities, related to the affinity between each component and the solid surface. The results were satisfactory, allowing a reliable description of the temperature effect on the hydrolysis process.

A parametric investigation was performed to check the influence of the operation conditions on the final output. Optimal operation conditions were calculated, enabling to simulate a complete methyl acetate conversion and product separation.

In perspective, further experiments will be conducted to collect new experimental data, to validate the model predictions.

Acknowledgements

This work is a part of activities at the Johan Gadolin Process Chemistry Centre (PCC), a centre of excellence in scientific research financed by Åbo Akademi University.

References

[1] J.A. Dinwiddie, W.A. Morgan, Fixed bed type reactor, U.S. Patent 2,976,132 (1961).
[2] E.M. Magee, Catalytic Conversion Process, Canadian Patent 631 (1961) 882.
[3] G.A. Gaziev, S.Z. Roginskii, M.J. Yanovskii, U.S.S.R. Patent 149,398 (1962).
[4] A.E. Rodrigues, C. Pereira, J.C. Santos, Chromatographic reactors, Chem. Eng. Technol. 35 (2012) 1171–1183.
[5] T. Falk, A. Seidel-Morgenstern, Comparison between a fixed-bed reactor and a chromatographic reactor, Chem. Eng. Sci. 54 (1999) 1479–1485.
[6] M.C. Bjorklund, R.W. Carr, The simulated countercurrent moving bed chromatographic reactor: a catalytic and separative reactor, Catal. Today 25 (1995) 159–168.
[7] M. Kawase, T.B. Suzuki, K. Inoue, K. Yoshimoto, K. Hashimoto, Increased esterification conversion by application of the simulated moving-bed reactor, Chem. Eng. Sci. 51 (1996) 2971–2976.
[8] A.K. Ray, R.W. Carr, Experimental study of a laboratory-scale simulated countercurrent moving bed chromatographic reactor, Chem. Eng. Sci. 50 (1995) 2195–2202.
[9] D.S.C. Azevedo, A.E. Rodrigues, Design methodology and operation of a simulated moving bed reactor for the inversion of sucrose and glucose–fructose separation, Chem. Eng. J. 82 (2001) 95–107.
[10] M. Minceva, P.S. Gomes, V. Meshko, A.E. Rodrigues, Simulated moving bed reactor for isomerization and separation of p-xylene, Chem. Eng. J. 140 (2008) 305–323.
[11] A.E. Rodrigues, C. Pereira, M. Minceva, L. Pais, A.M. Ribeiro, A. Ribeiro, M. Silva, N. Graça, J.C. Santos, Simulated Moving Bed Technology. Principles, Design and Process Applications, Elsevier Butterworth-Heineman, 2015.
[12] A.E. Rodrigues, L.M. Madeira, Y.-J. Wu, Sorption Enhanced Reaction Processes, World Scientific Publishing, 2017.
[13] D. Schweich, J. Villermaux, The chromatographic reactor. A new theoretical approach, Ind. Eng. Chem. Fund. 17 (1978) 1–7.
[14] M. Mazzotti, A. Kruglov, B. Neri, D. Gelosa, M. Morbidelli, A continuous chromatographic reactor: SMBR, Chem. Eng. Sci. 5 (1996) 1827–1836.
[15] M. Mazzotti, B. Neri, D. Gelosa, M. Morbidelli, Dynamics of a chromatographic reactor: esterification catalyzed by acidic resins, Ind. Eng. Chem. Res. 36 (1997) 3163–3172.
[16] T. Sainio, L. Zhang, A. Seidel-Morgenstern, Adiabatic operation of chromatographic fixed-bed reactors, Chem. Eng. J. 168 (2011) 861–871.
[17] M. Laatikainen, J. Heinonen, T. Sainio, Modeling of chromatographic separation of concentrated-acid hydrolysates, Sep. Purif. Technol. 80 (2011) 610–619.
[18] T.D. Vu, A. Seidel-Morgenstern, Quantifying temperature and flow rate effects on the performance of a fixed-bed chromatographic reactor, J. Chrom. A 1218 (2011) 8097–8109.
[19] N.S. Graça, L.S. Pais, V.M.T.M. Silva, A.E. Rodrigues, Dynamic study of the synthesis of 1,1-dibutoxyethane in a fixed-bed adsorptive reactor, Sep. Sci. Tech. 46 (2011) 631–640.
[20] Rui Faria, Carla S. Pereira, Viviana Silva, José Loureiro, A.E. Rodrigues, Sorption enhanced reactive process for the synthesis of glycerol ethyl acetal, Chem. Eng. J. 258 (2014) 229–239.
[21] D. Constantino, C. Pereira, R. Faria, A. Ferreira, J. Loureiro, A.E. Rodrigues, Synthesis of butyl acrylate in a fixed-bed adsorptive reactor over Amberlyst 15, AiChEJ 61 (2015) 1263–1274.
[22] V. Russo, R. Tesser, M. Trifuoggi, M. Giugni, M. Di Serio, A dynamic intraparticle model for fluid-solid adsorption kinetics, Comput. Chem. Eng. 74 (2015) 66–74.
[23] V. Russo, R. Tesser, D. Masiello, M. Trifuoggi, M. Di Serio, Further verification of adsorption dynamic intraparticle model (ADIM) for fluid-solid adsorption kinetics in batch reactors, Chem. Eng. J. 283 (2016) 1197–1202.
[24] V. Russo, D. Masiello, M. Trifuoggi, M. Di Serio, R. Tesser, Design of an adsorption column for methylene blue abatement over silica: from batch to continuous modelling, Chem. Eng. J. 302 (2016) 287–295.
[25] V. Russo, M. Trifuoggi, M. Di Serio, R. Tesser, Fluid-solid adsorption in batch and continuous processing: a review and insights on the modelling, Chem. Eng. Technol. 40 (2017) 799–820.
[26] Chemstations ChemCAD v.5.0 (http://www.chemstations.com/) (last visited 06/06/2018).
[27] C.R. Wilke, P. Chang, Corralation of diffusion coefficients in dilute solutions, AICHE J. 1 (1955) 264–270.
[28] R.C. Reid, J.M. Prausnitz, B.E. Polong, The Properties of Gases and Liquids, fourth ed., McGraw-Hill, New York, 1987.
[29] Sigma Aldrich specification sheet (https://www.sigmaaldrich.com/chemistry/chemical-synthesis/learning-center/technical-bulletins/al-142/dowex-resins.html).
[30] D.D. Do, Adsorption Analysis: Equilibria and Kinetics, Imperial College Press, London, 1998.
[31] P.N. Dwivedl, S.N. Upadhyay, Particle-fluid mass transfer in fixed and fluidized beds, Ind. Eng. Chem., Process Des. Dev. 16 (1977) 157–165.
[32] O. Levenspiel, Chemical Reaction Engineering, third ed., John Wiley & Sons, New York, 1999.

IV

processes

Article

Reactive Chromatography Applied to Ethyl Levulinate Synthesis: A Proof of Concept

Carmelina Rossano, Claudio Luigi Pizzo, Riccardo Tesser, Martino Di Serio and Vincenzo Russo *

Chemical Science Department, University of Naples Federico II, Via Cinthia, 80126 Naples, Italy; carmelina.rossano@unina.it (C.R.); claud_lp96@hotmail.it (C.L.P.); riccardo.tesser@unina.it (R.T.); diserio@unina.it (M.D.S.)
* Correspondence: v.russo@unina.it

Abstract: Levulinic acid (LA) has been highlighted as one of the most promising platform chemicals, providing a wide range of possible derivatizations to value-added chemicals as the ethyl levulinate obtained through an acid catalyzed esterification reaction with ethanol that has found application in the bio-fuel market. Being a reversible reaction, the main drawback is the production of water that does not allow full conversion of levulinic acid. The aim of this work was to prove that the chromatographic reactor technology, in which the solid material of the packed bed acts both as stationary phase and catalyst, is surely a valid option to overcome such an issue by overcoming the thermodynamic equilibrium. The experiments were conducted in a fixed-bed chromatographic reactor, packed with Dowex 50WX-8 as ion exchange resin. Different operational conditions were varied (e.g., temperature and flow rate), pulsing levulinic acid to the ethanol stream, to investigate the main effects on the final conversion and separation efficiency of the system. The effects were described qualitatively, demonstrating that working at sufficiently low flow rates, LA was completely converted, while at moderate flow rates, only a partial conversion was achieved. The system worked properly even at room temperature (303 K), where LA was completely converted, an encouraging result as esterification reactions are normally performed at higher temperatures.

Keywords: levulinic acid; ethyl levulinate; reactive chromatography; Dowex 50WX-8; ion-exchange resin

Citation: Rossano, C.; Pizzo, C.L.; Tesser, R.; Di Serio, M.; Russo, V. Reactive Chromatography Applied to Ethyl Levulinate Synthesis: A Proof of Concept. *Processes* **2021**, *9*, 1684. https://doi.org/10.3390/pr9091684

Academic Editor: Wenli Du

Received: 23 August 2021
Accepted: 15 September 2021
Published: 20 September 2021

1. Introduction

Levulinic acid (LA), also known as 4-oxopentanoic acid or γ-ketovaleric acid, is a highly versatile molecule that can be obtained from lignocellulosic biomass. The great interest around LA is due to its structure, composed of two high functionality groups (keto- and carboxylic- group) that furnish a wide range of possible derivatizations to value-added chemicals [1]. For all of these reasons, LA has been highlighted as one of the most promising platform chemicals, after screening approximately 300 substances [2]. Among the large number of utilizable chemicals derived from LA, levulinate esters potentially have the largest markets, especially from a biofuel perspective. Ethyl levulinate (EL) is gaining attention since it provides a better blending option with fuel, likewise other higher alcohols (i.e., butyl levulinate). The advantage of EL is due to the use of ethanol (EtOH) as the reactant in excess used in the esterification reaction, which is traditionally obtained from renewable resources with lower total costs, such as methanol and butanol [3]. Other applications of EL include its use as an additive for perfume formulations, as a plasticizer in biodegradable plastic polymers, and as an additive in de-icer formulations [4]. Homogeneous catalysts, such as sulfuric, chloridric, and phosphoric acid, are historically employed, but there are some drawbacks about the separation and recovery from the reaction medium [5–7]. Hence, heterogeneous catalysts are now the favorite [8–10]. Not long ago, Fernandes et al. [11] published an interesting paper in which the performance of zeolites, sulphated metal oxides, and a commercial cationic exchange resin, amberlyst-15, were compared, finding that ion exchange resins are surely good candidates. Very recently, Amberlyst-15 and Amberlite IR-120 were proven to be very active heterogeneous catalysts, showing no signs of deactivation after 100 h of reuse [12,13].

When scaling up the process from a batch to continuous operation, packed bed was demonstrated to be a reasonable choice [13]. The main drawback of the mentioned technology in using packed bed systems is the low rate of conversion due to the formation of water, which keeps the system at the thermodynamical conversion degree.

Different technologies could be used to overcome the mentioned problem, namely reactive chromatography (RC) and reactive distillation (RD). The main difference between RC and RD is based on the principle of separation. RC is an adsorptive separation process, where the components are separated based on their different affinities towards the adsorbent, while RD exploits the difference in boiling points of the components of the reaction. In the esterification reaction of levulinic acid with ethanol, water cannot be removed by RD as it is characterized by a higher boiling point than ethyl levulinate but lower than levulinic acid. For this reason, it is not possible to conduct this type of reaction in RD mode.

Reactive chromatography could solve this issue, as it is an operation unit that combines chemical reaction and chromatographic separation, allowing the intensification of the esterification process. In the field of process intensification, chromatographic reactors have gained more and more attention for their advantages related to a conversion increase through equilibrium shift and the reduced by-product formation. Indeed, the obtained reaction product is separated through the adsorption on the resin and in accordance with the adsorptive separation process principle, the difference in affinity between the sorbent and reaction products is the main reason for efficient separation [14].

Good performance shown by Amberlyst-15 as a catalyst, along with the adsorption capacity of the resin, suggest that LA esterification with ethanol could be conducted in a chromatographic reactor in which there is potential for catalysis and separation to be carried out in a single reactor. As is well known, cation exchange resins find employment as packing materials for ion exchange chromatography columns, in which the negatively charged analytes interact with the positive portion of the stationary phase and get separated depending on how strong the interaction is.

To support this, the studies of Mazzotti [15], Rodrigues [16], Vu et al. [17], and Russo et al. [18] used ion exchange resins for reactive chromatography experiments, conducting reactions such as acetic acid esterification and acetals synthesis, ethyl lactate production and xylene isomerization/separation, or esters hydrolysis.

Since Dowex 50WX-8 showed a good performance in similar systems, and as no applications of this concept appeared in the literature for the ethyl levulinate synthesis from LA, this work aimed to fill this gap, aiming to investigate how the different operation conditions affect the final conversion of the system.

2. Materials and Methods

2.1. Materials

The following reagents were procured from well-known companies and used without any further purification: levulinic acid (99 wt%) and ethyl levulinate (99 wt%) were supplied by Sigma Aldrich, ethanol (99 wt%) supplied by Carlo Erba Reagents. Dowex 50WX-8 ion exchange resin (by Acros Organics) was used as a solid acid catalyst. The main properties of the resin are reported in Table 1 and were taken from the material data sheet of the catalyst itself.

Table 1. Physical properties of the used Dowex 50WX-8 catalyst.

Catalyst	**Particle Size [µm]**	**Crosslinking Degree [%]**	**Ionic Form**	**Total Exchange Capacity [meq/cm^3]**	**Density [g/cm^3]**	**Water Retention Capacity [%]**	**Max. Operative Temperature [°C]**
Dowex 50WX8	150–300	8	H+	1.7	0.8	50–56	120

2.2. Methods

2.2.1. Chromatographic Reactor Setup

The setup for the chromatographic reactor is shown in Figure 1. Ethanol is stored in the tank (1) and pumped into the system by an HPLC pump (2) that allows for flow rate settings and pressure drop readings. The ethanol flux passes through a Rheodyne injector valve (3), where an injector combined with a 20 µL loop pulses the other reactant (LA) into the ethanol stream. The stream is then sent to the chromatographic reactor (4), consisting of a steel tube of 0.3 m length and 0.0078 m diameter jacketed with a heater regulated by a PID system (5). An online detector (Reach Device RD4, (6)) reveals the presence of solutes in the ethanol flux through UV (250 nm and 280 nm), IR, and conductivity detectors. A pin valve (7) is placed after the detector, for samples withdrawal. The accumulation tank (8) is provided with a pin valve for decumulation of the liquid stream. The pressure in the chromatographic reactor system is applied through a reductor (9) linked to a N_2 bottle (10). Packing of the tubular reactor (supplied by Phenomenex) was obtained after drying the resin and calculating the amount needed, considering the degree of swelling of the catalyst particle. About 6.5 g of Dowex 50WX8 was necessary to fill the tubular reactor. Ethanol was then streamed continuously for 6 h with a flow of 1.0 cm^3/min into the reactor to let the resin swell and pack the tube completely.

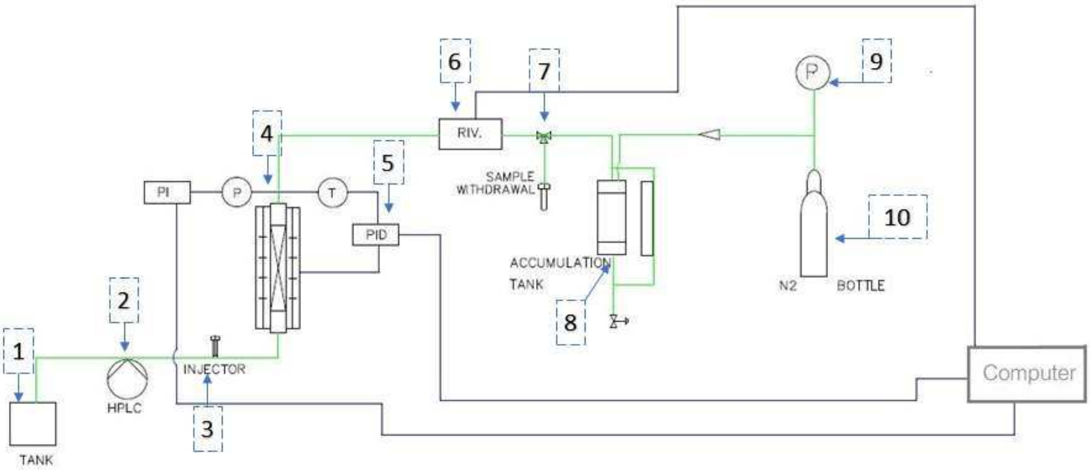

Figure 1. Chromatographic reactor setup scheme. (1) Tank; (2) HPLC pump; (3) injector; (4) chromatographic reactor; (5) PID; (6) online detector; (7) sample withdrawal valve; (8) accumulation tank; (9) reductor; (10) N_2 bottle.

The performance of the chromatographic reactor was evaluated with tests in which levulinic acid was pulsed into a stream of ethanol and data were collected from the online detector. To determine if the resin successfully separated the components of the system, tests pulsing EL were conducted and a comparison between the UV (250 nm) spectra was made. The summary of the experimental conditions is illustrated in Table 2.

Table 2. Experimental conditions for the chromatographic reactor runs.

Test	c_{LA} **[mol/L]**	c_{EL} **[mol/L]**	T **[K]**	Q **[cm^3/min]**	P **[bar]**	ΔP **[kg/cm^2]**
C1	6	-	303	0.8	2	9
C2	6	-	303	0.9	2	10
C3	6	-	303	1.1	2	13
C4	6	-	303	2.5	2	30
C5	6	-	303	5	2	54
C6	-	6	303	0.8	2	9
C7	-	6	303	0.9	2	10
C8	-	6	303	1.1	2	13
C9	-	6	303	2.5	2	30
C10	-	6	303	5	2	54
C11	6	-	313	1.1	2	13
C12	6	-	313	1.7	2	21
C13	6	-	313	1.8	2	23
C14	6	-	313	1.9	2	24
C15	6	-	313	2.5	2	30
C16	-	6	313	1.1	2	13
C17	-	6	313	1.7	2	21
C18	-	6	313	1.8	2	23
C19	-	6	313	1.9	2	24
C20	-	6	313	2.5	2	30
C21	6	-	323	1.8	2	23
C22	6	-	323	2.0	2	26
C23	6	-	323	2.5	2	30
C24	6	-	323	5.0	2	54
C25	-	6	323	1.8	2	23
C26	-	6	323	2.0	2	26
C27	-	6	323	2.5	2	30
C28	-	6	323	5.0	2	54

Each experiment was repeated three times to estimate the error on the experiment reproducibility. The average value was about 2.5% and the peaks shown in the next section were obtained as average values, for each test performed.

2.2.2. Take-up Test

When resins like Dowex 50WX8 are put in contact with reactants/reagents, they are subjected to a process known as take-up. This occurs because when resins adsorb solvents, especially polar ones like water (H_2O) or alcohols, there is a strong osmotic pressure difference between the liquid inside the pores and the solvent bulk. To decrease this difference, the resin takes up more solvent to dilute ion concentration into its pores.

Take-up tests were prepared to investigate how our reactive system affected the catalyst. Furthermore, evaluation of the swelling phenomenon is fundamental when a resin is to be used as a packing material for a reactor to avoid complete plugging of the system.

Since both the reagents (LA, EtOH) and the products (EL, water) are simultaneously in contact with the resin during the esterification process, 10 cm^3 of binary solutions of all the chemical species present in the system (LA/EtOH, LA/EL, LA/H_2O, EtOH/EL, EtOH/H_2O, EL/H_2O) with different molar fractions (0.8, 0.5, 0.2) were prepared and put in contact with ~1.5 g of dried Dowex 50WX8. The solutions were mixed from time to time with a rod to improve contact between the chemical species and the resin. The resin mass was weighed before and after 45 min of every take-up test. Known the density of the binary mixes, the value of the swelling phenomenon was calculated as:

$$\alpha\ [\%] = \frac{V^{s}_{resin} - V^{d}_{resin}}{V^{d}_{resin}} \times 100 \quad (1)$$

where α is the swelling percentage and V^{s}_{resin} and V^{d}_{resin} are the volumes of the swelled and dry resin, respectively.

3. Results and Discussion

3.1. Dowex 50WX8 Take-up Tests

Table 3 displays the results of all the take-up tests that were completed. The value of α was then calculated as the average value of all the swelling coefficients determined during the take-up tests, with this being α = 51.1 ± 5.6%.

Table 3. Swelling percentage of Dowex 50WX8 when put in contact with different molar ratios of the components of our reactive system.

Molar Fractions [–]				**α [%]**
LA	**EtOH**	**EL**	**H_2O**	
1	-	-	-	51.6
-	1	-	-	58.5
-	-	1	-	45.7
-	-	-	1	57.5
0.8	0.2	-	-	45.7
0.5	0.5	-	-	49.0
0.2	0.8	-	-	52.8
0.8	-	0.2	-	45.1
0.5	-	0.5	-	36.1
0.2	-	0.8	-	45.1
0.8	-	-	0.2	49.2
0.5	-	-	0.5	51.0
0.2	-	-	0.8	56.2
-	0.8	0.2	-	52.1
-	0.5	0.5	-	44.2
-	0.2	0.8	-	47.7
-	0.8	-	0.2	54.9
-	0.5	-	0.5	52.8
-	0.2	-	0.8	57.9
-	-	0.8	0.2	45.1
-	-	0.5	0.5	50.6
-	-	0.2	0.8	57.4

The resin volume in our reactive system was estimated to increase up to 1.5 times its original value.

As revealed, EL showed a lower take-up, probably due to both the relatively bigger dimensions and hindrance compared to the other molecules, which led to lower access to the catalyst pores and a lower affinity to the resin structure. The reported data will surely be of utmost importance when quantitatively modeling the reactive chromatography results.

3.2. Reactive Chromatography Results

Effect of the Stream Flow Rate

The first set of experiments consisted of pulsing LA at 303 K at different flow rates. The UV spectra results are reported in Figure 2.

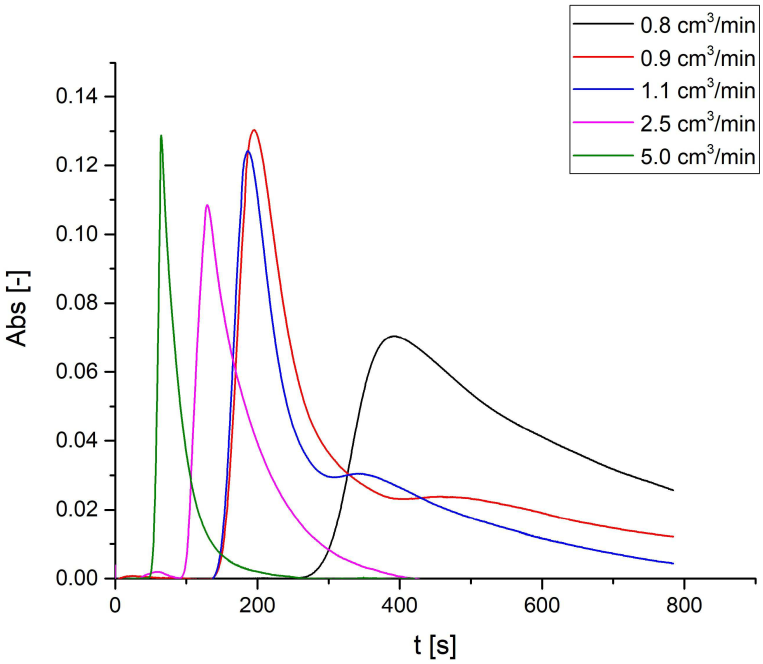

Figure 2. UV spectra of LA 6 M injected in the chromatographic reactor working at 303 K and at different flow rates.

As shown in the figure, the LA retention time decreased when the flow rate increased. This is what we expected because at higher flow rates, the time required to flow through the reactor is lower. In more detail, looking at the curve shape at the intermediate flow rate (0.9 and 1.1 cm^3/min tests), the formation of a second peak can be noted. Instead, the test at 0.8 cm^3/min flow rate shows a single, broad peak detected at a retention time similar to the second peak shown in the two tests at intermediate flow rates.

An explanation of this behavior can be ascribed to the time of interaction of the reagents with the resin that makes the reaction happen.

At lower flow rates, 0.8 cm^3/min, the entire quantity of LA pulsed into the reactor had enough time to interact with Dowex 50WX8 and it was totally converted, resulting in a single EL peak at the detection point.

At intermediate flow rate values, LA was only partially converted, and both the carboxylic acid and the ester were detected by the UV analyzer with detection times that were in line with their affinity values.

To confirm this hypothesis, a solution of EL 6 M in ethanol was pulsed into the chromatographic reactor at the same operative conditions and the UV spectra were compared with the corresponding LA spectra.

At high flow rates, like 5.0 and 2.5 cm^3/min, the LA did not have the time to interact with the resin and, thus, the UV analyzer only detected one peak and the chemical species exited the reactor at the same time. Thus, Dowex 50WX8 performed a good separation of the product and the reagent, allowing theoretical recovery of the pure product from the reactor outlet.

The UV spectra in Figure 3 confirm the previous hypothesis: if the fluid flow is slow enough, LA can be converted to EL completely (0.8 cm^3/min), otherwise only a fraction of it will react with ethanol forming EL.

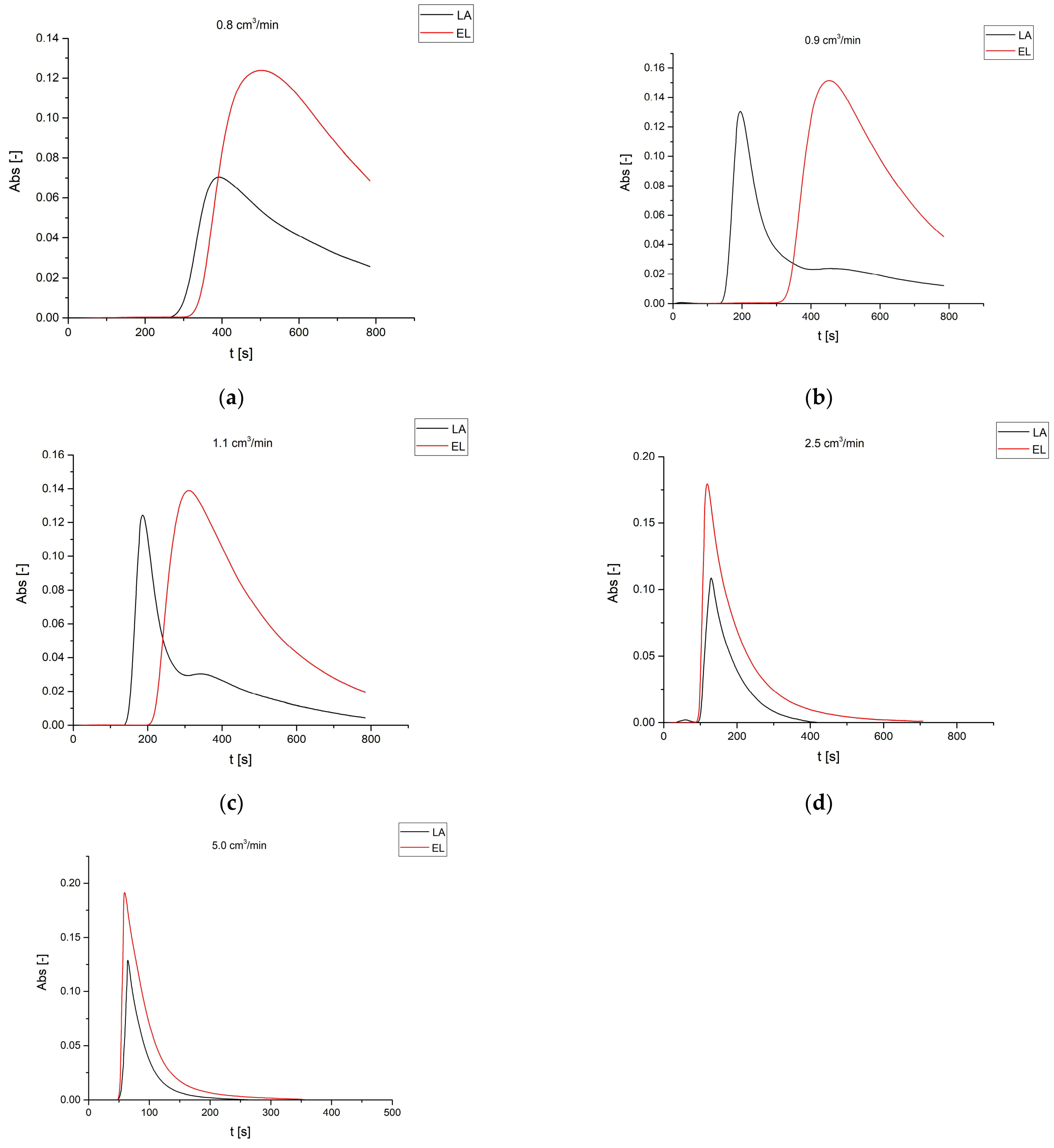

(**a**)

(**b**)

(**c**)

(**d**)

(**e**)

Figure 3. UV spectra of LA and EL 6 M at 303 K and different flow rates. (**a**) 0.8 cm^3/min. (**b**) 0.9 cm^3/min. (**c**) 1.1 cm^3/min. (**d**) 2.5 cm^3/min. (**e**) 5.0 cm^3/min.

To confirm this, through peak deconvolution, it was also possible to approximately determine LA conversion to EL at intermediate flow rates. LA conversion values were 58% and 87% for the tests with 1.1 and 0.9 cm^3/min flow rate, respectively.

3.3. *Effect of the Reactor Temperature*

The effect of temperature was evaluated performing tests at 313 K, in particular, data were collected from pulsing LA at 1.1 and 2.5 cm^3/min flow rates. In Figure 4, a comparison of the experiments at the same flow rates and different temperatures are shown.

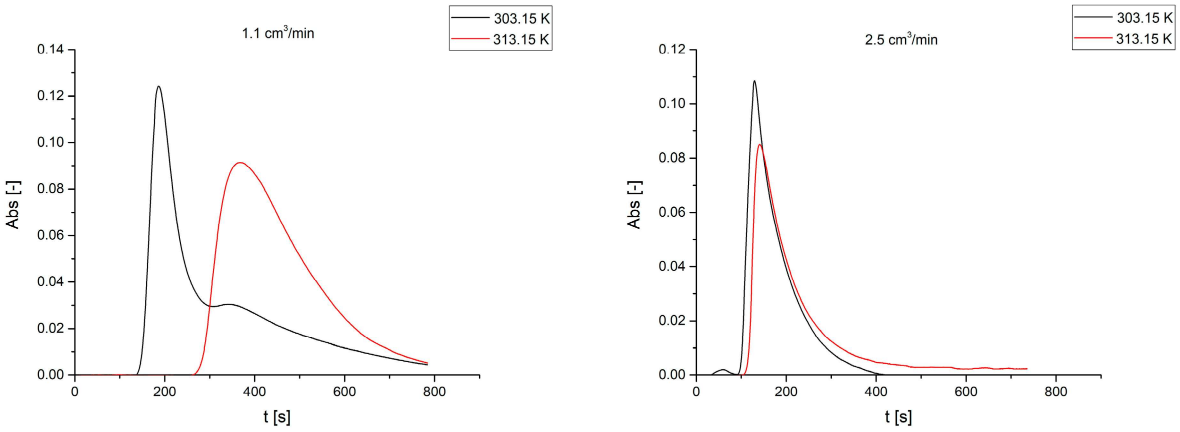

(**a**) (**b**)

Figure 4. UV spectra for LA 6 M injections at 1.1 cm^3/min (**a**) and 2.5 cm^3/min (**b**) flow rate at different temperatures.

At 2.5 cm^3/min flow rate, as expected, the rise in temperature did not make a significant difference since LA had no time to interact with the resin. At 1.1 cm^3/min flow rate, it can be noted that the conversion to EL was complete. The reaction kinetics were positively affected by higher temperatures, obtaining complete conversion of the carboxylic acid at higher flow rates.

Since we obtained two opposite outcomes (0 and 100% conversion), further tests were conducted to pinpoint the flow rate values that would give partial LA conversion at the same temperature, so that it could be verified that good separation would occur.

Figure 5 shows the results of test at 313 K and 1.7, 1.8, and 1.9 cm^3/min flow rates.

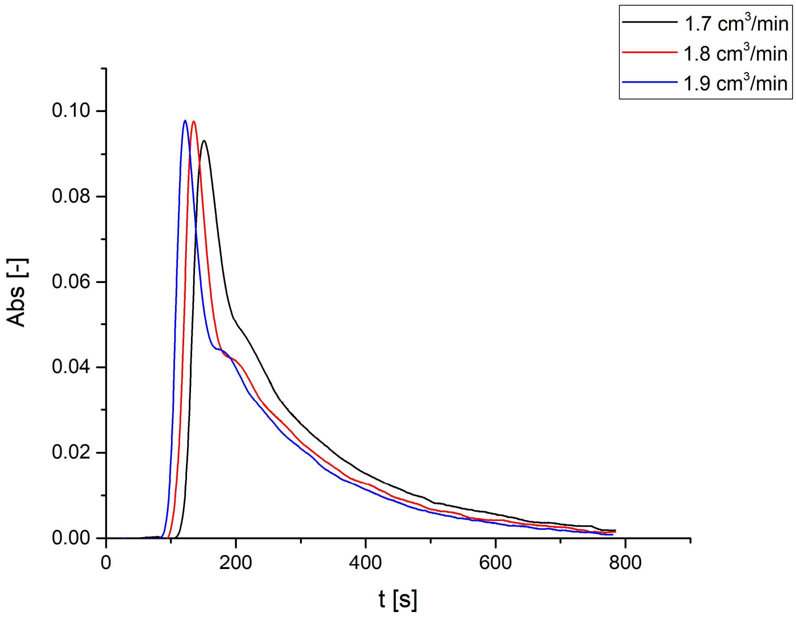

Figure 5. UV spectra of LA 6 M pulses at 313 K and different flow rates.

All three tests displayed the formation of two peaks, one was attributed to LA and the other, which was somewhat embedded into the first, to EL.

To prove that the conversion was not complete and that there was the presence of both LA and EL, a solution of EL 6 M was prepared and injected under the same operative conditions. In Figure 6, the results are shown and the correspondence confirms that the second peak in the LA injections spectra can be attributed to EL formation.

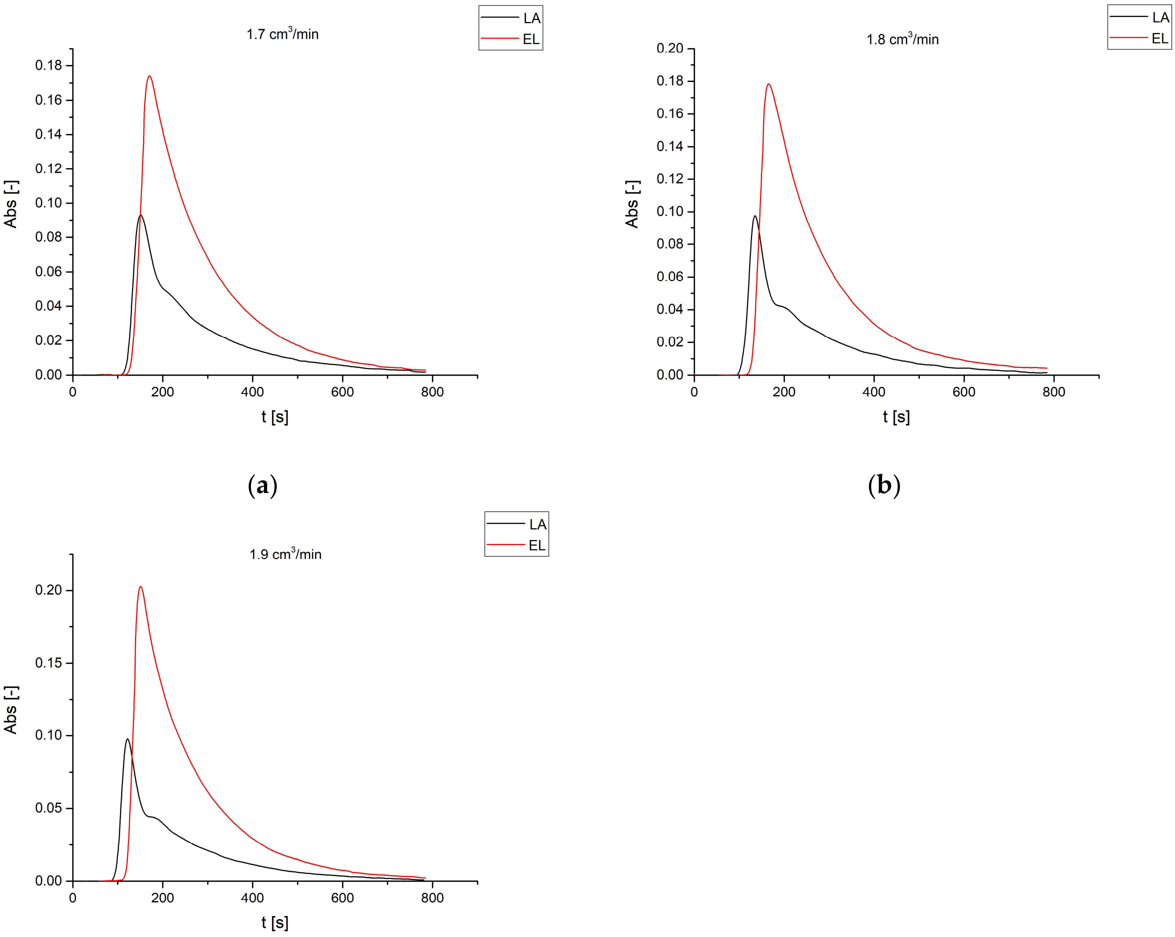

(**a**)

(**b**)

(**c**)

Figure 6. UV spectra of LA and EL 6 M at 313.15 K at different flow rates. (**a**): 1.7 cm^3/min. (**b**): 1.8 cm^3/min. (**c**): 1.9 cm^3/min.

Through peak deconvolution, the approximate LA conversion was determined. The conversion values were not much different for the tests at 1.7, 1.8, and 1.9 cm^3/min flow rate (65%, 67%, and 68% respectively) and, given the difficulty in peaks fitting due to the EL peaks being broad, these values are only indicative.

From these data, it was possible to confirm that the separation of EL from LA occurred at these operative conditions and that the range of conversion values was narrower than the one obtained with tests at 303 K and 0.9 and 1.1 cm^3/min flow rates.

Another set of experiments was carried out raising up the temperature to 323 K to further evaluate the performance of our chromatographic reactor setup. This time, no second peak appeared in any of our tests at different flow rates (1.8, 2, 2.5, and 5 cm^3/min) when LA 6 M pulses were sent through the resin-packed tubular reactor (Figure 7). If this was to be expected for the higher flow rates based on previous collected data, the nature of the single peaks at the lower flow rates remained to be demonstrated.

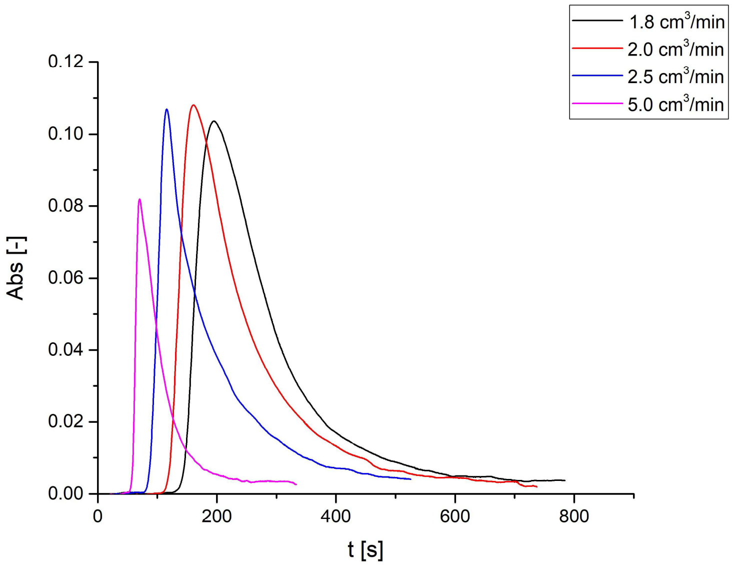

Figure 7. UV spectra of LA 6 M injections at 323 K and different flow rates.

EL 6 M injections at the same temperature and flow rate values demonstrated that at lower flow rates LA was completely converted to EL.

Further proof for the injection test at 1.8 cm^3/min (Figure 8) was given by the LA injection test with the same flow rate at lower temperature—the EL peak of that spectrum perfectly corresponded to the only peak in the LA injection spectrum at 323 K.

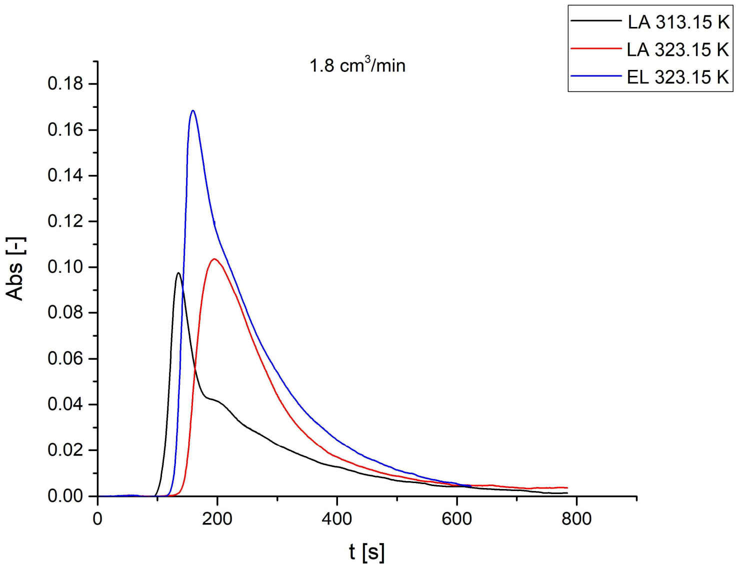

Figure 8. UV spectra of LA and EL 6 M at 313 and 323 K at 1.8 cm^3/min flow rate.

At 323 K, the reaction kinetics and the quantity of catalysts that completely packed the column allowed for complete conversion of LA to EL with flow rate values that gave the organic acid enough time to interact with the ion-exchange resin (Figure 9).

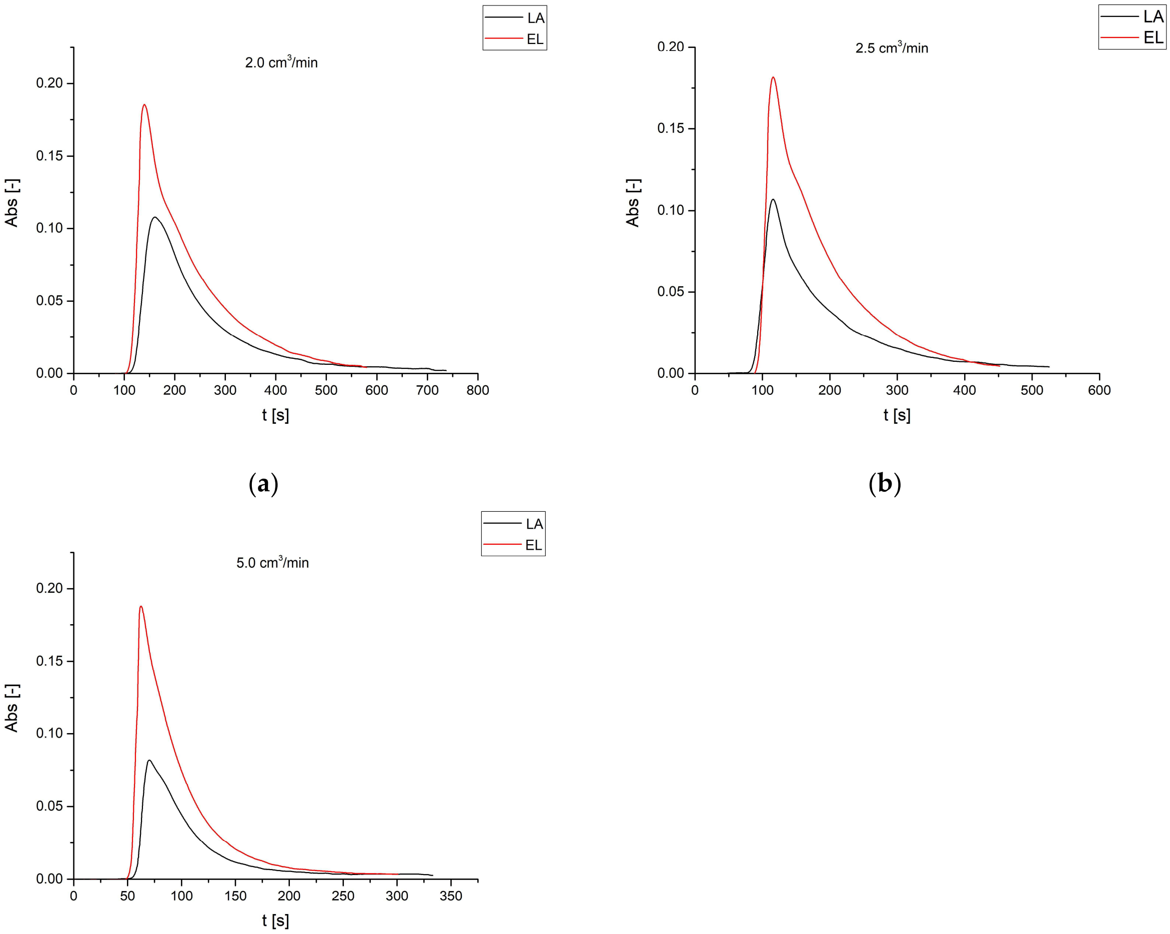

(**a**) (**b**)

(**c**)

Figure 9. UV spectra of LA and EL 6 M at 323 K at different flow rates. (**a**) 2.0 cm^3/min. (**b**) 2.5 cm^3/min. (**c**) 5.0 cm^3/min.

Water produced by the esterification reaction was mostly kept inside the solid. This should not have affected LA conversion largely, but too much water adsorbed in the resin could in fact reduce the quantity of EL obtained at the reactor outlet due to the EL hydrolysis taking place.

After many tests run with the chromatographic reactor setup, the resin showed that it was indeed starting to accumulate water. EL pulses started showing two peaks in the UV analyzer, which would only be explained by the presence of water in the system reacting with the ester and forming LA.

To remove water from the Dowex 50WX8 resin, a 0.05 cm^3/min flow of methanol was sent through the packed reactor for 24 h. The result of this treatment can be seen in the UV spectra in Figure 10.

From the UV spectra, it can be highlighted that methanol successfully removed water from the packed column since EL injections post-treatment did not result in LA formation.

The LA conversions achieved by the chromatographic reactor setup at the different operative conditions employed are summarized in Table 4.

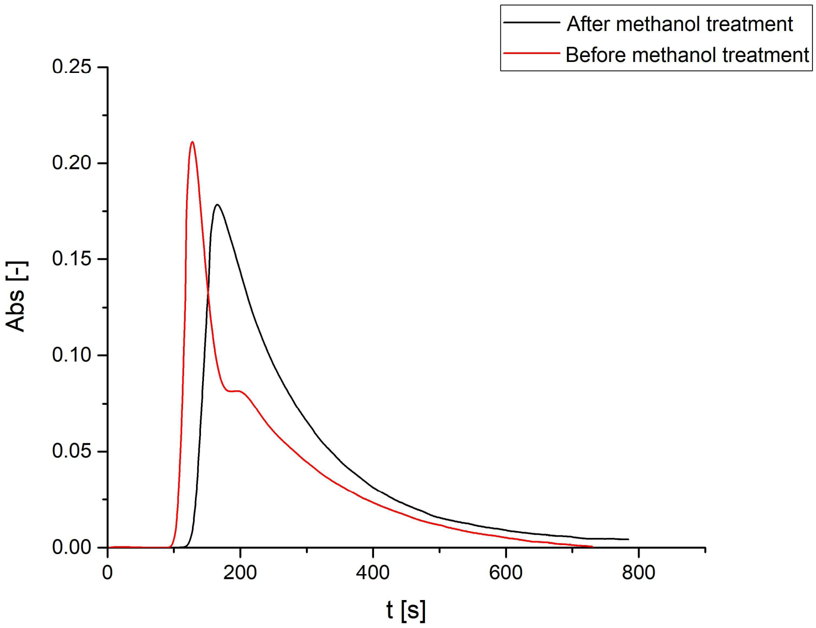

Figure 10. Efficiency of methanol treatment for water removal.

Table 4. LA conversions achieved at different operative conditions during the chromatographic reactor tests with LA 6 M pulses.

Test	T [K]	Q [cm^3/min]	X_{LA} [%] *
C1	303	0.8	100
C2	303	0.9	87
C3	303	1.1	58
C4	303	2.5	0
C5	303	5.0	0
C11	313	1.1	100
C12	313	1.7	65
C13	313	1.8	67
C14	313	1.9	68
C15	313	2.5	0
C21	323	1.8	100
C22	323	2.0	100
C23	323	2.5	0
C24	323	5.0	0

* X_{LA} values were determined by comparison with EL 6 M injections and with peak deconvolution.

As revealed, the trends are rather logical, as conversion decreases by increasing the flowrate, as lower residence times are achieved. The quantification of the data reported in this paper can give a real impact in the optimization of the chromatographic reactor operation conditions.

4. Conclusions

The possibility of conducting LA esterification with ethanol for production of EL in a chromatographic reactor setup was successfully verified using Dowex 50WX8, demonstrating that, in some cases, it is possible to achieve full LA conversion.

A tubular reactor was packed with Dowex 50WX8 to build a chromatographic reactor setup. Tests at different temperatures and flow rates were done to evaluate the catalytic and the separation efficiency of the resin itself.

The chromatographic separation method proved to work for LA esterification, as with sufficiently low flow rates, the LA pulses were completely converted to EL, while with moderate flow rates, the partially unconverted LA was well separated from the ester.

At flow rates higher than 2.5 cm^3/min, LA did not have time to interact with the resin surface. At temperatures near to room temperature (303 K), LA was completely converted to EL. This is a very encouraging result considering that this is not possible in a batch system due to the thermodynamic equilibrium. It was also proved that if the resin should trap too much water, as a by-product of the esterification, it is possible to clean it with a methanol treatment.

This promising reactive setup could be further investigated with a fluid-dynamic characterization and the development of a model that could describe the qualitative data obtained with the chromatographic reactor. Certainly, a higher experimental effort must be conducted to separately retrieve information about the kinetics of the reaction, a point that will be surely investigated in our future works.

Author Contributions: Conceptualization, V.R. and M.D.S.; methodology, V.R.; software, V.R. and R.T.; validation, C.R., C.L.P. and V.R.; formal analysis, V.R. and R.T.; investigation, C.R. and C.L.P.; data curation, C.L.P. and C.R.; writing—original draft preparation, C.R. and V.R.; writing—review and editing, V.R., R.T. and M.D.S.; supervision, V.R. and M.D.S.; project administration, V.R.; funding acquisition, M.D.S. All authors have read and agreed to the published version of the manuscript.

Funding: This research received no external funding.

Institutional Review Board Statement: Not applicable.

Informed Consent Statement: Not applicable.

Data Availability Statement: Data sharing not applicable.

Acknowledgments: Raffaele Morlando is cordially acknowledged for the support in the realization of the chromatographic reactor experimental setup.

Conflicts of Interest: The authors declare no conflict of interest.

Abbreviations

LA	Levulinic acid
EL	Ethyl levulinate
EtOH	Ethanol
H2O	Water
List of symbols	
T	Temperature [K]
t	Time [s]
V^d_{resin}	Volume of dried resin [cm^3]
V^s_{resin}	Volume of swelled resin [cm^3]
α	Swelling coefficient [%]

References

1. Liu, C.; Lu, X.; Yu, Z.; Xiong, J.; Bai, H.; Zhang, R. Production of levulinic acid from cellulose and cellulosic biomass in different catalytic systems. *Catalysts* **2020**, *10*, 1–22. [CrossRef]
2. Bozell, J.J.; Petersen, G.R. Technology development for the production of biobased products from biorefinery carbohydrates—the US Department of Energy's "Top 10" revisited. *Green Chem.* **2010**, *12*, 539. [CrossRef]
3. Leal Silva, J.; Grekin, R.; Mariano, A.; Filho, R. Making Levulinic Acid and Ethyl Levulinate Economically Viable: A Worldwide Technoeconomic and Environmental Assessment of Possible Routes. *Energy Technol.* **2017**, *6*, 613–639. [CrossRef]
4. Joshi, H.; Moser, B.R.; Toler, J.; Smith, W.F.; Walker, T. Ethyl levulinate: A potential bio-based diluent for biodiesel which improves cold flow properties. *Biomass Bioenergy* **2011**, *35*, 3262–3266. [CrossRef]
5. Brown, D.W.; Floyd, A.J.; Kinsman, R.G.; Roshan-ali, Y. Dehydration Reactions of Fructose in Non-aqueous Media. *J. Chem. Technol. Biotechnol.* **1982**, *32*, 920–924. [CrossRef]
6. Deuss, P.J.; Barta, K.; De Vries, J.G. Homogeneous catalysis for the conversion of biomass and biomass-derived platform chemicals. *Catal. Sci. Technol.* **2014**, *4*, 1174–1196. [CrossRef]
7. Schuette, H.A.; Cowley, M.A. Levulinic acid. II. the vapor pressures of its alkyl esters (C1–C6. *J. Am. Chem. Soc.* **1931**, *53*, 3485–3489. [CrossRef]

8. Nandiwale, K.Y.; Sonar, S.K.; Niphadkar, P.S.; Joshi, P.N.; Deshpande, S.S.; Patil, V.S.; Bokade, V.V. Catalytic upgrading of renewable levulinic acid to ethyl levulinate biodiesel using dodecatungstophosphoric acid supported on desilicated H-ZSM-5 as catalyst. *Appl. Catal. A Gen.* **2013**, *460–461*, 90–98. [CrossRef]
9. Pasquale, G.; Vázquez, P.; Romanelli, G.; Baronetti, G. Catalytic upgrading of levulinic acid to ethyl levulinate using reusable silica-included Wells-Dawson heteropolyacid as catalyst. *Catal. Commun.* **2012**, *18*, 115–120. [CrossRef]
10. Badgujar, K.C.; Badgujar, V.C.; Bhanage, B.M. A review on catalytic synthesis of energy rich fuel additive levulinate compounds from biomass derived levulinic acid. *Fuel Process. Technol.* **2020**, *197*, 106213. [CrossRef]
11. Fernandes, D.R.; Rocha, A.S.; Mai, E.F.; Mota, C.J.A.; Teixeira da Silva, V. Levulinic acid esterification with ethanol to ethyl levulinate production over solid acid catalysts. *Appl. Catal. A Gen.* **2012**, *425–426*, 199–204. [CrossRef]
12. Russo, V.; Rossano, C.; Salucci, E.; Tesser, R.; Salmi, T.; Di Serio, M. Intraparticle diffusion model to determine the intrinsic kinetics of ethyl levulinate synthesis promoted by Amberlyst-15. *Chem. Eng. Sci.* **2020**, *228*, 115974. [CrossRef]
13. Russo, V.; Tesser, R.; Rossano, C.; Cogliano, T.; Vitiello, R.; Leveneur, S.; Di Serio, M. Kinetic study of Amberlite IR120 catalyzed acid esterification of levulinic acid with ethanol: From batch to continuous operation. *Chem. Eng. J.* **2020**, *401*, 126126. [CrossRef]
14. Srivastava, N.; Kuddus, M. Use of Ion-Exchange Resin in Reactive Separation. In *Applications of Ion Exchange Materials in Chemical and Food Industries*; Inamuddin, T.A., Rangreez, M., Asiri, A., Eds.; Springer International Publishing: Cham, Switzerland, 2019; pp. 125–137. ISBN 978-3-030-06085-5.
15. Mazzotti, M.; Kruglov, A.; Neri, B.; Gelosa, D.; Morbidelli, M. A continuous chromatographic reactor: SMBR. *Chem. Eng. Sci.* **1996**, *51*, 1827–1836. [CrossRef]
16. Rodrigues, A.E.; Pereira, C.S.M.; Santos, J.C. Chromatographic Reactors. *Chem. Eng. Technol.* **2012**, *35*, 1171–1183. [CrossRef]
17. Vu, T.D.; Seidel-Morgenstern, A. Quantifying temperature and flow rate effects on the performance of a fixed-bed chromatographic reactor. *J. Chromatogr. A* **2011**, *1218*, 8097–8109. [CrossRef] [PubMed]
18. Russo, V.; Tesser, R.; Rossano, C.; Vitiello, R.; Turco, R.; Salmi, T.; Di Serio, M. Chromatographic reactor modelling. *Chem. Eng. J.* **2019**, *377*, 119692. [CrossRef]